STUDIES ON BOND AND CRACKING OF STRUCTURAL CONCRETE

by

Homayoun H. Abrishami

June 1994

Department of Civil Engineering and Applied Mechanics
McGill University
Montreal, Canada

A thesis submitted to
the Faculty of Graduate Studies and Research
in partial fulfilment of the requirements for the degree of
Doctor of Philosophy

National Library of Canada

Bibliothèque nationale du Canada

Acquisitions and Bibliographic Services Branch

Direction des acquisitions et des services bibliographiques

395 Wellington Street
Ottawa, Ontario
K1A 0N4

395, rue Wellington
Ottawa (Ontario)
K1A 0N4

Your file Votre référence

Our file Notre référence

ISBN 0-612-00099-0

Canadä

To:

All those who never quit human bonds

In the name of God

ABSTRACT

This thesis presents new testing methods to study the bond characteristics of reinforcing bars and pretensioned strands. For reinforcing bars, the new technique, which simulates a more uniform bond stress, enabled the study of both pullout failures and splitting failures. Variables studied included concrete cover, bar size and the effect of epoxy coatings on the bars. Analytical expressions for predicting the bond stress versus slip response and the bond stress distribution for different types of pullout tests are developed. For pretensioned strand, the testing technique enabled the study of the bond characteristics along both the transfer and the flexural bond lengths. Equations for predicting the transfer and development lengths are given.

The tensile behaviour of concrete members reinforced with a single reinforcing bar are studied. Variables studied included concrete strength, presence of steel fibres, bar size and the effect of epoxy coatings on the bars. Both transverse cracks and splitting cracks were studied and a factor accounting for the influence of splitting cracks on tension stiffening is introduced. A procedure for predicting the response of tension members, accounting for the concrete cover and bar size and the presence of steel fibres is given. Equations are suggested to determine the transfer length and crack spacing.

Experimental investigations were carried out to study the post-cracking behaviour of beams without stirrups. The influence of concrete strength and the presence of epoxy-coated reinforcement on the crack development, type of cracking, ductility and failure mechanism are discussed. Typical slab-column connections found in parking structures were tested, simulating the construction stages. The effects on crack development of both concrete quality and the presence of epoxy coatings on the reinforcement were studied. Modification factors for predicting crack widths in beams and two-way slabs, accounting for the presence of epoxy coatings, are given in a form suitable for implementation in codes of practice.

SOMMAIRE

Cette thèse présente de nouvelles méthodes expérimentales permettant d'étudier les caractéristiques d'adhérance de l'armature et des câbles prétendus. Pour l'armature, la nouvelle technique qui simule la contrainte d'adhérance plus uniforme a permis d'étudier aussi bien les ruptures par arrachement que celles par fendage. Les variables évaluées au cours de l'étude comprennent le recouvrement de béton, la dimension de l'armature et l'effet de l'enrobage d'époxy. Des expressions analytiques pour la prédiction de la contrainte d'adhérance versus le glissement résultant ainsi que la distribution des contraintes d'adhérance pour différents types d'essais d'arrachement sont développées. Pour les câbles prétendus, la nouvelle technique a permis d'évaluer les caractéristiques d'adhérance relatives aux longueurs de transfert et de flexion. Des équations pour la prédiction des longueurs de transfert et de développements sont également données.

Le comportement sous tension des éléments en béton armé d'une seul barre est étudié. Les variables évaluées au cours de l'étude comprennent la capacité du béton, la présence de fibres d'acier, la dimension de l'armature et l'effet de l'enrobage d'époxy. Tant les fissures transversales que les fissures de fendage ont été étudiés et un facteur tenant compte de l'influence des fissures de fendage sur la rigidité sous tension est introduit. Une procédure pour la prédiction de la réponse des éléments sous tension, prenant en considération le recouvrement de béton et la présence des fibres d'acier est présentée. Des équations sont suggérées afin de déterminer la longueur de transfert et l'espacement des fissures.

Des recherches expérimentales furent entreprises afin d'étudier le comportement post-fissuré de poutres sans étriers. L'influence de la résistance du béton et la présence d'armature enrobée d'époxy sur le développement des fissures, le type de fissures, ainsi que les mécanismes de ductilité et de rupture sont discutés. Des assemblages typiques dalles-poteaux, présentes dans les structures de stationnement, ont été testées en simulant les diverses étapes de construction. Les effets de la qualité du béton et de la présence d'armature enrobée d'époxy sur le développement des fissures furent étudiés. Des facteurs de modification pour la prédiction de l'ouverture des fissures dans les poutres et les dalles bi-directionnelles, tenant compte de la présence de l'enrobage d'époxy, sont présentés sous une forme convenant à leur implémentation dans les codes de pratique professionnelle.

ACKNOWLEDGEMENTS

Foremost, the author must thank God for giving him health, strength and patience during his Ph.D. program.

The author would like to take this opportunity to express his deepest gratitude to Professor Denis Mitchell, an excellent friend and teacher, for his continual encouragement, knowledgable advise and educational and scientific discussion throughout this research program. The author will never forget what he learned, all with pleasure, and wishes to follow Professor Mitchell's path both in teaching and research in the future.

The author would like to express his sincere thanks to Dr. William D. Cook for his skilful guidance and a very precise technical review of the final draft of this thesis. Special thanks are extended to Marco Di Franco for his expert assistance in preparing the figures and developing the photographs.

The experimental research was carried out in the structural laboratories in the Department of Civil Engineering and Applied Mechanics at McGill University. The author wishes to thank Ronald Sheppard, Brian Cockayne, Marek Przykorski, John Bartczak and Damon Kiperchuk for their assistance in constructing the specimens. The author also wishes to thank Arshad A. Khan, Phil Zeyl, Joanne Crabb, Nick Vanelli and Glenn Marquis for their help in testing of the specimens.

The financial assistance provided by Ministry of Culture and Higher Education of the Islamic Republic of Iran and the Network of Centres of Excellence program funded by the Minister of State, Science and Technology in Canada is highly appreciated. The financial support of the Protection and Coatings Committee of the Reinforcing Steel Institute of Canada is gratefully acknowledged. Thanks are extended to Harris Rebar, Nantucket Rebar and Bekaert Steel Wire Corporation for providing materials.

Most of all, the author is grateful to his mother who always provides the family with care and love, especially a year after this Ph.D. program started and his father passed away. A father who was his first teacher and supervisor.

TABLE OF CONTENTS

Chapter 2

Chapter 3

Chapter 4

Chapter 5

Chapter 6

LIST OF FIGURES

LIST OF TABLES

LIST OF SYMBOLS

A	=	effective area of concrete surrounding each bar
A_c	=	area of concrete cross section
A_f	=	area of steel fibres
A_s	=	area of steel reinforcement
b_w	=	width of beam web
c_1	=	a constant depending on the boundary conditions in a pullout specimen
c_2	=	a constant depending on the boundary conditions in a pullout specimen
c_3	=	a constant depending on the boundary conditions in a pullout specimen
c_4	=	a constant depending on the boundary conditions in a pullout specimen
d	=	distance from extreme compressive fibre to centroid of tension reinforcement
d_b	=	bar or strand diameter
d_c	=	distance from extreme tension fibre to centre of closest bar
d_{b1}	=	diameter of the reinforcement in direction 1
E_b	=	bond stiffness before cracking in a pullout specimen
E_c	=	modulus of elasticity of the concrete
E_f	=	modulus of elasticity of the steel fibres
E_s	=	modulus of elasticity of the reinforcing bar
E_d	=	bond stiffness after cracking in a pullout specimen
f_c	=	concrete stress
f_{cr}	=	tensile strength of concrete
f'_c	=	compressive strength of concrete (from a standard cylinder test)
f_{ps}	=	stress in prestressed reinforcement at nominal strength
f_{pu}	=	ultimate strength of strand
f_r	=	modulus of rupture
f_s	=	stress in the reinforcing bar or strand
f_{sp}	=	splitting tensile strength of concrete
f_{se}	=	effective stress in prestressed reinforcement after all losses
f_y	=	specified yield strength of steel reinforcement

k_1	=	coefficient to account for boundary conditions and loading of two-way slabs
K_s	=	stiffness of reinforcing bar
ℓ	=	embedment length
ℓ_d	=	development length
ℓ_{fb}	=	flexural bond length
ℓ_t	=	transfer length
L	=	length of reinforcement
M_{cr}	=	cracking moment
M_n	=	nominal moment resistance
P	=	applied load on the specimen
P_b	=	bottom force in the reinforcing bar or strand
P_t	=	top force in the reinforcing bar or strand
s	=	crack spacing
s_1	=	spacing of the reinforcement in direction 1
s_2	=	spacing of the reinforcement in direction 2
T	=	applied tensile load
T_{cr}	=	cracking load in a tension specimen
T_f	=	tensile load carried by fibres after yielding the reinforcement
T_{sp}	=	tensile force required to start splitting cracks
T_y	=	load in the reinforcement at yielding
u	=	bond stress
u_{av}	=	average bond stress
$u_{fb,\max}$	=	maximum bond stress along flexural bond length
$u_{\max}$	=	maximum bond stress
$u_{\min}$	=	minimum bond stress
u_{pf}	=	bond strength at pullout failure
u_{sp}	=	bond strength at splitting failure
u_{sr}	=	residual bond stress
$u_{t,\max}$	=	maximum bond stress along transfer length
V_c	=	factor shear strength provided by concrete

V_f	=	volume percentage of fibres in concrete
V_n	=	nominal shear strength
w_{av}	=	average crack width
w_{max}	=	maximum crack width
α	=	factor accounting for bond stress distribution
α_1	=	factor accounting for bond characteristics of reinforcement
α_2	=	factor accounting for load conditions
α_3	=	factor accounting for influence splitting cracks
β	=	ratio of distance between neutral axis and tension face to distance between neutral axis and centroid of reinforcing steel
δ	=	relative slip between concrete and steel
δ_{av}	=	average slip between concrete and steel
δ_c	=	slip of the concrete
δ_{pf}	=	average slip at pullout failure
δ_s	=	slip of the steel
δ_{sp}	=	average slip at splitting failure
δ_{sr}	=	average slip at residual bond stress
Δ_{cr}	=	deflection at cracking load
Δ_y	=	deflection at general yielding
Δ_u	=	deflection at ultimate load
ϵ_c	=	strain in the concrete
ϵ_s	=	strain in the steel
ϵ_{sm}	=	average strain in steel
ϵ_{sr}	=	strain in the reinforcing bar at crack location
σ_s	=	stress in steel at a crack
σ_{sr}	=	stress in steel at crack at a load corresponding to the cracking load
ρ	=	reinforcement ratio
ρ_{min}	=	minimum reinforcement ratio
ρ_{tl}	=	active steel reinforcement ratio
ϕ	=	ratio of top force to bottom force of reinforcement in a pullout / push-in bond specimen

Chapter 1

INTRODUCTION

"To engineers who, rather than blindly following the codes of practice, seek to apply the laws of nature"
T.Y. Lin, 1955

The behaviour of reinforced concrete members is strongly influenced by bond between the reinforcement and the concrete, which in turn strongly affects the cracking performance. Figure 1.1 shows schematically the stress distributions in a cracked reinforced concrete beam segment subjected to pure bending. Even for this simple loading case, the concrete stress, steel stress and bond stress distributions are quite complex. In order to study the behaviour of a reinforced concrete member it is necessary to understand, in some detail, the influence of both bond and cracking.

Chapter 1 presents an overview of some of the major studies carried out by other researchers in the general area of bond and cracking in reinforced concrete. The other chapters provide more detailed discussions of the research carried by others in specific areas. Chapter 2 presents a new testing technique to study bond characteristics of reinforcing bars and pretensioned strands. The effects of bar size, concrete cover and the presence of epoxy coating on the reinforcing bars are investigated. Both transfer length and flexural bond length of pretensioned strand are studied by this method of testing. In Chapter 3, equations are developed to predict the response of pullout specimens. These predictions involved first developing the governing differential equations relating bond stress and slip. These expressions were then applied to pullout tests with different boundary conditions to determine the bond stress distribution along reinforcing bars embedded in concrete. Also, analytical expressions are developed to predict the transfer length and development length of pretensioned strand.

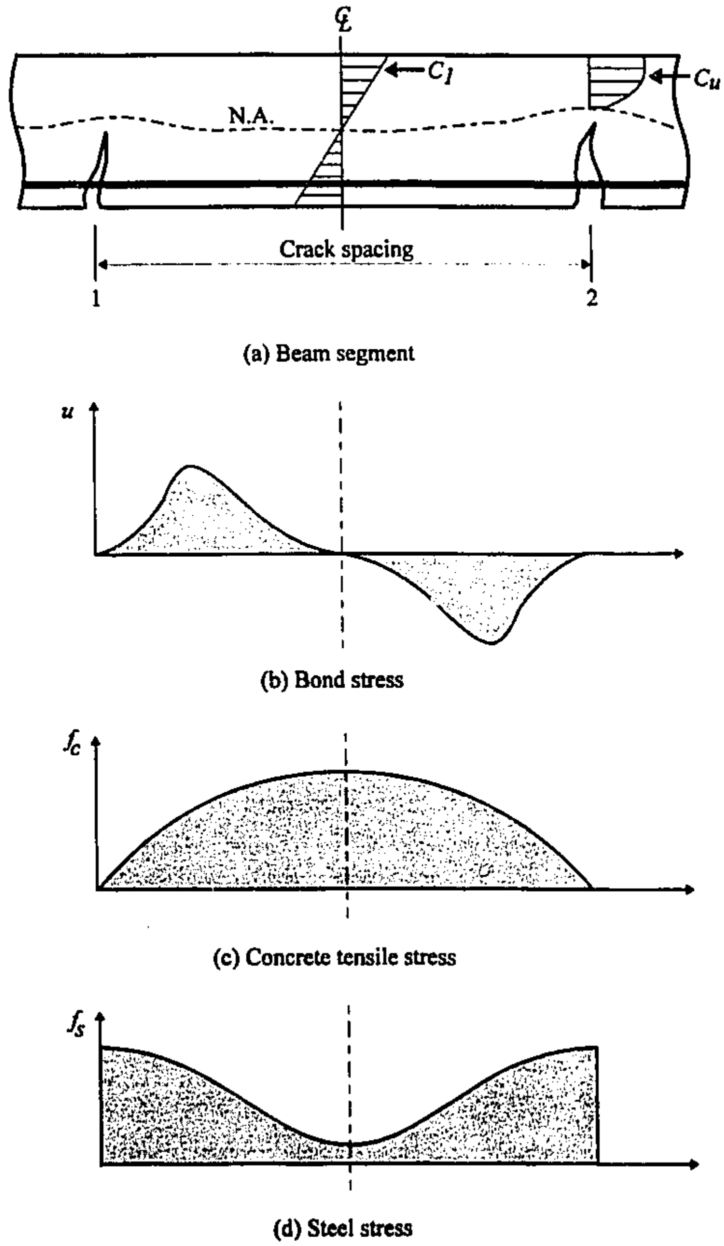

Figure 1.1: Stress distributions in a cracked reinforced concrete beam segment adapted from Nawy (1992)

Chapter 4 includes the response of reinforced concrete tension members, beams and two-way slabs. The influence of concrete strength, steel fibres and epoxy-coated reinforcement on both cracking and tension stiffening of reinforced concrete members subjected to pure tension is presented. This chapter also discusses the influence of epoxy-coated reinforcing bars on the responses of normal-strength and high-strength concrete beams. Failure mechanisms observed in tests of high-strength concrete beams are discussed. The effect of epoxy-coated reinforcing bars and concrete quality on cracking of slab-column connection specimens, representing typical parking garage structures, is also studied.

Chapter 5 presents an analytical investigation of the influence of concrete strength and presence of steel fibres on cracking and tension stiffening. Crack width predictions of concrete beams and slab-column connections reinforced with epoxy-coated bars are presented. Chapter 6 summarises the influence of high-strength concrete, steel fibres, epoxy-coated reinforcement and concrete quality on bond, cracking and structural deformations of tension members, beams and two-way slabs.

1.1 BOND CHARACTERISTICS OF REINFORCED CONCRETE

The transfer of forces across the interface between concrete and steel reinforcing bars is of fundamental importance in reinforced concrete structures. Bond stress is the equivalent shear stress acting parallel to the reinforcing bar on the interface between the bar and the concrete. The force transfer mechanism is a combination of (1) shear resistance due to adhesion, (2) frictional resistance and (3) mechanical anchorage. The mechanical anchorage is due to the presence of lugs or bar deformations in the case of reinforcing bars and is due to interlocking of the spiralling outer wires in the case of strands. This component of bond resistance arises mainly from the bearing of the lugs or spiral against the concrete.

ACI Committee 408 (1991) has suggested that for reinforcing bars embedded in concrete and subjected to monotonic loading typical values for the adhesion component range from 0.5 to 1.0 MPa, while those of the friction component range from 0.4 to 10 MPa (Chinn *et al.* 1955; Eligehausen *et al.* 1983). Based on research by Treece and Jirza (1987), ACI Committee 408 in comparing the performance of plain and epoxy-coated reinforcing bars has suggested that friction may contribute as much as 35% of the ultimate strength in failure governed by splitting of the concrete cover. In assessing the contribution of the lugs it is interesting to note that the CEB-FIP Model Code (1991) gives a bond strength for deformed bars which is as much as 2.25 times that for plain bars.

1.1.1 Previous Research on Bond Characteristics

Investigators have studied bond characteristics in reinforced concrete for nearly a century (Abrams 1913) and in pretensioned concrete for about 50 years (Armstrong 1949). The earliest published tests on bond between concrete and "iron bars" were carried out by Hyatt in 1877 (Abrams 1951). By 1909 Abrams (1913) had carried out tests on both beams and pullout specimens having a variety of deformations. Summaries of some of the major developments in the study of bond characteristics over the last century are given by ACI Committee 408 (1966; 1991) and CEB Task group VI (1981). The 1963 ACI Code (ACI 1963) specified a bond stress for working stress design and introduced an ultimate bond stress for ultimate strength design for determining the required embedment length of reinforcing bars. The magnitude of this average ultimate bond stress was taken as a function of the square root of the concrete compressive strength and was inversely proportional to the bar diameter. In 1971, the ACI Code (ACI 1971) introduced expressions for the required development length of reinforcing bars. These development length expressions were modified in the 1989 ACI Code (ACI 1989) (Revised 1992 (ACI 1992)) in order to introduce the influence of clear concrete cover, spacing between bars and the presence of transverse reinforcement. The empirically derived expressions were based on pullout tests, equivalent beam tests and beam tests. A standard pullout test method for determining bond strength is given by ASTM C234 (ASTM 1988). If the development length expression of the 1989 ACI Code is used to determine an equivalent bond strength, then this average bond stress, u , at ultimate is:

$$u = 16.7 \frac{\sqrt{f_c'}}{d_b} \qquad \text{(MPa, mm units)} \qquad (1.1)$$

where f_c' is the concrete compressive strength and d_b is the diameter of the reinforcing bar being developed.

Considerable research on bond between pretensioned strand and concrete has been reported since 1949 (Armstrong 1949). Janney (1954) was one of the earliest pioneers to research the physical characteristics of bond between pretensioned strand and concrete and its relationship to the transfer and development lengths. In a pretensioned concrete member there are two distinct regions having different bond characteristics; the transfer length region and flexural bond length region. The length of strand at the ends of a pretensioned member over which the stress in the steel builds-up is called the transfer length. The flexural bond length is the additional length required beyond the transfer length in order to develop the stress associated with the superimposed loading on the member. Experimental investigations to determine the transfer length and flexural bond lengths rely on measurements of the concrete surface strain or the steel strain along the strand.

A summary of the research carried out on bond characteristics of pretensioning strand has been presented by Cousins *et al.* (1990) and by Deatherage and Burdette (1990). Experimental studies were typically carried out on simple pullout specimens or beam tests having a wide variety of specimen geometries, types of loading and restraints. Based on the beam test results reported by Hanson and Kaar (1959) in 1959, an empirical relationship was adopted by the 1963 ACI Code (ACI 1963) which is still used in the 1989 ACI Code, Revised 1992 (ACI 1992). The ACI equation can be expressed as follows:

$$\ell_d = 0.048\, f_{se}\, d_b + 0.145\, (f_{ps} - f_{se})\, d_b \qquad \text{(MPa, mm)} \quad (1.2)$$

where ℓ_d is the development length, f_{ps} is the stress in the prestressed reinforcement at the critical section, f_{se} is the effective stress in the prestressed reinforcement after all losses and d_b is the nominal diameter of the strand. In this form the first term, ($0.048\, f_{se} d_b$), is the transfer length in mm and the second term, $0.145\, (f_{ps} - f_{se})\, d_b$, is the flexural bond length in mm.

More research is needed in order to gain a better understanding of the nature of bond and of the parameters which affect the bond strength.

1.1.2 Influence of Concrete Strength

The 1963 ACI Code (ACI 1963) introduced an ultimate bond stress for determining the stress that the bars could develop. In these earlier codes the bond stress was assumed to be uniform along the bar length. The magnitude of this average ultimate bond stress was taken as a function of the square root of the concrete compressive strength.

With the advent of higher concrete strengths, the 1989 ACI Code (ACI 1989) placed a limit on $\sqrt{f_c'}$ of 8.3 MPa (i.e., corresponding to a limit on f_c' of 69 MPa), when computing the required development length. In many design calculations it is often assumed that the bond stress is uniform along the bar, which implies that all lugs or bar deformations are bearing uniformly against the surrounding concrete. Research studies on bond performance of reinforcing bars embedded in high-strength concrete are limited (Hwang *et al* 1994). However, several researchers (e.g., Johnson and Ramirez (1989); Kim and White (1991)) have made conclusions about the influence of high strength concrete on the bond performance while studying flexural and shear behaviour of high-strength concrete beams.

Azizinamini *et al.* (1993) studied the influence of high-strength concrete on the behaviour of lap splices. They concluded that the assumption of a uniform bond stress distribution at the ultimate stage may not be correct for high-strength concrete. In addition, the normalized bond strength (u_{test} divided by $\sqrt{f_c'}$) is lower for high-strength concrete than for normal-strength concrete. They concluded that for small concrete covers increasing the splice length is not effective way of increasing the splice capacity and recommended some minimum amount of transverse reinforcement.

The effect of concrete compressive strength on transfer length of pretensioning strand has been investigated by several researchers (Kaar *et al.* 1963; Mitchell *et al.* 1993). A recent study by Mitchell *et al.* (1993) showed that the transfer length and development length diminished with an increase in compressive concrete strength, being inversely proportional to the square root of concrete compressive strength.

More experimental research is required to assess the influence of the more brittle, higher strength concretes on bond.

1.1.3 Influence of Epoxy Coatings on Reinforcing Bars

One of the design considerations when using epoxy-coated reinforcement is its effect on the bond between the epoxy-coated bar and the concrete. The influence of epoxy coating on bond and anchorage behaviour of reinforcing bars has been studied by Hamad *et al.* (1990), Choi *et al.* (1990) and Cleary and Ramirez (1991). Treece and Jirsa (1989) concluded that epoxy coating significantly reduces the bond strength and the amount of the reduction was dependent on the mode of failure: pullout failure or splitting failure. This reduction on bond strength was found to be approximately 65 percent and 85 percent in the case of splitting failure and pullout failure, respectively. Also, they concluded that the reduction in bond strength is insensitive to the variation in the coating thickness when the average coating thickness is between 5 mil and 14 mil (0.12 to 0.35 mm). The 1989 ACI Code (ACI 318 1989) provides a factor of 1.5 for the development length of epoxy-coated reinforcing bars with a concrete cover less than 3 bar diameters and a clear spacing between bars less than 6 bar diameters. For epoxy-coated bars with larger values of cover and spacing a factor of 1.2 applies.

1.1.4 Influence of Fibre-Reinforced Concrete

A summary of research carried out on the effect of fibre reinforced concrete on bond is given by Yan (1992). Swamy and Al-Noori (1974) were the first to investigate the improved performance in bond of deformed bars embedded in steel fibre reinforced concrete. A series of pullout specimens containing round straight steel fibres having a length of 25 mm and a diameter of 0.4 mm, as well as fibres with a length of 50 mm and a diameter of 0.5 mm were used in their experiments. Two different fibre contents, 3.5% and 7% by volume resulted in an increase of about 40% in bond strength over specimens without fibres. Ezeldin and Balaguru (1989), concluded that the presence of steel fibres improves the bond strength only slightly while a greater improvement was noticed in the ductility (i.e., the area under load-slip curve).

1.2 CRACKING AND STRUCTURAL DEFORMATIONS

Summaries of the considerable research carried out on cracking and its effect on structural deformations have been provided by the CEB Task Group on Cracking and Deformations (CEB Manual 1985) and by ACI Committee 224 (1988). The CEB-FIP Code (1978; 1991) limits the crack widths whereas North American Codes (ACI 1989; CSA 1984), limit the crack widths indirectly by limiting a crack control parameter. The ACI Code bases its crack control requirements on the Gergely-Lutz expression (Gergely-Lutz 1968) for maximum crack widths. The Gergely-Lutz expression for maximum crack width is:

$$w_{max} = 2.2\ \beta\ \epsilon_{scr} \sqrt[3]{d_c A} \tag{1.3}$$

where

w_{max} = maximum crack width

β = factor accounting for strain gradient

= 1.0 for uniform strain, or h_2 / h_1 for varying strains, where h_1 is the distance from the tension steel to the neutral axis and h_2 is the distance from the extreme tension fibre to the neutral axis

ϵ_{scr} = strain in reinforcing bar at crack location (may be taken as 0.6 ϵ_y in design)

d_c = distance from extreme tension fibre to centre of closest bar

A = effective area of concrete surrounding each bar, taken as the total area of concrete in tension which has the same centroid as the tension reinforcement, divided by the number of bars.

The major parameters affecting the development and characteristics of the flexural cracks in beams and one way slabs are: percentage of reinforcement, bond characteristics, size of the bar, concrete cover, and the effective concrete area in tension surrounding the bars.

The Gergely-Lutz expression underestimates the maximum crack widths in two-way slabs. In addition to those parameters affecting the crack widths in beams and one-way slabs, the boundary conditions in two-way slabs are significant factors influencing the crack widths. Based on the work of Nawy and Orenstein (1970) and Nawy and Blair (1971), ACI Committee 224 (1988) recommends the following equation for predicting the maximum crack width, w_{max}, in two-way slabs:

$$w_{max} = k_1\ \beta\ \epsilon_s \sqrt{\frac{d_{bl}\ s_2}{\rho_{tl}}} \qquad \text{(mm)} \tag{1.4}$$

where:

k_1 = coefficient, having a value of 0.81 for uniformly loaded restrained two-way square slabs and 0.90 for simply supported two-way square slabs subjected to a central concentrated load. For the other different boundary conditions see Nawy (1992), Nawy and Orenstein (1970), and Nawy and Kenneth (1971)

β = ratio of distance between neutral axis and tension face to distance between neutral axis and centroid of reinforcing steel (may be taken as 1.25 in design)

ϵ_s = average service load steel strain (may be taken as 0.4 ϵ_y in design)

d_{b1} = diameter of the reinforcement in direction 1 (closest to the concrete outer fibres)

s_1 = spacing of the reinforcement in direction 1

s_2 = spacing of the reinforcement in direction 2 (perpendicular to direction 1)

ρ_{t1} = active steel ratio

= area of steel A_s per unit width divided by (d_{b1} + $2c_1$) where c_1 is the clear concrete cover measured from the tensile face of concrete to the nearest edge of the reinforcing bar in direction 1

1.2.1 Previous Research on Cracking and Tension Stiffening

As early as 1899, Considère (1899), in testing small mortar prisms reinforced with steel wires, observed that their tensile load-deformation response was almost parallel to the bare bar steel response but remained well above it. In 1908, Mörsch (1909) explained this phenomenon which was later called "tension stiffening". After cracking there is no tensile stress in the concrete at crack locations but there are tensile stresses in the concrete between the cracks. After the formation of the first crack, the average tensile stress in the concrete between the cracks will be reduced and as further cracks develop, the average stress will be further reduced. In order to account for this effect the CEB-FIP Model Code (1978) based on tests of direct tension members (Leonhardt 1977) provides an empirical relationship to account for the stiffening effect of the concrete surrounding the reinforcement. The average strain in the reinforcement, ϵ_{sm} is given as:

$$\epsilon_{sm} = \frac{\sigma_s}{E_s}\left[1 - \beta_1 \beta_2 \left(\frac{\sigma_{sr}}{\sigma_s}\right)^2\right] \nless 0.4 \frac{\sigma_s}{E_s} \tag{1.5}$$

where:

σ_s = is the stress in the reinforcement at a cracked section due to the applied load;

σ_{sr} = is the stress in the reinforcing bar calculated on the assumption of a cracked section at a load corresponding to the cracking load;

β_1 = factor accounting for bond characteristics of reinforcement, 1.0 for high-bond bars, and 0.5 for plain bars;

β_2 = factor accounting for sustained or repeated loading, equal to 1.0 for short-term monotonic loading and 0.5 for sustained and/or repeated loading.

An alternative approach is to account for the tension stiffening effect of the concrete by introducing an average concrete tensile stress versus strain relationship. The suggested average tensile stress given by Vecchio and Collins (1986) and by Collins and Mitchell (1991) is:

$$f_c = \frac{\alpha_1 \; \alpha_2 \, f_{cr}}{1 + \sqrt{500 \; \epsilon_{cf}}} \tag{1.6}$$

where:

- α_1 = factor accounting for bond characteristics of reinforcement, 1.0 for deformed reinforcing bars, 0.7 for plain bars, wires, or bonded strands and 0.0 for unbonded reinforcement.
- α_2 = factor accounting for sustained or repeated loading, equal to 1.0 for short-term monotonic loading and 0.7 for sustained and/or repeated loading.

In applying this equation to predict the response of a member it must be noted that the stress in the reinforcement at a crack location cannot exceed the yield stress.

Several researchers have studied the behaviour of reinforced concrete tension elements, as well as the bond characteristics of reinforcement embedded in concrete (Mirza and Houde 1979; Williams 1986; Scott and Gill 1987; Wicke 1991; Reinhardt 1991). More recently, finite element methods (Gunther and Mehlhorn 1991; Stevens et al. 1991; Yannopoulos and Tassios 1991) and fracture mechanics techniques (Bažant 1992; Ouyang and Shah 1994) have been developed to model the influence of bond and cracking on the tensile response of reinforced concrete members.

1.2.2 Influence of Concrete Quality and Concrete Strength

Concrete quality, including mix design, curing and durability, is critical for control of cracking. The ACI Code (ACI 1989) and CSA Standards (1990; 1994a) require that for severe exposure conditions, a maximum water/cement ratio of 0.40 and a minimum concrete compressive strength of 35 MPa be provided. Both the ACI Code and the CSA Standards have a maximum chloride ion content of 0.15% by weight of cement for corrosion protection of non-prestressed construction that is exposed to chlorides in service.

Many recent innovations in advanced concrete technology have made it possible to produce concrete with exceptional performance characteristics. High-performance concrete (HPC) typically has high compressive and tensile strength, larger elastic modulus and very low permeability. High-performance concretes typically have low water/cement ratios, admixtures such as superplastizers and retarders, high quality aggregates (typically smaller sizes than in normal-strength concrete), and supplementary cementitious materials (e.g., silica fume or fly ash). The w/c ratio of normal concrete can vary between 0.45 and 0.70, while that of high-performance concrete ranges from 0.25 to 0.35. The very dense microstructure of HPC and the excellent bonding between the hydrated cement paste and the aggregate results in different cracking characteristics of HPC compared to normal-strength concrete. The significant advances in concrete technology over the past 15 years (ACI Committee 363 1992) now make it possible to obtain ready-mix concrete with strengths as high as 100 MPa in some regions of the country. To-date, the majority of high-strength concrete has been used in special structures, such as off-shore platforms and high-rise buildings.

High-strength concretes are typically much more brittle than traditional normal-strength concretes. In 1987 Thorenfeldt, Tomaszewicz and Jensen (1987) proposed an expression for the response of high-strength concrete in uniaxial compression for a standard cylinder. This stress-strain curve which, is a modification of that suggested by Popovics (1973) for normal-strength concrete, is as follows:

$$\frac{f_c}{f_c'} = \frac{\epsilon_c}{\epsilon_c'} \cdot \frac{n}{n - 1 + (\epsilon_c / \epsilon_c')^{nk}} \tag{1.7}$$

where:

f_c = compressive stress

f_c' = maximum stress

ϵ_c = compressive strain

ϵ_c' = strain when f_c reaches f_c'

n = curve fitting factor, as n becomes higher the rising curve becomes more linear

k = 1 when ϵ_c / ϵ_c' is less than 1, and k is a number greater than 1 when ϵ_c / ϵ_c' exceeds 1.

Collins and Poraz (1989) and Collins and Mitchell (1991) suggested that for $\epsilon_c / \epsilon'_c > 1$

$$k = 0.67 + f'_c / 62 \quad \text{MPa units}$$

and $$n = 0.80 + f'_c / 17 \quad \text{MPa units}$$

As the concrete strength increases, the post-peak unloading portion of the compressive stress-strain relationship is very steep, resulting in a brittle failure mode with very little ductility. These concretes, with very high compressive and tensile strengths, can result in less ductile responses of structural members. Because of this, many of the existing code provisions may need to be modified to account for the different characteristics of high-strength concrete (Collins *et al.* 1993). The modulus of rupture, which is an appropriate measurement of concrete tensile strength is used in predicting the flexural cracking load. The 1989 ACI Code (ACI 1989) uses a value of $0.62\sqrt{f'_c}$ (MPa) for the modulus of rupture for normal-strength concrete. Although this code expression shows that the modulus of rupture is increased as concrete strength is increased, experimental results show that higher values of modulus rupture are appropriate for high-strength concretes (Carrasquillo *et al.* 1981). The value of modulus rupture suggested by ACI Committee 363 (1992) is:

$$f_r = 0.94\sqrt{f'_c} \qquad \text{(MPa)} \qquad \textbf{(1.8)}$$

for concrete compressive strengths, f'_c , between 21 and 83 MPa.

Another design consideration is to ensure that members will not fail in a brittle manner upon first cracking. The 1989 ACI Code requires that beams be reinforced with a minimum amount of flexural reinforcement, ρ_{min}, such that:

$$\rho_{min} = \frac{1.4}{f_y} \qquad \text{(MPa)} \qquad \textbf{(1.9)}$$

It is clear that the minimum amount of flexural reinforcement required by this expression, is not a function of the concrete strength and hence may not provide an adequate amount of reinforcement for high-strength concrete beams. In order to correct this deficiency, ACI Committee 363 (ACI 1992) has recommended the following expression:

$$\rho_{min} = \frac{0.224\sqrt{f'_c}}{f_y} > \frac{1.4}{f_y} \qquad \text{(MPa)} \qquad \textbf{(1.10)}$$

A similar problem exists for the minimum amount of shear reinforcement. The traditional amount of minimum shear reinforcement is:

$$A_v = \frac{b_w\, s}{3\, f_y} \qquad \text{(MPa, mm)} \qquad \textbf{(1.11)}$$

in which, A_v is shear reinforcement, b_w is web width, s is spacing of shear reinforcement and f_y is the yield stress of the shear reinforcement.

Roiler and Russell (1990) carried out an experimental investigation on the shear strength of high-strength concrete beams containing minimum shear reinforcement, according to the requirements of the 1983 ACI Code (ACI 1983). They concluded that two out of three beams failed in shear at a strength that was not only less than the calculated nominal strength, V_n, but also less than the calculated concrete contribution, V_c. For concrete strengths above 69 MPa the 1989 ACI code limits the shear carried by the concrete to:

$$V_c = 0.167\sqrt{69}\, b_w\, d \qquad \text{(MPa, mm)} \qquad \textbf{(1.12)}$$

unless the minimum amount of shear reinforcement is increased by multiplying the amount from Equation (1.11) by $f'_c / 35$ but not more than three times the amount required by Equation (1.11). In Equation (1.12), d is the distance from the extreme compression fibre to the centroid of longitudinal tension reinforcement.

Another behavioural feature that affects the response in shear, is that, in contrast to the rough crack surfaces typical of lower strength concrete, the crack surfaces in higher strength concrete tend to be smoother. This difference in crack surfaces may result in a reduction in the shear carried by aggregate interlock, and thus a reduction in the shear carried by the concrete, V_c. ACI Committee 363 (1992) has suggested that the margin of safety against shear failure of beams designed by the ACI Code (ACI 1989), is smaller for high-strength concrete beams than for normal-strength concrete beams. Johnson and Ramirez (1989) concluded that in beams with higher concrete strengths, due to the redistribution of forces at diagonal tension cracking, the shear strength may be reduced unless adequate amount and detailing of longitudinal and web reinforcement is provided. Experimental research carried out at Cornell University (Pastor *et al.* 1984; El-Zanaty *et al.* 1986a; El-Zanaty *et al.* 1986b) and by Ahmad *et al.* (1986) and Ahmad and Lue (1987) indicate that current ACI Code provisions for shear are not conservative for high-strength concrete particularly for beams having low longitudinal steel ratios. Collins *et al.* (1993) concluded that due to the more brittle nature of the high-strength concrete, if cracks form they may propagate more extensively than they would in traditional concrete and this may result in premature shear failures, particularly in large lightly reinforced beams. There is a need for more data on the minimum amount of web reinforcement required to prevent brittle failure after the formation of diagonal cracking and to control diagonal cracking at service load levels.

More experimental research is required to understand the influence of high-strength concretes on the cracking performance and stiffness of reinforced concrete members.

1.2.3 Influence of Epoxy Coatings on Reinforcing Bars

There are several methods of protecting reinforcement against corrosion. These include increasing the concrete cover, improving the concrete quality, providing cathodic protection of the reinforcement and using fusion bonded epoxy coatings on the reinforcing bars. The Federal Highway Administration (FHWA) initiated research on epoxy coatings in the 1960's. The National Bureau of Standards concluded that the only impervious and tough/bendable coatings were the epoxy powder coatings applied by the electrostatic spray fusion-bonding process that had been developed for the coating of steel pipe for the pipeline industry (Clifton *et al.* 1974).

The first major field application of epoxy coated reinforcing bars was in a Pennsylvania bridge deck over the Schuykill River near Philadelphia in 1973. In 1981 the American Society for Testing Materials (ASTM 1990) Standards Specification for Epoxy-Coated Reinforcing Bars was issued permitting a range of epoxy thicknesses between 5 and 12 mils (0.13 and 0.3 mm).

Treece and Jirsa (1989), in studying the influence of epoxy coating on the bond strength, also noted that the width and spacing of cracks were significantly increased when the bars were coated with epoxy. They also concluded that the cracking load and deflections were not significantly affected by the presence of epoxy coatings.

Further experimental investigations are needed to quantify the influence of epoxy coatings on the cracking behaviour and stiffness of a variety of structural members.

1.2.4 Influence of Fibre-Reinforced Concrete

The concept of using fibres to improve the characteristics of mortar dates back to Roman times. The principal reason for incorporating fibres into a cement matrix is to increase the toughness and tensile strength, and improve the cracking and deformation characteristics of the composite. For many applications, this same objective can also be accomplished using conventional steel reinforcing bars or wires. Research performed by Romualdi and Batson (1963) and Romualdi and Mandel (1964) in the late 1950's and early 1960's represented the first significant steps towards the development of steel fibre reinforced concrete (SFRC) technology. Although patents have been granted since the turn of the century for various methods of reinforcing concrete with steel, the development of SFRC technology did not begin to progress much until the late 1950's. A summary of research in this area has been reported by PCA (1991).

The addition of fibres to concrete makes it more homogeneous and isotropic and can significantly improve the tensile strength and ductility. When concrete cracks, the randomly oriented fibres arrest the microcracking mechanism and limit crack propagation, thus significantly improving the tensile strength and ductility. Also, the addition of fibres has been found to improve the bond-slip behaviour between concrete and reinforcing bars under both monotonic loading and cyclic loading, particularly once cracking has occurred (Spencer *et al.* 1982; Ezeldin and Balaguru 1990).

The reported data concerning the effect of steel fibres on the tensile strength of cement composites vary considerably. It has been shown that the addition of 1.5% fibres by volume will increase direct tensile strength of mortar by about 40%. The increase in splitting tensile strength is somewhat higher, with reported increases of as much as 100% (ACI Committee 544 1984). Several investigators have reported compressive strength results for conventional SFRC ranging from a loss in strength to as much as a 40% increase (ACI Committee 544 1974). In general, with adequately consolidated specimens, the addition of steel fibres has little effect on compressive strength of conventional SFRC (fibre contents ranging from 0.5% to 2.0% by volume).

More research is required to investigate the use of fibres to overcome the brittleness of concrete subjected to tension, particularly high-strength concrete. A better understanding of crack control and tension stiffening in fibre-reinforced concrete is needed.

1.3 RESEARCH OBJECTIVES

The primary objectives of this research program are:

1) To study the bond characteristics of reinforcing bars and pretensioning strands. The experimental studies include the development of a new testing method to determine the bond stress versus slip response. Parameters to be investigated include the diameter of reinforcing bars and pretensioning strand and the presence of different epoxy coating thicknesses.

2) To predict the response of typical reinforcing bar pullout specimens and to predict the transfer and development length of pretensioned strand, using the bond stress versus slip relationships determined experimentally.

3) To study tension stiffening and cracking of reinforced concrete members subjected to pure tension. Different concretes including normal-strength, high-strength and steel fibre-reinforced concrete are investigated. The influence of reinforcing bar size and the presence of two different epoxy coating thicknesses are studied.

4) To study the influence of epoxy-coated reinforcement on the response of normal and high-strength concrete beams. Features investigated include the propagation of cracks, crack lengths, crack spacings, crack widths and failure mechanisms.

5) To investigate the responses of specimens representing typical slab-column connections used in parking garage structures. The influence of epoxy-coated reinforcement and concrete quality on cracking is investigated.

Chapter 2

DETERMINATION OF BASIC BOND CHARACTERISTICS FOR REINFORCED CONCRETE

"I commend the conference to all those concerned about and with the bond question, be it between concrete and its reinforcement or between peoples."

R.E. Rowe, President of CEB

Bond in Concrete, Riga, Latvia, 1992

Investigators have studied bond characteristics in reinforced concrete for nearly a century (Abrams 1913) and in pretensioned concrete for about 50 years (Hoyer 1939; Janney 1954). Experimental studies were typically carried out on simple pullout specimens or beam tests having a wide variety of specimen geometries, types of loading and restraints (CEB Task Group VI 1981; FIP 1982; ACI Committee 408 1991). The wide variation of test specimens and testing methods makes the comparison of the experimental results very difficult. Typical pullout specimens have nonuniform bond stress distributions along the reinforcing bars and hence can only be used to determine the average bond strength. Due to the absence of a standard test method capable of determining the bond stress versus slip relationship, it is not possible to perform detailed analyses, such as finite element modelling, of the bond interaction for a variety loading situations (Keuser and Mehlhorn 1987).

It is clear that there is a need to develop a more rational approach for understanding bond behaviour. The objectives of the research reported in this chapter are:

1) To develop new testing methods for determining the bond characteristics of both reinforcing bars and pretensioned strand.

2) To simulate a more uniform bond stress distribution along reinforcing bars.

3) To study both splitting and pullout types of failure.

4) To study bond behaviour of pretensioned strand in a very direct manner, from measured forces in the strand.

5) To investigate bond behaviour of pretensioned strand along both the transfer length and the flexural bond length.

2.1 BOND CHARACTERISTICS OF REINFORCING BARS IN CONCRETE

The transfer of forces across the interface between concrete and steel reinforcing bars is of fundamental importance in reinforced concrete structures. Bond stress is the equivalent unit shear stress acting parallel to the reinforcing bar on the interface between the bar and the concrete. Due to the transfer of forces through bond stress, between the concrete and the bar, the force in the reinforcing bar changes along its length. Hence the bond stress is related to the rate of change of steel stress. Consequently, in order to have bond stress it is necessary to have a changing steel stress.

Forces are transferred from the reinforcing bar to the concrete primarily by inclined compressive forces radiating out from the bar. This force transfer mechanism was recognized by Abrams (1913) as shown in Fig. 2.1. The actual bond distribution would not be uniform for this case.

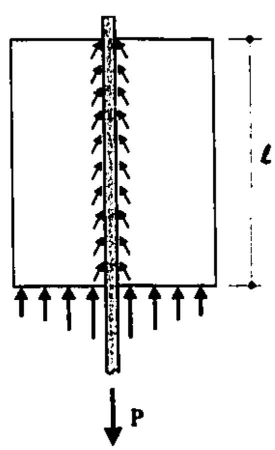

Figure 2.1: Pullout specimen and force transfer mechanism adapted from Abrams (1913)

The radial components of these inclined compressive forces are balanced by circumferential tensile stresses in the concrete surrounding the bar (see Fig. 2.2). The ability of a deformed bar to transfer its load into the surrounding concrete is typically limited by the failure of this ring of tension when the thinnest part of the ring splits (splitting failure) as shown in Fig. 2.3. However, if a relatively small diameter bar is embedded in a large block of concrete the bar might pullout of the concrete (pullout failure) due to concrete shear failure over a cylindrical surface at the extremities of the bar deformations (see Fig. 2.4).

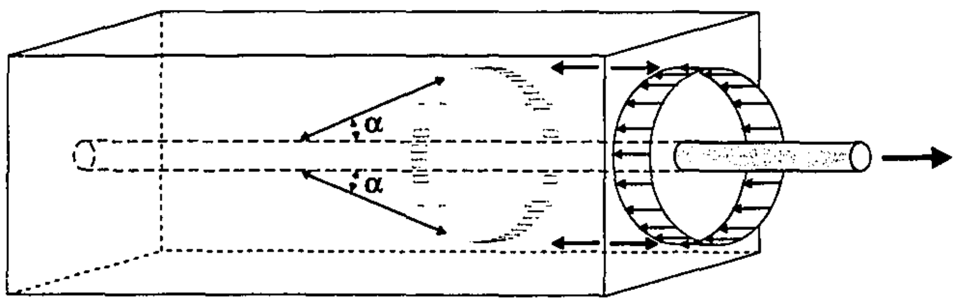

Figure 2.2: Tensile stress rings from Tepfers (1973)

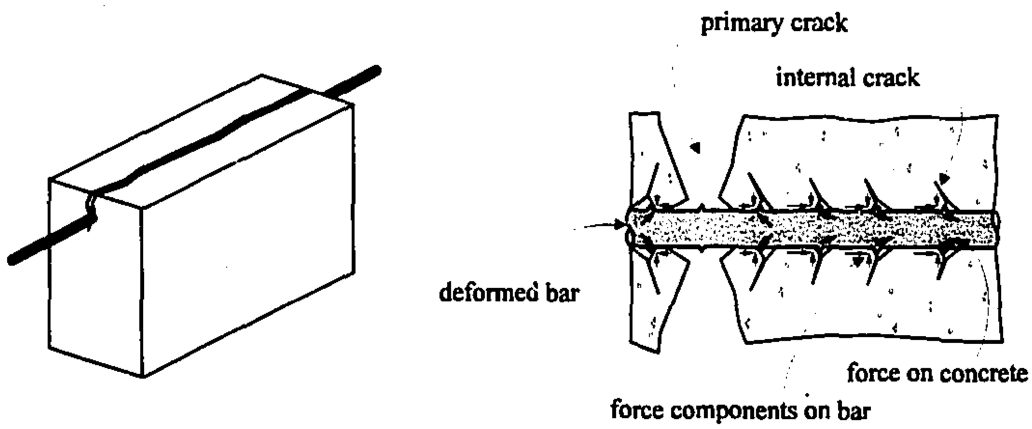

(a) Splitting failure

(b) Internal cracking

Figure 2.3: Splitting failure and internal cracking adapted from Goto (1971)

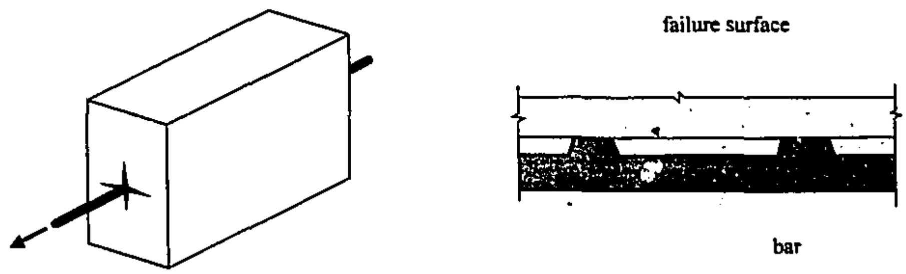

(a) Pullout failure (b) Pullout failure surface

Figure 2.4: Pullout failure and close-up of failure surface

Different methods of testing have been used to determine the bond characteristics of reinforcing bars embedded in concrete. Bond tests can be classified into two groups; pullout tests; and bond-beam tests. Figure 2.5 shows some different variations of pullout specimens while Fig. 2.6 shows the three different types of bond-beam specimens. The standard pullout test (ASTM 1988) is widely used for comparing relative bond strengths and provides a very simple means of testing. The deficiencies of this test are that it produces high bond stress concentrations, results in lateral restraint at the base of the concrete cylinder and introduces compressive stresses along the axis of the cylinder. The aspects of nonuniform bond stress in this test are discussed below. Several variations of the eccentric pullout test (Fig. 2.5b) have been used to study the mechanics of bond and slip under conditions representing more closely that of bars in flexural members (Lutz *et al.* 1966). A modified pullout test method (see Fig. 2.5c) was developed by Hajnal-Kónyi (1957) to determine pullout strengths of reinforcing bars embedded in concrete that is subjected to tensile stresses. Although this test method produces tensile stresses in the concrete, these tensile stresses are not uniform and the bond stresses are not uniform. Many investigators (Broms 1963; Falkner 1969; Wilhelm *et al.* 1971; Mirza and Houde 1979) have studied the bond characteristics in the transfer length and crack development using tension specimens as illustrated in Fig. 2.5d. While these tests provide information on the bond stress variations over the transfer lengths, which is useful in studying crack spacing, crack widths and tension stiffening, the tests do not provide information on the bond strength. To study the influence of splitting cracks, Tepfers (1973) developed the ring test shown in Fig. 2.5e. Although this test has some of the same deficiencies as the standard pullout test, it has a shorter embedment length and is useful in making comparative studies of the effects of cover and bar size on bond splitting cracks. Figure 2.5f illustrates a variation of the pullout test (Losberg and Olsson 1979), having an extremely short embedment length. The short embedment length was used in an attempt to produce more uniform bond stresses. This method of testing results in a pullout type of failure which gives unrealistically high bond strengths due to the very short embedment length and due to the confinement over the embedment length which precludes splitting failures.

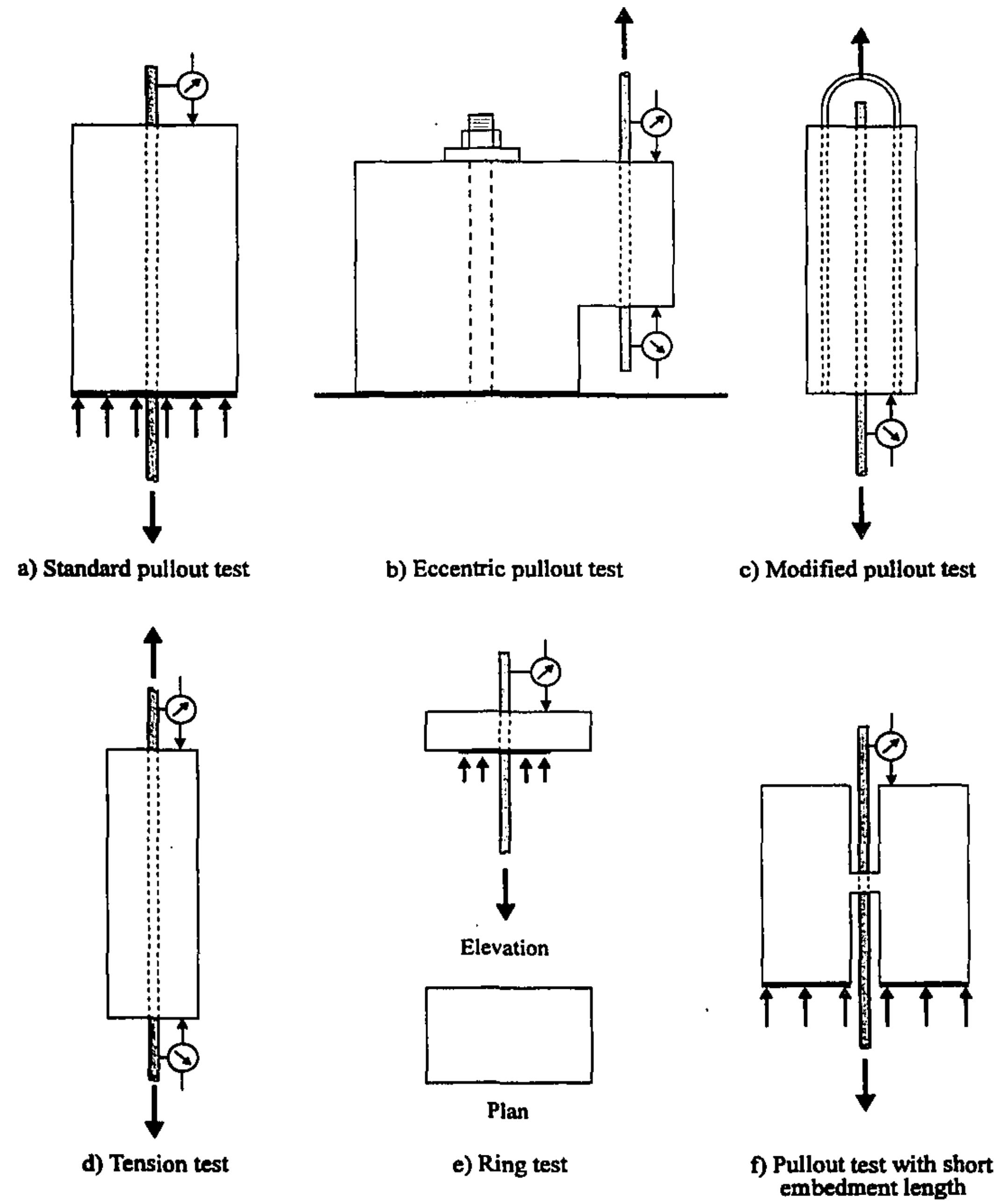

Figure 2.5: Simple bond test methods

Figure 2.6a shows the test beam recommended by ACI Committee 208 (1945) for determining bond strength. One advantage of this beam is that the concrete is in tension rather than compression while the disadvantage of this bond beam specimen is that due to high bearing stresses at the supports the resulting bond strengths are too high for certain practical situations. The hammerhead beam specimen was developed in response to some of the criticism of the ACI 208 bond beam (Mathey and Watstein 1961).

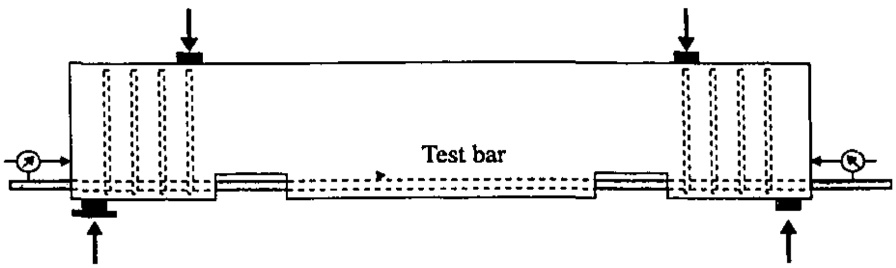

a) Bond-test beam recommended by ACI Committee 208 (1945)

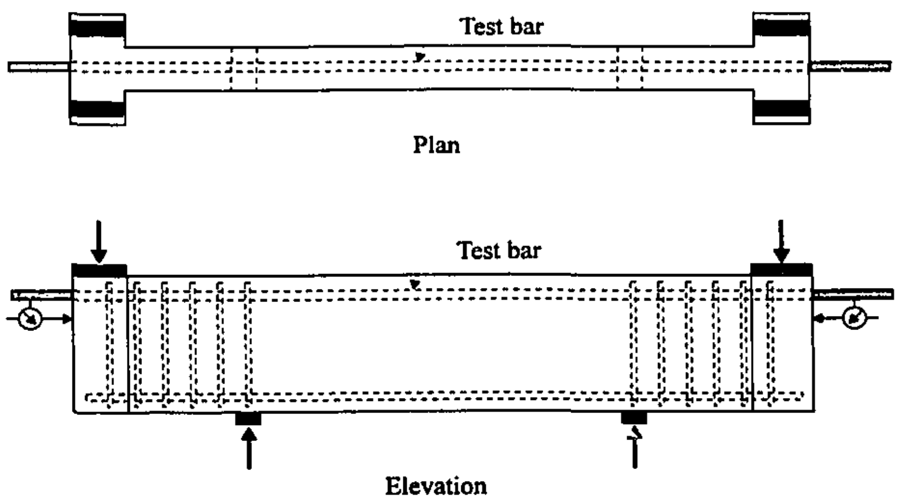

b) Bond-test beam recommended by ACI Committee 408 (1964)

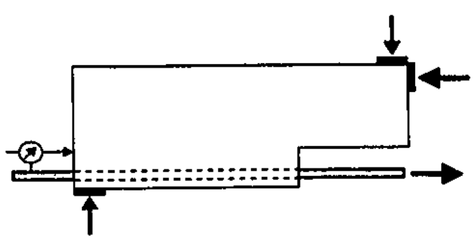

c) Beam-end test adapted from Wilhelm et al. (1971)

Figure 2.6: Different types of beam tests to study bond

Figure 2.6b shows the details of this beam specimen which was revised by ACI Committee 408 in 1964. The indirect loading method eliminated much of the concern about the confinement due to concentrated loads close to the test area. The desire to have a smaller, simpler test setup led to the development of smaller beam-end specimens or stub cantilever specimens as shown in Fig. 2.6c (Mirza and Hsu 1969; Wilhelm *et al.* 1971).

One similarity of all of the test methods shown in Fig. 2.5 and 2.6 is that the reinforcing bar is loaded at one end and in most of the tests the relative bar slip is measured at the unloaded end only. Non-uniform bond stresses result when only one end of the bar is loaded. Another disadvantage of these tests is that they typically can only be used to study one type of bond failure, either pullout or splitting.

The distribution of steel stress and bond stress in a typical pullout test is illustrated in Fig. 2.7. The steel stresses are measured using electrical strain gauges either on the surface of the bar or installed in specially grooved bars so as not to affect the bond surface (Mirza and Houde 1979). The bond stresses are calculated from the rate of change of the steel stresses.

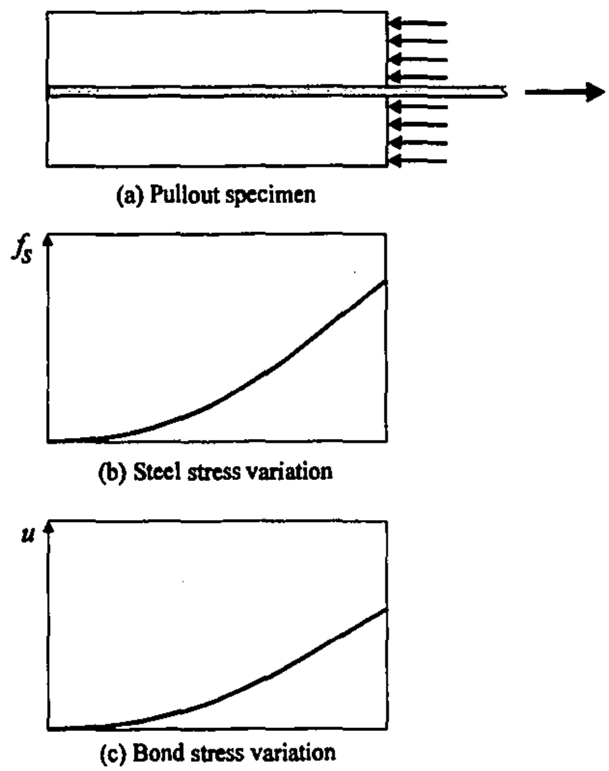

Figure 2.7: Distribution of steel stresses and bond stresses along embedment length of pullout specimen

As has been found by many researchers (CEB 1981; Yankelevsky 1985; Yerex *et al.* 1985) the bond stress distribution in this type of test is not uniform. Several researchers (Losberg and Olsson 1979) have performed pullout tests on very short embedment lengths in an attempt to simulate more closely "uniform" bond stress (see Fig. 2.8). Concern has been expressed that these very short embedment lengths give extremely high bond strengths which may not be realistic (Berggren 1965) and may give results with considerable variability (Bažant and Şener 1988).

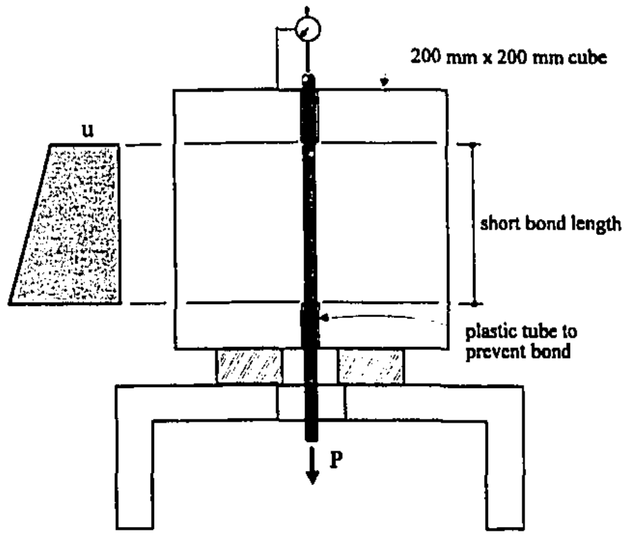

Figure 2.8: Pullout test on very short embedment length, adapted from Losberg and Olsson (1979)

2.1.1 Testing Technique for Simulating Uniform Bond Stress

Figure 2.9 illustrates the equilibrium conditions for a portion of a reinforcing bar of length, dx . The bond stress, u , can be expressed as the change in the stress in the reinforcement over the length, dx as follows:

$$u\ (\pi\ d_b\ dx) = A_s\ (\ f_s + df_s\ ) - A_s f_s \tag{2.1}$$

or

$$u = \frac{d_b}{4} \cdot \frac{df_s}{dx} \tag{2.2}$$

where d_b and A_s are the diameter and area of the reinforcing bar and f_s is the stress in the reinforcement.

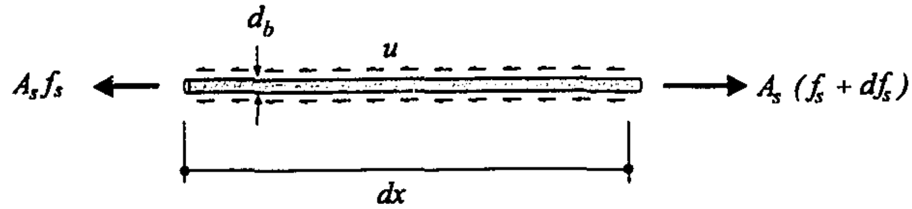

Figure 2.9: Bond stresses acting on reinforcing bar

Equation 2.2 demonstrates that the bond stress is proportional to the rate of change of the stress in the reinforcement, df_s / dx . Hence, if the stress in the reinforcement varies linearly, then the bond stress must be uniform.

Figure 2.10 illustrates the technique developed in this research program (Abrishami and Mitchell 1992a and 1992b) to simulate a more uniform bond stress and to determine the complete bond stress versus slip relationship. This procedure is described below:

Step 1 - A reinforcing bar, instrumented with strain gauges, is tensioned to an initial force level, P_o in a loading frame, as shown in Fig. 2.10(a) and Fig. 2.11(a).

Step 2 - Concrete is cast around this tensioned bar (see Fig. 2.10(b) and Fig. 2.11(b)) and cured in order to achieve the desired concrete properties before testing.

Step 3 - In order to create a small bond stress, the tension in the reinforcing bar at the bottom of the specimen is increased by a small force, ΔP_b , while the tension in the reinforcing bar at the top is reduced by ΔP_t (see Fig. 2.10(d)), so as to produce a linear variation in the strains measured on the reinforcing bar. The linear variation in strains results in a linear variation of stress in the reinforcing bar (see Fig. 2.10(e)) and hence produces uniformly distributed bond stress as shown in Fig. 2.10(f). The bond stress is given by:

$$u = \frac{P_b - P_t}{\pi \, d_b \, \ell} \qquad \textbf{(2.3)}$$

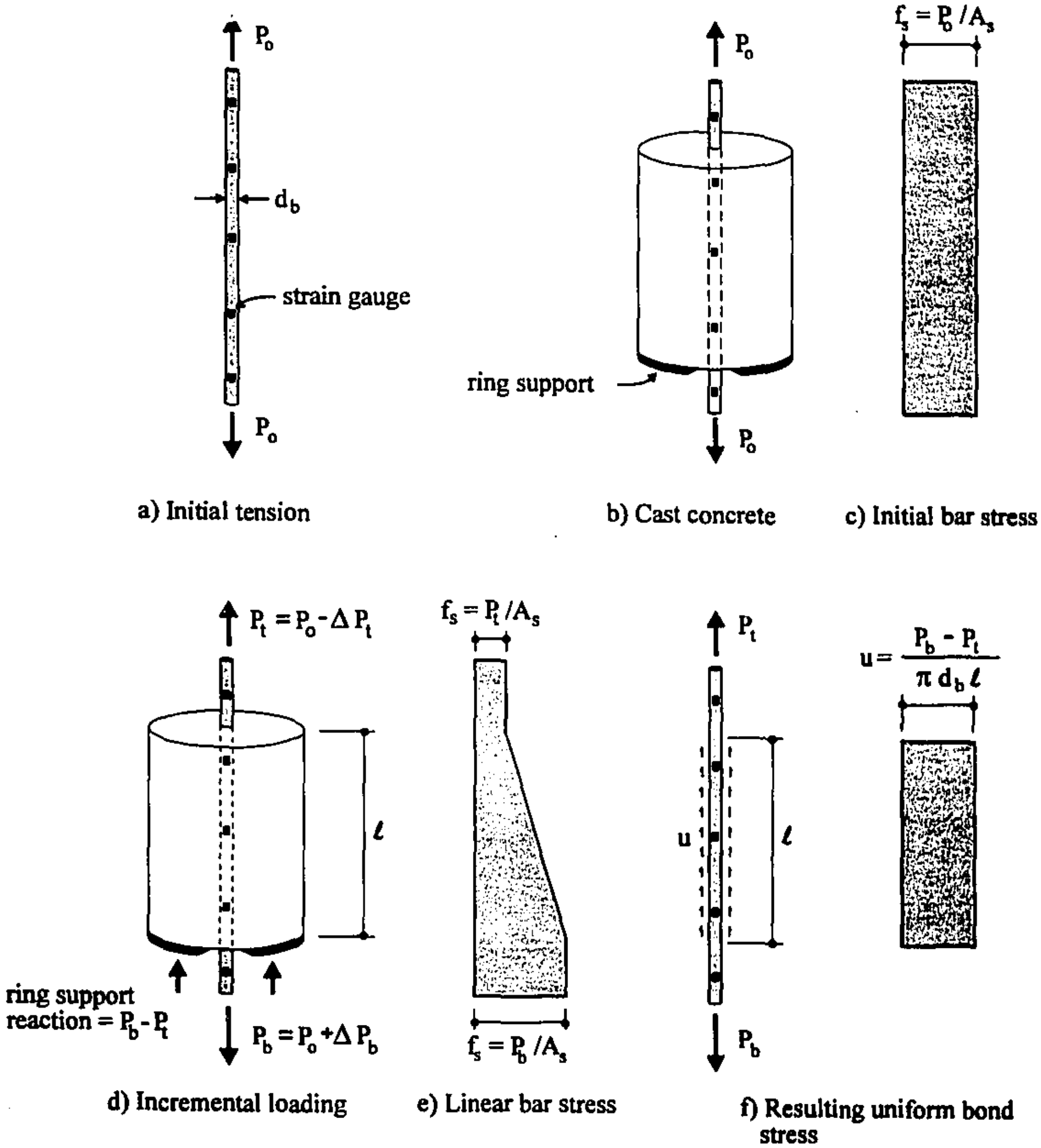

Figure 2.10: Testing technique for simulating uniform bond stress

where P_b and P_t are the bottom and top forces in the reinforcing bar, respectively and ℓ is the embedment length. The changes in tension in the reinforcing bar, both above and below the concrete cylinder, are equilibrated by a compressive reaction at the bottom of the cylinder as shown in Fig. 2.10(d).

Step 4 - Steps 3 is repeated for each increment of loading.

Step 5 - For each increment of loading the relative slips between the concrete and the steel at the top and bottom of the test specimen are measured. The complete response of a specimen is obtained by plotting the bond stress versus the average of the slips measured at the top and the bottom for each load increment.

Figure 2.11(a) shows the test set-up after tensioning the reinforcing bar and before casting the concrete while Fig. 2.11(b) shows the set-up during loading. The load is applied through threaded screws at the top and the bottom and the loads are recorded by load cells at these locations. This method of loading permits performing the experiment under strain control, rather than load control, enabling the post-peak response to be determined. Because of the initial tensioning of the bar, the bar remains in tension during the testing, which helps to keep the applied loading aligned with the bar axis.

This test method has a number of parameters which affect the bond stress distribution. The boundary conditions at the top and bottom of the specimen are different. Due to the bearing stresses at the bottom of specimen, higher but very localized bond stress is expected. Also releasing the load at the top of the reinforcing bar causes slight lateral expansion (Hoyer effect) while increasing the load at the bottom of the specimen reduces the bar diameter which may affect the bond stress distribution. The purpose of this testing technique is to simulate a more uniform bond stress than the other methods of testing such as the pullout tests illustrated in Fig. 2.5.

2.1.2 Test Program

In the test series used to verify the testing procedure a concrete mix was designed to give a concrete compressive strength of 25 MPa at the time of testing (age of about 5 days) and to give a 35 MPa compressive strength at 28 days. The three sizes of concrete specimens tested were 150 mm diameter by 300 mm long, 200 mm diameter by 300 mm long and 200 mm diameter by 100 mm long cylinders.

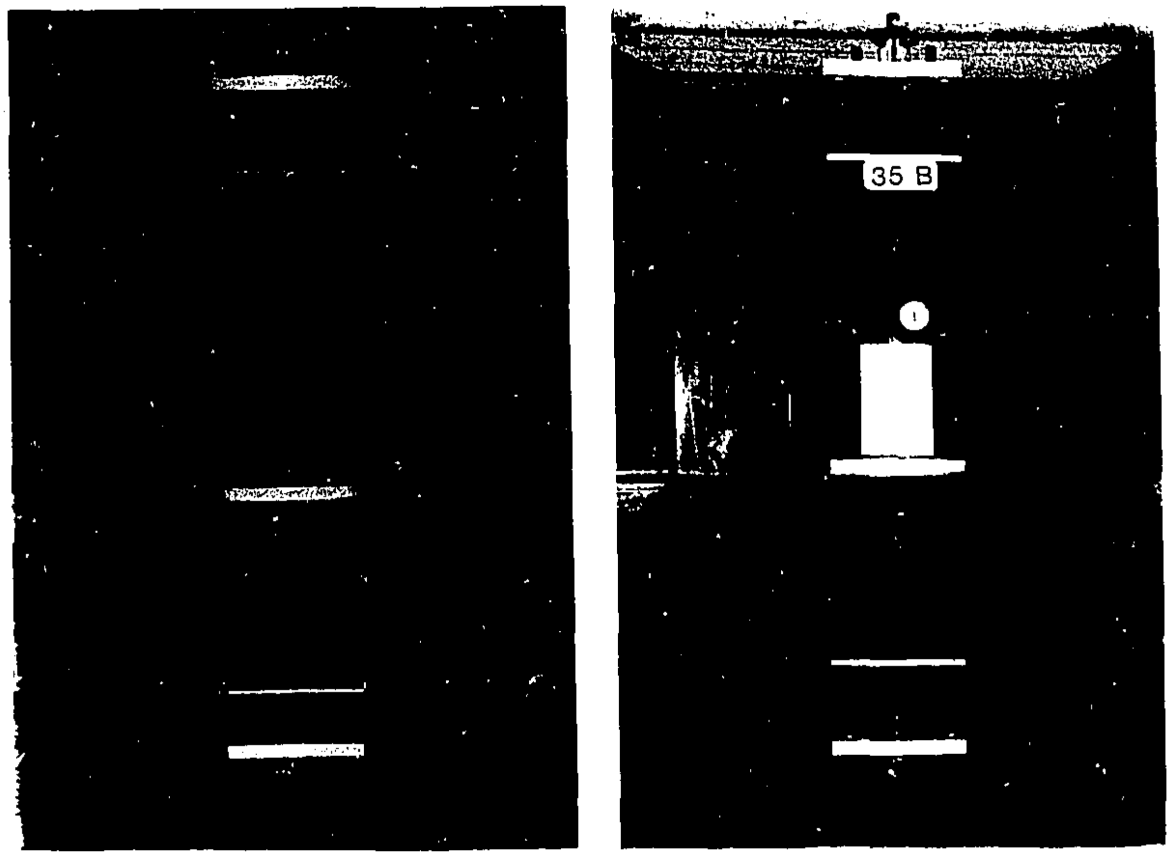

(a) Bar after tensioning and before casting the concrete

(b) Specimen under load

Figure 2.11: Test setup and loading frame

The reinforcing bar sizes used were No. 15, No. 20, No. 25, No. 30 and No. 35 bars, all having a specified yield stress of 400 MPa. Table 2.1 presents the details of the specimens tested including the concrete strengths for each specimen. The reinforcing bars were instrumented with five strain gauges, two outside of the concrete and three along the embedment length. Strain gauges having a 6 mm gauge length were glued to the surface of the reinforcing bars. These small gauges were used in order to minimize the reduction of bond surface area due to the presence of the gauges (less than a 1% reduction in bar surface area).

Table 2.1: Summary of results of tests simulating uniform bond stress

Specimen	Cylinder dia. x length (mm x mm)	d_b (mm)	f_c' (MPa)	failure mode	Bond strength (MPa)	Slip at max. bond stress (mm)
35A	150 x 300	35.7	25.5	S	3.0	0.36
35B	200 x 300	35.7	25.0	S	3.6	0.21
30A	150 x 300	29.9	26.0	P	5.5	0.55
30B	200 x 300	29.9	22.0	S	4.0	0.31
25A	150 x 300	25.2	28.0	P	8.5	0.60
25B	200 x 300	25.2	25.1	S	3.6	0.31
20A	150 x 300	19.5	25.5	S	4.2	0.36
20B	200 x 300	19.5	25.0	S	5.6	0.35
15C	200 x 100	16.0	22.3	S	5.3	0.16

S = splitting failure, specimen tested with greased split-ring support
P = pullout failure, specimen tested with ring support

2.1.3 Test Results

As observed by other researchers, there were two distinct modes of bond failure; splitting and pullout failures. Figure 2.12 illustrates the complete behavioural response of a typical specimen failing by splitting of the concrete surrounding the bar. The uniform bond stress versus average slip response is shown schematically in Fig. 2.12(a). The relationship between bond stress and slip, before reaching the peak stress is nearly linear. For small values of bond stress (point **A** in Fig. 2.12(a)), the bottom slip is much greater than the top slip (see point **A** in Fig. 2.12(c)). The bond stress is computed from the difference between the top and bottom bar forces. As the peak bond stress is approached, the measured slip at the top becomes close to the measured bottom slip.

The peak bond stress occurs at point **B** (see Fig. 2.12(c)) when the difference between the bottom and top forces is a maximum (see point **B** in Fig. 2.12(a)). At the peak bond stress, vertical splitting cracks were evident on the surface of the concrete starting at the bottom of the test specimen. Figure 2.12(d) illustrates a typical variation of strains in the reinforcing bar over the embedment length. Between points **B** and **C** in Fig. 2.12(a), the splitting crack extends vertically over the entire embedment length (see Fig. 2.13). Due to the post-peak reduction in bond stress, the difference between the bottom and top forces reduces (see point **C** in Fig. 2.12(b)). By continued testing it can be shown that for a splitting type of failure mechanism there is still considerable bond stress beyond point **C**. At point **D**, the bottom and top slips are equal as shown in Fig. 2.12(b) resulting in an almost constant residual bond strength (see Fig. 2.12(c)). This residual bond strength is due to the ability of the concrete to transmit local forces across the rough crack interfaces even though the splitting crack has extended along the entire specimen length (see Fig. 2.13).

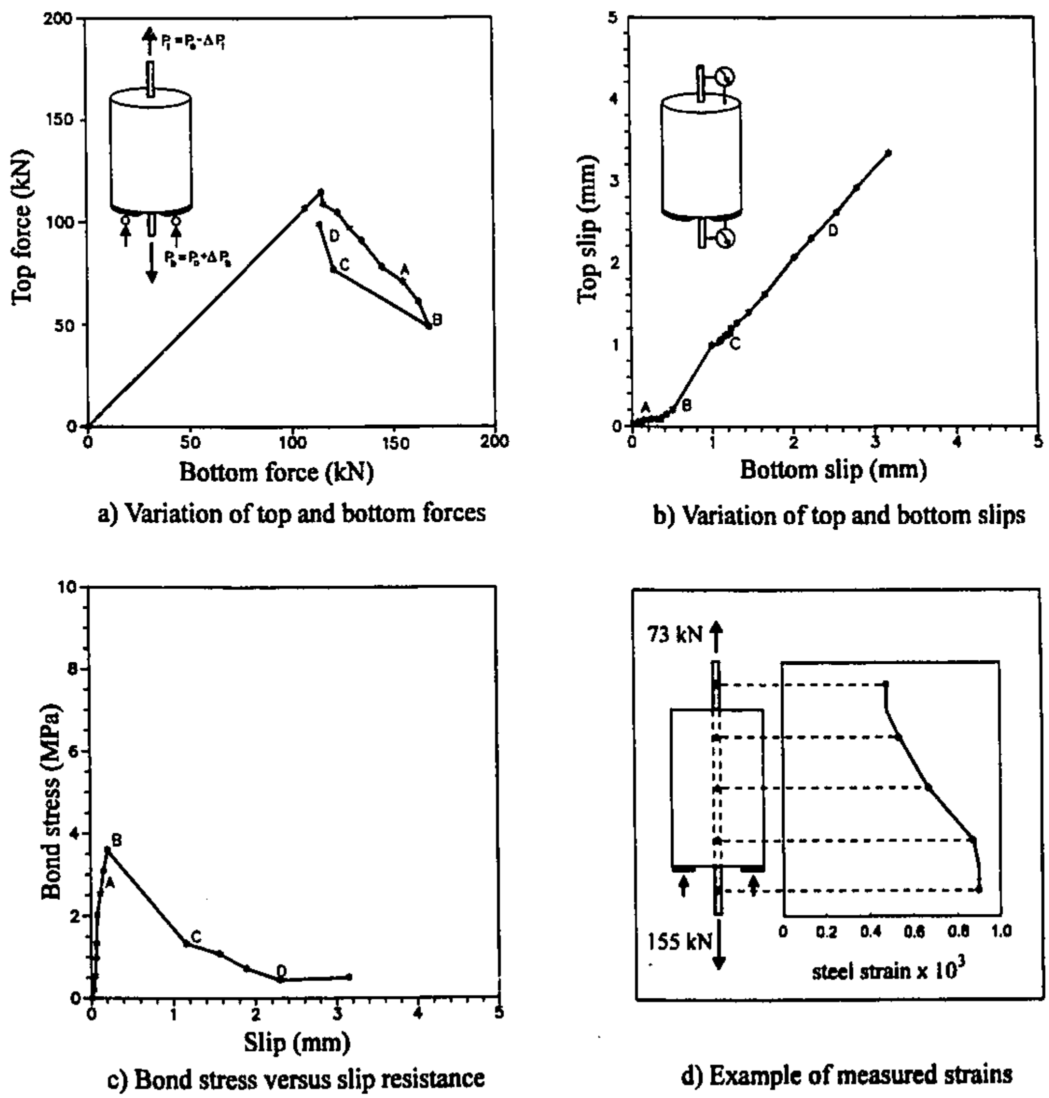

Figure 2.12: Measured response of specimen failing by splitting, Specimen 35B

Figure 2.14 shows the experimentally determined relationships between bond stress and average slip for specimens having No. 20 and No. 35 reinforcing bars. Both specimens had about the same concrete strength and failed by splitting. It should be noted that in order to produce splitting failures an attempt was made to reduce, as much as possible, the friction due to the compressive reaction at the base of the concrete cylinder. This was accomplished by using a greased split ring at the support. The split ring had a 110 mm diameter central hole and an outer diameter equal to the diameter of the cylinder being tested. It is clear from Fig. 2.14 that the specimen with the smaller bar has greater bond strength than the specimen with the larger diameter bar. It was found that the values of slip at the peak bond stress were similar. The results of these tests follow very closely with the behavioral description given above for splitting failures. Figure 2.15 illustrates the influence of concrete clear cover on the response of two specimens having the same bar size. As expected, the bond strength (i.e., the maximum bond stress) and initial stiffness increase as the amount of concrete surrounding the bar increases. Figure 2.16 shows the rough crack interface, after testing, for Specimen 35A that exhibited a splitting failure.

Figure 2.17 illustrates the difference between the response of a specimen (25B) exhibiting a splitting type of failure with that of a specimen (25A) failing by pullout. In order to obtain pullout failures, the reaction ring at the base of the cylinder was not split and was not greased in order to prevent splitting cracks from initiating at the cylinder base (see Fig. 2.17). The two specimens have the same bar size but have different concrete covers. It is interesting to note that the initial stiffnesses are about the same. The maximum bond stress reached in the specimen with the pullout failure exceeds that of the specimen failing by splitting. For this case of uniformly distributed bond stress, the pull-out failure is very brittle compared to the splitting failure.

Figure 2.18 shows a close-up of a specimen which failed by pullout. The splitting crack formed at the peak bond stress. Failure took place by shearing of the concrete along a cylindrical surface at the extremities of the bar deformations as illustrated in Fig. 2.4(b). The photograph also illustrates the uniform nature of this local shearing failure achieved with this new testing technique.

Figure 2.19 compares the response of two specimens having No. 25 and No. 30 reinforcing bars that failed by pullout. The smaller bar exhibits a greater initial stiffness as well as greater bond strength.

The experimental results for these investigations are summarized in Table 2.1.

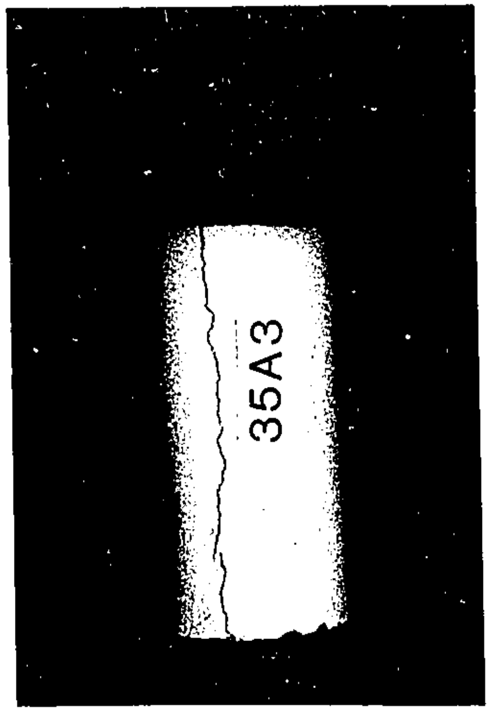

Figure 2.13: Splitting crack in Specimen 35A

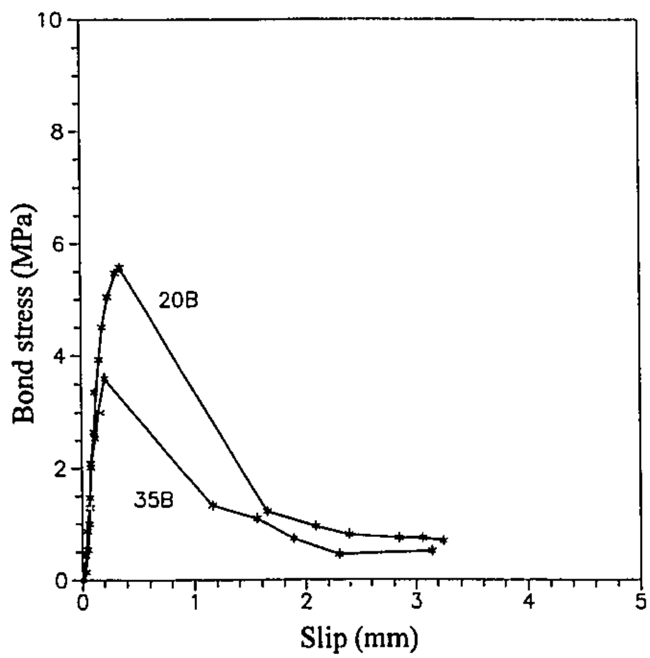

Figure 2.14: Influence of bar size on the bond stress versus slip response

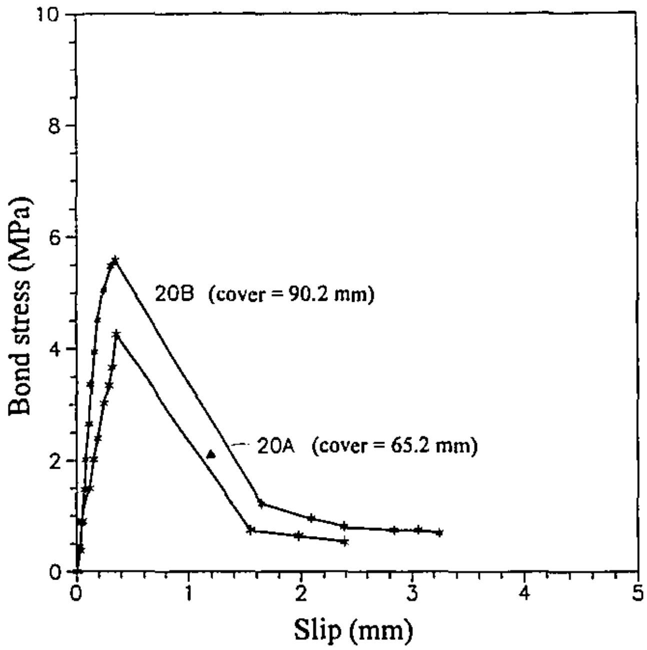

Figure 2.15: Influence of concrete cover on the bond stress versus slip response

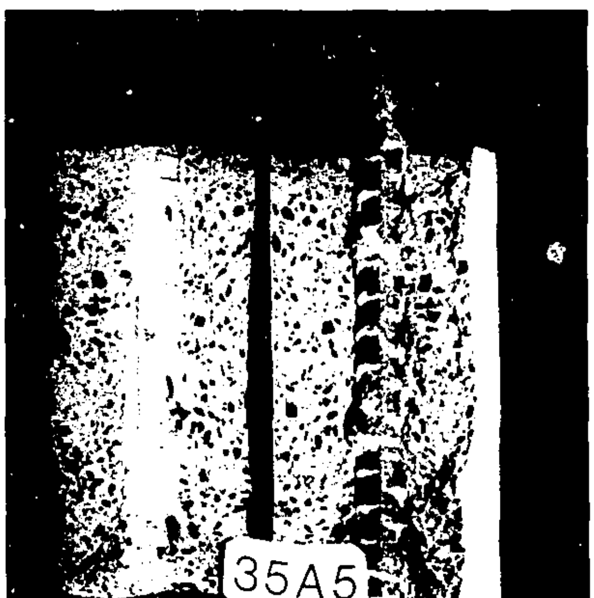

Figure 2.16: Rough crack interface due to splitting failure in Specimen 35A

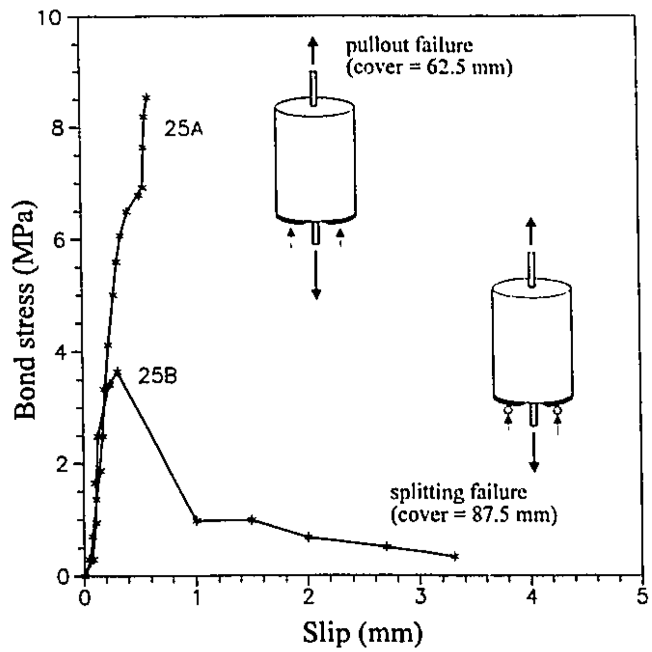

Figure 2.17: Comparison of bond stress versus slip responses for splitting and pullout failures

Figure 2.18: Close-up of pullout failure surface around bar in Specimen 25A

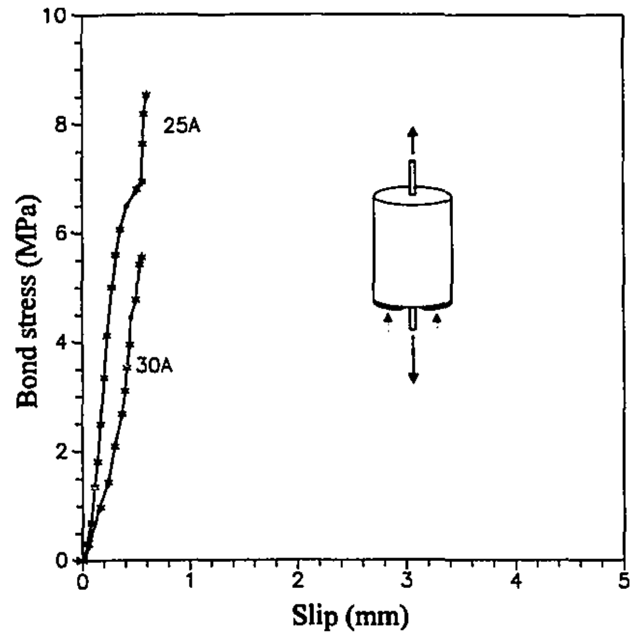

Figure 2.19: Influence of bar size on the bond stress versus slip response for specimens failing by pullout

2.2 BOND CHARACTERISTICS OF PRETENSIONED STRAND

Pretensioned members rely on the bond between the pretensioning steel (usually strand) and the concrete, both to apply prestress to the concrete and to develop additional stress in the pretensioning steel. The length of strand at the ends of a pretensioned member, over which the stress in the steel builds-up, is called the transfer length. The flexural bond length is the additional length required beyond the transfer length in order to develop the stress associated with the superimposed loading.

Upon tensioning of the strand in the pretensioning bed the diameter of the strand is reduced due to Poisson's effect. After the concrete reaches sufficient strength, the strands are released from the abutment of the pretensioning bed, and at the free ends of the beams the stress in the strands returns to zero. With this reduction of steel stress along the transfer length, the diameter of the strand expands and wedges against the surrounding concrete. This wedging action caused by the lateral expansion, called the Hoyer effect (Hoyer 1939), results in improved bond performance over the transfer length.

Janney (1954) was one of the pioneers to research the physical characteristics of bond between pretensioned strand and concrete and its relationship to the transfer and development lengths. Janney concluded that the following three factors contribute to bond between the prestressing steel and the surrounding concrete:

1) Adhesion on the concrete and steel interface;
2) Friction between the concrete and steel; and
3) Mechanical resistance due to interlocking of the spiral twisting of the outer wires forming the strand.

Although there are several methods of measuring bond, as described by Weerasekera (1991), experimental investigations to determine the transfer and flexural bond lengths rely on measurements of the concrete surface strain or the steel strain along the strand. Figure 2.20 shows the determination of the transfer length obtained by measuring the variation of the concrete surface strains near the ends of a beam.

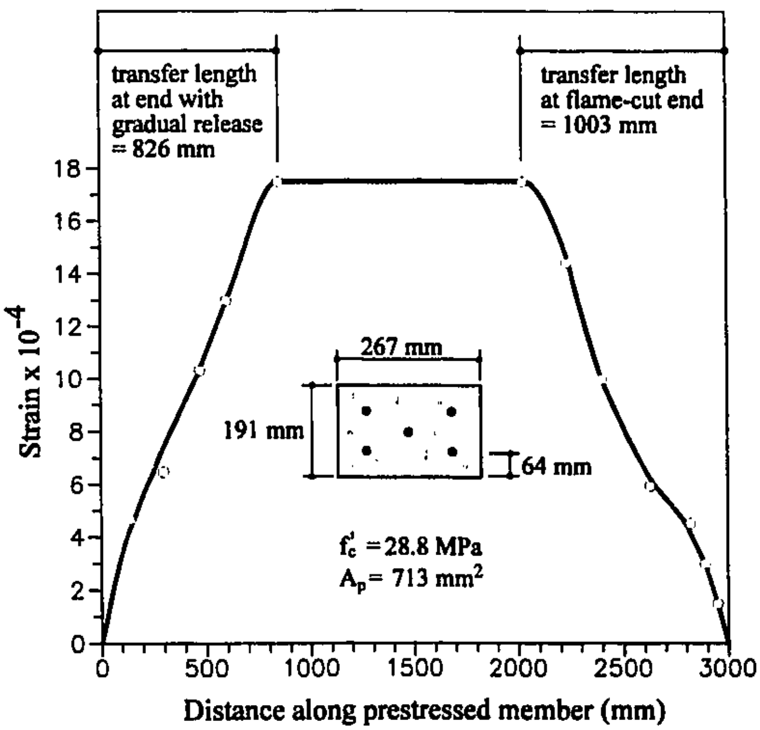

Figure 2.20: Determination of transfer length by measuring concrete surface strain, adapted from Kaar *et al.* (1963)

The transfer length is assumed to be the length required to produce a constant compressive strain at the concrete surface. Figure 2.21 shows the development of strain in the strands of simply supported pretensioned beams subjected to single-point loading at midspan (Mitchell *et al.* 1993).

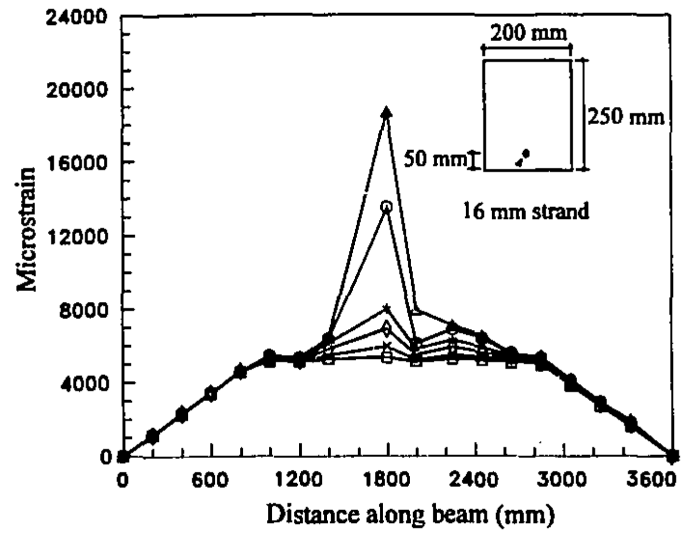

Figure 2.21: Measured strand strains in pretensioned beam for increasing point load at midspan, adapted from Mitchell *et al.* (1993)

2.2.1 Simulation of the Transfer Length and the Flexural Bond Length

In a pretensioned concrete member there are two distinct regions having different bond characteristics; the transfer length region and the flexural bond length region. Figure 2.22 shows the variation of the stress in the pretensioned strand after release. The stress in the strand varies linearly from zero, at the end of the beam to a maximum at the end of the transfer length, ℓ_t (see Fig. 2.22(b)). Figure 2.22(c) shows the pretensioning forces acting on a segment of the beam along the transfer length. In order to simulate the bond action in this region the strand tension is reduced on one side of the segment relative to the other side.

Figure 2.23 shows the same beam subjected to external loading. The variation of the stress in the strand in Fig. 2.23(b) indicates the two different bond phenomena over the transfer and flexural bond lengths. The external loading results in increased strand stresses along the beam. Figure 2.23(c) shows the prestressing forces acting on a segment of the beam along the flexural bond length. In order to simulate the bond action in this region the strand tension is increased on one side of the segment relative to the other side.

It must be recognized that, due to release, the pretensioning force in the strand reduces towards the end of the beam along the transfer length, while due to the external loads the force in the strand increases towards the critical section. In order to simulate these different phenomenon, two testing techniques were developed. These testing methods are described below.

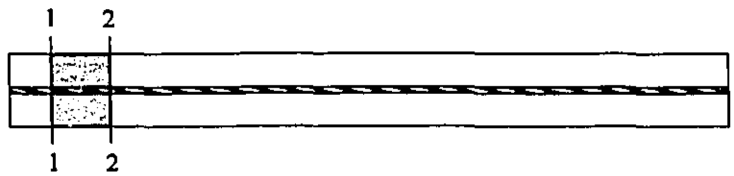

(a) Pretensioned beam after release

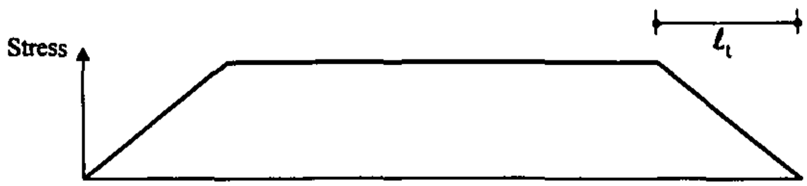

(b) Idealized variation of stress in strand after release

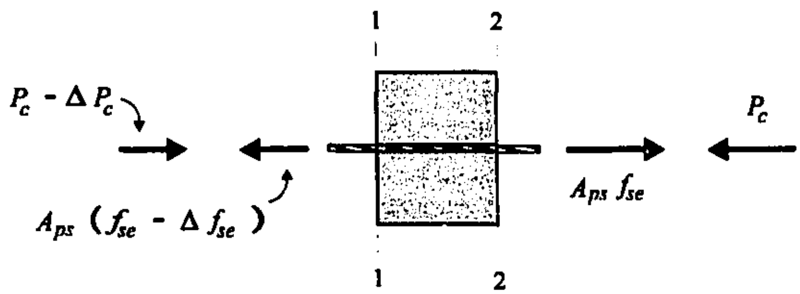

(c) Forces on strand and concrete along transfer length

Figure 2.22: Idealized variation of strand stress along pretensioned beam after release

2.2.2 Testing Technique for Simulating Transfer and Flexural Bond Stresses

Figure 2.24 illustrates the technique developed (Abrishami and Mitchell 1992b and 1993) to study bond characteristics of pretensioned strand along the transfer length. This procedure simulates the applied forces on the strand as described below:

Step 1 - Seven-wire strand, is tensioned to an initial force level, P_o , in a loading frame, as shown in Fig. 2.24(a) and in Fig. 2.26(a).

Step 2 - Concrete is cast around this tensioned strand (see Fig. 2.24(b) and Fig. 2.26(b)) and cured in order to achieve the desired concrete properties before testing.

Step 3 - In order to create a small bond stress the tension in the strand at the top is reduced by a small force, ΔP_t (see Fig. 2.24(c)).

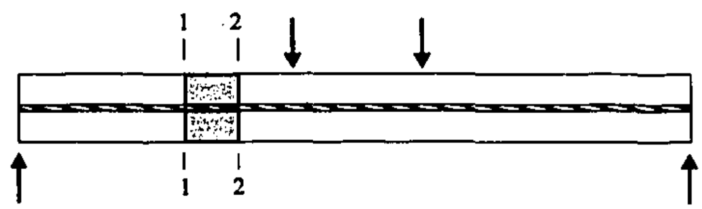

(a) Pretensioned beam under load

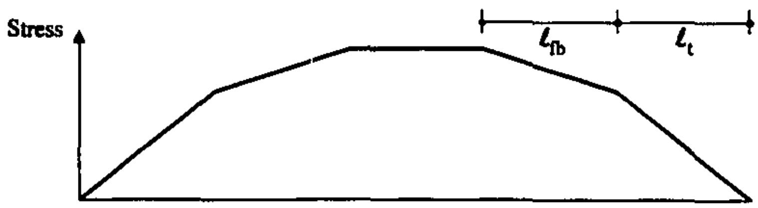

(b) Idealized variation of stress in strand

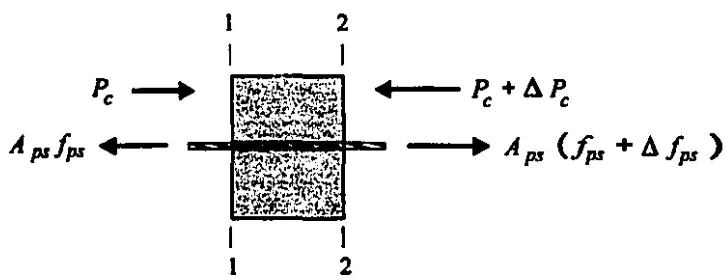

(c) Longitudinal forces on strand and concrete along flexural bond length

Figure 2.23: Idealized variation of strand stress along pretensioned beam subjected to external loading

At this stage the bond stress is given by:

$$u = \frac{P_b - P_t}{\pi \, d_b \, \ell} \tag{2.4}$$

where P_b is the force in the strand at the bottom of the specimen (approximately equal to P_o , the initial force), P_t is the top force in the strand, and ℓ is the embedment length. The difference in strand tension at the top and bottom of the concrete cylinder are equilibrated by a compressive reaction at the bottom of the cylinder as shown in Fig. 2.24(c).

Step 4 - Step 3 is repeated for increments in loading reduction at the top of the specimen.

Step 5 - For each increment of loading the relative slips between the concrete and the steel at the top and bottom of the test specimen are measured. The complete response of a specimen is obtained by plotting the bond stress versus the average of the slips measured at the top and the bottom for each load increment.

In order to study the bond characteristics of strand along the flexural bond length the steps described above are used, except for Step 3. In Step 3 the top tension is not reduced, but instead, the tension in the strand at the bottom of the specimen is increased by a small force ΔP_b and the top and bottom slips are measured (see Fig. 2.25(c)). At this stage the bond stress is given by:

$$u = \frac{P_b - P_t}{\pi \, d_b \, \ell} \tag{2.5}$$

This incremental load increase is repeated to determine the entire bond stress versus slip response. Figure 2.25 shows the steps for the testing method to study the bond behaviour along the flexural bond length. Figure 2.26(a) shows the test set-up after tensioning the strand and before casting the concrete while Fig. 2.26(b) shows the set-up during loading.

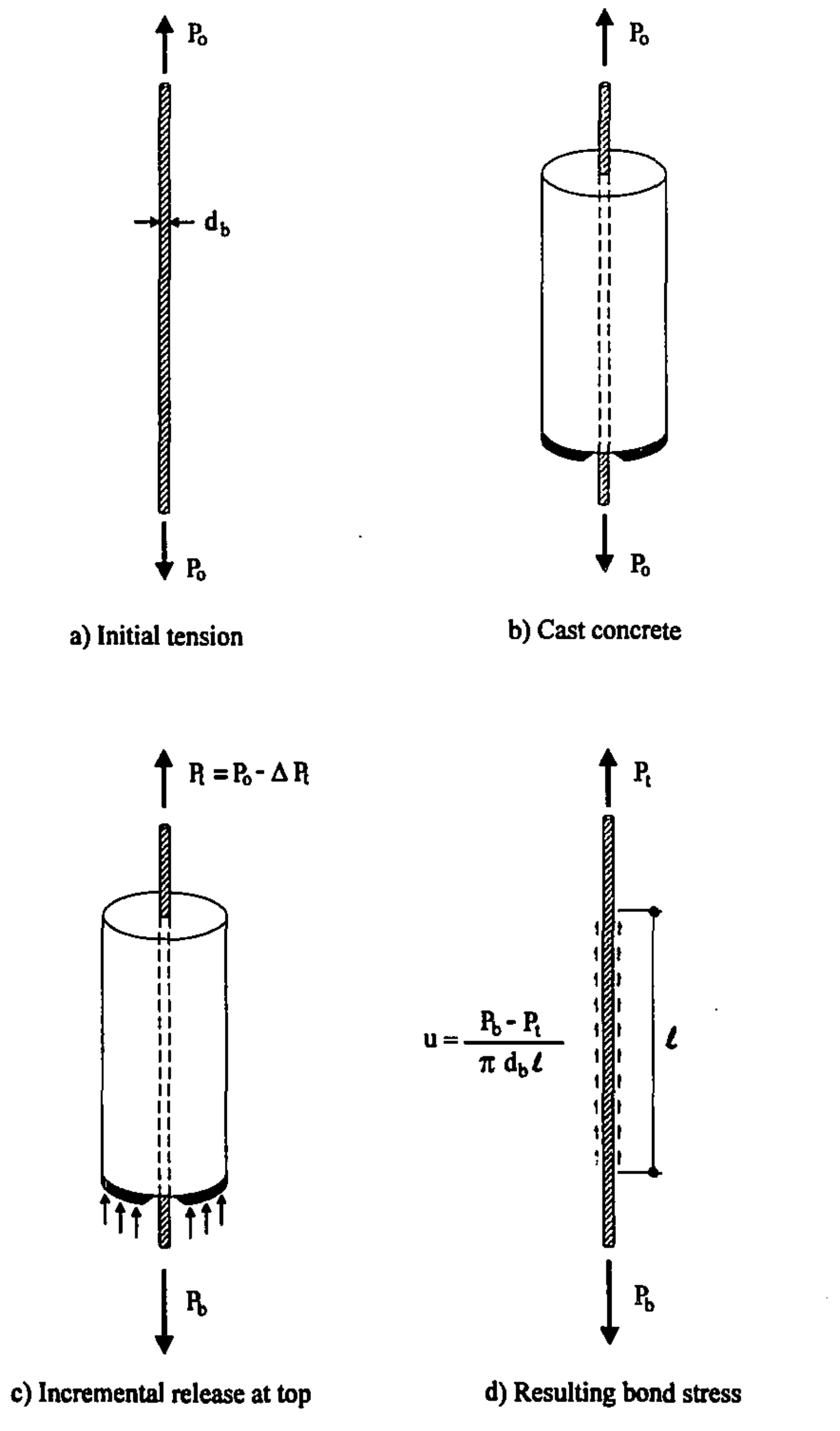

Figure 2.24: Testing technique to simulate bond behaviour along transfer length

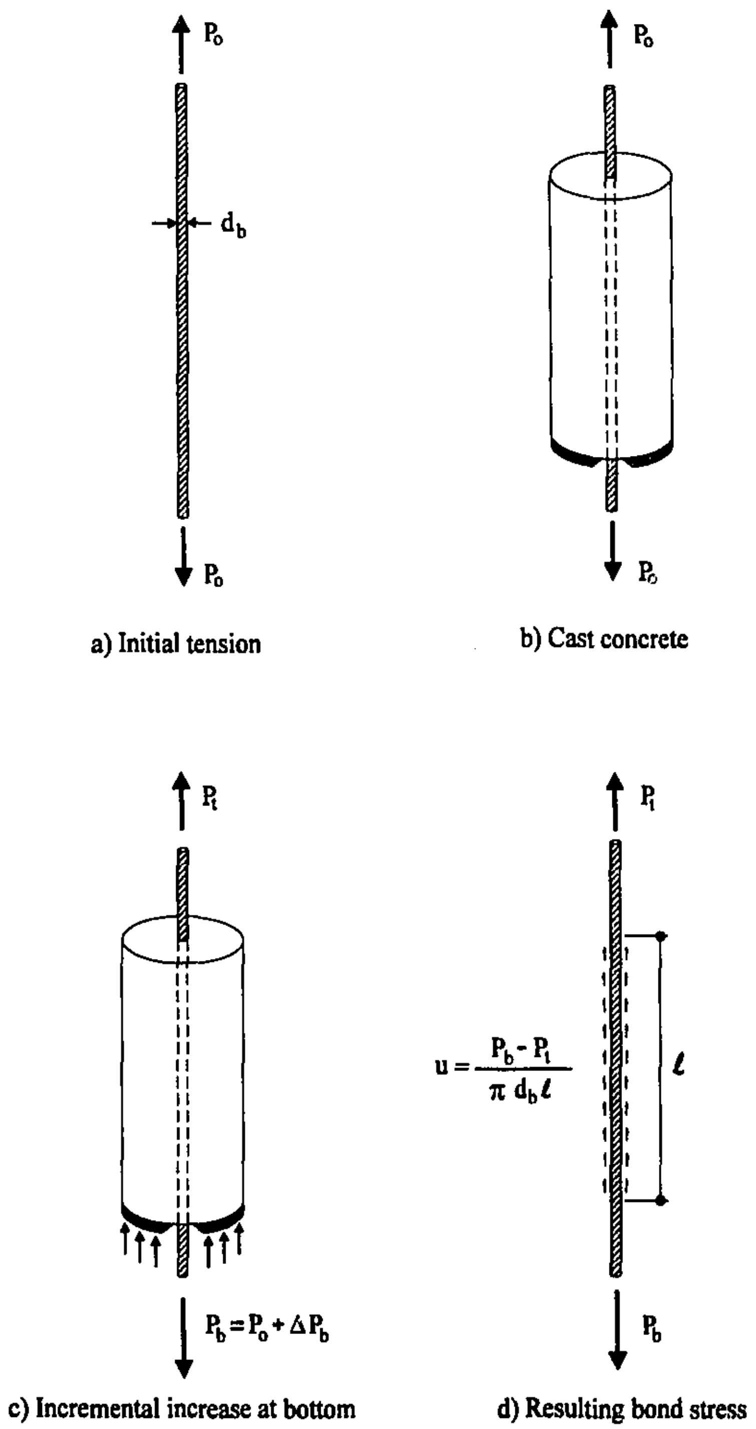

Figure 2.25: Testing technique to simulate bond behaviour along flexural bond length

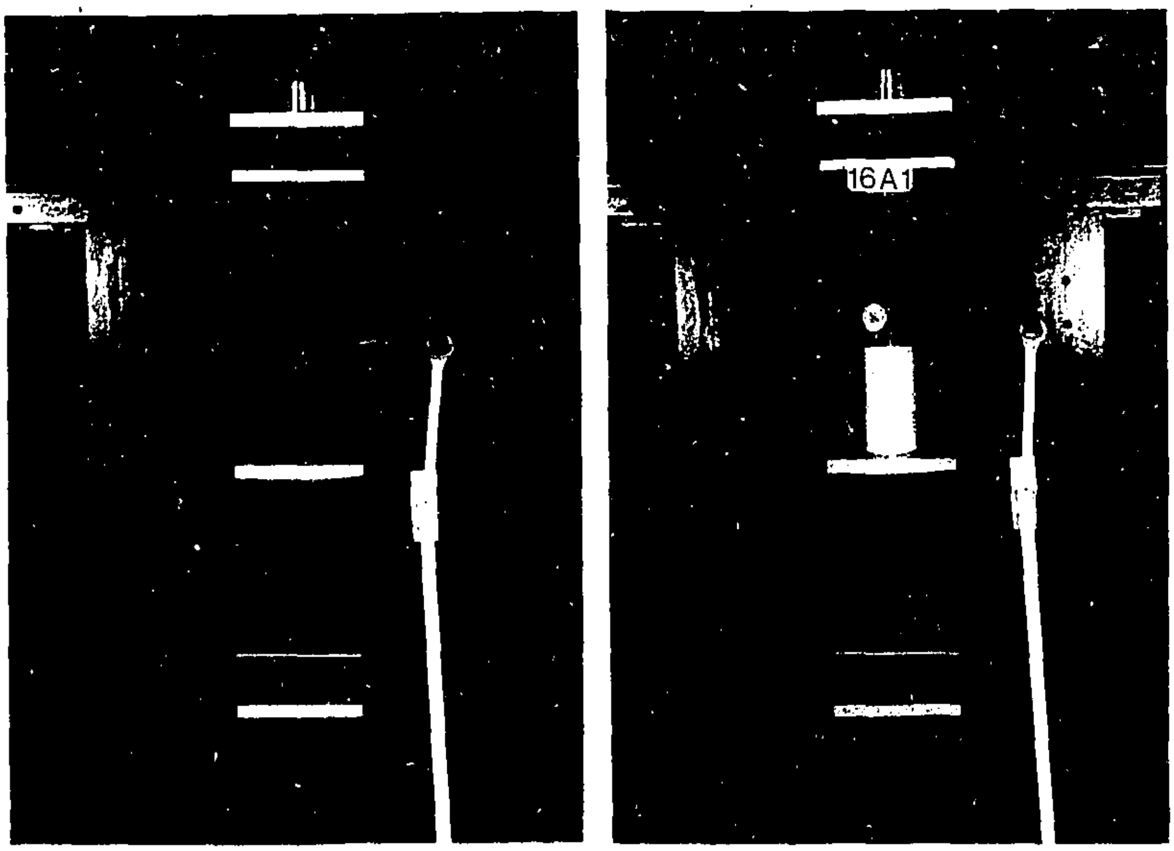

Figure 2.26: Test setup and loading frame, (a) strand after tensioning and before casting the concrete and (b) specimen under load

For both the transfer and flexural bond length tests the tensions in the strand are adjusted by threaded screws and the loads at the top and bottom are recorded by load cells. This method of loading permits performing the experiment under strain control, rather than load control, enabling the post-peak bond response to be determined. Because of the method of release of the strand in the transfer test method, the bond characteristics obtained are representative of those obtained due to gradual release rather than a sudden release. This new testing method uses the same loading frame used to simulate "uniform bond stress" on reinforcing bars.

2.2.3 Test Program

In this test series a concrete mix was designed to give a concrete compressive strength of 25 MPa at the time of testing (age of about 5 days) and to give a 35 MPa compressive strength at 28 days. The specimens were 150 mm diameter by 300 mm long cylinders. Standard concrete cylinders of 150 mm diameter by 300 mm long were used to determine the material characteristics.

The prestressing steel used in this investigation was seven-wire strand. The nominal diameters of the strand sizes used were 9.5 mm, 13 mm and 16 mm. The 9.5 and 13 mm diameter strands had an ultimate tensile strength of 1860 MPa and the 16 mm diameter strand had an ultimate tensile strength of 1760 MPa. Tables 2.2 and 2.3 present the details of the specimens tested. For each size of strand, three specimens were tested to determine bond characteristics along the transfer length and three specimens were used to examine the bond response along the flexural bond length. The 9.5 mm diameter strand had slight rusting on the surface while the two other types of strand had no signs of rusting but had been exposed to the air for about two years.

2.2.4 Transfer Length Test Results

In the testing of the specimens simulating a portion of the transfer length it is noted that all bond failures that occurred were by "pullout" of the strand rather than by splitting of the concrete, as expected. In all of the test specimens, no surface cracks were observed on the concrete cylinders. The bond stress was computed from the difference between the top and bottom strand forces.

Table 2.2: Summary of transfer length test results

Specimen	d_b (mm)	f_c' (MPa)	Initial tension P_o (kN)	P_t at bond failure (kN)	P_b at bond failure (kN)	Average bond strength (MPa)	Top slip at bond failure (mm)
9.5A1	9.5	26.0	80	7	76	7.7	1.74
9.5A2	9.5	25.0	69	6	66	6.7	1.60
9.5A3	9.5	25.0	73	1	71	7.8	1.92
13A1	13	25.8	128	36	121	6.9	1.09
13A2	13	25.5	123	32	116	6.9	1.29
13A3	13	25.3	127	26	118	7.5	1.36
16A1	16	25.0	161	17	142	8.3	1.36
16A2	16	25.8	160	41	147	7.1	1.05
16A3	16	26.5	161	23	147	8.2	1.04

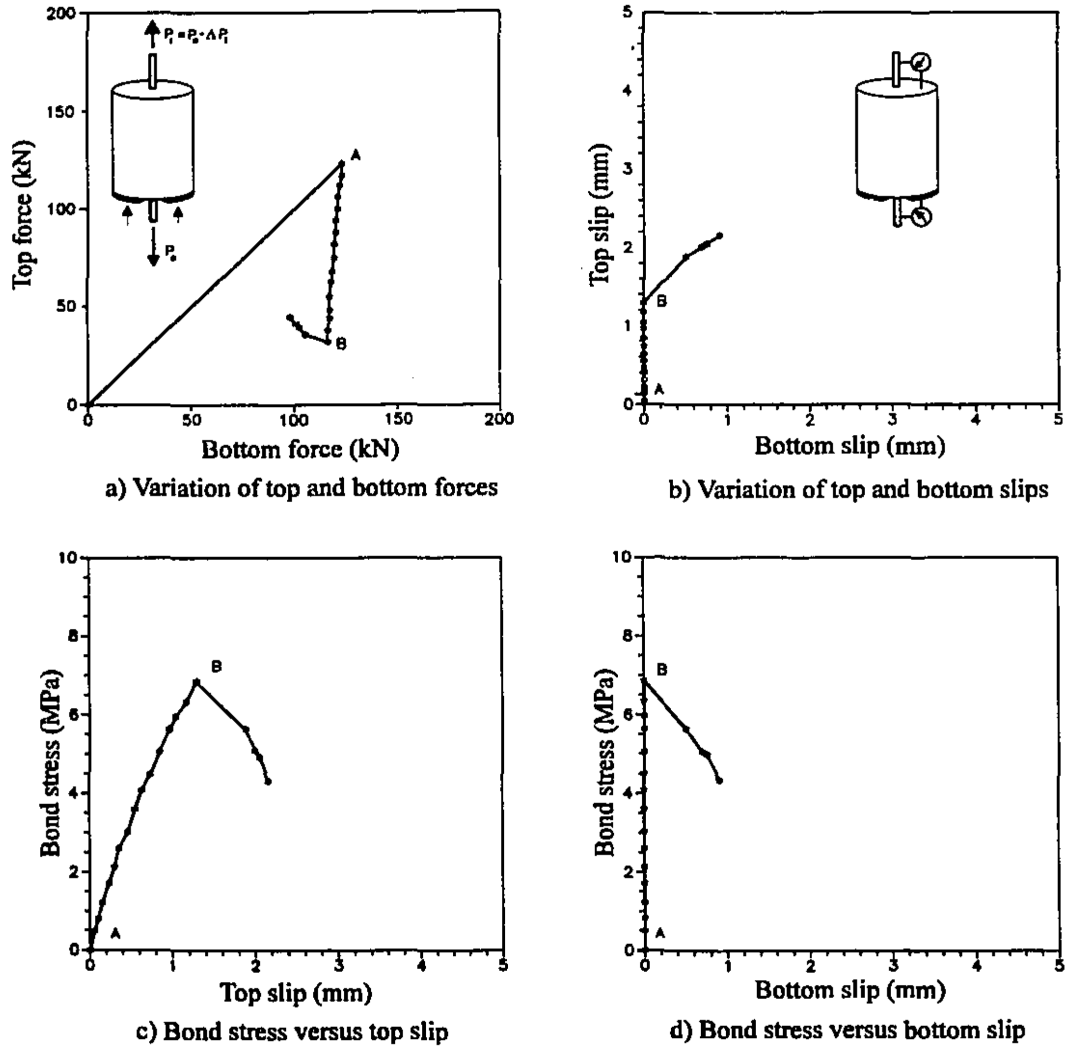

Figure 2.27: Measured response of transfer length specimen 13A2

Figure 2.27 illustrates the complete response for a typical transfer length test specimen. Figure 2.27(a) shows the top force versus bottom force in the strand due to the loading. At point **A**, the top force is equal to bottom force due to the pretensioning of the strand (a strand stress of about 0.7 f_{pu}) before casting the concrete. During testing, the tension in the strand is reduced by ΔP_t (see Fig. 2.27(a)). Due to the reduction of the force at the top of the strand the force at the bottom of the strand undergoes a very slight reduction. After point **A**, the unloading results in a top force which is smaller than the bottom force and hence bond stress is created. Figure 2.27(b) compares the top slip with the bottom slip during testing.

Figure 2.27(c) shows the bond stress versus top slip response while the Fig. 2.27(d) shows the bond stress versus bottom slip response. The peak bond stress occurs at point **B** (see Fig. 2.27(c) and Fig. 2.27(d)) when the difference between the bottom and top forces is a maximum. With the reduction of strand force at the top of the specimen the strand slips, relative to the concrete at the top of the specimen. Before reaching point **B** no slip is observed at the bottom of the specimen. As can be seen from Figure 2.27(c) the relationship between the bond stress and slip, before reaching the peak stress is nearly linear. Bottom slip starts when the maximum bond stress is reached, that is when bond failure occurs. The deflection control of the testing enables the post-peak response to be determined. After the peak stress is reached the bond stress reduces (see Fig. 2.27(c and d)). The increments in top and bottom slip after bond failure are the same which indicates that the strand is pulling through the concrete.

Figure 2.28 compares the response of the three transfer length specimens failing by pullout having strand diameters of 9.5 mm, 13 mm and 16 mm. An increase in the strand diameter gives an increase in the bond stress versus slip stiffness. The 16 mm diameter strand also has a larger bond strength than 13 mm diameter strand. It is noted that the 9.5 mm diameter strand was slightly rusted, which may have resulted in some increased bond strength. The experimental results are summarized in Table 2.2. The maximum bond stresses varied from 6.7 to 8.3 MPa, with an average bond strength of 7.5 MPa.

2.2.5 Flexural Bond Length Test Results

In the testing of the specimens simulating a portion of the flexural bond length it is noted that all bond failures that occurred were by "pullout" of the strand rather than by splitting of the concrete, as expected. In all of the test specimens no surface cracks were observed on the concrete cylinders. The bond stress was computed from the difference between the top and bottom strand forces. Figure 2.29 illustrates the complete response of a typical flexural bond length test specimen failing by pullout.

Figure 2.29(a and b) show the variations of top and bottom forces and the variations of the slips at the top and bottom. At point **A**, the top force is equal to bottom force due to the pretensioning of the strand before casting the concrete. During the test the tension in the bottom of the strand is increased by ΔP_b (see Fig. 2.29(a)). Due to the increase in the force at the bottom of the strand the force at the top of strand also increases slightly. At point **B** (see

Fig. 2.29(c and d)) slip has progressed to the top of the specimen but the maximum bond stress has not been reached.

Figure 2.29(c) shows the bond stress versus bottom slip response while Fig. 2.29(d) shows the bond stress versus top slip response. At the peak bond stress (point **C** in Fig. 2.29(c and d)), the difference between the bottom and the top forces is a maximum. In spite of the considerable slip that occurs after the peak bond stress is reached there is still significant bond resistance. After slip occurs at the top (point **B**) the increments in the top and bottom slip are the same (see Fig. 2.29(b)).

Table 2.3: Summary of flexural bond length test results

Specimen	d_b (mm)	f'_c (MPa)	Initial tension P_o (kN)	P_t at bond failure (kN)	P_b at bond failure (kN)	Average bond strength (MPa)	Bottom slip at bond failure (mm)
9.5B1	9.5	24.3	37	39	77	4.2	0.68
9.5B2	9.5	26.0	20	22	70	5.4	1.35
9.5B3	9.5	25.0	19	21	65	4.9	1.27
13B1	13	25.0	62	66	110	3.6	0.71
13B2	13	25.0	62	67	110	3.5	0.72
13B3	13	25.1	62	67	107	3.3	0.68
16B1	16	23.6	90	95	150	3.6	0.54
16B2	16	26.8	90	98	154	3.7	0.78
16B3	16	26.0	61	67	114	3.1	0.59

Figure 2.30 compares the response of the three flexural bond length specimens failing by pullout, having strand diameters of 9.5 mm, 13 mm and 16 mm. The experimental results are summarized in Table 2.3. The maximum bond stresses varied from 3.1 to 5.4 MPa, with an average bond strength of 3.9 MPa.

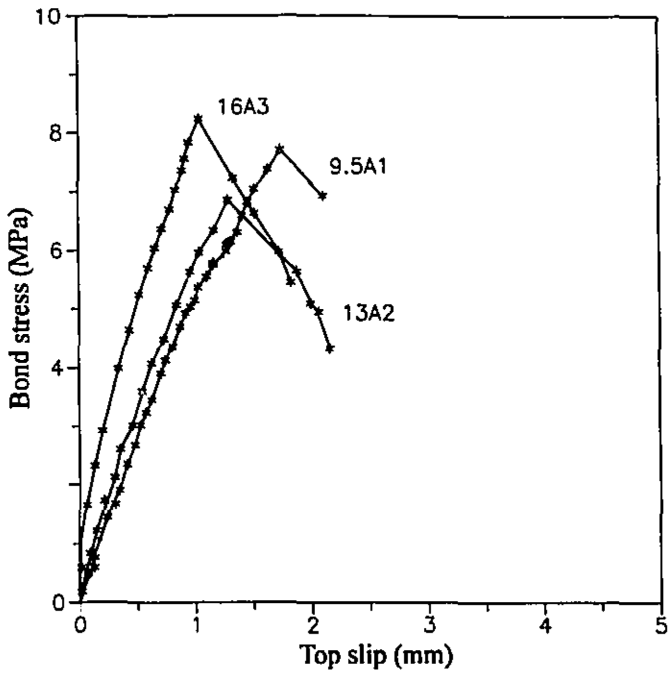

Figure 2.28: Comparison of bond stress versus slip response for transfer length tests for 9.5, 13 and 16 mm diameter strands

2.2.6 Comparison of Transfer and Flexural Bond Responses

Figure 2.31 compares the bond stress versus average slip response of two specimens, having 13 mm diameter strand, tested to simulate the transfer length and flexural bond length regions. As can be seen from this figure the bond strength in the transfer length, $u_{t,\max}$, is greater than the bond strength in the flexural bond length, $u_{fb,\max}$. The average ratios $u_{t,\max} / u_{fb,\max}$ are 1.5, 2.0 and 2.3 for strand sizes of 9.5, 13 and 16 mm, respectively. This ratio increases with increasing strand diameter. After bond failure, the flexural bond length specimen exhibits a more ductile response, with a nearly constant bond stress, while the transfer length specimen exhibits a more brittle bond failure (see Fig. 2.31).

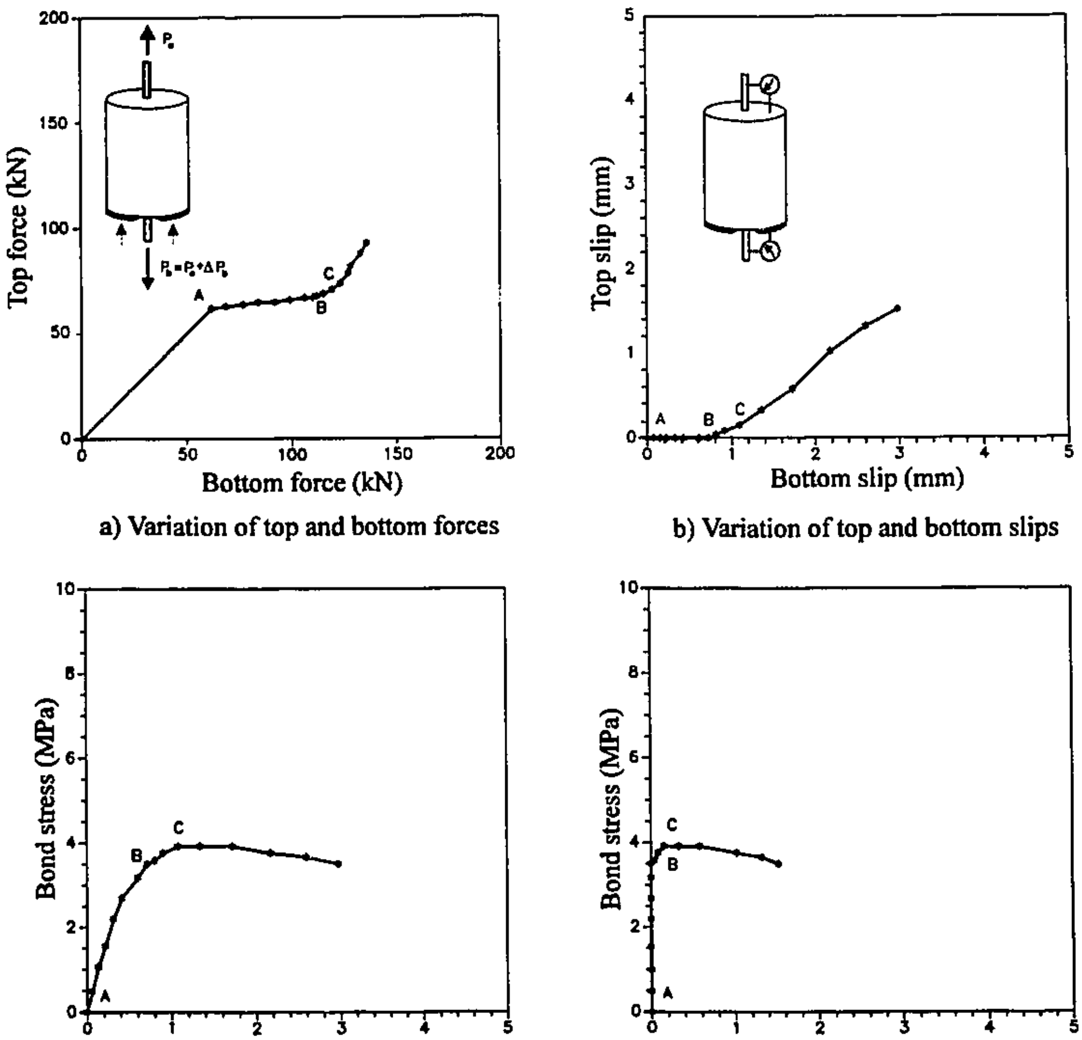

a) Variation of top and bottom forces

b) Variation of top and bottom slips

c) Bond stress versus bottom slip

d) Bond stress versus top slip

Figure 2.29: Measured response of flexural bond length for specimen 13B2

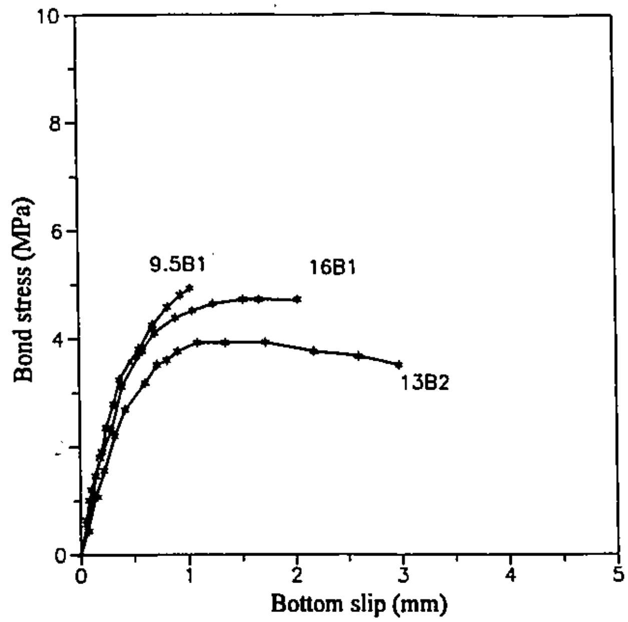

Figure 2.30: Comparison of bond stress versus slip response for flexural bond length tests for 9.5, 13 and 16 mm strands

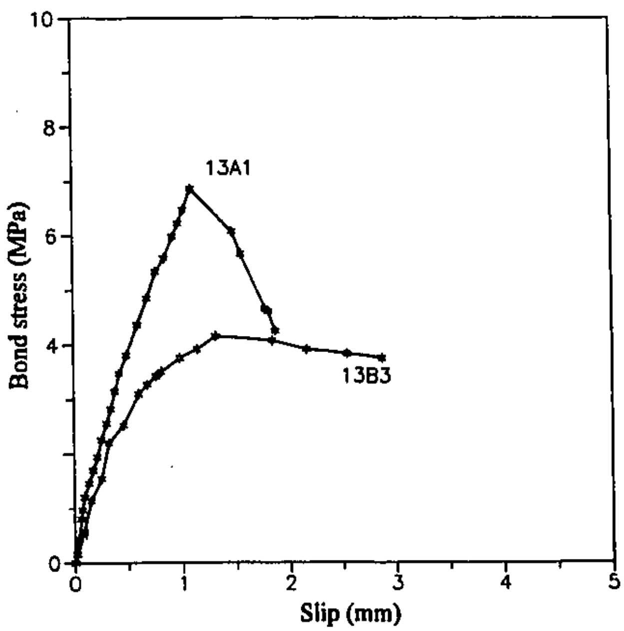

Figure 2.31: Comparison of bond stress versus slip response for transfer length specimen 13A1 and flexural bond length specimen 13B3

2.3 INFLUENCE OF EPOXY-COATED REINFORCING BARS ON BOND STRENGTH

Since 1973, the use of epoxy-coated bars has been steadily increasing in an attempt to reduce corrosion. Several researchers have shown that epoxy-coated bars significantly reduce the bond strength (Treece and Jirza 1989; Hamad *et al.* 1990; Choi *et al.* 1990; Cleary and Ramirez 1991) which must be accounted for in design. The primary reason for the reduction in bond strength appears to be the loss of adhesion between the epoxy-coated bars and the surrounding concrete, causing a reduction in bond resistance. This smooth epoxy coating gives rise to reductions in the bond transfer mechanisms involving adhesion and friction between the bar and the concrete. Those reductions lead to larger mechanical interlocking forces (see Fig. 2.3) and hence larger tensile stresses in the concrete surrounding the bar, resulting in more splitting cracks (Treece and Jirza 1989).

2.3.1 Modifications to Testing Technique for Simulating Uniform Bond Stress

A loading frame was constructed to enable a study the influence of epoxy coating on bond strength. This loading frame was a modification of the loading frame which was used in previous experiments (Abrishami and Mitchell 1992a; Abrishami and Mitchell 1992b; Abrishami and Mitchell 1993). The modifications to this loading frame enabled a series of pullout specimens to be cast all at once and then tested one after another. This testing technique simulates a uniform bond stress distribution along the reinforcing bar embedded in the concrete. The testing procedure, shown in Fig. 2.32, is described below:

Step 1 - Concrete is cast around the reinforcing bar, instrumented with strain gauges (see Fig. 2.32(a)) and cured in order to achieve the desired concrete properties before testing.

Step 2 - In order to create a small bond stress a small tensile force ΔP_b is applied in the reinforcing bar at the bottom of the specimen and a compressive force ΔP_t is applied to the reinforcing bar at the top of the specimen is adjusted (see Fig. 2.32(b)) so as to produce a linear variation in the strains measured on the reinforcing bar. This linear variation in strains results in a linear variation of stress in the reinforcing bar (see Fig.

2.32(c)) and hence produces uniformly distributed bond stress as shown in Fig. 2.32(d). The bond stress is given by:

$$u = \frac{P_b + P_t}{\pi \, d_b \, \ell} \tag{2.6}$$

where P_b and P_t are the bottom and top forces in the reinforcing bar, respectively, and ℓ is the embedment length. The changes in tension in the reinforcing bar, both above and below the concrete cylinder are equilibrated by a compressive reaction at the bottom of the cylinder as shown in Fig. 2.32(b).

Step 3 - Step 2 is repeated for increments in loading. For each increment of loading the relative slips between the concrete and the steel at the top and bottom of the test specimen are measured. The response of a specimen is obtained by plotting the bond stress versus the average of the slips measured at the top and the bottom for each load increment.

Figure 2.33 shows the test set-up during loading. The load is applied through threaded screws at the top and the bottom and the loads are recorded by load cells at these locations. This method of loading permits performing of the experiment under strain control rather than load control.

2.3.2 Test Program

A total of eighteen pullout specimens having uncoated bars and two different thicknesses of epoxy coatings on the reinforcing bars were tested. A series of fifteen specimens were cast using ready-mix concrete. The concrete specimens were 150 mm diameter by 300 mm long with one single bar at the centre. The compressive concrete strength at the time of testing was 36 MPa. In addition to these specimens, three more short pullout specimens having 150 mm diameter and 100 mm long were cast. These three specimens had one single No. 10 bar at the centre and the concrete compressive strength was 23 MPa.

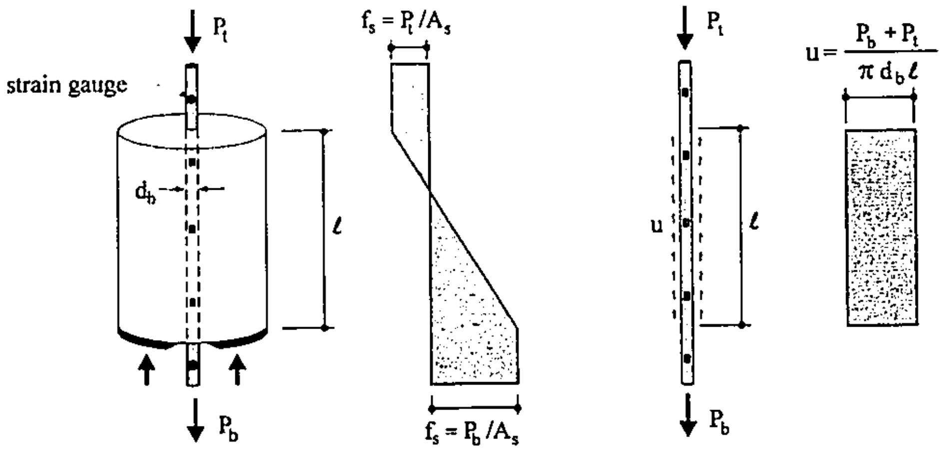

a) Incremental loading b) Linear bar stress c) Resulting uniform bond stress

Figure 2.32: Testing technique to simulate uniform bond stress distribution

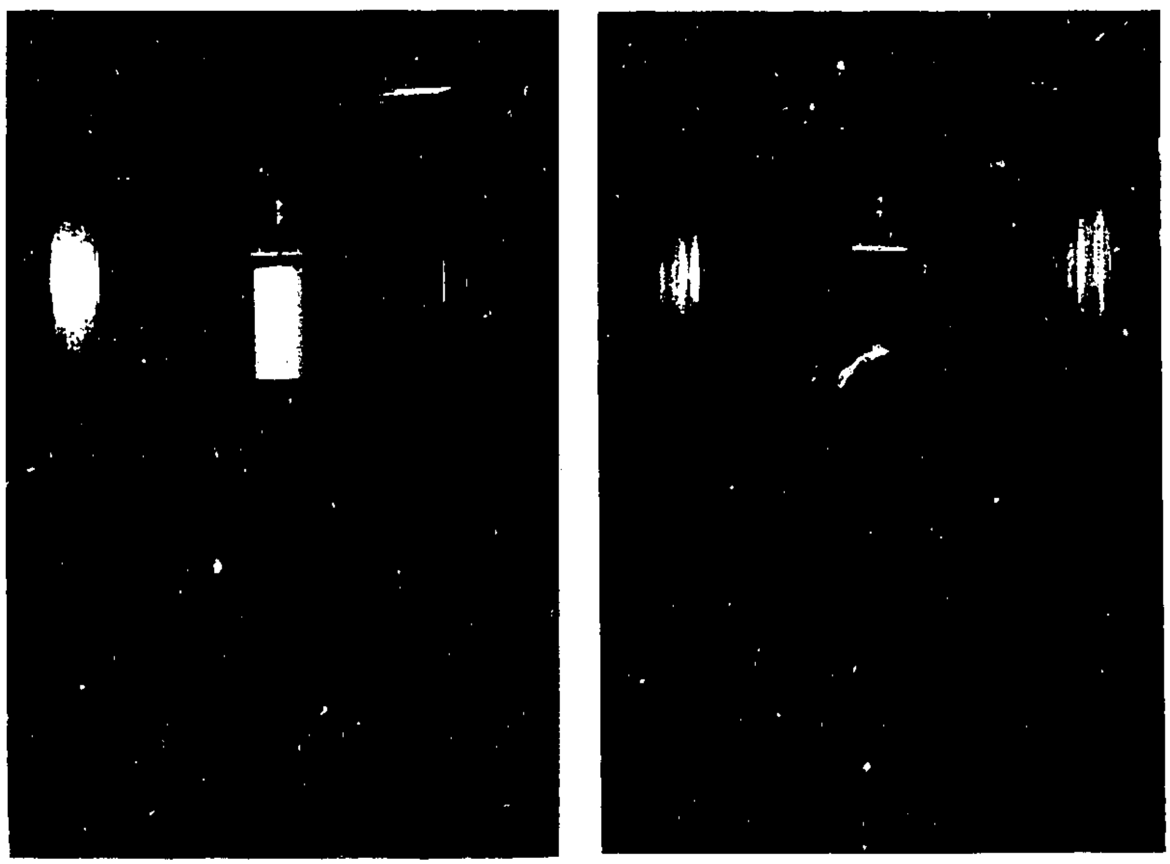

Figure 2.33: Test setup and loading frame

The reinforcing bar sizes used were No. 10, No. 15, No. 20, No. 25, and No. 30 bars, all having a specified yield stress of 400 MPa. For each reinforcing bar size, three different surface conditions, including uncoated bars and two different epoxy coating thicknesses (6 to 8 mil and 10 to 12 mil) were used. Table 2.4 presents the details of the specimens tested. The reinforcing bars were instrumented with five strain gauges, two outside of the concrete and three along the embedment length. Strain gauges having a 2 mm gauge length, were glued to the surface of the reinforcing bars. These small gauges were used in order to minimize the reduction of bond surface area due to the presence of the gauges.

2.3.3 Test Results

After reaching the maximum bond stress, all the specimens tested had very brittle failures and therefore it was not possible to record the post-peak responses. Figure 2.34 shows the bond stress versus slip of three specimens having No. 20 bar size with uncoated and two different epoxy-coated bars. As can be seen from this figure the specimen containing uncoated bar had higher stiffness than companion specimens containing epoxy-coated bars. Also the bond strength of uncoated bar is greater than bond strength of the epoxy-coated bars.

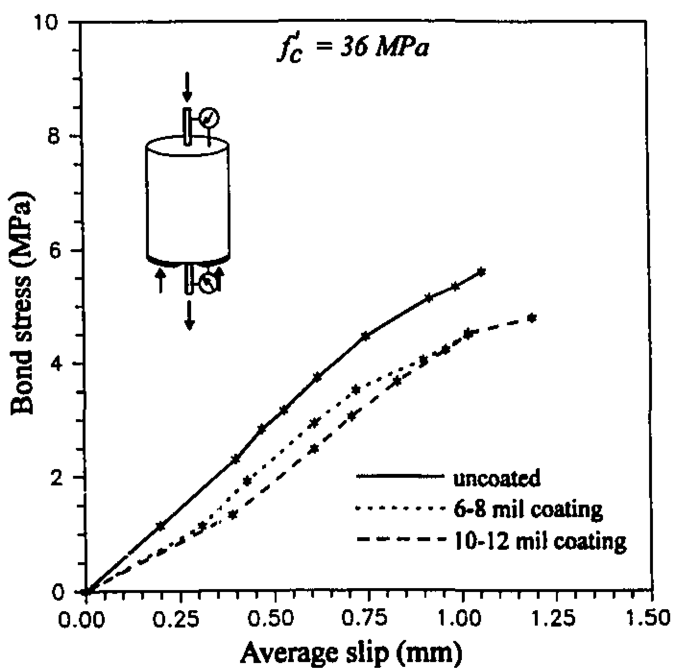

Figure 2.34: Bond stress versus average slip response for specimens 20UC, 20C1 and 20C2

Table 2.4 presents the bond strength of all the specimens tested in this study. In this table the bond strength ratio is the ratio of bond strength of the epoxy-coated bar to the bond strength of the uncoated bar. As can be seen, the bond strength in specimens having epoxy-coated bars can be reduced up to 17 percent. The thicker, 10-12 mil, coatings also resulted in lower bond strengths than the 6-8 mil coatings.

Table 2.4: Summary of results of bond tests with epoxy coated bars

specimen	Cylinder dia. x length (mm x mm)	d_b (mm)	f_c' (MPa)	Bond strength (MPa)	Slip at max. bond stress (mm)	Bond strength ratio
30UC	150 x 300	29.9	36	3.48	0.93	1
30C1	150 x 300	29.9	36	3.34	0.92	0.96
30C2	150 x 300	29.9	36	2.90	0.80	0.83
25UC	150 x 300	25.2	36	4.31	0.78	1
25C1	150 x 300	25.2	36	4.47	0.93	1.04
25C2	150 x 300	25.2	36	4.00	0.84	0.93
20UC	150 x 300	19.5	36	5.59	1.06	1
20C1	150 x 300	19.5	36	4.50	1.02	0.80
20C2	150 x 300	19.5	36	4.79	1.19	0.86
15UC	150 x 300	16.0	36	6.76	1.17	1
15C1	150 x 300	16.0	36	7.17	1.15	1.06
15C2	150 x 300	16.0	36	6.22	1.28	0.92
10UC	150 x 300	11.3	36	*	*	*
10C1	150 x 300	11.3	36	*	*	*
10C2	150 x 300	11.3	36	*	*	*
S10UC	150 x 100	11.3	23	5.67	0.48	1
S10C1	150 x 100	11.3	23	5.19	0.54	0.91
S10C2	150 x 100	11.3	23	4.94	0.62	0.87

* - Reinforcing bar yielded in the specimen before bond failure
UC, C1, and C2, representing uncoated bar, 6-8 mil coating thickness and 10-12 mil coating thickness on the reinforcement, respectively

2.4 COMPARISON OF RESULTS FROM THE NEW TESTING METHODS

The bond strength of different series, tested with the two different testing techniques described in Section 2.1 and Section 2.3 were compared. The comparison is available only for specimens reinforced with uncoated bars and having the same bar size (see Table 2.1 and Table 2.4). All of the specimens reported in Table 2.4 had splitting failures and therefore can be compared with the specimens failing by splitting given in Table 2.1. Specimen 20A is compared with specimen 20UC, both having the same bar size and concrete cover (i.e., $c/d_b = 3.3$). Due to the higher compressive and tensile strength of the concrete in specimen 20UC compared to that of specimen 20A, the bond strength of specimen 20UC is 1.30 times that of specimen 20A. Based on the ACI Code (1989), the bond strength is proportional to the square root of compressive strength which is 1.2 for above specimens.

Although the concrete compressive strength of specimen 30UC is greater than specimen 30B, Specimen 30UC has less bond strength than specimen 30B due to the smaller concrete cover. The ratio of concrete cover to bar size (c/d_b) of specimen 30B is 2.8 compared to 2.0 for specimen 30UC.

Specimen 25UC has a bond strength which is 1.2 times that of specimen 25B even though its c/d_b ratio is smaller (i.e., 2.5 versus 3.5, respectively). However specimen 25UC has a higher concrete strength than that in specimen 25B, giving a ratio of tensile strengths equal to 1.2. Since both specimens have relatively high c/d_b ratios, it is expected that the concrete tensile strength would govern the bond strength.

These comparisons indicate that the two testing methods give comparable results, although no tests were performed which had identical concrete strengths and identical c/d_b ratios.

Chapter 3

ANALYTICAL STUDIES OF BOND BEHAVIOUR

"You can only predict things after they've happened"
Eugene Lones

A number of analytical studies on bond stress versus slip responses of reinforcement embedded in concrete have been reported (ACI Committee 408 1991; CEB Task Group VI 1981). In general these studies can be classified into three groups; 1) finite difference or finite element models, which result in solving the differential equations of bond stress distribution (Edwards and Yannopoulos 1979; Plaines *et al.* 1982; Tassios and Koroneos 1984; Ciampi *et al.* 1982), 2) an assumed bond stress distribution function along the embedment length of the reinforcing bars which is based on experimental results (Guiriani 1981; Shah and Somayai 1981; Bertero and Bresler 1968; Bertero *et al.* 1978) and, 3) more recently, models based on fracture mechanics (Bertero *et al.* 1978; Gerstle *et al.* 1982; Gyltoft *et al.* 1982; Ouyang and Shah 1994).

3.1 ANALYTICAL APPROACH TO STUDY PULLOUT SPECIMENS

The purpose of this section is to demonstrate the manner in which the bond performance of pullout test specimens, subjected to different types of loading, can be predicted. The use of bond stress versus slip relationships together with the differential equation for bond, enables various testing techniques employed by other researchers to be compared.

The bond stress distribution in a typical pullout test is not uniform. Several researchers have attempted to study the real distribution of bond stress along a reinforcing bar embedded in concrete (CEB 1981; Russo *et al.* 1990; Nilson 1972; Yankelevski 1985; Yerex *et al.* 1985;

Viwathanatepa *et al.* 1979). Due to the non-uniformity in the bond stress distribution, there is as yet, no theoretical method for evaluating bond strength of a reinforcing bar embedded in concrete (ACI Committee 408 1991; CEB Task Group VI 1981). Hence an "average bond stress" or "average bond strength" is used in codes of practice. Several studies have shown that there is a significant variation of the actual bond stress distribution, with the maximum bond stress in some cases being much greater than the average bond stress. In addition, it has been shown that the bond stress distribution varies greatly as slip develops (Hamad and Jirsa 1979; Pillai and Kirk 1988). It has also been demonstrated that an average bond stress-slip relation is not suitable for detailed analysis in finite element models (Keuser and Mehlholn 1987).

As part of this research program a new testing technique (Abrishami and Mitchell 1992) was developed to simulate uniform bond stress distribution to better understand bond characteristics of reinforcing bars in concrete structures. This testing technique is described in Chapter 2.

3.1.1 Bond Stress versus Slip Response -- A Fundamental Material Characteristic

The relationship between bond stress, u , and the relative slip, δ , between the steel reinforcing bar and the concrete, is of fundamental importance in predicting the complex interaction between the two materials. Many researchers have attempted to determine experimentally the bond stress versus slip response. These results were typically reported as the average bond stress versus slip at one end of the specimen due to the significant variation of bond stress along the embedment length. A new testing technique (Abrishami and Mitchell 1992), which attempts to simulate a uniform bond stress distribution, has enabled a more accurate determination of the bond stress versus slip response. Figures 3.1(a) and 3.1(b) show the bond stress versus slip response obtained from tests simulating a uniform bond stress distribution for specimens failing in pullout and splitting, respectively. Also shown in these figures are the proposed analytical relationships for the bond stress versus slip response.

3.1.2 Governing Differential Equation for Bond

Figure 3.2(a) shows the forces acting on a reinforced concrete element of length, dx, while Fig. 3.2(b) illustrates the equilibrium conditions for a reinforcing bar of length, dx.

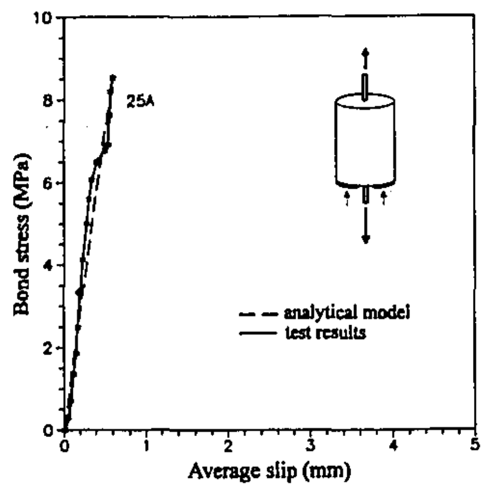

a) pullout failure

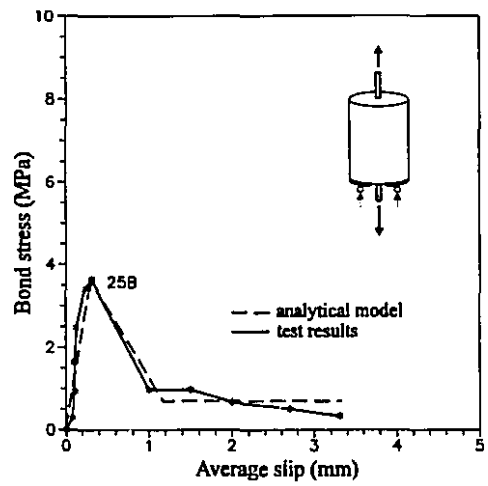

b) splitting failure

Figure 3.1: Bond stress versus slip response

The equilibrium equations obtained from these two figures can be written as:

$$A_c df_c + A_s df_s = 0 \tag{3.1}$$

and

$$u(\pi d_b dx) = A_s(f_s + df_s) - A_s f_s \tag{3.2a}$$

or:

$$u = \frac{d_b}{4} \frac{df_s}{dx} \tag{3.2b}$$

where A_c and A_s are the concrete and reinforcing bar areas, f_c and f_s are the concrete and steel stresses, d_b is the diameter of the reinforcing bar and u is the bond stress. The bond stress, u , is a function of the slip, δ , that is $u = u(\delta)$. The slip, $\delta(x)$, at a distance x along the rebar, is defined as the relative displacement between the reinforcing bar and concrete, that is:

$$\delta(x) = \delta_s(x) - \delta_c(x) \tag{3.3}$$

where $\delta_s(x)$ is the displacement of the steel at point x and $\delta_c(x)$ is the displacement of the concrete at point x . Differentiation of this equation gives:

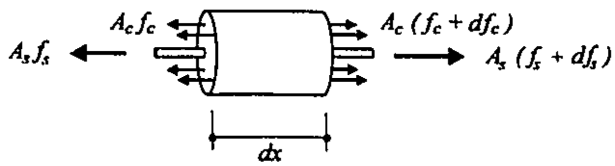

a) Forces acting on reinforced concrete element of length, dx

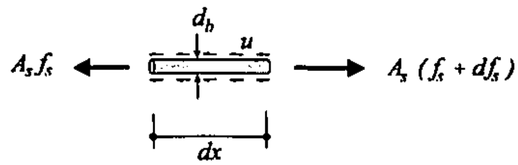

b) Equilibrium conditions for a reinforcing bar of length, dx

Figure 3.2: Bond stress resulting from changing stress in reinforced concrete

$$\frac{d\delta(x)}{dx} = \epsilon_s(x) - \epsilon_c(x) \tag{3.4}$$

where ϵ_s and ϵ_c are reinforcement and concrete strains, respectively. The linear elastic relationship between stress and strain can be expressed as follows:

$$f_s = E_s \, \epsilon_s \tag{3.5}$$

$$f_c = E_c \, \epsilon_c \tag{3.6}$$

in which E_s and E_c are Young's moduli of the reinforcing steel and concrete, respectively. Differentiation of Eq. (3.4), after substituting values from Eqs.(3.5) and (3.6), gives:

$$\frac{d^2\delta(x)}{dx^2} = \frac{1}{E_s} \frac{df_s}{dx} (1 + n\rho) \tag{3.7}$$

where: $\rho = A_s / A_c$ and $n = E_S / E_c$. Substituting df_s / dx from Eq. (3.2) into Eq. (3.7) gives:

$$\frac{d^2\delta}{dx^2} - k_s \, u = 0 \tag{3.8}$$

where: $k_s = 4(1 + n\rho) / (d_b E_s)$. Equation (3.8) is the general differential equation for bond slip response as a function of x .

3.1.3 Response Predictions of Bond Specimens Failing by Pullout

Figure 3.3 shows a standard pullout test specimen subjected to: (a) a standard pullout test, (b) a "push-in" test and (c) a combination of (a) and (b).

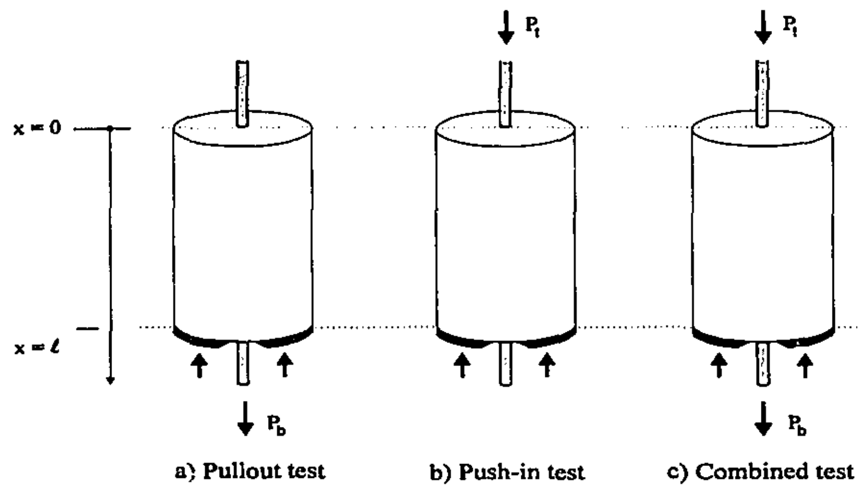

Figure 3.3: Typical pullout test specimen subjected to different types of loading

A mathematical model used to predict the response of a specimen failing by pullout is shown in Fig. 3.4.

The bond stress can be written as:

$$u = E_b\, \delta \qquad 0 \leq \delta \leq \delta_{pf} \tag{3.9}$$

$$u = 0 \qquad \delta > \delta_{pf} \tag{3.10}$$

where $E_b = u_{pf} / \delta_{pf}$. Eq. (3.8) can be simplified as:

$$\frac{d^2\delta}{dx^2} - k_s\, E_b\, \delta = 0 \tag{3.11}$$

assuming $k = \sqrt{k_s\, E_b}$ in Eq.(3.11) and integrating twice gives:

$$\delta = c_1 e^{kx} + c_2 e^{-kx} \tag{3.12}$$

where c_1 and c_2 are constants depending the boundary conditions. Substituting δ from Eq. (3.12) in Eq. (3.9) gives:

$$u = E_b\,(c_1\,e^{kx} + c_2\,e^{-kx}) \quad 0 \le \delta \le \delta_{pf} \tag{3.13}$$

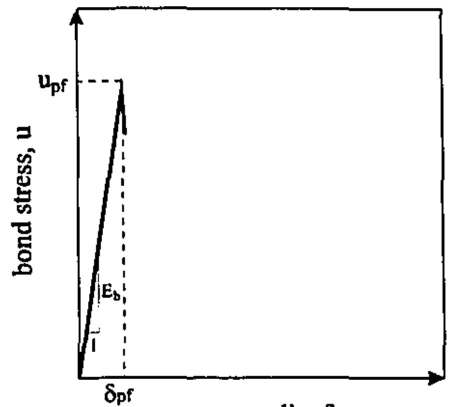

Figure 3.4: Analytical bond model for pullout failure

Example No. 1 - Predicting Response of Standard Pullout Test

The standard pullout specimen is subjected to a tensile force, P_b , at the bottom of the reinforcing bar as shown in Fig. 3.3(a). The boundary conditions can be written as follows:

at $\quad x = 0 \quad \epsilon_c = 0 \quad \epsilon_s = 0$

at $\quad x = \ell \quad \epsilon_c = -\dfrac{P_b}{E_c\,A_c} \quad \epsilon_s = \dfrac{P_b}{E_s\,A_s}$

These boundary conditions result in:

$$c_1 = c_2 = \frac{1}{k(e^{kl} - e^{-kl})}\left(\frac{1}{E_s\,A_s} + \frac{1}{E_c\,A_c}\right) P_b \tag{3.14}$$

The slips at the top of the specimen, δ_t , ($x = 0$) and the bottom of the specimen, δ_b, ($x = l$) are:

$\delta_t = c_1 + c_2$

and

$$\delta_b = c_1 \, e^{kt} + c_2 \, e^{-kt}$$

The average slip, δ_{av} , at the top and bottom of the specimen is used to predict the response of the standard pullout test. Replacing c_1 and c_2 in Eq. (3.12), the relationship between the pullout force, P_b , and average slip, δ_{av} , can be expressed as:

$$P_b = \left[\frac{2k \, (e^{kt} - e^{-kt})}{2 + e^{kt} + e^{-kt}} \left(\frac{E_s \, A_s}{1 + n\rho} \right) \right] \delta_{av} \tag{3.15}$$

Example No. 2 - Predicting Response of "Push-in" Test

The push-in test specimen is subjected to a compressive force, P_t , at the top of the reinforcing bar as shown in Fig. 3.3(b). The boundary conditions can be written as follows:

at $\quad x = 0 \quad \epsilon_c = 0 \quad \epsilon_s = -\dfrac{P_t}{E_s A_s}$

at $\quad x = \ell \quad \epsilon_c = -\dfrac{P_t}{E_c \, A_c} \quad \epsilon_s = 0$

These boundary conditions result in:

$$c_1 = \left(\frac{1}{k(e^{k\ell} - e^{-kt})} \right) \left(\frac{e^{-kt}}{E_s \, A_s} + \frac{1}{E_c \, A_c} \right) P_t \tag{3.17}$$

$$c_2 = \left(\frac{1}{k \, (e^{kt} - e^{-kt})} \right) \left[\left(\frac{e^{-kt}}{E_s \, A_s} + \frac{1}{E_c \, A_c} \right) + \frac{1}{k \, E_s \, A_s} \right] P_t \tag{3.16}$$

using the same procedure described above, the response of "push-in" test as a relationship between the "push-in" force, P_t , and average slip, δ_{av} , can be expressed as:

$$P_t = \left[\frac{2k \, (e^{kt} - e^{-kt})}{2 + e^{kt} + e^{-kt}} \left(\frac{E_s \, A_s}{1 + n\rho} \right) \right] \delta_{av} \tag{3.18}$$

As expected this relationship is identical to Eq. (3.15) for the pullout test.

Example No. 3 - Predicting Response of a Combination Pullout / Push-in Test

For this combined loading case the specimen is subjected to a tensile force, P_b , at the bottom of the reinforcing bar and a compressive force, P_t , at the top of the reinforcing bar as shown in Fig. 3.3(c). The boundary conditions can be written as:

$$\text{at} \quad x = 0 \quad \epsilon_c = 0 \quad \epsilon_s = -\frac{P_t}{E_s A_s}$$

$$\text{at} \quad x = \ell \quad \epsilon_c = -\frac{(P_b + P_t)}{E_c\, A_c} \quad \epsilon_s = \frac{P_b}{E_s\, A_s}$$

Assuming $P_t = \phi P$ and $P_b = (1 - \phi)P$, where $P = P_t + P_b$. These boundary conditions result in:

$$c_1 = \frac{1}{k}\,(e^{k\ell} - e^{-k\ell})^{-1}\left[\frac{\phi\, e^{-k\ell}}{E_s\, A_s} + \frac{(1-\phi)}{E_s\, A_s} + \frac{1}{E_c\, A_c}\right] P \tag{3.19}$$

and

$$c_2 = \frac{1}{k}\left[(e^{k\ell} - e^{-k\ell})^{-1}\left(\frac{\phi\, e^{-k\ell}}{E_s\, A_s} + \frac{(1-\phi)}{E_s\, A_s} + \frac{1}{E_c\, A_c}\right) + \frac{\phi}{E_s\, A_s}\right] P \tag{3.20}$$

Using the same method described in Examples 1 and 2, the total applied force, P , is determined as a function of average slip, δ_{av} as:

$$P = \left[\frac{2k\,(e^{k\ell} - e^{-k\ell})}{2 + e^{k\ell} + e^{-k\ell}}\left(\frac{E_s\, A_s}{1 + n\rho}\right)\right]\delta_{av} \tag{3.21}$$

For the linear range of response this equation gives the same result as the pullout test when $\phi = 0$ and the same result as push-in test when $\phi = 1$ (see Eqs. (3.15) and (3.18)).

3.1.4 Response Predictions of Bond Specimens Failing by Splitting

A mathematical model used to predict the response of a specimen failing by splitting is shown in Fig. 3.5.

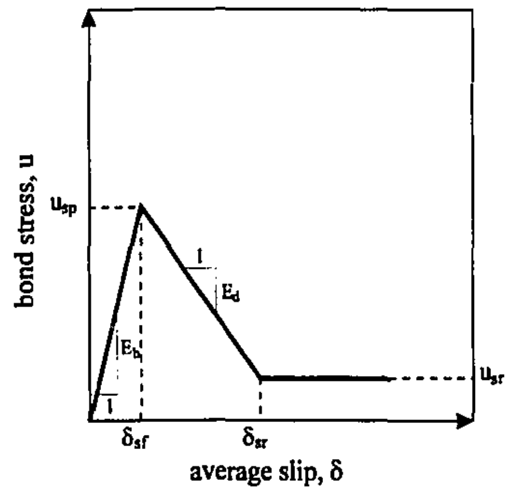

Figure 3.5: Analytical bond model for splitting failure

The bond stress can be expressed as:

$$u = E_b\,\delta \qquad 0 < \delta < \delta_{sf}$$

$$u = E_d\,\delta + E_b\,\delta_{sf} - E_d\,\delta_{sf} \qquad \delta_{sf} < \delta < \delta_{sr}$$

$$u = u_{sr} \qquad \delta > \delta_{sr}$$

where $E_b = u_{sf} / \delta_{sf}$ and $E_d = (u_{sr} - u_{sf}) / (\delta_{sr} - \delta_{sf})$

The governing differential equation for bond is:

$$\frac{d^2\delta}{dx^2} - k_s\,E_b\,\delta = 0 \qquad 0<\delta<\delta_{sf} \tag{3.22}$$

$$\frac{d^2\delta}{dx^2} - k_s\,E_d\,\delta = k_s\,E_d\,\delta_{sf}\left(\frac{E_b}{E_d}-1\right) \qquad \delta_{sf}<\delta<\delta_{sr} \tag{3.23}$$

For the ascending branch, assuming $k = \sqrt{k_s\,E_b}$ for $0 < \delta < \delta_{sf}$, Eq. 3.22 gives:

$$\delta = c_1 e^{kx} + c_2 e^{-kx} \tag{3.24}$$

$$u = E_b\,(c_1\,e^{kx} + c_2\,e^{-kx}) \tag{3.25}$$

For the descending branch, assuming $k = \sqrt{-k_s\,E_d}$ for $\delta_{sf} < \delta < \delta_{sr}$, Eq. (3.23) gives:

$$\delta(x) = c_3 \cos(kx) + c_4 \sin(kx) - m \tag{3.26}$$

$$u(x) = E_d\,\big(c_3 \cos(kx) + c_4 \sin(kx)\big) \tag{3.27}$$

In which $m = \delta_{sf}\,(E_b/E_d - 1)$

Example No. 4 - Predicting Response of Standard Pullout Test

The standard pullout specimen is subjected to a tensile force, P_b, at the bottom of reinforcing bar as shown in Fig. 3.3(a). The boundary conditions can be written as follows:

at $\quad x = 0 \quad \epsilon_c = 0 \quad \epsilon_s = 0$

at $\quad x = \ell \quad \epsilon_c = -\dfrac{P_b}{E_c\,A_c} \quad \epsilon_s = \dfrac{P_b}{E_s\,A_s}$

For $0 < \delta < \delta_{sf}$ these boundary conditions result in:

$$c_1 = c_2 = \frac{1}{k(e^{kt} - e^{-kt})}\left(\frac{1}{E_s\,A_s} + \frac{1}{E_c\,A_c}\right) P_b \tag{3.28}$$

$$P_b = \left[\frac{2k(e^{kt} - e^{-kt})}{2 + e^{kt} + e^{-kt}}\right]\left(\frac{E_s\,A_s}{1 + n\rho}\right)\delta_{av} \tag{3.29}$$

In which δ_{av} is the average of the slips at the top and the bottom of the specimen.

For $\delta_{sf} < \delta < \delta_{sr}$ these boundary conditions result in:

$$c_3 = \frac{-1}{k \sin(k\ell)} \left(\frac{1}{E_s A_s} + \frac{1}{E_c A_c} \right) P_b \tag{3.30}$$

$$c_4 = 0 \tag{3.31}$$

$$P_b = \left[\frac{-2k \sin(k\ell)}{1 + \cos(k\ell)} \left(\frac{E_s A_s}{1 + n\rho} \right) \right] (\delta_{av} + m) \tag{3.32}$$

Example No. 5 - Predicting Response of "Push-in" Test

The push-in test specimen is subjected to a compressive force, P_t , at the top of reinforcing bar as shown in Fig. 3.3(b), the boundary conditions can be written as follows:

at $\quad x = 0 \quad \epsilon_c = 0 \quad \epsilon_s = -\dfrac{P_t}{E_s A_s}$

at $\quad x = l \quad \epsilon_c = -\dfrac{P_t}{E_c A_c} \quad \epsilon_s = 0$

For $0 < \delta < \delta_{sf}$ these boundary conditions result in:

$$c_2 = \left[\left(\frac{e^{-kt}}{E_s A_s} + \frac{1}{E_c A_c} \right) \left(\frac{1}{k\,(e^{kt} - e^{-kt})} \right) + \frac{1}{k\,E_s A_s} \right] P_t \tag{3.33}$$

$$c_1 = \left(\frac{e^{-kt}}{E_s A_s} + \frac{1}{E_c A_c} \right) \left(\frac{1}{k\,(e^{kt} - e^{-kt})} \right) P_t \tag{3.34}$$

$$P_t = \left[\frac{2k(e^{kt} - e^{-kt})}{2 + e^{kt} + e^{-kt}} \right] \left(\frac{E_s A_s}{1 + n\rho} \right) \delta_{av} \tag{3.35}$$

and for $\delta_{sf} < \delta < \delta_{sr}$ these boundary conditions result in:

$$c_3 = \frac{-1}{k\sin(k\ell)} \left(\frac{\cos(k\ell)}{E_s\, A_s} + \frac{1}{E_c\, A_c} \right) P_t \tag{3.36}$$

$$c_4 = \frac{-P_t}{k\, E_s\, A_s} \tag{3.37}$$

$$P_t = \left[\frac{-2k\, \sin(k\ell)}{1 + \cos(k\ell)} \left(\frac{E_s\, A_s}{1 + n\rho} \right) \right] (\delta_{av} + m) \tag{3.38}$$

Example No. 6 - Predicting Response of a Combination Pullout / Push-in Test

The specimen is subjected to a tensile force, P_b at the bottom of reinforcing bar and a compressive force, P_t at the top of reinforcing bar as shown in Fig. 3.3(c). The boundary conditions can be written as:

at $\quad x = 0 \quad \epsilon_c = 0 \quad \epsilon_s = -\dfrac{P_t}{E_s A_s}$

at $\quad x = \ell \quad \epsilon_c = -\dfrac{(P_b + P_t)}{E_c\, A_c} \quad \epsilon_s = \dfrac{P_b}{E_s\, A_s}$

Using the same method described in Examples 4 and 5, the total applied force, P, which is the summation of top force, P_t , and bottom force, P_b , is determined as a function of the average slip, δ_{av} for $0 < \delta < \delta_{sf}$:

$$c_1 = \frac{1}{k} (e^{k\ell} - e^{-k\ell})^{-1} \left[\frac{\phi\, e^{-k\ell}}{E_s\, A_s} + \frac{(1-\phi)}{E_s\, A_s} + \frac{1}{E_c\, A_c} \right] P \tag{3.39}$$

$$c_2 = \frac{1}{k} \left[(e^{k\ell} - e^{-k\ell})^{-1} \left(\frac{\phi\, e^{-k\ell}}{E_s\, A_s} + \frac{(1-\phi)}{E_s\, A_s} + \frac{1}{E_c\, A_c} \right) + \frac{\phi}{E_s\, A_s} \right] P \tag{3.40}$$

and

$$P = \left[\frac{2k\, (e^{k\ell} - e^{-k\ell})}{2 + e^{k\ell} + e^{-k\ell}} \left(\frac{E_s\, A_s}{1 + n\rho} \right) \right] \delta_{av} \tag{3.41}$$

For $\delta_{sf} < \delta < \delta_{sr}$:

$$c_3 = \frac{-1}{k\sin(k\ell)}\left[\frac{\phi\cos(kl)}{E_s A_s} + \frac{1}{E_c A_c} + \frac{(1-\phi)}{E_s A_s}\right] P \tag{3.42}$$

$$c_4 = \frac{-\phi}{k E_s A_s} P \tag{3.43}$$

and

$$P = \left[\frac{-2k \sin(k\ell)}{1 + \cos(k\ell)}\left(\frac{E_s A_s}{1 + n\rho}\right)\right] (\delta_{av} + m) \tag{3.44}$$

3.1.4 Sample Pullout Tests and Results

In order to predict the bond stress distribution, a number of pullout specimens were tested. The concrete mix was designed to give a concrete compressive strength of 25 MPa at the time of testing. The three sizes of concrete specimens tested were 150 mm diameter by 300 mm long, 200 mm diameter by 300 mm long and 150 mm diameter by 150 mm long. The reinforcing bar sizes used were No. 25 and No. 35, all having a specified yield stress of 400 MPa. Table 3.1 presents the details of the specimens tested.

Specimens labelled "A" and "B" were tested with a new testing technique (see Section 2.1) and the specimens labelled "C" and "D" were tested as standard pullout specimens. In both cases the load is applied through threaded screws and is recorded by load cells. This method of loading permits performing of the experiment under strain control rather than load control, enabling the post-peak response to be determined. Two different types of failure, splitting failure and pullout failure were investigated. A summary of the test results is given in Table 3.1. Table 3.2 presents the bond stiffness obtained from the test results. These values are used to study the bond stress distribution along the reinforcing bar.

Table 3.1: Summary of pullout test results

Specimen	Cylinder diameter x length (mm)	d_b (mm)	Failure mode	Maximum pullout force (kN)	Maximum average bond stress (MPa)	Average slip (mm)
25A	150 x 300	25.2	P	201	8.5	0.60
25B	200 x 300	25.2	S	86	3.6	0.31
25C	150 x 300	25.2	P	111	4.7	0.64
25D	150 x 150	25.2	P	52	4.4	0.37
35A	150 x 300	35.7	S	98	3.0	0.36
35B	200 x 300	35.7	S	119	3.6	0.21
35C	150 x 300	35.7	S	76	2.3	0.52
35D	150 x 150	35.7	S	33	2.0	0.30

P = pullout failure

S = splitting failure

Table 3.2: Bond stiffness of pullout specimens, (MPa / mm)

	25A	25B	25C	25D	35A	35B	35C	35D
E_b	13.86	12.90	7.99	12.77	9.61	18.91	4.54	7.24
E_d	*	-3.84	*	*	-2.83	-2.35	-4.25	-0.97

* Pullout failure

3.1.5 Comparison of Predicted Bond Stress Distributions in Different Pullout Specimens

The test specimens, having the properties described above, were used to study the bond stress distributions along reinforcing bars embedded in concrete. Based on equations developed in previous sections, the bond stress distributions were predicted as described below:

a) Pullout Failure

Figure 3.6 shows the bond stress distributions predicted using Eq. (3.13) for specimens 25C and 25A. As can be seen the predicted bond stress distribution in a standard pullout test is not uniform, as expected. The ratio of maximum to average bond stress is 1.37 and the ratio of maximum to minimum bond stress is 1.67. A suitable combination of pullout and push-in forces can simulate a nearly uniform bond stress distribution along the bar (see Fig. 3.6(b)). In this case the ratio of maximum to average bond stress is 1.10 and the ratio of maximum to minimum bond stress is 1.16. These predictions demonstrate that with a combination of pullout and push-in forces a nearly uniform bond stress distribution results.

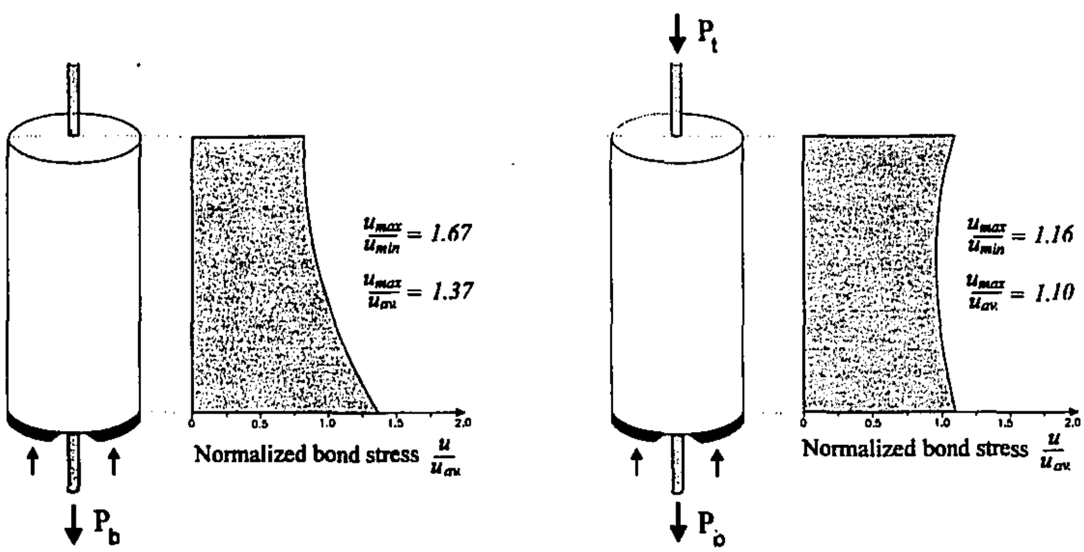

a) Specimen 25C

b) Specimen 25A

Figure 3.6: Bond stress distribution in specimens failing by pullout

b) Splitting Failure

The response of a bond specimen, governed by splitting has two distinct regions of response, before cracking and after cracking. These are discussed below:

1) Before cracking

Figure 3.7 shows the bond stress distributions predicted using Eq. (3.25) for specimens 35C and 35A. For the standard pullout test the ratio of maximum to average bond stress is 1.26 and the ratio of maximum to minimum bond stress is 1.39. A suitable combination of pullout and push-in forces can simulate a nearly uniform bond stress distribution along the bar (see Fig. 3.7(b)). The ratio of maximum to average bond stress is 1.11 and the ratio of maximum to minimum bond stress is 1.12.

2) After cracking

Equation (3.27) is used to study bond stress distribution in a splitting type of failure after cracking. Figure 3.7(c) shows the bond stress distribution in specimen 35C while Fig. 3.7(d) shows the bond stress distribution in specimen 35A. The predicted bond stress distribution is almost uniform, even for the case of the standard pullout test, once significant splitting cracks have formed. As can be seen, the combined pullout and push-in test can achieve almost uniform bond stress for specimens failing by splitting.

3.1.6 Effect of Specimen Size

The predicted ratios of maximum to minimum bond stress given in Fig. 3.6 and 3.7 are dependent on the length of the specimen (300 mm length was used for the predictions). As the length of the specimen decreases, the bond stress becomes more uniform. Because of this, early attempts by the other researchers to determine bond strength under nearly uniform bond stress, involved very short embedment lengths. However, these very short embedment lengths gave rise to unrealistically high bond strength results. On the other hand, the use of a longer embedment length in a simple pullout test gives a large variation between the maximum and minimum bond stress. For this reason the bond strength determined, an assumed average bond stress, is not representative.

The combined "push-in" and "pullout" specimen enables a reasonable size of specimen to be used (say 300 mm long) while achieving a nearly uniform bond stress distribution. Hence, the bond strength obtained from such a test represents a more realistic material characteristic.

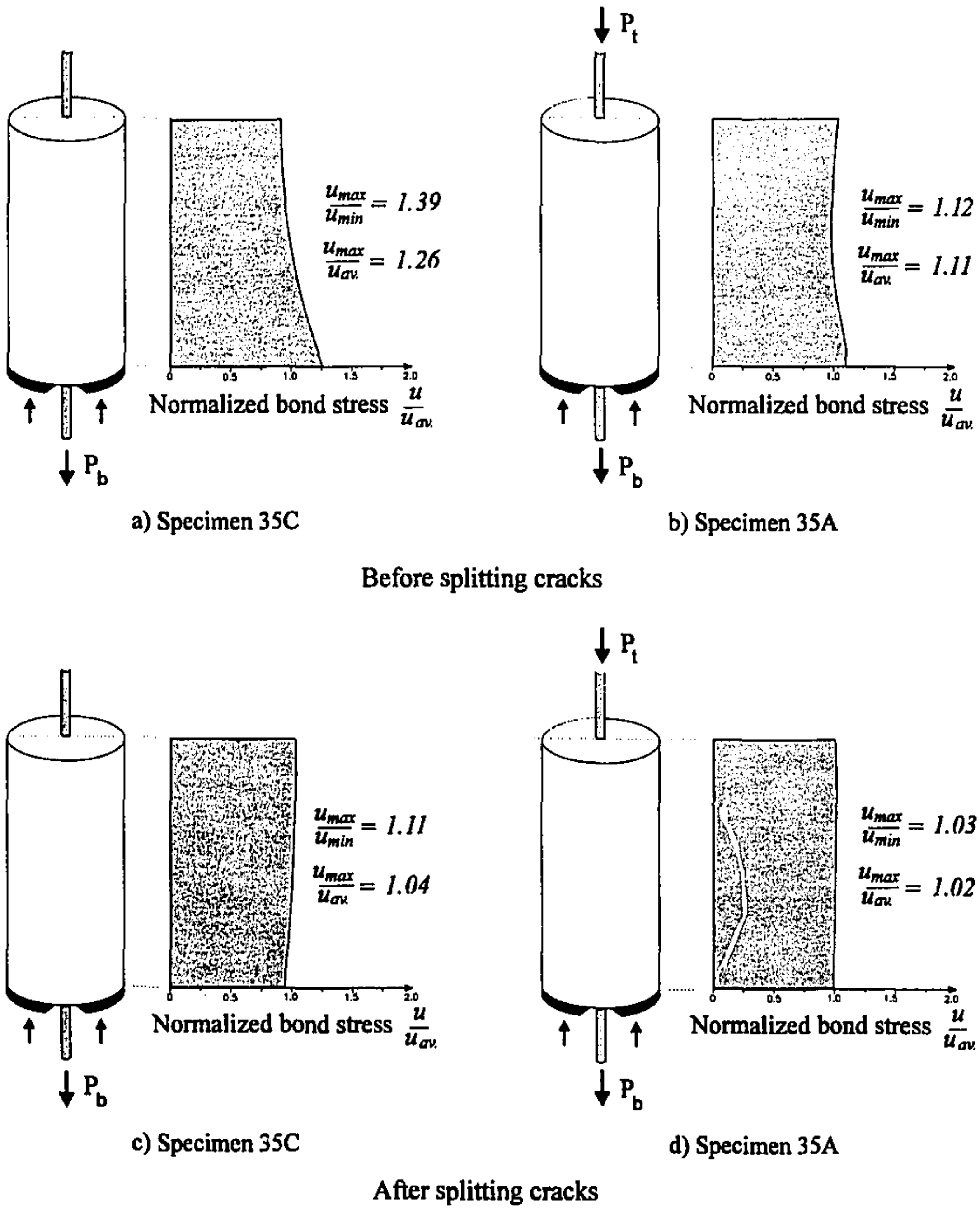

Figure 3.7: Bond stress distribution in specimens failing by splitting

3.2 ANALYTICAL STUDY TO DETERMINE TRANSFER LENGTH AND DEVELOPMENT LENGTH OF PRETENSIONED STRAND

Pretensioned members rely on the bond between the pretensioning steel (usually strand) and the concrete. In a pretensioned concrete member there are two distinct regions having different bond characteristics; the transfer length region and the flexural bond length region (see Fig. 3.8). The length of strand at the ends of a pretensioned member over which the stress in the steel builds-up is called the transfer length. The flexural bond length is the additional length required beyond the transfer length in order to develop the stress associated with the superimposed loading. Experimental investigations to determine the transfer length and flexural bond length rely on measurements of the concrete surface strain at the level of the strand or the steel strain measured along the strand.

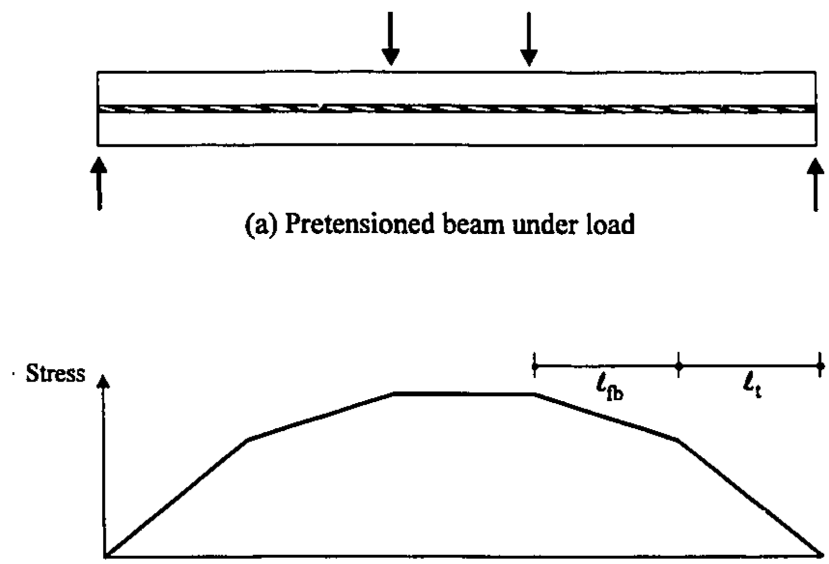

(a) Pretensioned beam under load

(b) Idealized variation of stress in strand

Figure 3.8: Transfer length and flexural bond length in a pretensioned member

Based on the beam test results reported by Hanson and Kaar (1959), an empirical relationship was adopted by the ACI Building Code in 1963 (ACI 1963) which is still used in the 1989 ACI Code (ACI 1989). The ACI equation appears in the following form:

$$\ell_d = \left(f_{ps} - \frac{2}{3} f_{se} \right) d_b \qquad \text{(ksi, in. units)} \qquad \textbf{(3.45)}$$

where ℓ_d is the development length, f_{ps} is the stress in the prestressing steel at the critical section, f_{se} is the effective stress in the prestressing steel after all losses and d_b is the nominal diameter of the strand. Equation (3.45) can be expressed as follows:

$$\ell_d = \frac{f_{se}}{3} d_b + (f_{ps} - f_{se}) d_b \qquad \text{(ksi, in. units)} \qquad \textbf{(3.46)}$$

or in MPa, mm units:

$$\ell_d = 0.048\, f_{se}\, d_b + 0.145\, (f_{ps} - f_{se})\, d_b \qquad \textbf{(3.47)}$$

In this form, the first term is the transfer length and the second term is the flexural bond length. Figure 3.9 shows the variation of strand stress along the transfer length and flexural bond length predicted by the ACI Code expression.

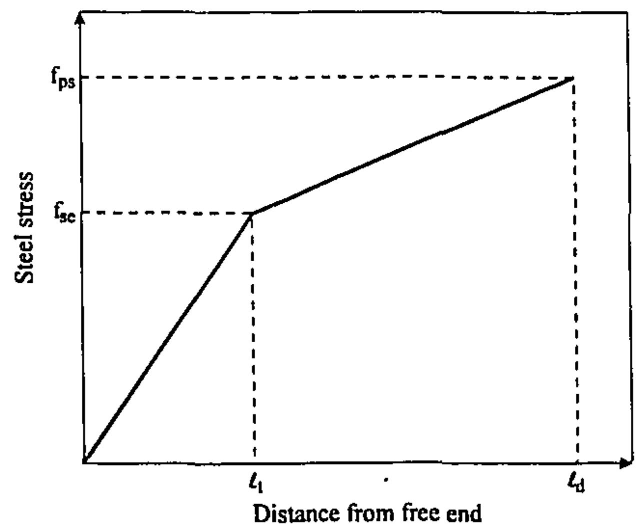

Figure 3.9: Development of stress in pretensioned strand

Zia and Mostafa (1977) developed empirical equations for the transfer length and flexural bond length of prestressing strand based on a linear regression analysis of available research data published before 1977. These equations allow for adjustment for different concrete strengths.

Cousins *et al.* (1990) also proposed an analytical model for both transfer length and development length, assuming both elastic and inelastic regions along the transfer length and the flexural bond length. The analysis considers both uncoated and epoxy-coated strand. Mitchell *et al.* (1993) studied the influence of concrete strength on transfer and development length and developed equations for these lengths accounting for a wide range of concrete strengths. A summary of the research conducted to determine the transfer and development length equations is given by Tabatabai and Dickson (1993) and Deatherage *et al.* (1994).

In order to predict the transfer length and development length of pretensioning strand, a new testing technique was developed to investigate the bond characteristics of pretensioned strand (Abrishami and Mitchell 1993). The key feature of this method is the determination of the bond strength in a more direct manner, from measured forces in the strand, rather than from strains measured on the strand or on the concrete surface in beam specimens. The bond specimen includes a standard sized cylinder, 150 mm in diameter and 300 mm long, containing a single strand. The method of testing is described in Section 2.2. The complete response of a specimen is obtained by plotting the bond stress versus the slip. It is noted that all bond failures that occurred were by "pullout" of the strand rather than by splitting of the concrete, as expected. Figure 3.10(a) and 3.10(b) show the typical bond stress versus slip responses of two specimens along the transfer length and flexural bond length, respectively. The bond strengths obtained from these tests were used to determine transfer and development lengths.

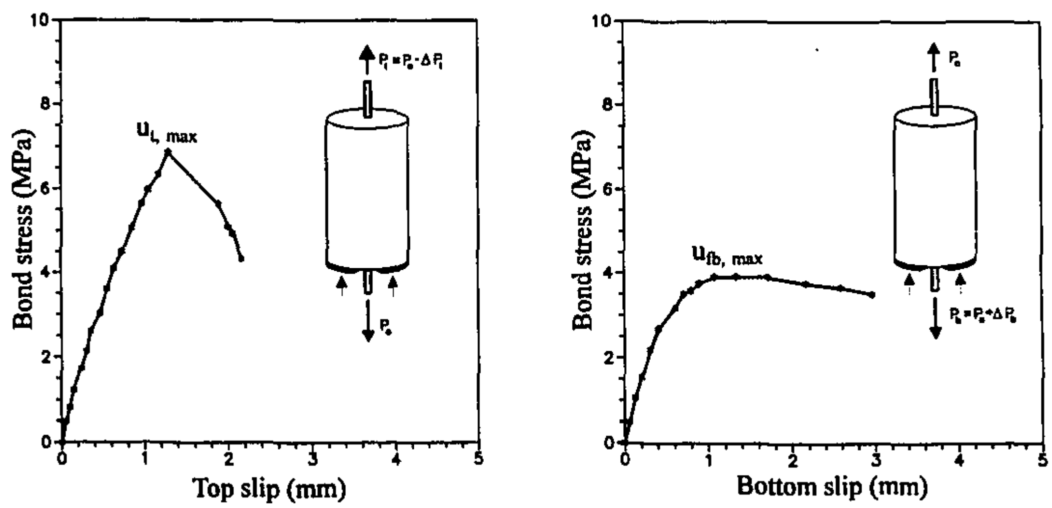

a) Transfer length test

b) Flexural bond length test

Figure 3.10: Bond stress versus slip along transfer and flexural bond lengths

3.2.1 Governing Differential Equation

Figure 3.11 illustrates the equilibrium conditions for a portion of a pretensioned strand of length, dx . The bond stress, u , can be expressed as the change in the stress in the strand over the length, dx , as follows:

$$u\ (\pi d_b\ dx) = A_s\ (f_s + df_s) - A_s f_s \tag{3.48}$$

or:

$$u = \frac{A_s}{\pi d_b} \frac{df_s}{dx} \tag{3.49}$$

where d_b is the diameter and A_s is the area of the pretensioning strand and f_s is the stress in the strand. Equation 3.49 demonstrates that the bond stress is proportional to the rate of the change of the stress in the strand, df_s/dx . Hence, if the stress in the strand varies linearly, then the bond stress must be uniform and if the strand stress varies parabolically, the bond stress must be linear.

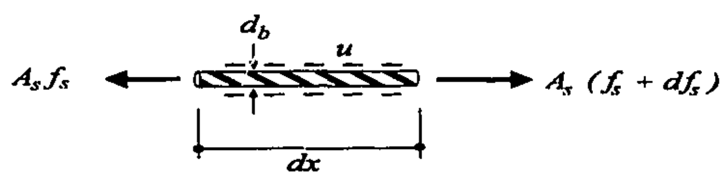

Figure 3.11: Forces acting on a pretensioning strand

3.2.2 Proposed Analytical Model for Transfer Length

Figure 3.12 illustrates the stress distribution in the strand as well as the bond stress distribution along the transfer length in a pretensioned member. Parabolic variations in strand stress are assumed near the end of the strand and near the end of the transfer length while a linear variation is assumed in the middle region of the transfer length (see Fig. 3.12(b)). Based on these stress distributions and using Eq. (3.49), the bond stress distribution, including an elastic region and inelastic region, can be obtained as shown in Fig. 3.12(c). It is clear that at the free end of the pretensioned member the force in the strand is zero, while at the other end of the transfer length (see Fig. 3.12(d)), the stress in the strand is equal to the stress in the strand at release, f_{pi} . The following expression is derived by integrating the bond stress, u, along the transfer length and equating the resultant with the initial force in the strand:

$$\frac{u_{t,\max}}{2}\left(\ell_1 + 2\ell_2 + \ell_3\right) = A_s\, f_{pi} \tag{3.50}$$

and hence the transfer length, ℓ_t , can be written as:

$$\ell_t = \frac{A_s}{\pi\, d_b}\frac{f_{pi}}{u_{t,\max}} - \ell_2 \tag{3.51}$$

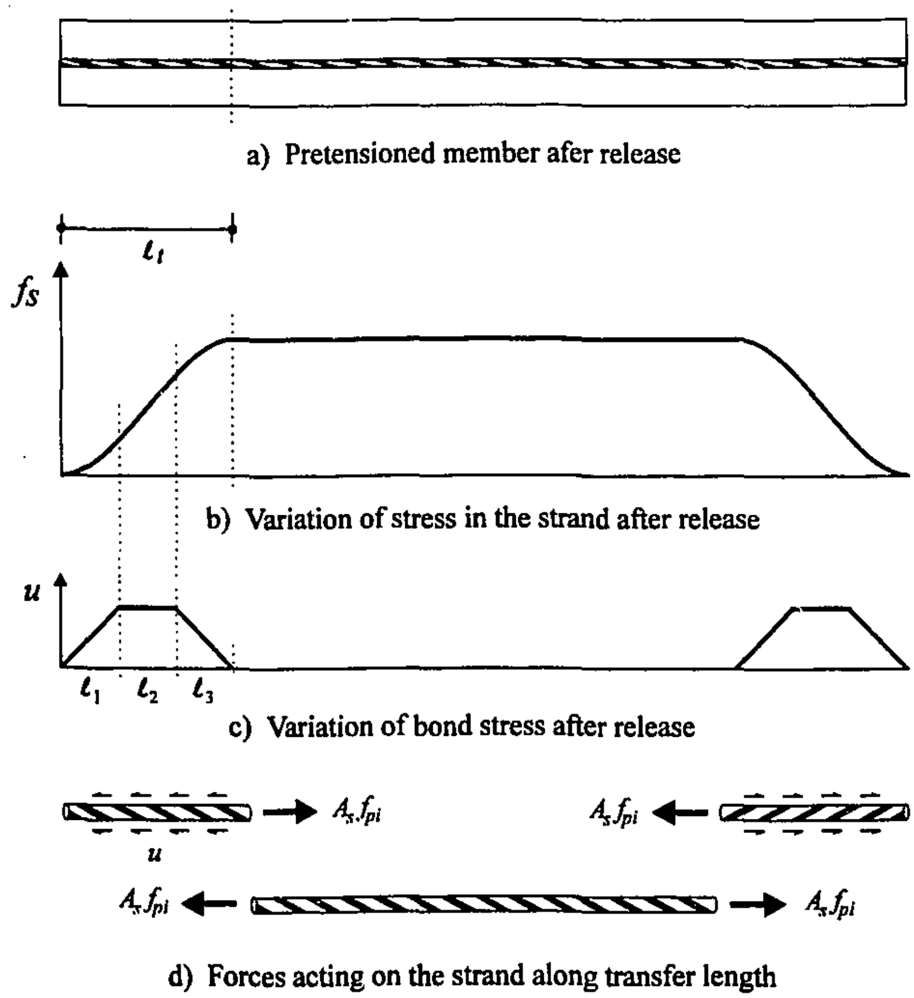

Figure 3.12: Assumed bond stress distribution along the transfer length

where ℓ_2 is the length of the inelastic region along the transfer length, f_{pi} is the stress in the strand at release and $u_{t,max}$ is the maximum bond stress achieved along the transfer length.

The minimum value of ℓ_2 is zero giving a triangular bond stress distribution as shown in Fig. 3.13(a) and the maximum value of ℓ_2 is ℓ_t resulting in a uniform bond stress distribution as shown in Fig. 3.13(b). Hence the upper and lower bounds on the predicted transfer lengths are:

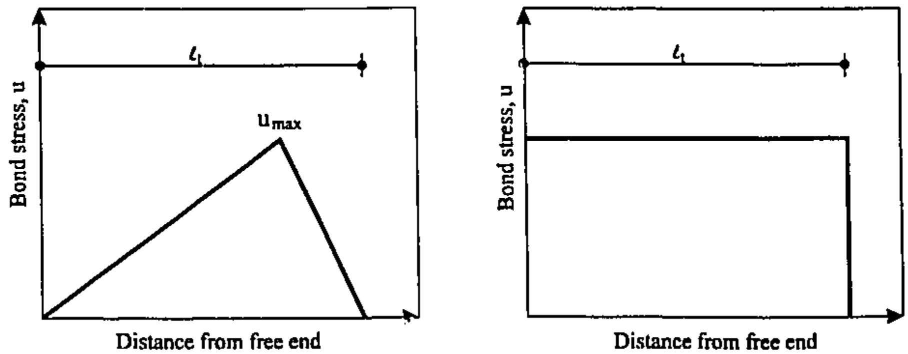

Figure 3.13: Linear and uniform bond stress distribution along the transfer length

(a) upper bound from triangular bond stress distribution:

$$\ell_t = 2\frac{f_{pi}}{u_{t,max}}\frac{A_s}{\pi d_b} \tag{3.52}$$

(b) lower bound from uniform bond stress distribution:

$$\ell_t = \frac{f_{pi}}{u_{t,max}}\frac{A_s}{\pi d_b} \tag{3.53}$$

3.2.3 Proposed Analytical Model for Flexural Bond Length

Figure 3.14 shows the stress distribution in the strand as well as the bond stress distribution along the flexural bond length in a pretensioned member. Using the same approach described above for the transfer length, the bounds on the flexural bond length can be expressed as:

(a) upper bound from triangular bond stress distribution:

$$l_{fb} = 2\frac{(f_{ps}-f_{se})}{u_{fb,\max}}\frac{A_s}{\pi d_b} \tag{3.54}$$

(b) lower bound from uniform bond stress distribution:

$$\ell_{fb} = \frac{(f_{ps}-f_{se})}{u_{fb,\max}}\frac{A_s}{\pi d_b} \tag{3.55}$$

where $u_{fb,\max}$ is the maximum bond stress along the flexural bond length, f_{ps} is the stress in the strand at the critical section and f_{se} is the stress in the strand after all losses.

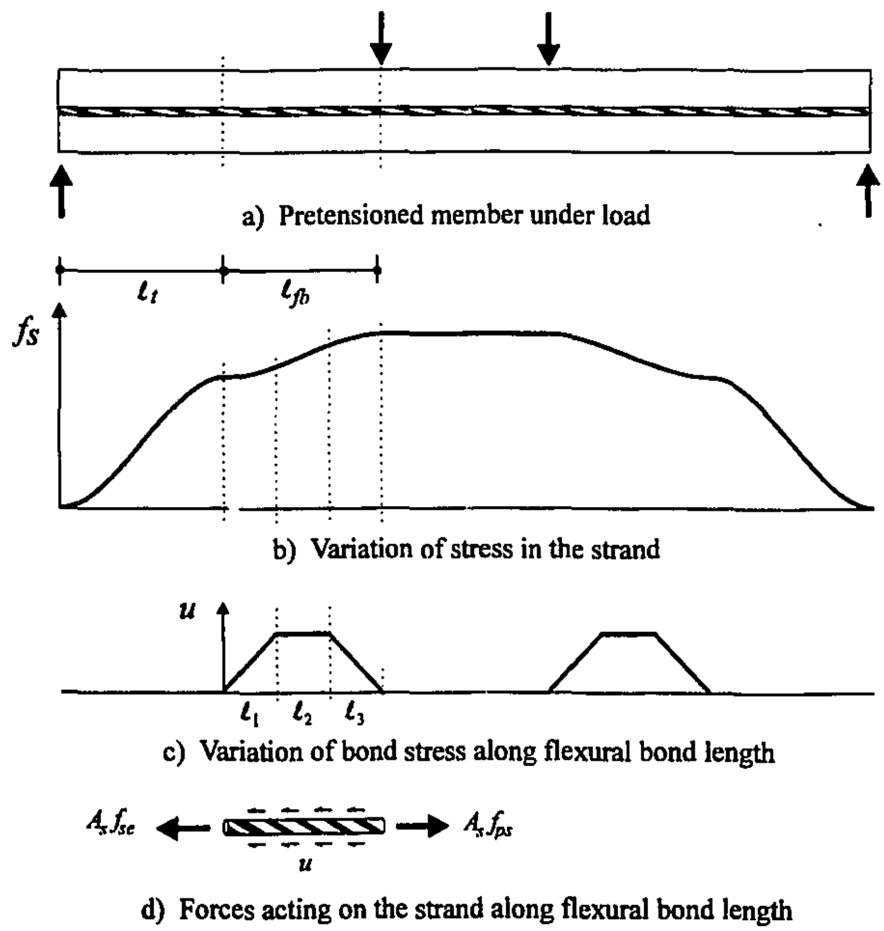

Figure 3.14: Assumed bond stress distribution along the flexural bond length

3.2.4 Prediction of Transfer Length and Development Length

From Eqs. (3.52) and (3.53) the transfer length can be expressed as:

$$\ell_t = k\alpha \frac{f_{pi}}{u_{t,\max}} \tag{3.56}$$

where $k = A_s/\pi d_b$ is a factor which depends on the strand size, and α is a parameter which reflects the bond stress distribution (varying from 1, for uniform bond stress to 2, for a triangular bond stress distribution). From Eqs. (3.54) and (3.55) the flexural bond length can be expressed as:

$$\ell_{fb} = k\alpha \frac{(f_{ps}-f_{se})}{u_{fb,\max}} \tag{3.57}$$

Both the bond strength along the transfer length and flexural bond length have been determined experimentally (see Section 2.2) and are functions of the concrete strength.

It is important to account for the different stages in the life of a pretensioned member. At release, the stress in the strand is f_{pi} . With time this stress will reduce from f_{pi} to f_{se} due to relaxation of the strand as well as creep and shrinkage of the concrete (see Fig. 3.15). It is assumed that before loading the member the stress in the strand drops to f_{se} , but without a change in the transfer length. Thus the transfer length is a function of f_{pi} and the flexural bond length is a function of the required stress increase in the strand, $f_{ps} - f_{se}$ as shown in Fig. 3.15.

3.2.5 Sample Test Results from Experimental Studies

In order to determine the bond strength along the transfer length and the flexural bond length a new experimental testing technique was developed (Abrishami and Mitchell 1993) as described in Section 2.2. The bond specimens all had a concrete compressive strength of 25 MPa at the time of testing. Three different seven-wire strand diameters, 9.5, 13 and 16 mm were used.

Specimens ladled "A", represent transfer length tests and specimens ladled "B" represent flexural bond length tests. The values of bond strengths along the transfer lengths and the flexural bond lengths are summarized in Table 3.3.

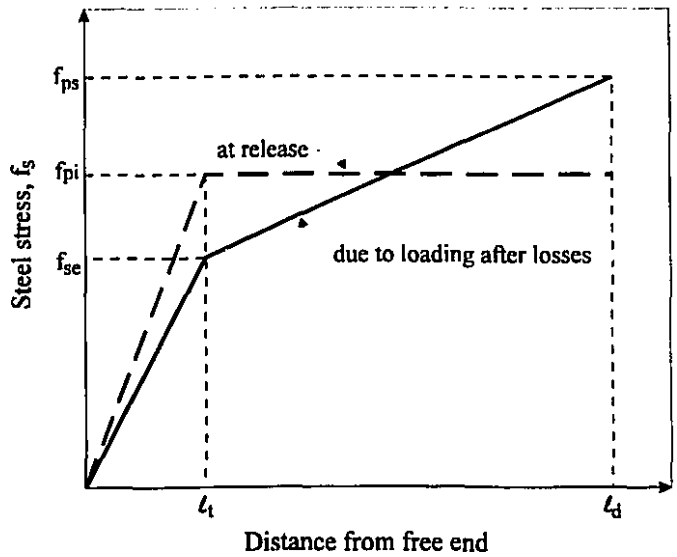

Figure 3.15: Assumed steel stress distribution along the flexural bond length

As can be seen from Table 3.3, the bond strengths varied from 6.7 MPa to 8.3 MPa along the transfer length. Also the bond strengths varied from 3.1 to 5.4 MPa along the flexural bond length. The average of these values were used in the transfer length and development length expressions. In computing the average bond strength, the higher bond strengths for the slightly rusted 9.5 mm strand were not included in the data.

3.2.6 Influence of Concrete Strength on Transfer and Development Length

The bond strengths given in Table 3.3 were obtained from tests on bond specimens having a concrete compressive strength of 25 MPa. Several researchers have shown that the transfer length and flexural bond length are inversely proportional to $\sqrt{f_c'}$ (e.g., Mitchell *et al* 1993). Hence, to include the effect of concrete strength on both the transfer and development lengths, Eqs. (3.56) and (3.57) can be expressed as:

$$\ell_t = k\alpha \sqrt{\frac{25}{f_{ci}^{\prime}} \frac{f_{pi}}{u_{t,\max}}} \qquad \text{(MPa, mm)} \qquad \textbf{(3.58)}$$

and:

$$\ell_d = k\alpha \sqrt{\frac{25}{f_{ci}^{\prime}} \frac{f_{pi}}{u_{t,\max}}} + k\alpha \sqrt{\frac{25}{f_c^{\prime}} \frac{(f_{ps}-f_{se})}{u_{fb,\max}}} \qquad \text{(MPa, mm)} \qquad \textbf{(3.59)}$$

For seven wire strand, k is about 0.19 d_b. The assumption of a triangular bond stress distribution is more compatible with the measured variation of relative slip along the length of the strand (see Fig. 3.10) than the assumption of a uniform bond stress distribution. Therefore the factor α will be conservatively taken as 2. The average values of $u_{t,\max}$ and $u_{fb,\max}$ are 7.46 and 3.47 MPa, respectively. Hence:

$$\ell_t = 0.255 \frac{f_{pi}}{\sqrt{f_{ci}^{\prime}}} d_b \qquad \text{(MPa, mm)} \qquad \textbf{(3.60)}$$

and:

$$\ell_d = 0.255 \frac{f_{pi}}{\sqrt{f_{ci}^{\prime}}} d_b + 0.548 \frac{(f_{ps}-f_{se})}{\sqrt{f_c^{\prime}}} d_b \qquad \text{(MPa, mm)} \textbf{(3.61)}$$

3.2.7 Comparison of Proposed Equation with ACI Development Length Expression

Table 3.4 compares the development lengths predicted from Eq. (3.61) with those predicted using the ACI empirical expression (Eq. (3.47)). These predicted lengths are based on a concrete strength, $f_{ci}^{\prime}$ = 21 MPa at release, initial prestressing stress, f_{pi} = 1290 MPa, an ultimate concrete strength of $f_c^{\prime}$ = 25 MPa, an effective prestressing stress, after all losses, f_{se} = 1080 MPa and a stress in the pretensioning strand at the critical section, f_{ps} = 0.90 f_{pu} = 1674 MPa.

Table 3.3: Experimentally determined bond strengths for strand

Specimen	d_b (mm)	$u_{t,max}$ (MPa)	$u_{fb,max}$ (MPa)
9.5A1	9.5	7.7	----
9.5A2	9.5	6.7	----
9.5A3	9.5	7.8	----
13A1	13	6.9	----
13A2	13	6.9	----
13A3	13	7.5	----
16A1	16	8.3	----
16A2	16	7.1	----
16A3	16	8.2	----
9.5B1	9.5	----	4.2
9.5B2	9.5	----	5.4
9.5B3	9.5	----	4.9
13B1	13	----	3.6
13B2	13	----	3.5
13B3	13	----	3.3
16B1	16	----	3.6
16B2	16	----	3.7
16B3	16	----	3.1

As can be seen from Table 3.4, both methods give the same development length. However, the ACI equations have a shorter transfer length and a longer flexural bond length than that proposed. The basic bond tests performed as part of this research program enable a direct comparison of the bond strengths for both the transfer length and the flexural bond length. In addition, the proposed expressions account for a wide range of concrete strengths.

Table 3.4: Comparison of predicted and ACI expression for development length

d_b (mm)	Development length, (mm)		
	ACI $\ell_d = \ell_t + \ell_{fb}$	Proposed $\ell_d = \ell_t + \ell_{fb}$	$\ell_{d,prop.} / \ell_{d,ACI}$
9.5	1311 = 493 + 818	1300 = 682 + 618	0.99
13	1794 = 674 + 1120	1779 = 933 + 846	0.99
16	2208 = 829 + 1379	2190 = 1148 + 1042	0.99

Chapter 4

EXPERIMENTAL STUDIES OF CRACKING IN REINFORCED CONCRETE ELEMENTS

"The basics apply to the most sophisticated structures"

Ben C. Gerwick, Jr., 1988

The primary objective of this chapter is to study the basic concepts necessary to understand the behaviour of simple structural members such as tension elements, beams and slabs. The effects of different concretes, such as normal-strength, high-strength and steel-fibre reinforced concrete, are studied. Different sizes of uncoated reinforcing bars and bars with one of two different epoxy coating thicknesses were used to investigate the influence of epoxy coatings on the post-cracking response of typical reinforced concrete elements.

4.1 RESPONSE OF MEMBERS SUBJECTED TO PURE TENSION

This section describes the experimental program and test results of series of tension specimens carried out. The purpose of these series of tests was to determine the influence on cracking of:

(a) reinforcing bar size;

(b) epoxy-coating on the reinforcing bars;

(c) concrete strength; and

(d) steel fibre-reinforced concrete.

Forces are transferred from the reinforcement to the concrete by bond stress which is of fundamental importance in the response of reinforced concrete members subjected to tension.

Fig. 4.1 illustrates the manner in which the axial load is shared between the concrete and the reinforcement and how this load sharing is influenced by the formation of cracks. Prior to cracking (see Fig.4.1(a)) the load carried by the concrete, T_c , and the load carried by the steel, T_s , remain constant along the length of the member. After the first primary crack forms, T_c and T_s are no longer constant along the member (see Fig. 4.1(b)).

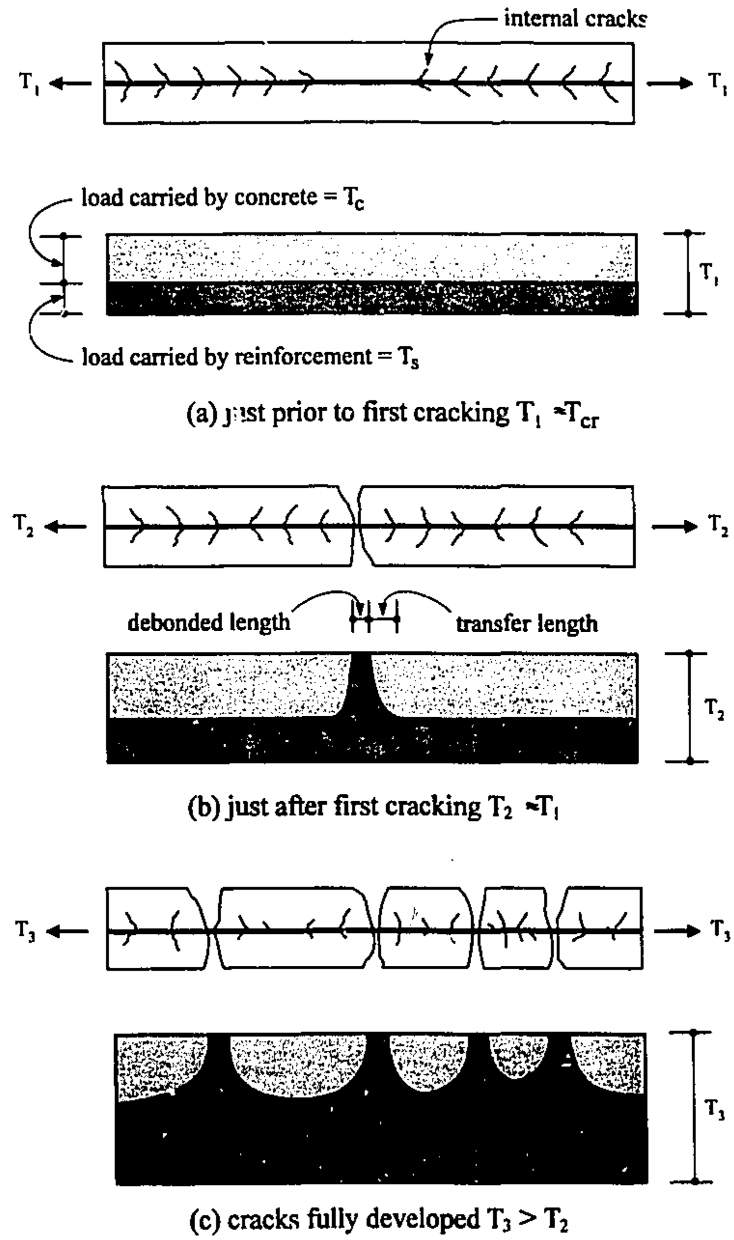

Figure 4.1: Load sharing between concrete and reinforcement, adapted from Collins and Mitchell (1991)

The load sharing along the length of the member for a fully developed crack pattern is shown in Fig. 4.1(c). The distribution of steel stress, f_s , bond stress, u , and concrete stress, f_c , is shown in Fig. 4.2. Figure 4.3 shows the tension versus elongation response of a reinforced concrete element and the response of the reinforcement alone ("bare bar" response). The tension carried by the concrete, T_c , stiffens the response. This "tension stiffening" effect is important in reducing deformations in reinforced concrete elements.

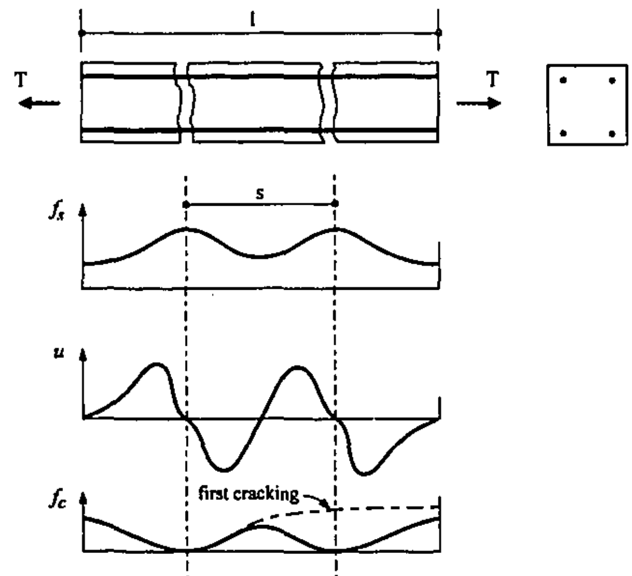

Figure 4.2: Distribution of steel stress, bond stress and concrete stress in a tension specimen, adapted from CEB Manual (1985)

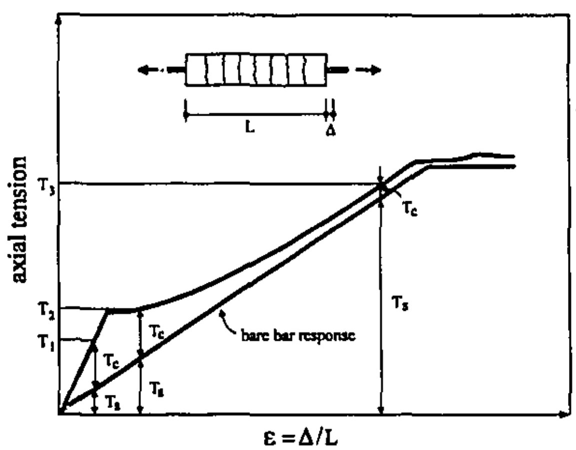

Figure 4.3: Influence of tension in concrete on load-deformation response, adapted from Collins and Mitchell (1991)

4.1.1 Response of Normal-Strength Concrete Tension Specimens

This section describes the behaviour of fifteen tension specimens each containing a single reinforcing bar. The purpose of this part of the study is to investigate the influence of bar size and epoxy coating thickness on tension stiffening and cracking in normal-strength concrete specimens. Both splitting cracks and transverse tensile cracks are studied.

4.1.1.1 Test Program

Figure 4.4 shows the geometry and instrumentation for a typical tension specimen. All of the specimens had a length of 1500 mm. A single reinforcing bar with minimum concrete cover of approximately 40 mm, was provided in each specimen. The specimen was varied so that the reinforcement ratio, ρ, was a constant 1.23%. The reinforcing bar extended 250 mm outside of the ends of the concrete.

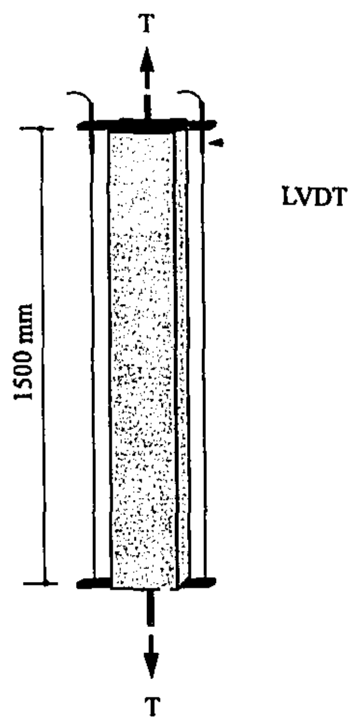

Figure 4.4: Typical tension specimen

The concrete compressive strength, f_c', was obtained by testing standard cylinders having a diameter of 150 mm and a height of 300 mm. The modulus of rupture, f_r, was determined from flexural tests on 100 mm by 100 mm by 400 mm long beams which were subjected to third-point loading over a span of 300 mm.

Tests to determine the splitting tensile strength, f_{sp}, were carried out on 150 mm diameter by 300 mm long cylinders. The average compressive strength, f_c', modulus of rupture, f_r, and splitting strength, f_{sp}, of the concrete were 34.9, 4.3 and 3.1 MPa, respectively. The testing of the tension specimens, as well as the concrete specimens, was carried out at an average concrete age of 105 days.

The nominal diameters of the bar sizes used were 10 mm, 15 mm, 20 mm, 25 mm and 30 mm and all had a specified yield strength of 400 MPa. Three different surface conditions were provided on each reinforcing bar size. The specimens labelled "C0" contained uncoated bars, while those labelled "C1" and "C2" contain bars with epoxy coating thicknesses of 6-8 mils and 10-12 mils, respectively. Table 4.1 presents the details of the specimens tested.

The test setup consisted of a loading frame transmitting the load through a set of tension grips at the top and the bottom of the reinforcing bar. This resulted in tension being transferred from the steel reinforcing bar to the reinforced concrete section. A linear voltage differential transducer (LVDT) was placed along each side of the specimen as shown in Fig. 4.4. These transducers, which were clamped to the steel reinforcing bar just outside of the concrete, measured the total elongation of the reinforced concrete specimen. At each load stage the cracks were measured using a crack width comparator. The complete response of each specimen is described by plotting the applied tension versus the average member elongation.

4.1.1.2 Load Deflection Responses

Figure 4.5 shows the tension versus elongation responses of two specimens, C0-10 and C0-30, reinforced with No. 10 and No. 30 uncoated reinforcing bars, respectively. Also shown in this figure is the response of a bare bar (i.e., without concrete). Due to shrinkage of the concrete the elongation of the specimens is negative prior to load application. An average free shrinkage strain of -0.3×10^{-3} was determined from strain measurements on 100 mm by 100 mm by 400 mm long shrinkage specimens which had the same curing conditions as the test specimens.

Table 4.1: Details of normal-strength concrete tension specimens

Specimen	Cross-sectional dimensions (mm)	d_b (mm)	Measured yielding stress, f_y (MPa)	Type of cracking	$T_{sp} / A_s f_y$	Average crack spacing (mm)	Max. crack spacing (mm)
C0-10	90 x 90	11.3	420	T	---	167	200
C1-10	90 x 90	11.3	460	T	---	187	260
C2-10	90 x 90	11.3	460	T	---	167	240
C0-15	95 x 170	16.0	480	T-S	1.00	214	295
C1-15	95 x 170	16.0	480	T-S	0.68	300	340
C2-15	95 x 170	16.0	480	T-S	0.63	300	385
C0-20	100 x 245	19.5	440	T-S	0.37	375	430
C1-20	100 x 245	19.5	440	T-S	0.34	500	650
C2-20	100 x 245	19.5	440	S	0.32	---	---
C0-25	105 x 387	25.2	440	S	0.22	---	---
C1-25	105 x 387	25.2	450	S	0.17	---	---
C2-25	105 x 387	25.2	450	S	0.19	---	---
C0-30	110 x 515	29.9	530	S	0.19	---	---
C1-30	110 x 515	29.9	530	S	0.17	---	---
C2-30	110 x 515	29.9	530	S	0.12	---	---

T = transverse cracks
S = splitting cracks

As can be seen, each specimen includes elastic uncracked, post cracking and post yielding regions. In specimen C0-10, containing a No. 10 reinforcing bar, no splitting cracking was observed during the test and therefore the specimen showed significant tension stiffening even after transverse cracking (Fig. 4.5(a)). Specimen C0-30 experienced only splitting cracks during the test and hence rapidly lost its tension stiffening after these cracks formed (See Fig. 4.5(b)).

Figure 4.6(a) shows the tension versus elongation responses of specimens containing uncoated reinforcing bars. Figures 4.6(b) and 4.6(c) give the tension versus elongation responses for the specimens containing bars with epoxy coating thicknesses of 6-8 mils and 10-12 mils, respectively.

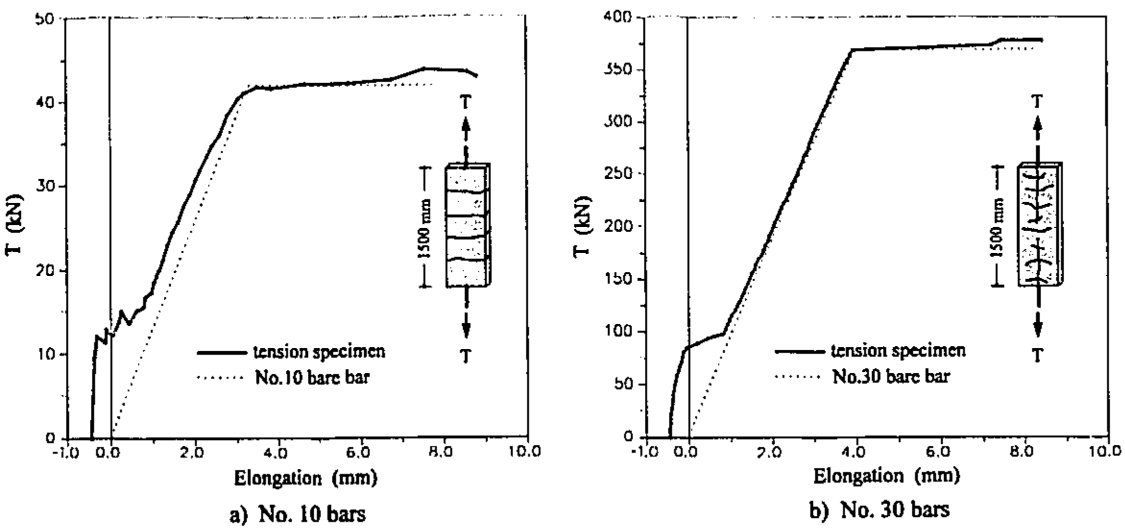

Figure 4.5: Tension responses of normal-strength concrete specimens reinforced with uncoated bars

Table 4.1 shows the ratio of the tensile force at the start of splitting cracks to the yield force of the reinforcing bar ($T_{sp} / A_s f_y$). As can be seen, no splitting cracks were observed in the specimens containing No. 10 bars. The splitting cracks in the tension specimen containing an uncoated No. 15 bar started just as the reinforcing bar yielded. Also, this table shows that splitting cracks started at lower tensions for specimens reinforced with epoxy-coated bars than for those containing uncoated bars. Also longer splitting cracks were observed at the top and bottom of the specimens as the bar size increased.

4.1.1.3 Cracking Behaviour

Figure 4.7 shows the crack patterns for specimens having different sizes of reinforcing bars having 6-8 mil epoxy coating. As can be seen, specimen C1-10, containing a No. 10 bar, has only transverse cracks, while specimen C1-30, containing No. 30 bar, exhibits only splitting cracks. The potential for forming splitting cracks increases as the bar diameter, d_b , increases and as the concrete cover, c , decreases. Recently, North American codes of practice (ACI 1989; CSA 1994b) have introduced development length expressions which account for the ratio c / d_b.

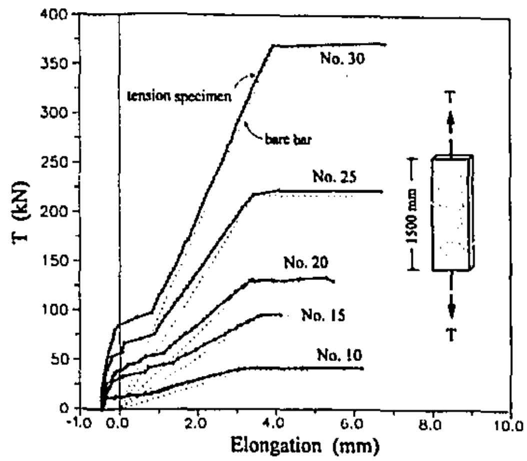

a) uncoated bars

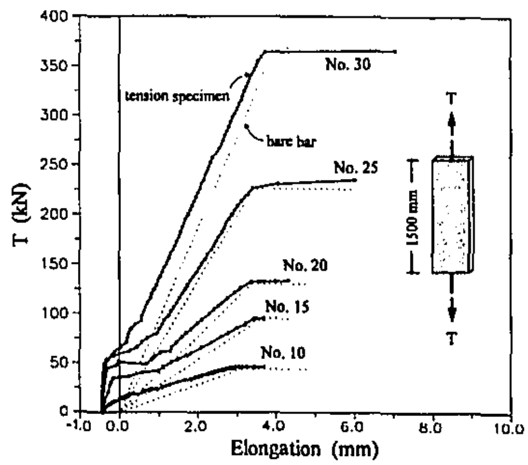

b) 6-8 mil epoxy-coated bars

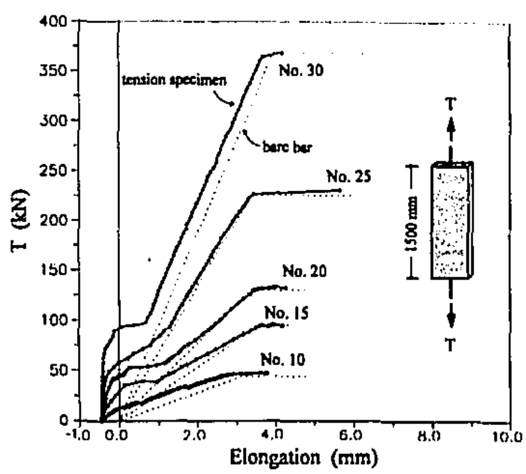

c) 10-12 mil epoxy-coated bars

Figure 4.6: Tension versus elongation responses of normal-strength concrete specimens

The first crack which appeared in specimen C0-15 was a transverse crack, while the first crack which appeared in specimen C2-15, containing a 10-12 mil epoxy-coated bar, was a splitting crack. Concrete codes (ACI 1989; CSA 1994b) have introduced modification factors for calculating the development length of epoxy-coated bars, which depend on the ratio c/d_b . This accounts for the detrimental effect splitting cracks have on the development length especially in the presence of epoxy-coated bars. The splitting crack observed in the specimen with an epoxy-coated bar is due to less bond strength in this specimen compared to the companion specimen with an uncoated bar. The first crack observed in specimens, C0-25, C1-25 and C2-25, having No. 25 bars, was a splitting crack. Specimen C0-20, containing an uncoated No. 20 bar, had an initial crack that was transverse to the longitudinal axis, whereas specimens C1-20 and C2-20, with epoxy-coated bars, had initial cracks which were splitting cracks.

Figure 4.8 compares the crack widths of tension specimens reinforced with different bar sizes. Figure 4.8(a) shows the influence of bar size on the crack width of tension specimens C0-10, C0-15 and C0-20, containing uncoated bars. Figure 4.8(b) compares the crack widths of specimens with the 6-8 mil epoxy coating thickness on the reinforcing bars (C1-10, C1-15 and C2-20), while Fig. 4.8(c) compares the crack widths of the specimens with the 10-12 mil epoxy coating thickness on the reinforcing bars (C2-10, and C2-15). As can be seen, specimens containing larger bar sizes have larger crack widths.

The average crack spacing was measured on the specimens having transverse cracks. Table 4.1 shows the average crack spacing for the different specimens. The specimens with smaller bars have smaller crack spacings than those with the larger bars and the specimens containing epoxy-coated bars have larger crack spacings than the specimens with uncoated bars, except for the specimen with a No. 10 bar having a 10-12 mil epoxy coating thickness (C2-10).

Figure 4.7: Transverse tensile cracks and splitting cracks in specimens C1-30, C1-25, C1-20, C1-15 and C1-10

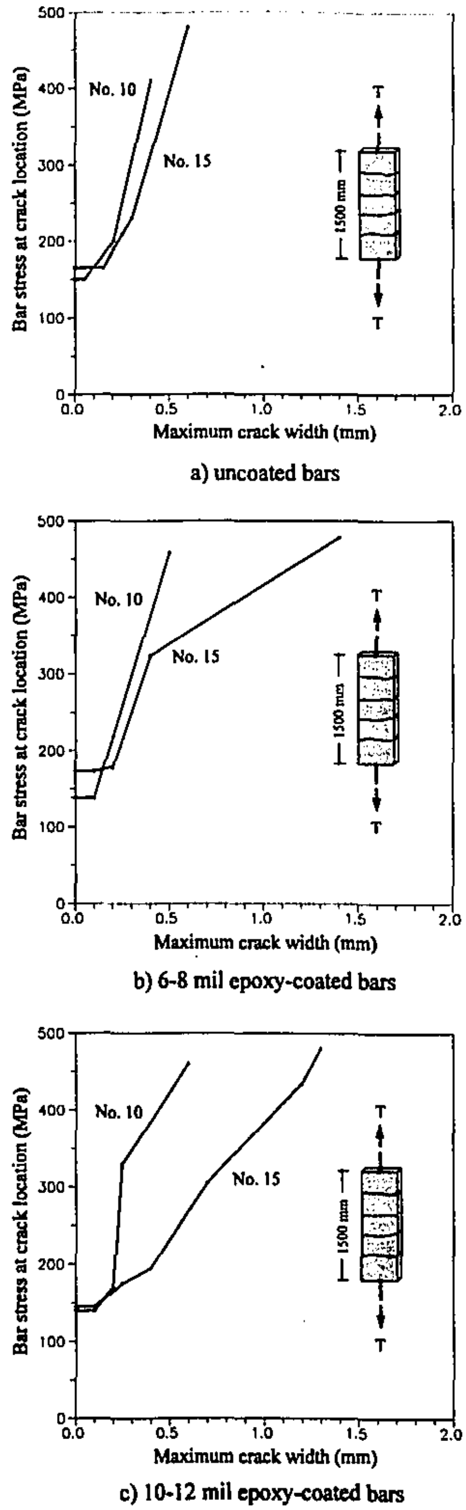

Figure 4.8: Influence of bar size on crack widths for normal-strength concrete specimens

4.1.2 Influence of High-Strength Concrete

In order to determine the effect of high-strength concrete, fifteen high-strength concrete tension specimens, reinforced with a single bar, were tested. The main interest was to investigate the effect of high-strength concrete on the tension stiffening and cracking behaviour of tension specimens. The high-strength concrete specimens had an average concrete strength of 90 MPa, a modulus of rupture of 9.8 MPa and a tensile splitting strength of 6.3 MPa. Table 4.2 presents the details of the specimens tested. At each load stage the cracks were measured using a crack width comparator.

4.1.2.1 Load Deflection Responses

Figures 4.9(a) and 4.9(b) show the tension versus elongation responses of specimens made with normal-strength and high-strength concrete and reinforced with No. 10 and No. 30 bars. Also shown in these figures are the responses of the bare bars (i.e., without concrete). Due to shrinkage of the concrete the elongation of the specimens is negative prior to load application. The average shrinkage strain of the normal-strength and high-strength concrete specimens was about -0.3×10^{-3}. It must be noted, however, that the normal-strength concrete specimens were tested at an age of 105 days, whereas the high-strength concrete specimens were tested at an age of 135 days. In the specimens reinforced with a No. 10 bar, the high-strength concrete specimen exhibits a larger stiffness than the normal-strength concrete specimen, both before and after cracking. Also the high-strength concrete specimens have a higher cracking load than the specimens made with normal-strength concrete. The high-strength concrete specimens reinforced with a No. 30 bar exhibited a higher cracking load than the specimen made with normal-strength concrete. Due to presence of splitting cracks, the responses of the high-strength and normal-strength concrete specimens are similar after cracking.

Figure 4.10 shows the responses of tension specimens reinforced with different bar sizes. Figures 4.11 and 4.12 compare the influence of high-strength concrete on the responses of specimens reinforced with No. 20 and No. 25 bar sizes. These tests demonstrate how the type of cracking influences tension stiffening. As the c/d_b ratio reduces (i.e., for the larger bar sizes) splitting cracks become more predominant (see Fig. 4.9) and give rise to significant reductions in tension stiffening.

Table 4.2: Details of high-strength concrete tension specimens

Specimen	Section dimension (mm)	d_b (mm)	Measured yield stress, f_y (MPa)	Type of cracking	$T_{sp} / A_s f_y$	Average crack spacing (mm)	Max. crack spacing (mm)
HC0-10	90 x 90	11.3	420	T	---	167	300
HC1-10	90 x 90	11.3	430	T-S	0.88	187	320
HC2-10	90 x 90	11.3	430	T-S	0.90	214	270
HC0-15	95 x 170	16.0	490	T-S	0.42	500	750
HC1-15	95 x 170	16.0	490	T-S	0.41	750	850
HC2-15	95 x 170	16.0	480	T-S	0.41	750	930
HC0-20	100 x 245	19.5	440	S	0.36	---	---
HC1-20	100 x 245	19.5	450	S	0.32	---	---
HC2-20	100 x 245	19.5	450	S	0.32	---	---
HC0-25	105 x 387	25.2	440	S	0.26	---	---
HC1-25	105 x 387	25.2	480	S	0.23	---	---
HC2-25	105 x 387	25.2	460	S	0.16	---	---
HC0-30	110 x 515	29.9	530	S	0.18	---	---
HC1-30	110 x 515	29.9	530	S	0.17	---	---
HC2-30	110 x 515	29.9	520	S	0.14	---	---

T = transverse cracks
S = splitting cracks

Therefore the specimens with very large bar sizes exhibit responses which approach the bare-bar responses after cracking. The influence on tension stiffening of epoxy coating on the bars is also apparent from Fig. 4.11 and Fig. 4.12. The presence of epoxy coating on the bars gives rise to more splitting cracks and hence gives reduced values of tension stiffening. Also, as the epoxy coating thickness increases, the tension stiffening decreases.

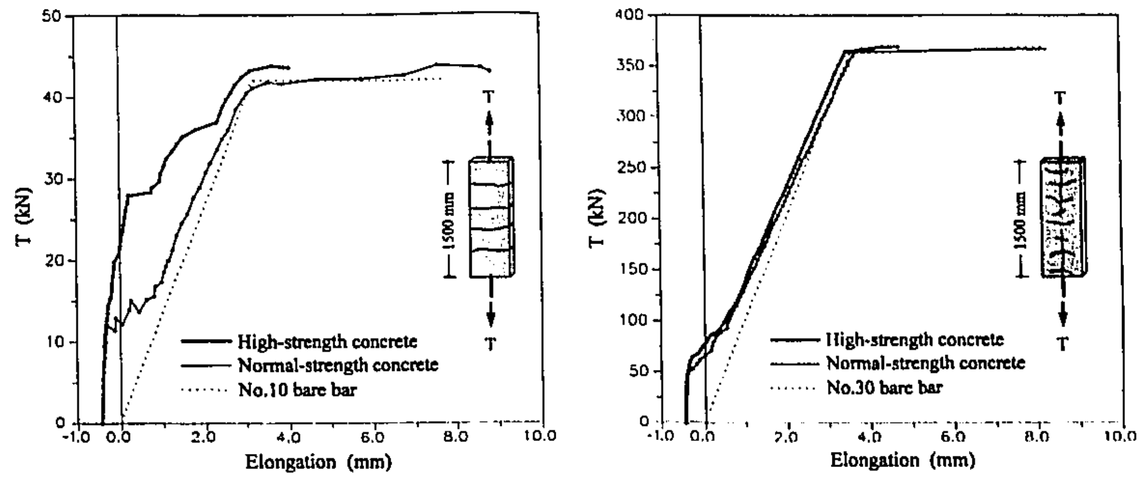

a) No. 10 uncoated bars b) No. 30 6-8 mil epoxy-coated bars

Figure 4.9: Influence of concrete strength on tension stiffening

Table 4.2 shows the ratio of the tensile force corresponding to the formation of splitting cracks to the yield force. All of the high-strength concrete specimens showed splitting cracks except specimen HC0-10, reinforced with a No. 10 uncoated reinforcing bar (see Table 4.2). By comparing Tables 4.1 and 4.2, it is evident that more splitting cracks were observed for the high-strength concrete specimens. Table 4.2 also shows that splitting cracks started at smaller tensile forces for the specimens reinforced with epoxy-coated bars, than for the specimens with uncoated bars. Also the length of the splitting cracks at the top and bottom of the specimens increased for larger bar sizes.

4.1.2.2 Cracking behaviour

Figure 4.13 shows the crack patterns of the high-strength concrete specimens having different sizes of reinforcing bars with the 6-8 mil epoxy coating. As can be seen more splitting cracks were observed for the specimens reinforced with larger bar sizes.

Figures 4.14 and 4.15 show the crack widths of specimens reinforced with No. 10 and No. 15 bar sizes, respectively. These figures show that the use of higher strength concrete generally reduced the crack widths at service load levels.

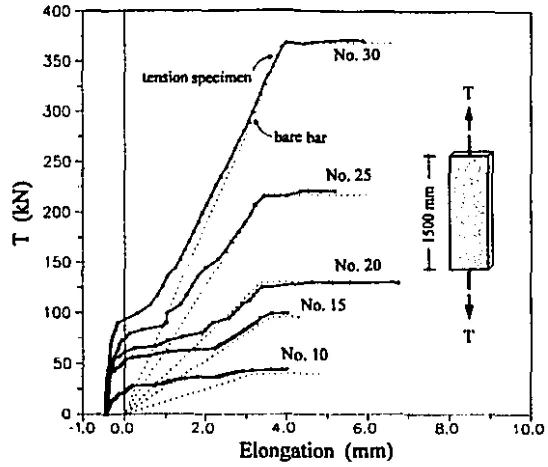

a) uncoated bars

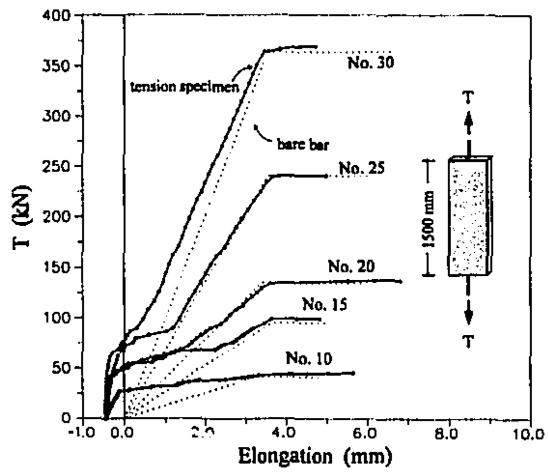

b) 6-8 mil epoxy-coated bars

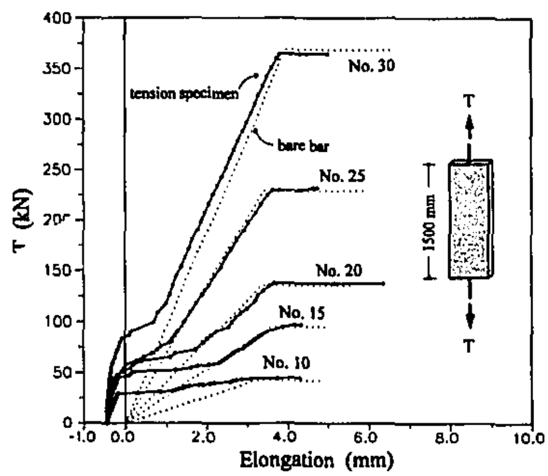

c) 10-12 mil epoxy-coated bars

Figure 4.10: Tension versus elongation responses of high-strength concrete specimens

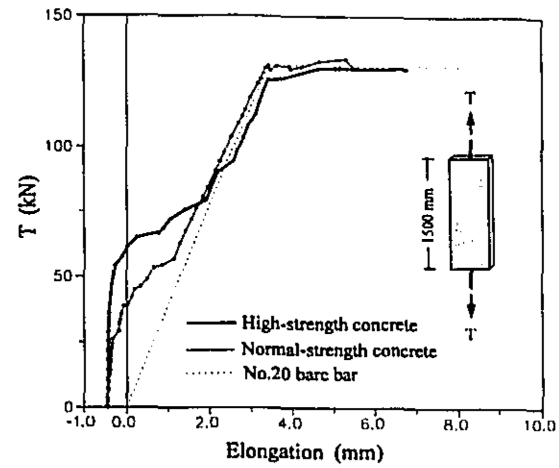

a) No. 20 uncoated bars

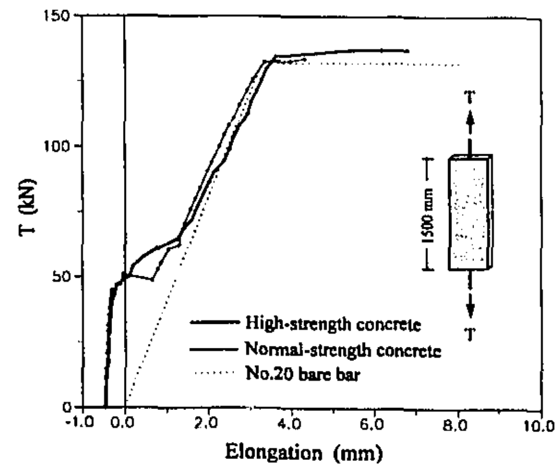

b) No. 20 6-8 mil epoxy-coated bars

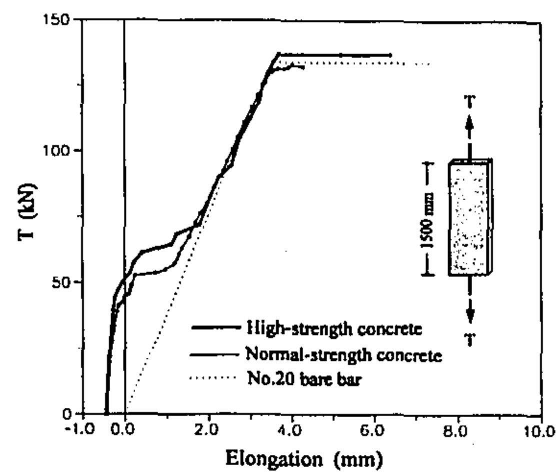

c) No. 20 10-12 mil epoxy-coated bars

Figure 4.11: Influence of concrete strength on tension stiffening for specimens with No. 20 bars

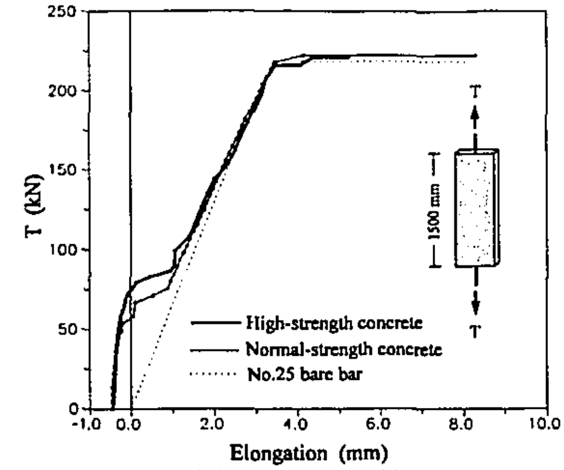

a) No. 25 uncoated bars

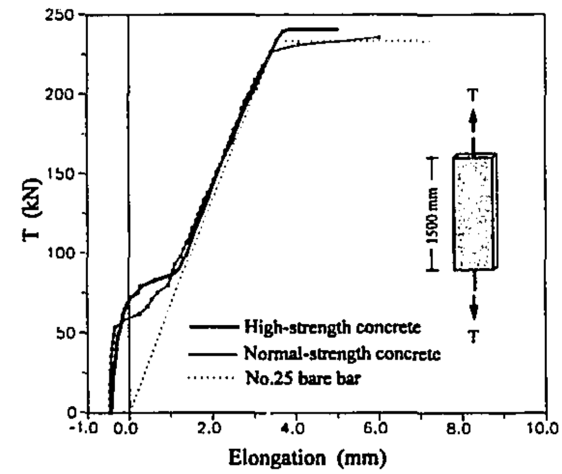

b) No. 25 6-8 mil epoxy-coated bars

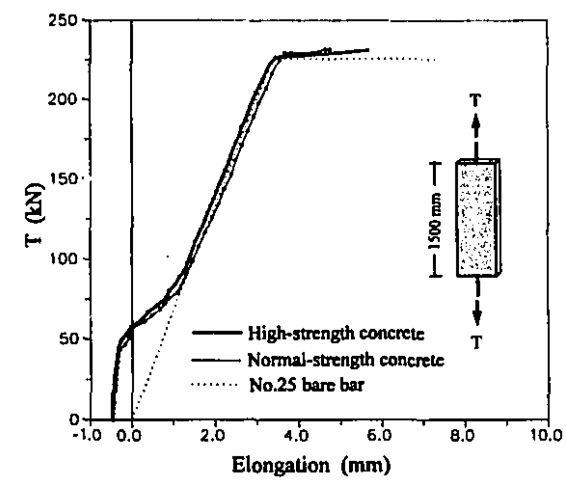

c) No. 25 10-12 mil epoxy-coated bars

Figure 4.12: Influence of concrete strength on tension stiffening for specimens with No. 25 bars

Figure 4.13: Transverse tensile cracks and splitting cracks in specimens HC1-10, HC1-15, HC1-20, HC1-25 and HC1-30

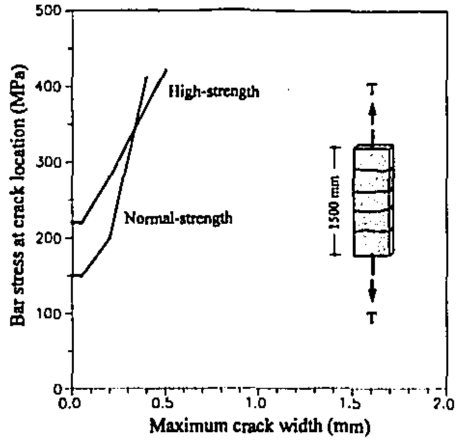

a) uncoated bars

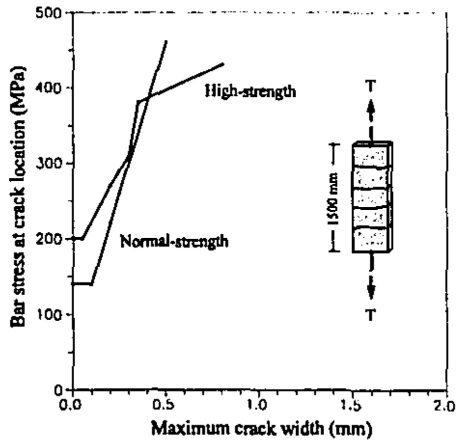

b) 6-8 mil epoxy-coated bars

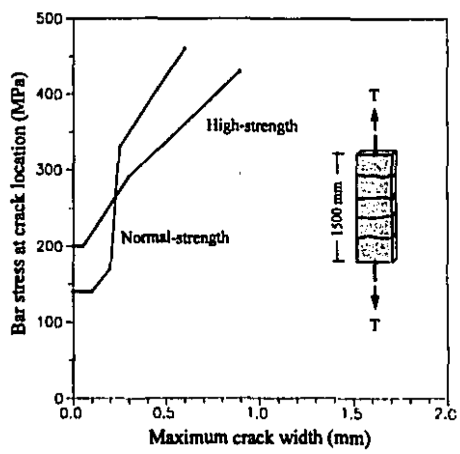

c) 10-12 mil epoxy-coated bars

Figure 4.14: Influence of concrete strength on maximum crack widths for specimens with No. 10 bars

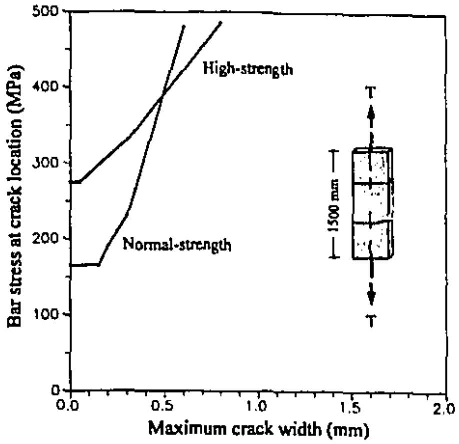

a) uncoated bars

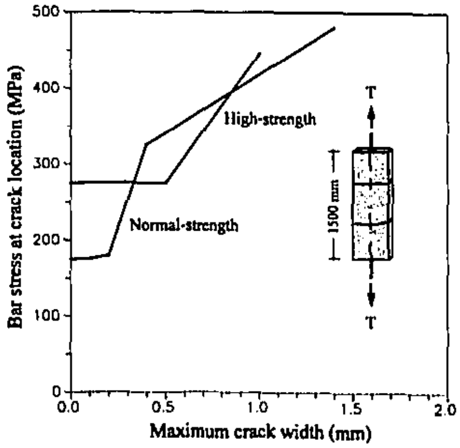

b) 6-8 mil epoxy-coated bars

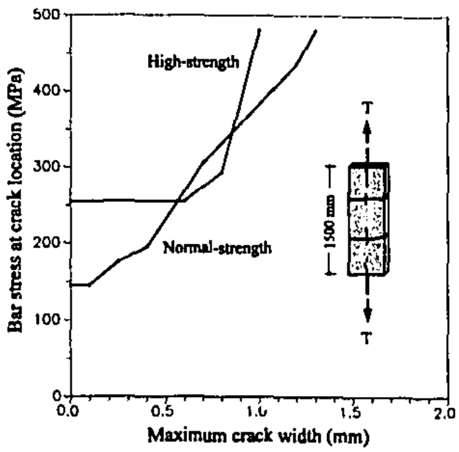

c) 10-12 mil epoxy-coated bars

Figure 4.15: Influence of concrete strength on maximum crack widths for specimens with No. 15 bars

4.1.3 Influence of Steel Fibres on Response of Tension Specimens

Addition of fibres to concrete makes it more homogeneous and isotropic and can significantly improve the tensile strength and ductility. Tensile behaviour of steel fibre concrete has been studied by several researchers (Lim *et al* 1987; Mitchell *et al* 1994). This section describes the behaviour of twelve tension specimens. Six specimens were constructed with normal-strength concrete and six specimens were constructed with high-strength concrete. In each batch of six specimens the variables were the presence of fibres (with or without) and the thickness of epoxy coatings on the bars (no coating, 6-8 mil coating and 10-12 mil coating). The purpose of this section is to investigate the effect of steel fibres on the behaviour of reinforced concrete elements subjected to pure tension. The influence of concrete strength and thickness of epoxy coatings were also studied.

4.1.3.1 Material Properties

In this testing program, hooked-end steel fibres, produced by the Bekaert Steel Wire Corporation, were used to attain 1 percent fibre reinforcement (76.8 kg/m^3) by volume of concrete. The fibres had lengths of 30 mm and a diameter of 0.5 mm. The tensile strength of the fibre was 1200 MPa. Four different types of concrete were used in the testing program. These included normal-strength concrete, with and without steel fibres and high-strength concrete, with and without steel fibres. The concrete compressive strengths, f_c' , were obtained by testing standard cylinders, having a diameter of 150 mm and a height of 300 mm. Figure 4.16 shows the typical compressive stress-strain responses of the normal and high-strength concretes, with and without steel fibres. As can been seen, the addition of 1% steel fibres has increased the compressive strength by about 10%. However, the ductility of the compressive stress-strain response has been significantly improved, for both normal and high-strength concrete (see Fig. 4.16).

The modulus of rupture, f_r , was determined from flexural test specimens 100 mm by 100 mm by 300 mm long, loaded at their third points. Figure 4.17 shows the load-deflection responses obtained from the modulus of rupture tests for the normal-strength concrete, with and without steel fibres. As expected, the plain concrete specimen has no ductility, with brittle failure occurring when the first crack forms. After the initial cracking of the fibre-reinforced concrete, the specimen exhibited a sudden drop in load carrying capacity, but had some post-peak resistance due to the presence of fibres which were bridging the cracks.

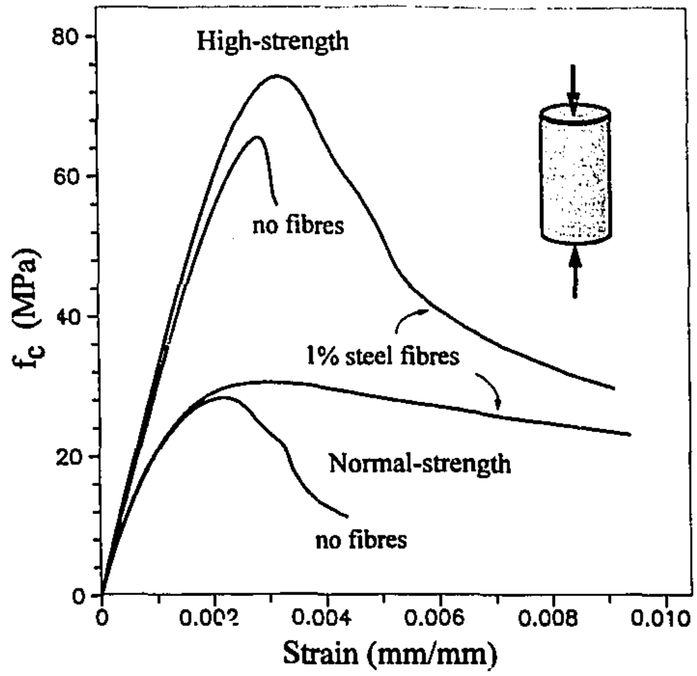

Figure 4.16: Compressive stress-strain responses of different concretes

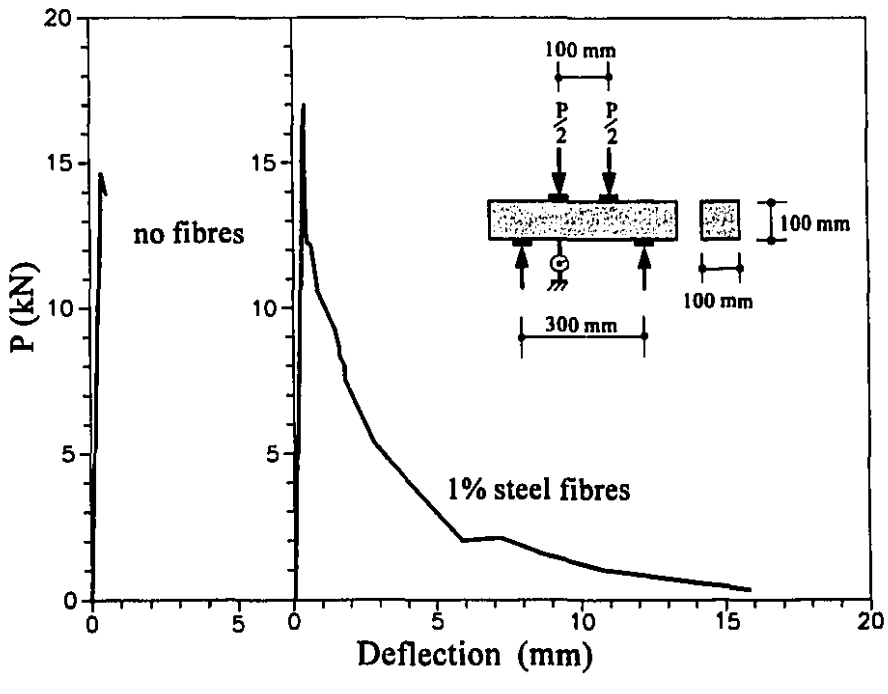

Figure 4.17: Load-deflection responses of modulus of rupture tests

The splitting tensile tests were carried out on 150 mm diameter by 300 mm long cylinders. The results showed that the addition of fibres had a major effect on increasing the splitting tensile strength, f_{sp} . A summary of the concrete material test results is shown in Table 4.3.

Table 4.3: Influence of steel fibres on concrete strength

		f'_c (MPa)	f_{sp} (MPa)	f_r (MPa)
Normal-strength	No Fibres	28.5	2.8	4.4
	1% Steel Fibres	30.8	4.8	5.1
High-strength	No Fibres	65.8	5.1	---
	1% Steel Fibres	74.6	7.5	6.8

All of the reinforcing bars used in the tension specimens were No. 15, with a specified yield strength of 400 MPa and a measured yield stress of 480 MPa. Three different surface conditions were provided on the No. 15 bars. The specimens labelled "C0" contained uncoated bars, while those labelled "C1" and "C2" contained bars with an epoxy coating thicknesses of 6-8 mils and 10-12 mils, respectively. Specimens C0, C1 and C2 were constructed with the normal-strength concrete, having a compressive strength at the time of testing of 34.9 MPa (at an age of 105 days). Specimens FC0, FC1 and FC2 were constructed with normal-strength concrete containing 1% steel fibres. The fibre reinforced concrete in these specimens had a compressive strength at the time of testing of 30.8 MPa (at an age of 75 days). Specimens HC0, HC1 and HC2 were constructed with high-strength concrete, having a compressive strength at the time of testing of 90 MPa (at an age of 135 days). Specimens FHC0, FHC1 and FHC2 were constructed with high-strength concrete containing 1% steel fibres, with the fibre reinforced concrete having a compressive strength at the time of testing of 74.6 MPa (at an age of 75 days), 66.8 and 66.8 MPa (at an age of 55 days), respectively. Tables 4.4 and 4.5 summarize the composition and material properties of the concrete used in the test specimens.

4.1.3.2 Test Program

The test program consisted of a series of twelve tension specimens. Figure 4.18 shows the geometry and instrumentation for a typical tension specimen. All of the specimens had cross-sectional dimensions of 95 mm by 170 mm and had lengths of 1500 mm. A single No.15 bar was provided in each specimen giving a reinforcement ratio, ρ, of 1.23%. The reinforcing bar extended 250 mm outside of the ends of the concrete.

Table 4.4: Composition and properties of the concretes used in tension specimens

Concrete	Normal-Strength 28-35 MPa	High-Strength 65-75 MPa	High-Strength 90 MPa
Cement, (kg/m^3)	355	515*	515*
Water, (L/m^3)	160	143	135
Sand, (kg/m^3)	790	846	850
Coarse aggregate, (kg/m^3)	1040	959	960
Water reducing agent, (mL/m^3)	1110	1551	1565
Air entraining agent, (mL/m^3)	200	--	--
Superplasticizer, (L/m^3)	--	13.0	21.0
Water/cement ratio	0.45	0.30	0.29
Coarse aggregate size, (mm)	5 to 20	5 to 10	5 to 10
Slump, (mm)	150	200	60
Air, (%)	7.0	3.0	1.8
Density, (kg/m^3)	2300	2480	2505

* Blended cement containing 7 - 8% of silica fume

Table 4.5: Properties of concretes used in fibre-reinforced tension test series

Specimen	f'_c (MPa)	f_{sp} (MPa)	f_r (MPa)
C0	34.9	3.1	4.3
C1	34.9	3.1	4.3
C2	34.9	3.1	4.3
FC0	30.8	4.8	5.1
FC1	30.8	4.8	5.1
FC2	30.8	4.8	5.1
HC0	90	6.3	9.8
HC1	90	6.3	9.8
HC2	90	6.3	9.8
FHC0	74.6	7.5	6.8
FHC1	66.8	7.2	---
FHC2	66.8	7.2	---

The test setup consisted of a loading frame transmitting the load through a set of tension grips at the top and the bottom of the reinforcing bar. This resulted in tension being transferred from the steel reinforcing bar to the reinforced concrete section. A linear voltage differential transducer (LVDT) was placed along each side of the specimen as shown in Fig. 4.19. These transducers, which were clamped to the steel reinforcing bar just outside of the concrete, measured the total elongation of the reinforced concrete specimen. At each load stage the cracks were measured using a crack width comparator. The complete response of each specimen is described by plotting the applied tension versus the average member elongation.

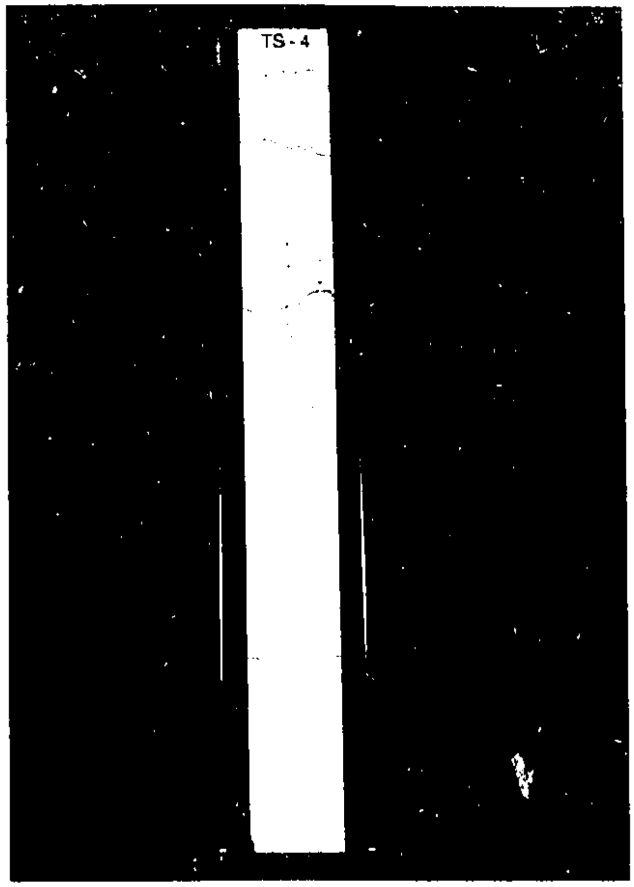

Figure 4.18: Tension specimen C1 under load

4.1.3.3 Load Deflection Responses

Figure 4.19 shows the tension versus elongation responses of two specimens made with normal-strength concrete and reinforced with uncoated bars. Also shown in this figure is the response of a bare bar. Due to shrinkage of the concrete, the elongation of the specimens is negative prior to load application. An average free shrinkage strain of -0.3×10^{-3} was determined from strain measurements on 100 x 100 x 400 mm long shrinkage specimens which had the same curing conditions as the test specimens. As can be seen, the presence of 1% of steel fibres in the concrete has resulted in an increase in stiffness before cracking and an increase in the cracking load. After cracking, the specimen without fibres shows some tension stiffening as indicated in Fig. 4.19. In this specimen, at crack locations, the reinforcing bar must carry all of the tension in the specimen. When the applied load causes localized yielding of the bar at a crack then an abrupt loss of stiffness occurs (see Fig. 4.19). A key feature of fibre-reinforced concrete is the ability of the fibres to bridge across cracks. Hence, at the locations of cracks in the fibre-reinforced concrete, the fibres help the reinforcing bar to carry tension. This results in a significant increase in the tension stiffening after cracking as can be seen in Fig. 4.19. This ability also enables fibre-reinforced concrete members to develop loads greater than the yield force in the reinforcing bar.

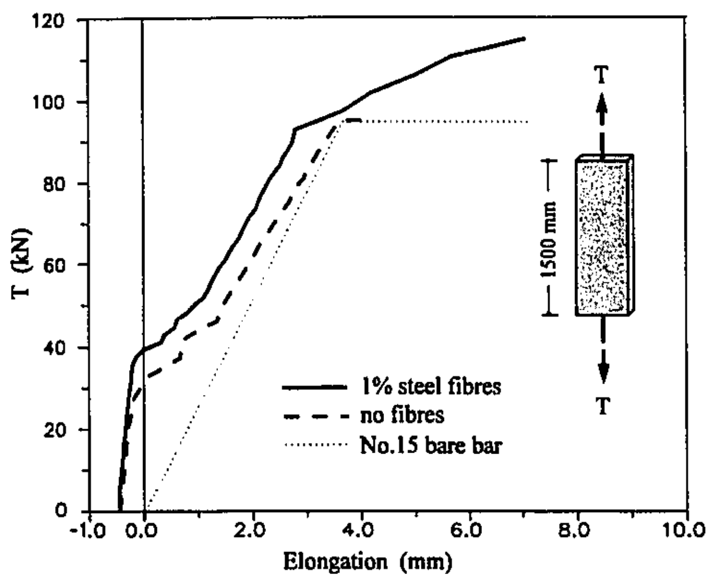

Figure 4.19: Tension responses of normal-strength concrete specimens reinforced with uncoated bars

Figure 4.20 shows the tension versus elongation responses of four specimens containing uncoated reinforcing bars. Before cracking, the high-strength concrete specimens exhibit larger stiffness than the normal-strength concrete specimens. Also, the high-strength concrete specimens have a higher cracking load than the specimens made with normal-strength concrete. After cracking in the high-strength specimens there is a larger energy release at crack locations which gives a sudden jump in the tension versus elongation response (see Fig. 4.20). It is interesting to note that the responses of the high-strength and normal-strength concrete specimens, that did not contain fibres, are almost identical after the development of significant cracking. The addition of fibres produces an increase in the tension stiffening for both strengths of concrete and enables the specimens to develop tensions greater than the yield force in the reinforcing bar.

Figures 4.21 and 4.22 give the tension versus elongation responses for the specimens containing bars with epoxy coating thicknesses of 6-8 mils and 10-12 mils, respectively.

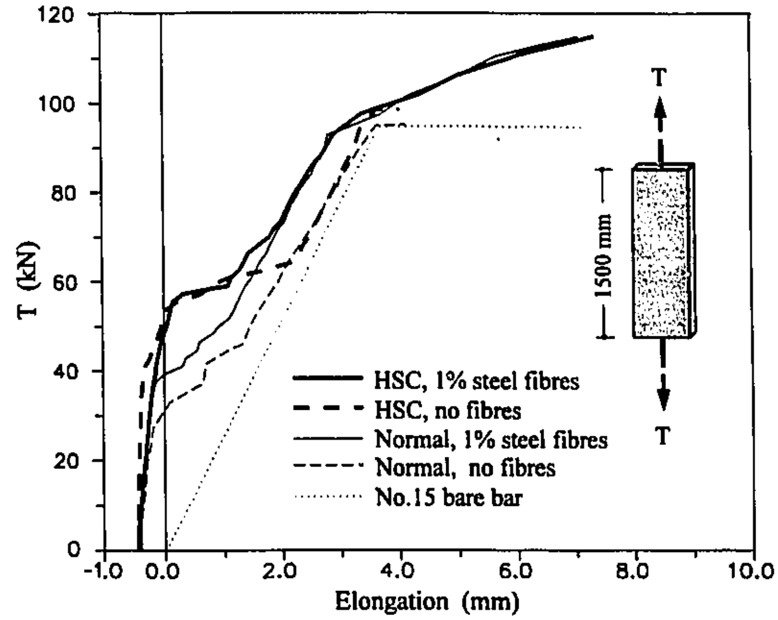

Figure 4.20: Tension responses of specimens reinforced with uncoated bars

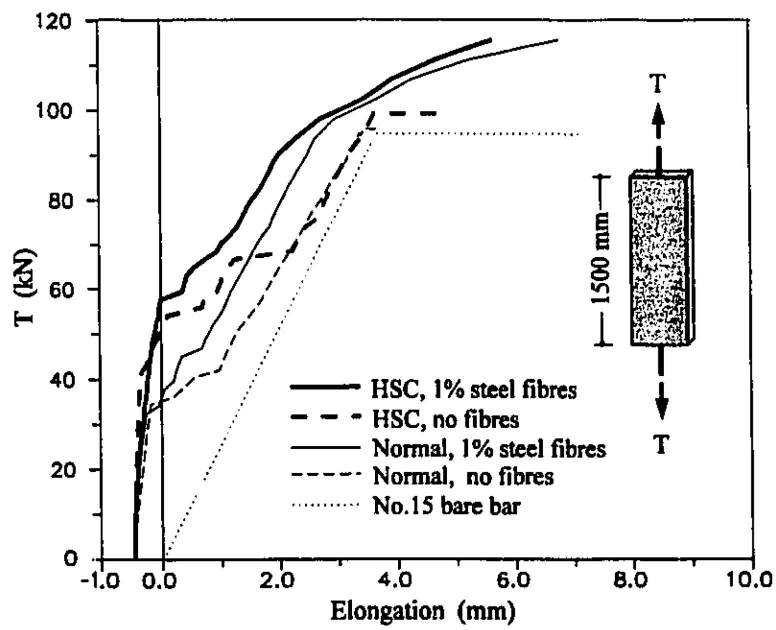

Figure 4.21: Tension responses of specimens reinforced with 6-8 mil epoxy-coated bars

As can be seen the influence of concrete strength and the presence of steel fibres is similar to that observed in the specimens with uncoated bars.

Figure 4.23 compares the tension responses of the specimens to indicate the influence of epoxy coating thickness. It can be concluded that for these tension specimens, in which splitting cracking was not a dominant feature, the presence of and thickness of epoxy coating did not have a significant effect on the tension stiffening.

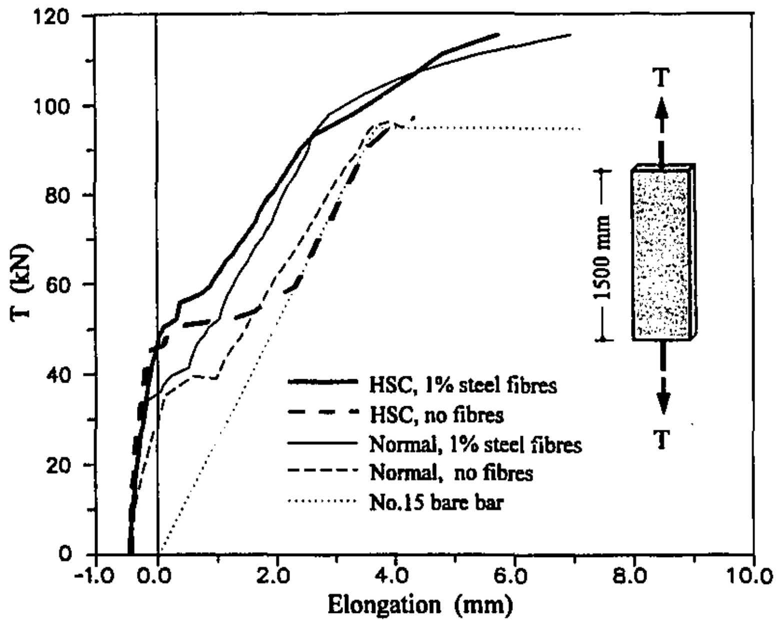

Figure 4.22: Tension responses of specimens reinforced with 10-12 mil epoxy-coated bars

4.1.3.4 Cracking Behaviour

A typical crack pattern of the tension specimen constructed with normal-strength concrete with no fibres is shown in Fig. 4.18(b). As can be seen, both tensile transverse cracks and splitting cracks were observed during the test. In the specimens constructed with high-strength concrete, without fibres, more splitting cracks along the specimens were observed. In the specimens using steel fibres, no splitting cracks were observed during the test.

Figure 4.24 shows the crack widths of different specimens constructed with normal-strength and high-strength concrete, with and without fibres, and reinforced with uncoated bars.

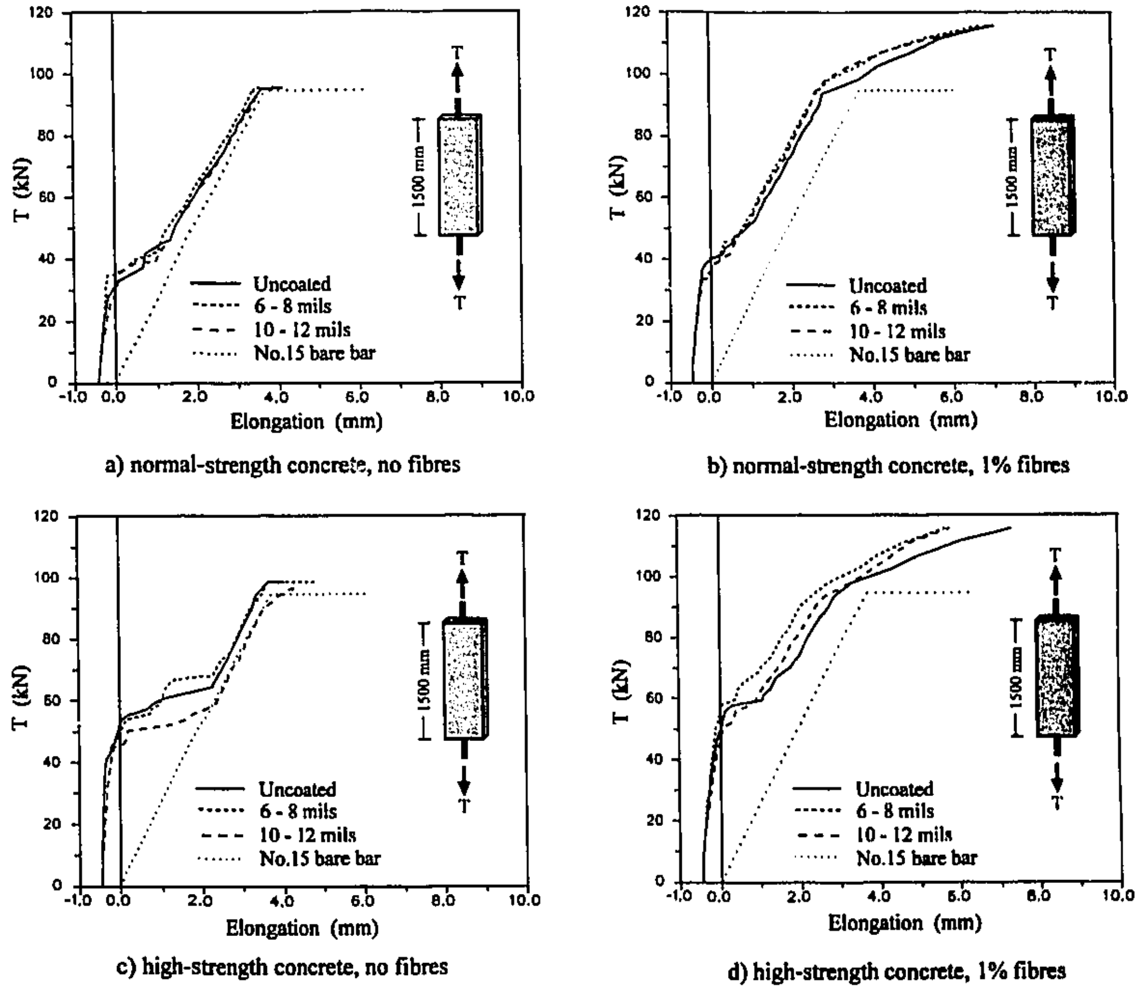

Figure 4.23: Influence of epoxy coating thickness on the tension response

Figure 4.24(a) shows the influence of steel fibres on the crack widths of normal-strength concrete specimens (CO and FCO) and high-strength concrete specimens (HCO and FHCO), respectively. As can be seen from these figures, adding fibres significantly reduced the crack widths. Figure 4.24(b) shows the influence of concrete strength on the crack widths of specimens constructed without fibres (CO and HCO) and with fibres (FCO and FHCO), respectively. These figures also show that the use of higher strength concrete reduced the crack widths. Figure 4.25 compares the crack width of specimens reinforced with uncoated bars and bars with epoxy coating thicknesses of 6-8 mils and 10-12 mils. Specimens containing epoxy-coated bars have higher crack widths than those with uncoated bars. In addition, increasing the coating thickness resulted in larger cracks.

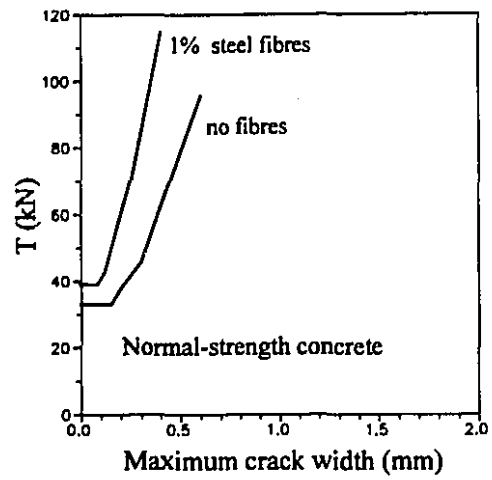

a) Influence of steel fibres

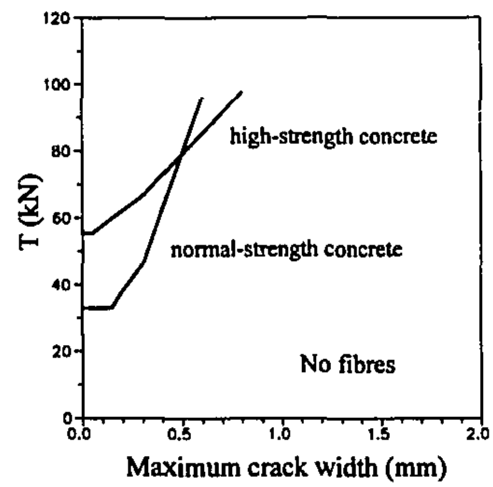

b) Influence of concrete strength

Figure 4.24: Influence of fibres and concrete strength on crack widths in specimens with uncoated bars

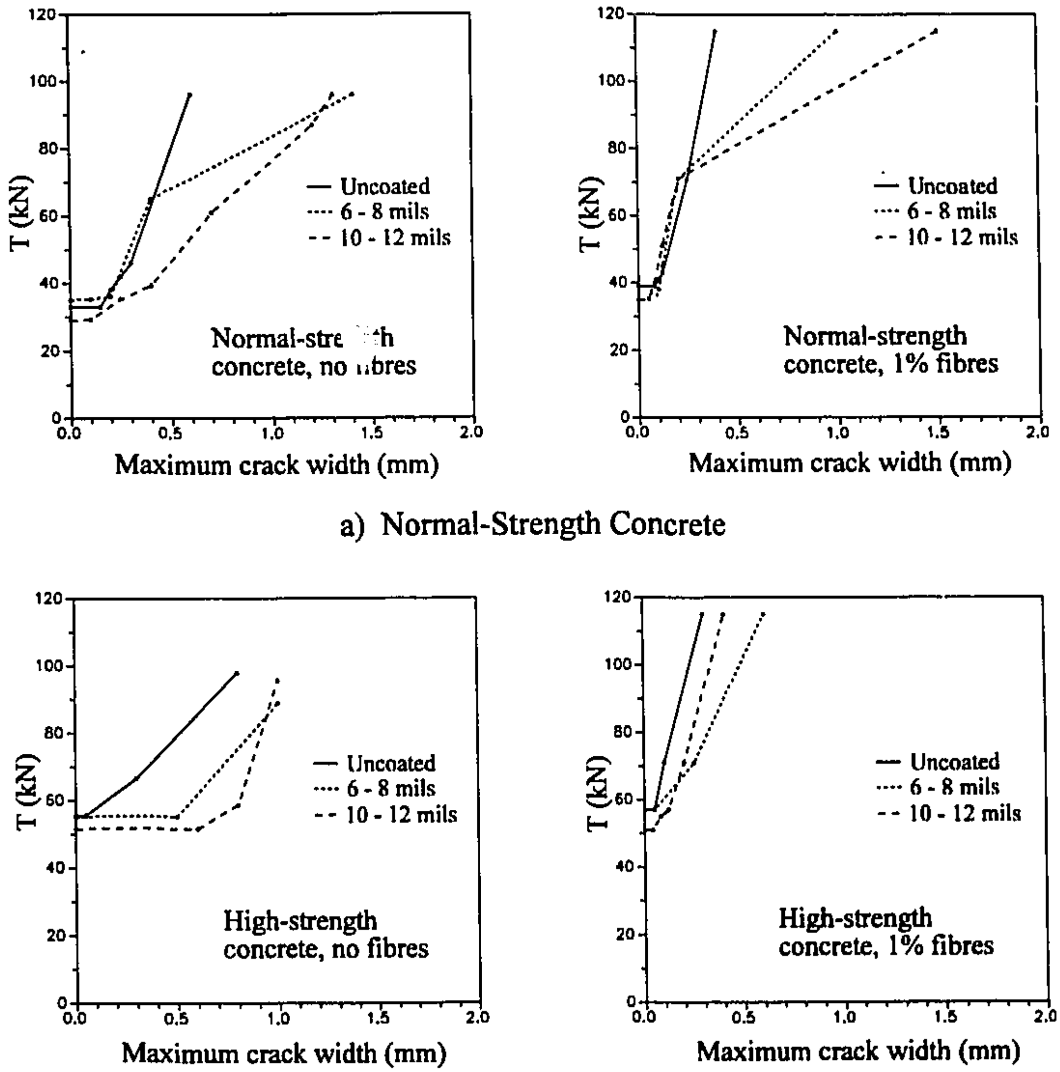

Figure 4.25: Influence of epoxy coating on crack widths

4.2 RESPONSE OF MEMBERS SUBJECTED TO FLEXURE

The importance of obtaining a better understanding of the failure mechanism of reinforced concrete beams without web reinforcement has resulted in a large number of experimental and analytical investigations (e.g., Kim and White 1991; Bažant and Kazemi 1991; Reineck 1991; Kani *et al.* 1979; Abrishami *et al.* 1994). This section examines the flexural behaviour of normal and high-strength concrete beams, constructed with either uncoated bars or with bars having one of two different epoxy coating thicknesses. This enabled a study of the effect of concrete strength and coating thickness on the flexural response, crack control, ductility and failure mechanism. This initial program examined the response of beams without web reinforcement in order to study the combined effects of bending, shear and bond in high-strength concrete members.

4.2.1 Test Program

The test program consisted of a series of six beams, the details of which are given in Fig. 4.26. All of the beams were 200 mm wide, 400 mm deep and had a span of 4.5 m. Two No. 20 bars were provided in each beam giving a reinforcement ratio, ρ_s, of 0.0088. The clear concrete cover provided was 50 mm. It is noted that no shear reinforcement was used in this study. Two types of concrete, normal and high-strength, were used in this test series. Table 4.6 gives the composition of these concretes. The concrete compressive strengths were obtained by testing standard cylinders, having a diameter of 150 mm and a height of 300 mm. Figure 4.27 shows compressive stress-strain responses of the normal and high-strength concretes having average compressive strengths of 32 MPa and 90 MPa at the time of testing, respectively. The average splitting tensile strengths, f_{sp} , were 3.0 MPa and 6.3 MPa for the normal and high-strength concretes, respectively. The splitting tests were carried out on 150 mm diameter by 300 mm long cylinders. The average moduli of rupture, f_r , were 4.1 MPa and 9.8 MPa for the normal and high-strength concretes, respectively. These tests were carried out on 100 mm by 100 mm by 400 mm long beams which were subjected to third-point loading over spans of 300 mm.

Figure 4.28 shows a typical stress-strain response for the No. 20 reinforcing bars which all came from the same lot. Three different surface conditions were provided on the No. 20 bars. The beams labelled "UCB" contained uncoated bars, while those labelled "C1B" and "C2B" contained bars with epoxy coating thicknesses of 6 to 8 mils (0.15 to 0.2 mm) and 10 to 12 mils (0.25 to 0.3 mm), respectively.

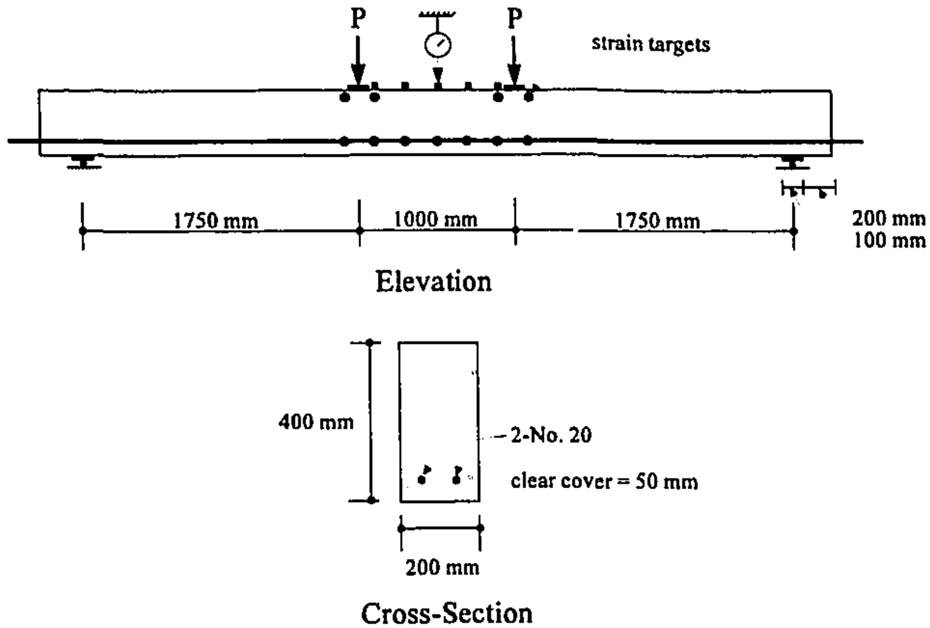

Figure 4.26: Details of beam specimens and instrumentation

Beams UCB, C1B and C2B were constructed with normal-strength concrete, while beams HUCB, HC1B and HC2B were made with high-strength concrete. The beams were simply supported and were subjected to two point loads as shown in Fig. 4.26. The loads were applied by means of hydraulic actuators and controlled by load cells. At each load increment the midspan deflection was measured by linear voltage differential transformers (LVDT's). Longitudinal strains were obtained from mechanical strain targets, having a gauge length of 200 mm, glued to the concrete at the level of the reinforcement with matching strain targets located either on the top surface or 60 mm from the top surface of the specimens (see Fig. 4.26). At each load stage the cracks were measured using a crack width comparator.

4.2.2 Test Results

First flexural cracking

Table 4.7 shows the loads, P_{cr} , when the first flexural cracks were observed. This table also shows the crack widths and the lengths or heights of the first cracks above the bottom face of each beam. As expected, the high-strength concrete beams had larger applied loads at first cracking than the normal-strength concrete beams.

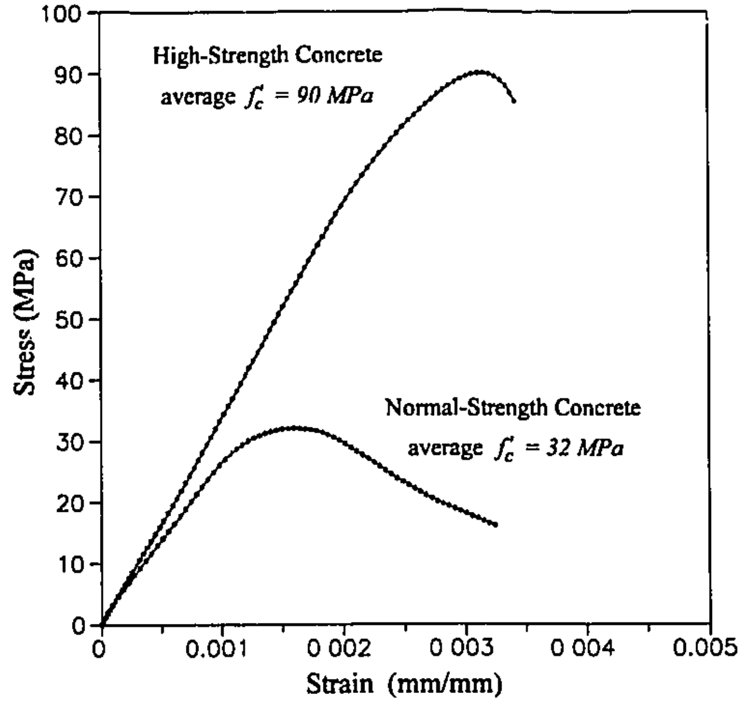

Figure 4.27: Typical stress-strain responses of normal and high-strength concretes

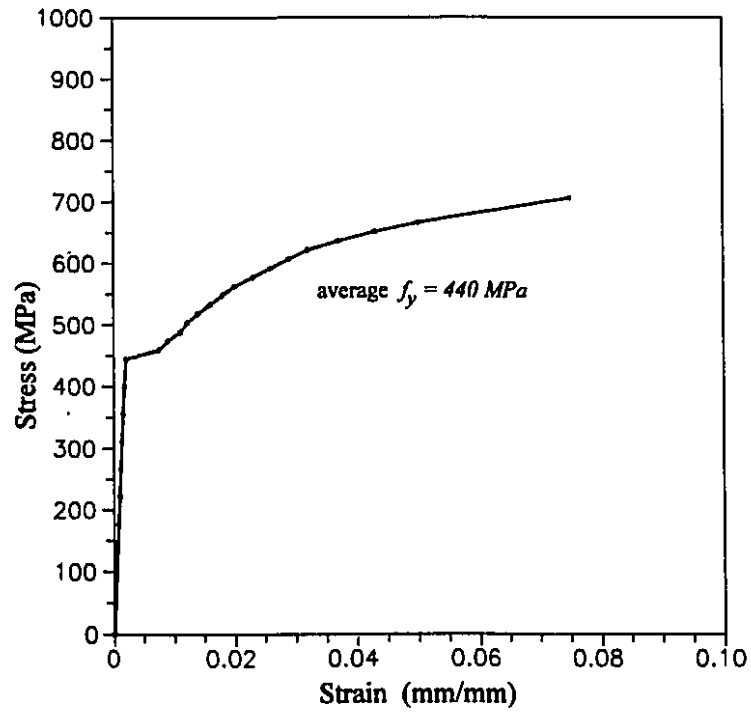

Figure 4.28: Typical stress-strain response of reinforcing bars

Table 4.6: Composition and properties of the concretes used in flexural specimens

Concrete	Normal-Strength	High-Strength
Cement, (kg/m^3)	355	515*
Water, (L/m^3)	160	135
Sand, (kg/m^3)	790	850
Coarse aggregate, (kg/m^3)	1040	960
Water reducing agent, (mL/m^3)	1110	1565
Air entraining agent, (mL/m^3)	200	--
Superplasticizer, (L/m^3)	--	21.0
Water/cement ratio	0.45	0.29
Coarse aggregate size, (mm)	5 to 20	5 to 10
Slump, (mm)	150	60
Air, (%)	7.0	1.8
Density, (kg/m^3)	2300	2505

* Blended cement containing 7 - 8% of silica fume

All of the first cracks in the normal-strength concrete beams were hairline in width, while the first cracks in the high-strength concrete beams were slightly wider (about 0.05 mm). Due to the larger cracking stress of the high-strength concrete, a larger amount of energy is released upon cracking, resulting in the propagation of longer and wider initial cracks (see Table 4.7).

Load-deflection behaviour

The load-deflection responses of all six beams tested are shown in Fig. 4.29. As can been seen, there are three different behavioral stages, pre-cracking, post-cracking and post-yielding. As expected, the high-strength concrete beams had higher stiffnesses than the normal-strength concrete beams both before and after cracking. The high-strength concrete beams had higher loads at cracking, at yielding and at ultimate than the normal-strength concrete beams. As can be seen from Fig. 4.29, the presence of the epoxy coatings on the reinforcement did not significantly affect the stiffness or ultimate capacity.

Table 4.8 gives the applied loads and corresponding midspan deflections at flexural yielding and at ultimate load and the modes of failure. The presence of different thicknesses of epoxy coating on the reinforcement has little effect on the loads to cause both flexural yielding and ultimate. The measured midspan deflections of the high-strength concrete beams are smaller than those of the normal-strength concrete beams at both yield and ultimate load levels. The maximum deflections achieved varied from 42.8 mm for specimen HC2B (high-strength beam with largest thickness of epoxy coating) to 83.4 mm for specimen UCB (normal-strength beam with uncoated bars).

Table 4.7: Conditions at first cracking

Beam	P_{cr} (kN)	M_{cr} (kNm)	Deflection (mm)	Crack width (mm)	Crack length (mm)
UCB	6.2	17.2	1.5	hairline	63
C1B	4.0	13.4	1.2	hairline	50
C2B	4.4	14.1	1.1	hairline	46
HUCB	9.5	23.0	1.2	0.05	124
HC1B	8.4	21.1	0.8	0.05	200
HC2B	9.9	23.7	1.1	0.05	240

Note: Moment at midspan = $P \times 1.75 + 6.4$ kNm

The displacement ductilities, taken as the deflection at maximum load level divided by the deflection at first yielding, Δ_u/Δ_y, are also shown in Table 4.8. From Table 4.8 and Fig. 4.29 it is evident that the presence of epoxy coating decreases the ductility, for both the normal and high-strength concrete beams. It is also noted that, as the epoxy coating thickness increases, the ductility decreases. The lowest displacement ductility was 1.91 for the high-strength concrete beam, HC2B, reinforced with bars having the 10-12 mils epoxy coating. Both the normal and high-strength concrete beams (UCB and HUCB), having uncoated bars had the maximum observed displacement ductilities of 3.37 and 3.44, respectively.

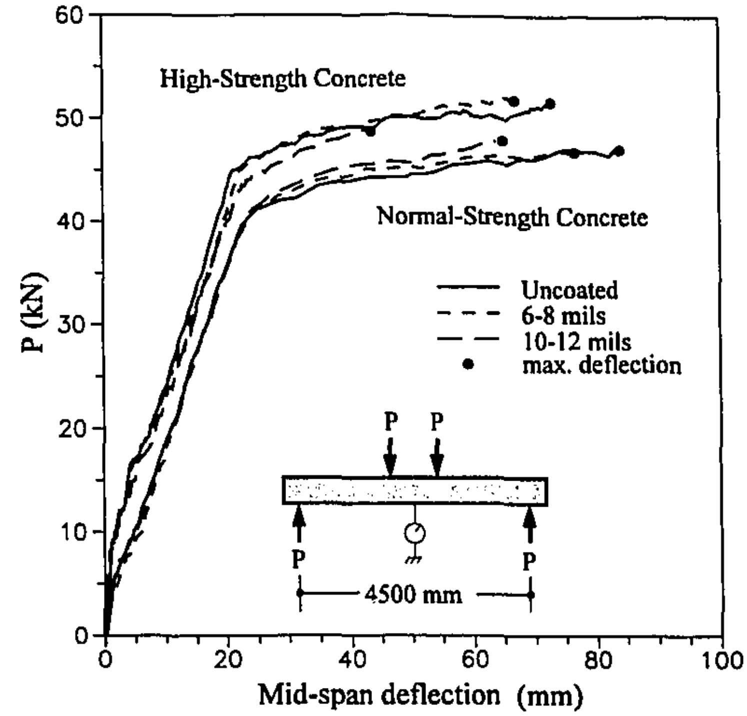

Figure 4.29: Load-deflection responses of beam specimens with different epoxy coating thicknesses on the reinforcement

Table 4.8: Summary of test results at yielding and ultimate

Beam	Yielding		Ultimate		Ductility	Mode of
	P_y (kN)	Δ_y (mm)	P_u (kN)	Δ_u (mm)	Δ_u/Δ_y	failure*
UCB	42.2	24.7	48.5	83.4	3.37	F
C1B	42.5	25.2	48.3	77.0	3.05	F
C2B	42.3	26.6	48.8	63.9	2.40	F
HUCB	44.5	21.0	50.8	72.3	3.44	F-B
HC1B	44.5	22.5	51.6	66.9	2.97	F-B
HC2B	43.3	22.4	48.8	42.8	1.91	F-B

* F = Flexural yielding followed by concrete crushing

F-B = Flexural yielding followed by diagonal tension and bond splitting failure

4.2.3 Comparison of test results and analysis

In order to predict the flexural response of the specimens the computer program "RESPONSE" (Collins and Mitchell 1991) was used. This program, which carries out a "plane sections" analysis is capable of simulating the concrete compressive stress-strain curves for a wide range of concrete strengths. The predicted moment capacities using program RESPONSE and using the ACI Code (ACI 1989) equations are compared with the test results in Table 4.9. The test results include the dead load moment due to the beam self-weight and the moment due to the loading apparatus (6.4 kNm at midspan). The predictions using the ACI equations and program RESPONSE, neglecting strain hardening of the reinforcement, both provide similar and conservative predictions of the flexural capacities. Comparisons of the predicted capacities, accounting for strain hardening of the reinforcement, with the observed capacities indicates that the normal-strength concrete beams were capable of developing high strains in the reinforcement. Although the high-strength concrete beams reached flexural yielding, they failed due to diagonal tension and bond splitting cracks, before attaining significant strain hardening in the reinforcement.

Table 4.9: Comparison of predicted and experimental results

Beam	Observed Ultimate M_u (kNm)	Prediction using "RESPONSE" no strain hardening (kNm)	Prediction using "RESPONSE" with strain hardening (kNm)	ACI Prediction M_n no strain hardening (kNm)
UCB	91.3	83.9	88.3	83.3
C1B	90.9	83.9	88.3	83.3
C2B	91.8	83.9	88.3	83.3
HUCB	95.3	87.5	106.5	87.5
HC1B	96.6	87.5	106.5	87.5
HC2B	91.8	87.5	106.5	87.5

4.2.4 Influence of epoxy coating and concrete strength on cracking

Three different types of cracks were observed during the tests; flexural cracks, splitting cracks and diagonal tension cracks. Flexural cracking occurred early in the testing in the constant moment region. This was followed by flexural cracks outside of this region and splitting cracks appearing at the level of reinforcement before reaching yielding of the reinforcement. Before yielding, all of the beams had splitting cracks, except the high-strength concrete beam (HUCB) that was reinforced with uncoated bars. More splitting cracks were observed in the beams having bars with the 10-12 mils epoxy coating than in the beams having bars with the 6-8 mils coating. More extensive splitting cracks were observed in the constant moment region of the normal-strength concrete beams, than in the high-strength concrete beams having the same coating thickness. Before reaching the ultimate load, diagonal cracks were observed in the normal-strength concrete beams. Eventually crushing occurred in the compressive zone causing flexural failure of the normal-strength concrete beams. In these beams, diagonal cracks had formed close to failure which turned into splitting cracks at the level of the bars. This was more noticeable in beam HC2B, having the 10-12 mils epoxy coating on the bars. Figure 4.30 shows the three normal-strength concrete beams after failure. In the high-strength concrete beams, after flexural yielding, diagonal tension cracks formed which initiated splitting cracks near the ends of the beams. The failures of the high-strength concrete beams were very sudden, with simultaneous crushing of the concrete compression zone and bond-splitting failures near the beam ends. Figure 4.31 compares the appearance of the three high-strength concrete beams after failure. The small adhesion between the concrete and the coated bars and the larger splitting forces led to the total loss of the concrete cover during failure for beams HC1B and HC2B.

Figure 4.32 compares the average crack widths of normal and high-strength concrete beams for different bar coating thicknesses. These flexural crack widths were measured at the level of the reinforcement and the average crack width was determined from the cracks in the constant moment region. It is clear that the higher strength concrete beams displayed smaller average crack widths than the companion normal-strength concrete beams. Table 4.10 gives the average crack spacings (determined over the constant moment region), average crack widths and maximum crack widths for the six specimens tested. It is clear that the presence of epoxy coating results in fewer cracks (i.e., larger crack spacings), but larger crack widths.

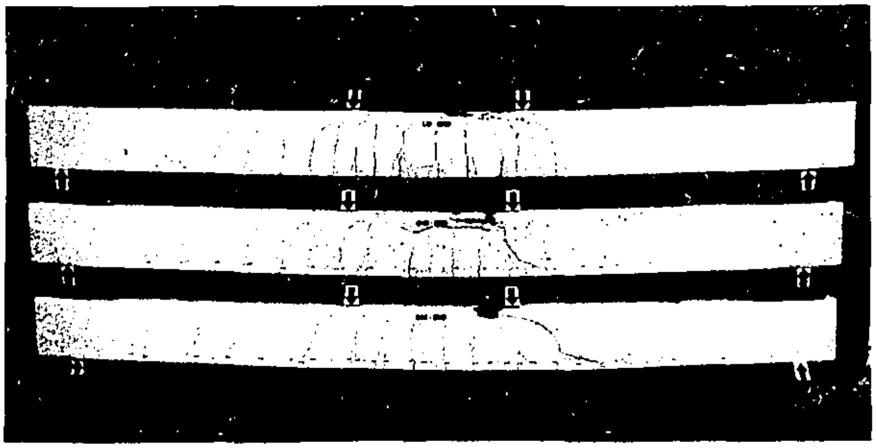

Figure 4.30: Normal-strength concrete beams after failure; top, beam UCB; middle, beam C1B; and bottom, beam C2B.

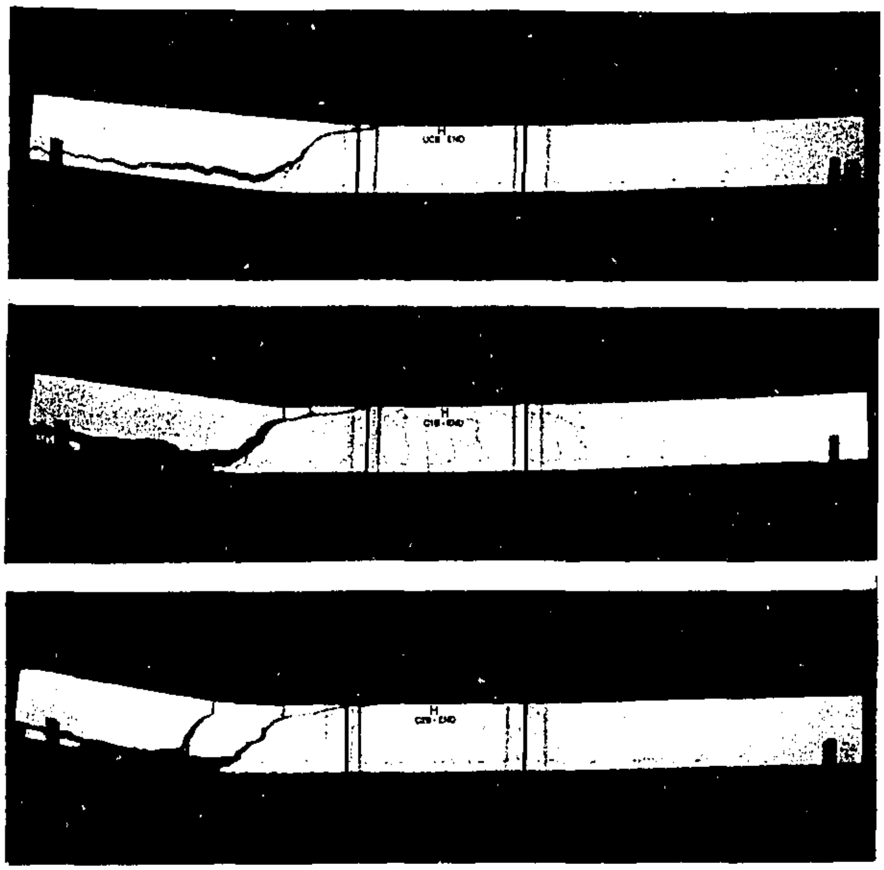

Figure 4.31: High-strength concrete beams after failure; top, Beam HUCB; middle, Beam HC1B; and bottom, beam HC2B.

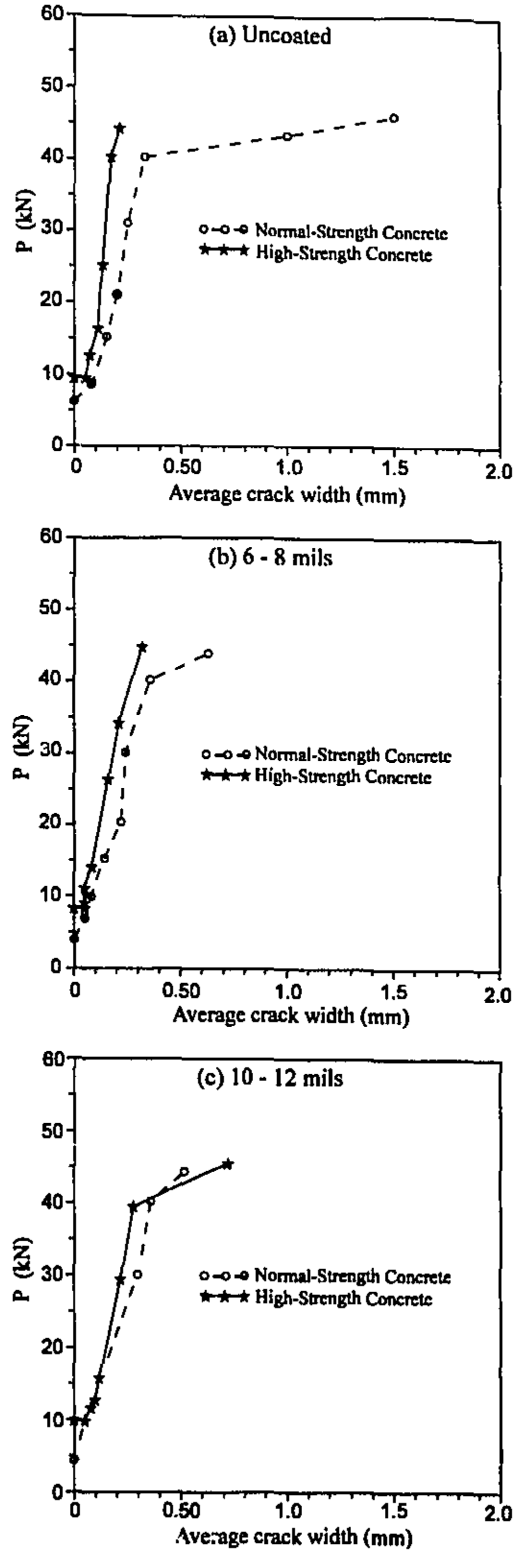

Figure 4.32: Influence of concrete strength on average crack widths

Table 4.10: Observed crack widths at service load level (0.6 of M_n)

Beam	Average Crack Spacing (mm)	Average Crack Width (mm)	Maximum Crack Width (mm)
UCB	143	0.17	0.22
C1B	167	0.23	0.30
C2B	167	0.24	0.35
HUCB	125	0.13	0.25
HC1B	200	0.16	0.25
HC2B	250	0.19	0.27

Figure 4.33 shows the load versus average crack widths and the load versus maximum crack widths for all of the beams. The beams with uncoated bars showed smaller average crack widths at service load moments (assumed to be 60% of M_n) than the beams with the coated bars. This figure also shows that for normal-strength concrete, the coating thickness has a significant effect on the maximum crack width at service load levels. Figures 4.32 and 4.33 demonstrate that the use of high-strength concrete, with its higher tensile strength, results in smaller flexural crack widths at service load levels. In addition, the maximum crack width is not as sensitive to the presence of epoxy coating on the reinforcement when high-strength concrete is used.

4.2.5 Failure Mechanisms

In the normal-strength concrete beams, after significant flexural cracking and the development of large strains in the reinforcement, diagonal tension cracks formed with flexural failure of the beams occurring by crushing of the compression zone. In the high-strength concrete beams, after flexural yielding, the ductility was limited by sudden failures. Figure 4.34 shows the sequence of events leading to the sudden failure of specimen HC1B, captured by slow motion video taping. The diagonal tension crack precipitated the failure by propagating towards the loading point and towards the tension reinforcement. This resulted in simultaneous flexural-shear crushing near the load point and bond-splitting along the reinforcement towards the support.

There are several contributing factors which resulted in the sudden failures in the high-strength concrete beams.

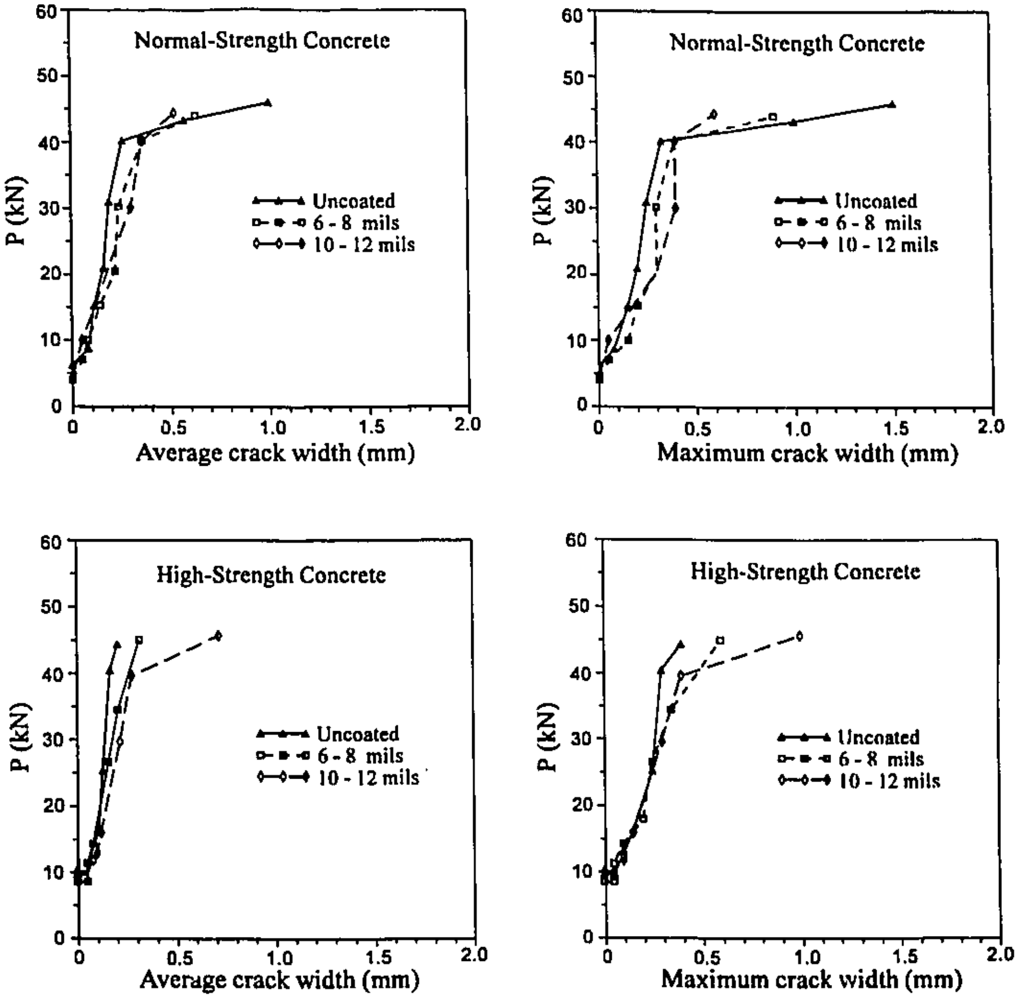

Figure 4.33: Influence of coating thicknesses on average and maximum crack widths

As observed by other researchers (ACI 1992; Johnson and Ramirez 1989) there is less aggregate interlock across diagonal tension cracks in high-strength concrete beams. This is due to the fact that cracks pass through the aggregates, instead of around the aggregates, because of the higher strength of the aggregate-paste interface. Therefore, for beams without shear reinforcement, upon opening of the diagonal crack, significant dowel forces are set up in the longitudinal reinforcement. In addition, the presence of high-strength concrete gives rise to highly concentrated bond stresses at the critical section (Azizinamini *et al.* 1993). The highly concentrated bond stresses at the location of the diagonal crack results in higher bond splitting forces adjacent to this critical section.

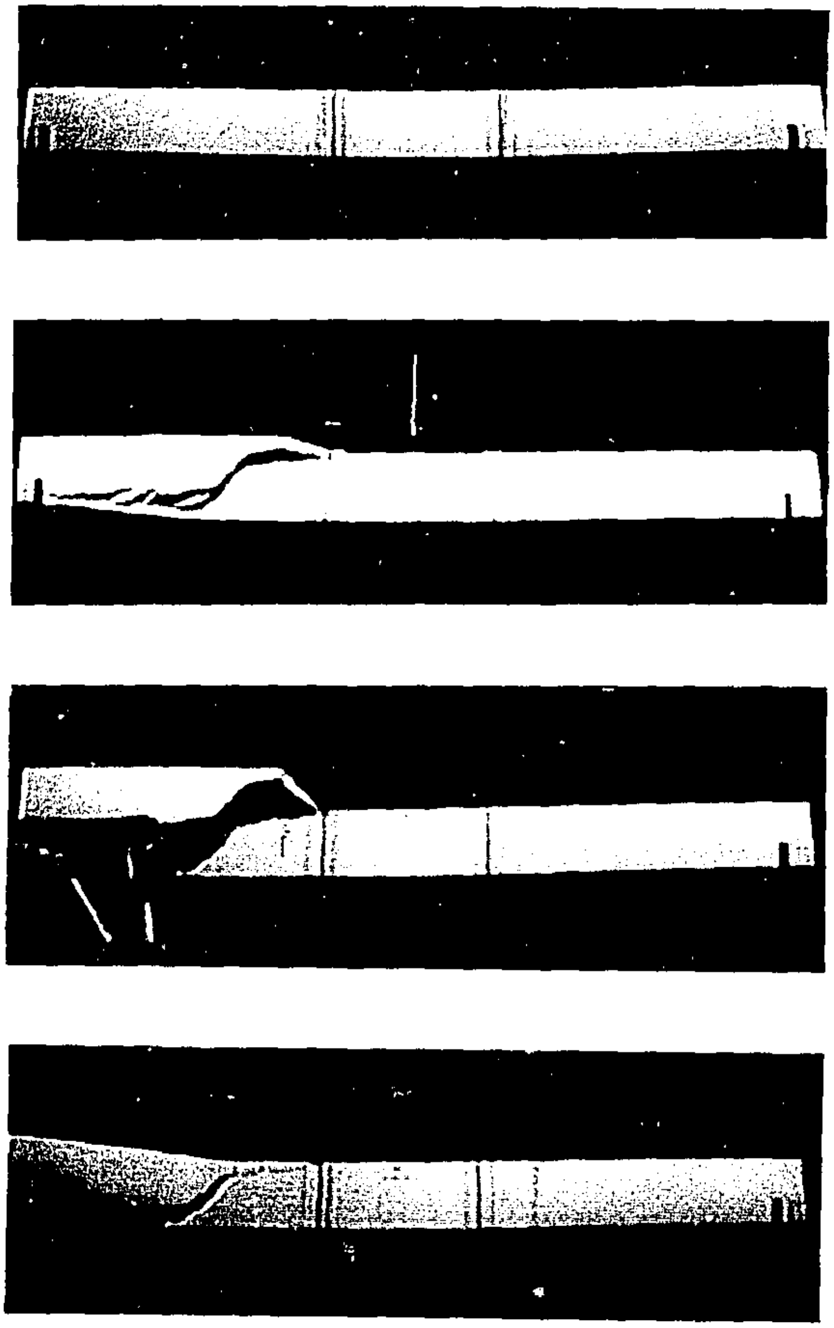

Figure 4.34: Sequence of failure in high-strength concrete beam HC1B

The combined effects of higher dowel forces and higher bond stresses in high-strength concrete beams can result in a sudden splitting failure in the concrete in a plane through the reinforcing bars. Figure 4.34(c) shows this failure mechanism. The high-strength concrete beams with epoxy coated bars displayed less ductility (see Table 4.8) and resulted in complete loss of the concrete cover (see Fig. 4.34(d)).

It is important to note that the high-strength concrete beams tested would not have required minimum shear reinforcement using the ACI code (ACI 1989) approach. The presence of shear reinforcement would have a twofold effect: it would help to control the diagonal tension cracks and would help to control the dowel-splitting and bond-splitting cracks. An intermediate layer of longitudinal bars would result in higher shear capacity (Collins *et al.* 1993) and would have reduced the dowel forces in the tension reinforcement.

4.3 RESPONSE OF SLAB-COLUMN CONNECTIONS

Although some research has been conducted by Nawy and Orenstein (1970), Nawy and Blair (1971) and Clark (1973) on the prediction of flexural crack widths in two way slabs, little work has been done on the effect of epoxy coatings on the flexural cracking (Abrishami *et al.* 1994). The research reported in this section investigates the effect of epoxy-coatings on reinforcement on the cracking behaviour of slab-column connections. The influence of concrete quality and thickness of epoxy coatings were also studied.

4.3.1 Test Program

A typical parking garage structure was chosen as the prototype structure. Figure 4.35(a) shows the prototype structure with a 4 bay by 4 bay flat plate slab having 5 m spans. The computer program "ADOSS" (CPCA 1987) was used to design the 200 mm thick slab according to the CSA Standard (CSA 1984). A typical test specimen, shown in Figure 4.35(b), represents a full-scale interior slab-column connection. The test program consisted of a series of six slab-column connection specimens, each with slab dimensions of 2 m by 2 m by 200 mm thick supported on a 300 by 300 mm column. Figure 4.36 shows the geometry and reinforcement details for a typical specimen. The No. 15 top reinforcing mat had a 40 mm cover and the No. 15 bottom bars had a 20 mm cover.

The slabs were divided into two series: one with normal-strength concrete having a water cement ratio of 0.45 and no special curing conditions and the other series with high-performance concrete having a water cement ratio of 0.31 and subjected to 5 days of moist curing. Each series of slabs was constructed with uncoated bars and bars with two different epoxy-coating thicknesses. All the specimens were stripped from their timber formwork after 4 days. Table 4.11 summarizes the material properties of the concretes used in the test specimens. The concrete compressive strengths, f_c' , were obtained by testing standard field cured cylinders, having a diameter of 150 mm and a height of 300 mm. The stress-strain relationships of the normal and high-performance concretes are shown in Fig. 4.37. The modulus of rupture, f_r , was determined from flexural test specimens 100 mm by 100 mm by 400 mm long, and 150 mm by 150 mm by

600 mm long, loaded at their third points over spans of 300 mm and 450 mm, respectively. The splitting tensile tests were carried out on 150 mm diameter by 300 mm long cylinders. Figure 4.38 shows the measured shrinkage of the normal-strength and high-performance concrete control beams (100 mm by 100 mm by 400 mm). As can be seen, the high-performance concrete had less shrinkage than the normal-strength concrete. All of the control specimens used to determine the concrete properties were cured in the same manner as the slab-column specimens. The average concrete strengths are summarized in Table 4.12.

All of the reinforcing bars in the slab were No. 15 bars, with a specified yield strength of 400 MPa and a measured yield stress of 480 MPa. Three different surface conditions were provided on the No. 15 bars. The specimens labelled "C0" contained uncoated bars, while those labelled "C1" and "C2" contained bars with epoxy coating thicknesses of 6-8 mils and 10-12 mils, respectively. Specimens C0, C1 and C2 were constructed with the normal-strength concrete, while specimens HC0, HC1 and HC2 were constructed with high-performance concrete.

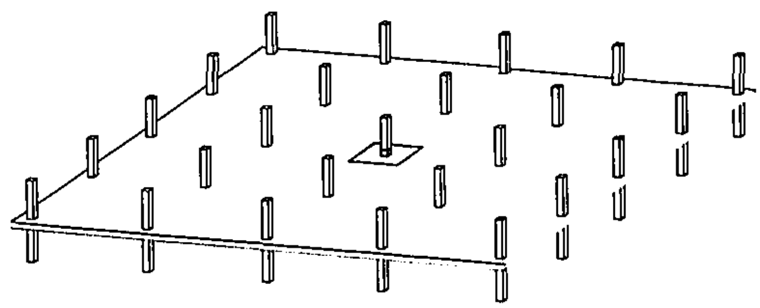

(a) prototype structure (5 m x 5 m bays)

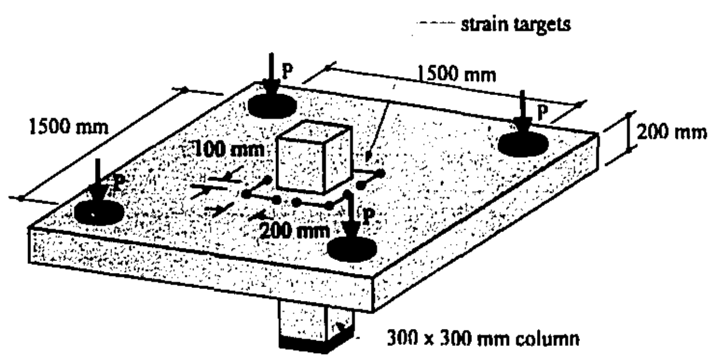

(b) slab-column specimen (2 m x 2 m)

Figure 4.35: Prototype structure and test specimen

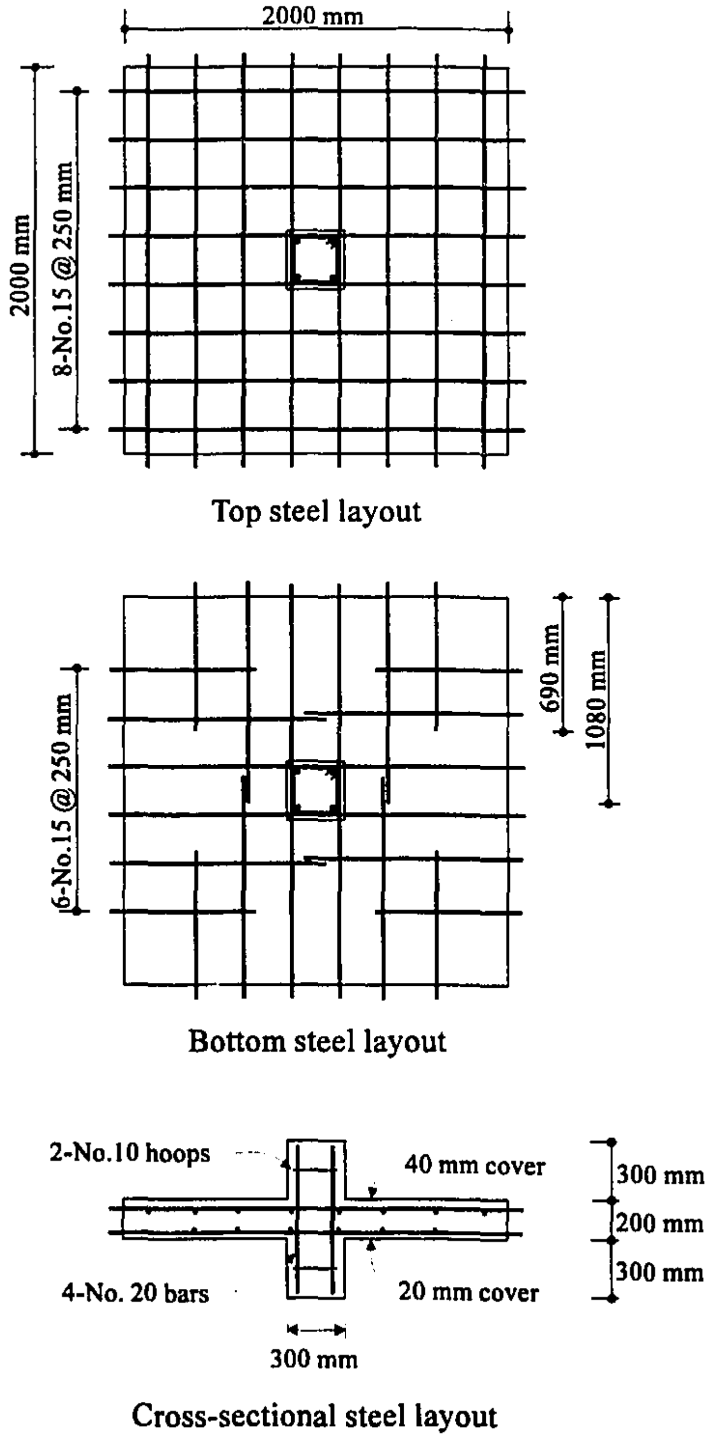

Figure 4.36: Reinforcement details of slab specimens

Table 4.11: Composition and properties of the concretes used in the slab specimens

Characteristics	Normal-strength concrete, 28 MPa	High-performance concrete, 34 MPa
Cement (Type 10), (kg/m^3)	355	495
Fine aggregates, (kg/m^3)	790	665
Coarse aggregates, (kg/m^3)	1040	1080
Water, (l/m^3)	160	155
Water-Cement ratio	0.45	0.31
Air-entraining agent, (ml/m^3)	175	800
Water-reducing agent, (ml/m^3)	1010	1550
Superplasticizer, (l/m^3)	---	3200
Slump, (mm)	175	80
Air content, (%)	7.2	9

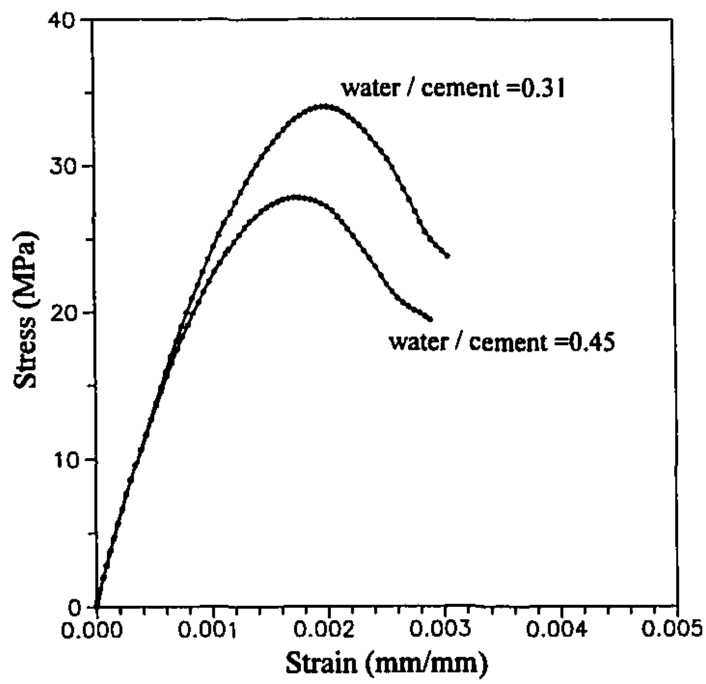

Figure 4.37: Concrete stress-strain relationships

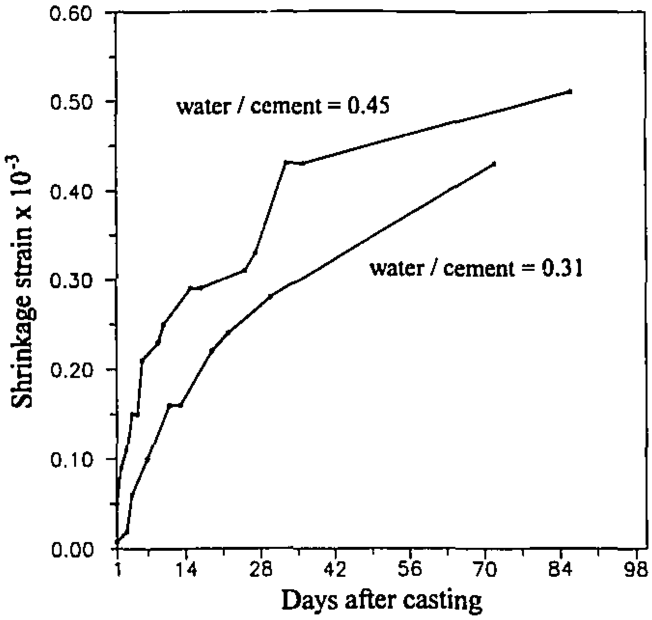

Figure 4.38: Measured shrinkage of the normal and high-performance concretes

Table 4.12: Measured concrete properties of slab specimens

	7 days	21 days			
	f'_c (MPa)	f'_c (MPa)	f_{sp} (MPa)	f_r* (MPa)	f_r** (MPa)
Normal-strength concrete, w/c = 0.45	24.0	27.6	3.0	3.4	2.9
High-performance concrete, w/c = 0.31	30.1	34.2	3.3	4.1	3.4

* Modulus of rupture from 100 mm by 100 mm by 400 mm beam specimens
** Modulus of rupture from 150 mm by 150 mm by 600 mm beam specimens

The test setup consisted of four hydraulic jacks transmitting loads through threaded rods passing through holes in the slab to loading plates on the top surface of the slab (see Fig. 4.35(b)). Four linear voltage differential transducers (LVDT's) measured the deflections of the slab at the loading points which were 1.5 m apart. At each load stage the cracks were measured using a crack width comparator. Strain targets were glued to the top surface of the slab around the column to determine strains.

To simulate the stages of construction in the prototype structure each specimen was loaded as described in Fig. 4.39. The specimens were first loaded at an age of seven days to produce moments in the slab at the face of the column equal to the moments in the prototype structure due to the slab self weight (4.8 kPa) and an additional superimposed construction load of 1.0 kPa. This simulated the loading condition in the prototype structure after removal of the forms. The test specimens were then unloaded and at an age of 21 days were reloaded. During the second loading, load stages were taken at loads corresponding to the self weight of the slab (4.8 kPa), an additional superimposed dead load of 1.0 kPa, one half the live load and the full live load of 2.4 kPa. The loading was then cycled three times between loads corresponding to service dead load and full service loading (dead plus full live load) as shown in Fig. 4.39. After this cycling, the loads were increased until yielding occurred in the reinforcement.

The self-weight of test specimen plus a concentrated load, P, equal to 23.6 kN at each corner produced a moment at the column face equal to the moment due to self-weight in the prototype structure. Additional loads at each corner of 5.3 kN and 13.0 kN, were used to simulate the additional moment at the face of the column due to construction loads and live loads, respectively. The moment at the face of the column is $1.2\ P + 3.77$ kNm, accounting for the self weight of the specimen, the weight of the loading apparatus and the applied loading (a concentrated load, P, at each corner).

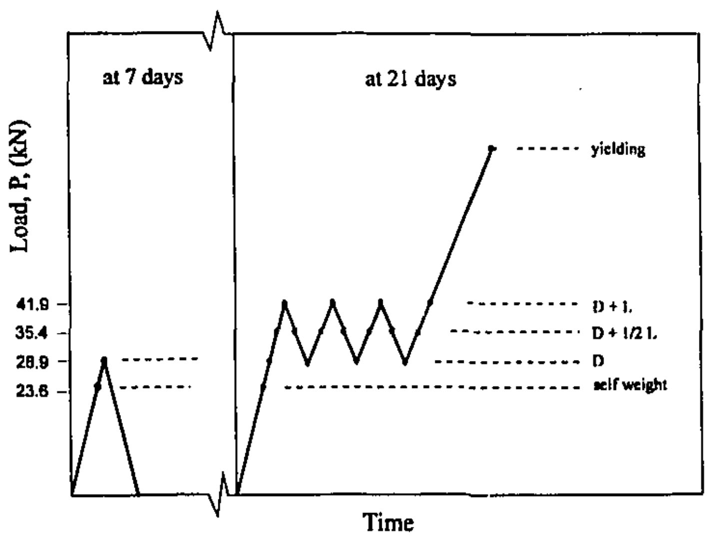

Figure 4.39: Load stages in test specimens to simulate construction and loading of prototype structure.

4.3.2 Influence of epoxy coating and concrete quality on load versus strain response

Figure 4.40(a) and Fig. 4.40(b) show the load versus average strain responses of the normal-strength (C0, C1 and C2) and the high-performance specimens (HC0, HC1 and HC2), respectively. The average strain was calculated from the eight strains measured from the strain targets on the top surface of the slab around the column perimeter (see Fig. 4.35(b) and Fig. 4.40).

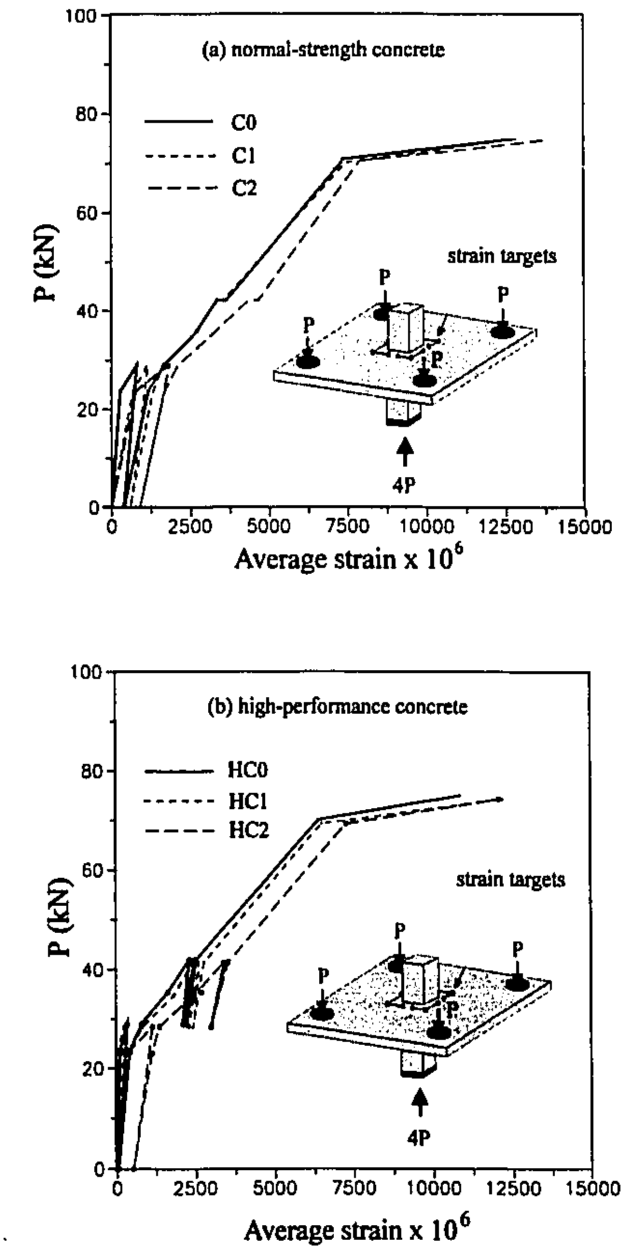

Figure 4.40: Load versus average strain responses of test specimens

The strain targets were positioned at a distance of 100 mm from the face of the column and were located to give gauge lengths of 200 mm. Larger measured average strains would result in larger slab deflections. For the normal-strength specimens the presence of the 6-8 mil epoxy coating resulted in only a slight increase in the average strain measured and about a 30 percent increase for the 10-12 mil coating thickness. For the high-performance concrete specimens the presence of the 6-8 mil coating thickness resulted in about a 15 percent increase in the average strain, while the 10-12 mil coating thickness resulted in an increase of about 40 percent. If Fig. 4.40(a) and Fig. 4.40(b) are compared, it is evident that the use of high-performance concrete resulted in reduced average strains for each coating thickness. The presence of epoxy coating on the reinforcement, particularly for the larger coating thickness, results in larger slab deflections. The use of high-performance concrete, as currently required in the ACI Code and the CSA Standard, would reduce the slab deflections and hence would compensate for the influence of epoxy coating on the reinforcement.

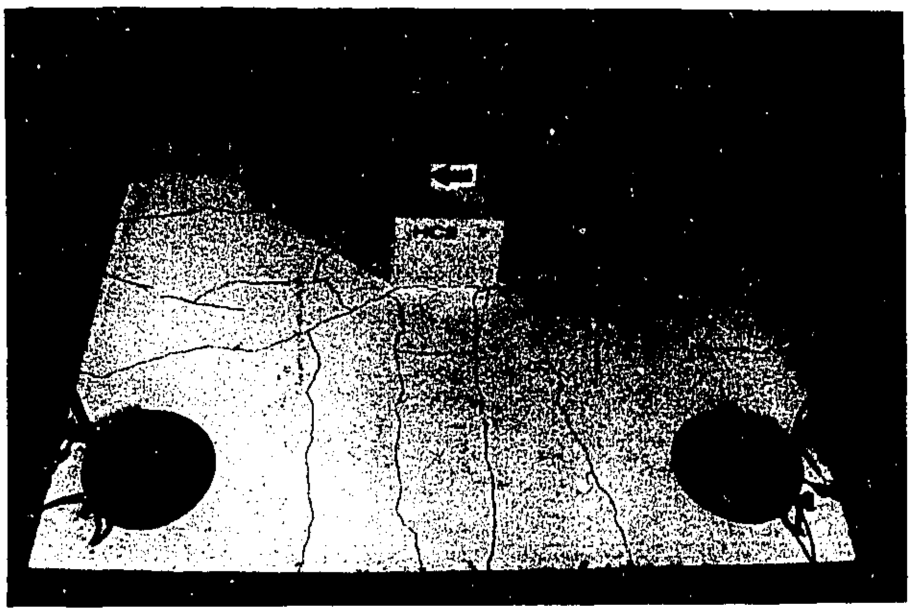

Figure 4.41: Specimen HC2 during the test

4.3.3 Influence of epoxy coating and concrete quality on cracking

Figure 4.42 shows the crack patterns and measured crack widths for the specimens loaded at 7 days. The load stage shown corresponds to the load level in the prototype slab at first removal of forms (i.e., self weight plus a construction load of 1.0 kPa). It is clear from this figure that high-performance concrete significantly decreases both the number of cracks and the crack widths. It is also evident that the presence of epoxy coating increases the crack widths. In addition, the specimens with the 10-12 mil epoxy coating had a larger number of cracks.

Figure 4.43 shows the crack patterns and measured crack widths for the specimens loaded at 21 days. This load stage corresponds to the load levels in the prototype slab due to self weight, superimposed dead load, and full live load. As can be seen, the use of high-performance concrete results in a slight decrease in the average crack width.

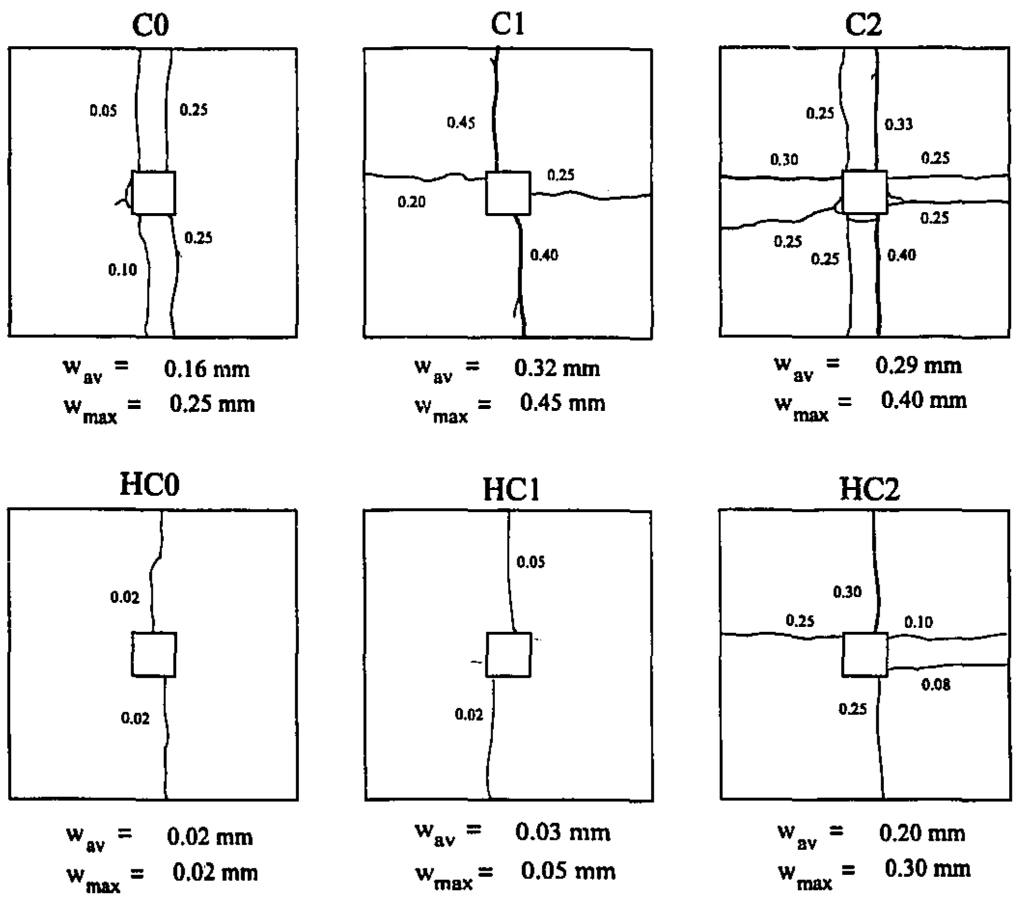

Figure 4.42: Crack patterns and crack widths on top surface of slabs due to simulation of self-weight and construction loads at an age of 7 days

Also, specimens reinforced with epoxy-coated bars showed larger crack widths than specimens reinforced with uncoated bars. An increased coating thickness resulted in larger average crack widths.

Figure 4.44(a) and Fig. 4.44(b) show the influence of epoxy coating on the maximum crack width of slab specimens constructed with normal-strength concrete and high-performance concrete, respectively. These figures show that, in the service load range, the presence of epoxy coating increases the maximum crack width. Figure 4.45 illustrates the influence of concrete quality on maximum crack width for different epoxy coating thicknesses. It is clear from Fig. 4.42, Fig. 4.43 and Fig. 4.45 that the use of high-performance concrete results in smaller average crack widths.

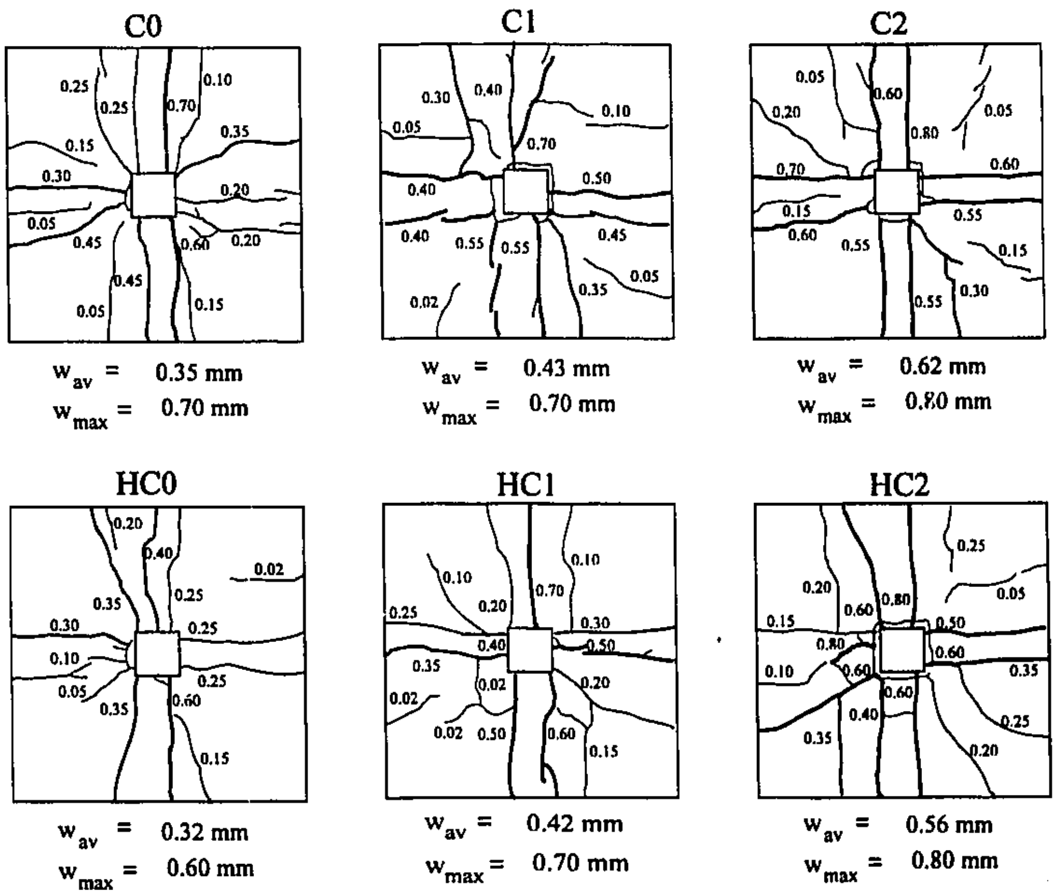

Figure 4.43: Crack patterns and crack widths on top surface of slabs due to simulation of dead loads and full live load at an age of 21 days

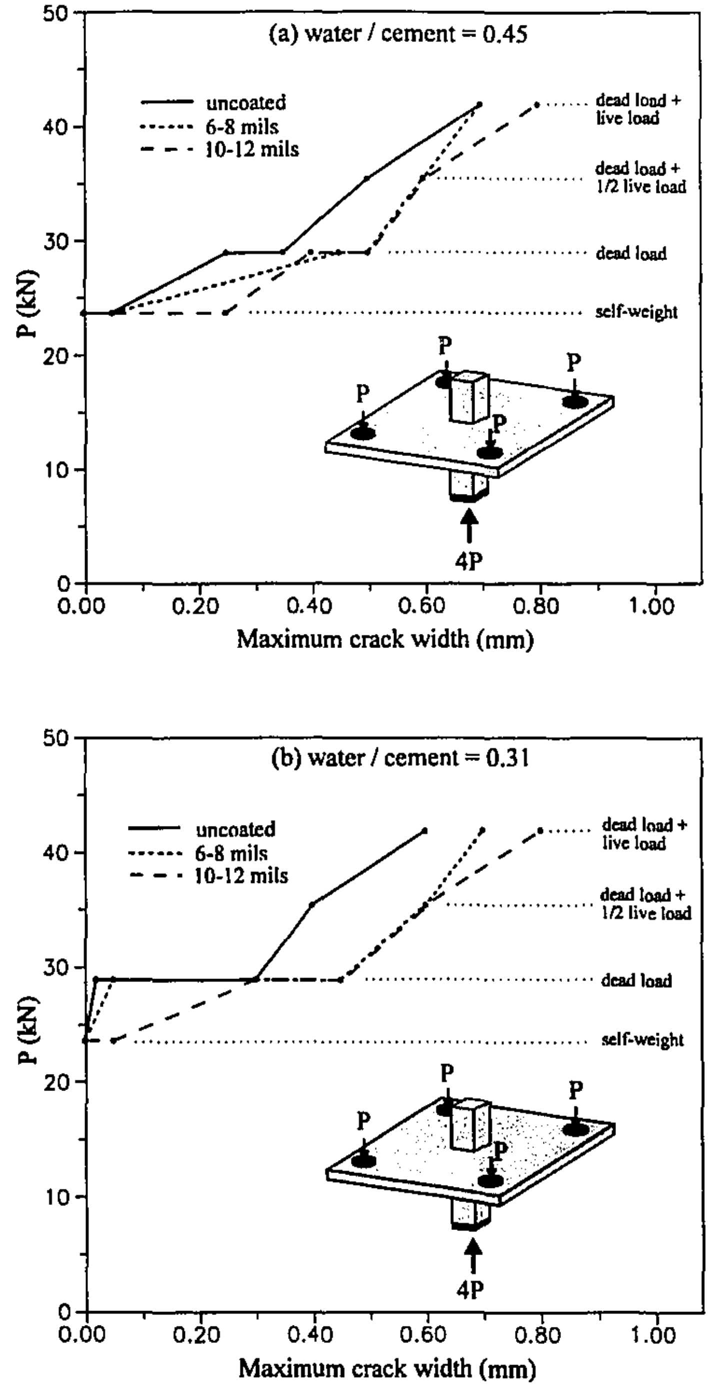

Figure 4.44: Influence of epoxy coating on maximum crack widths

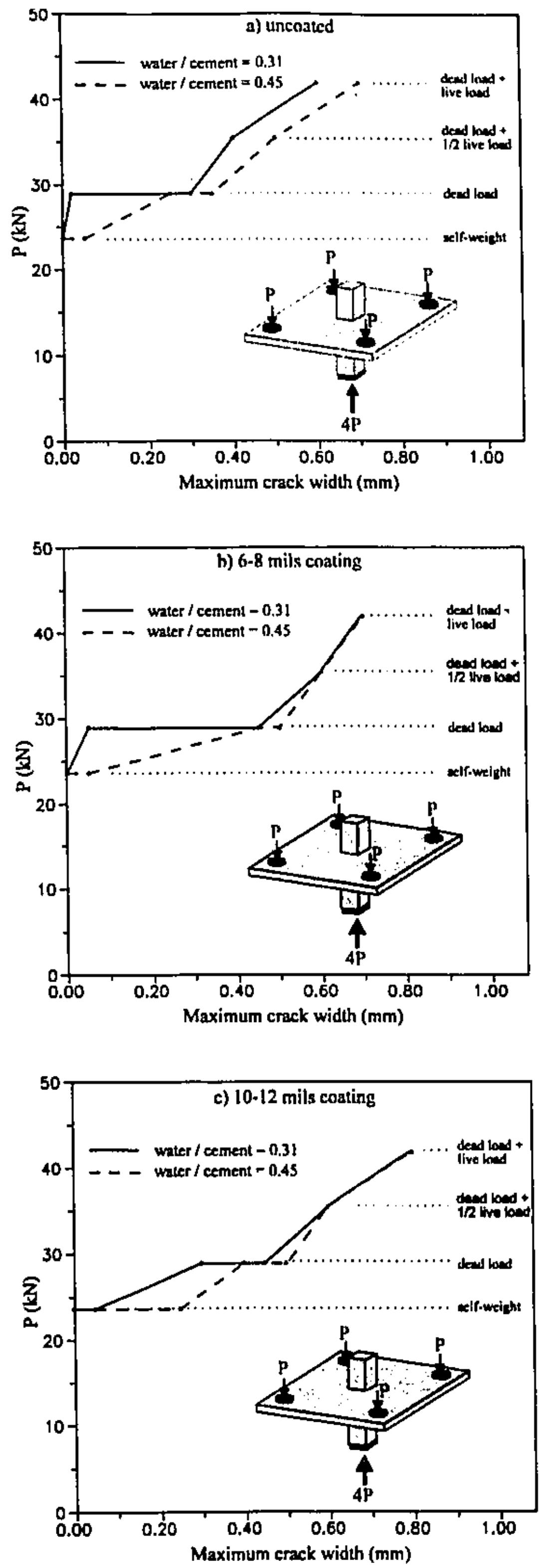

Figure 4.45: Influence of concrete quality on maximum crack widths

Chapter 5

ANALYTICAL STUDIES OF POST-CRACKING BEHAVIOUR

"There is nothing more practical than a simple theory"
Robert Maillart

Nonlinear behaviour of reinforced concrete is strongly influenced by concrete cracking. Analytical studies such as numerical methods and finite element techniques are employed to determine the response of reinforced concrete structures. A summary of research carried out in recent years on the application of finite elements to model the behaviour of reinforced concrete is given in a report of the ASCE Task Committee on Finite Element Analysis of Reinforced Concrete (ASCE 1982). Lutz (1970) carried out finite element analyses on single bar specimens to study the bond stress distribution, the variation of concrete and steel stresses, and the variation of circumferential stresses in the concrete. oA number of computer programs (e.g., NONLAX (Ghoneim 1978) and ADINA (1981)) have been developed to enable prediction of the non-linear response of reinforced concrete. The development of a constitutive relationship for predicting the response of reinforced concrete after cracking requires extensive experimental studies.

This chapter presents analytical studies of the post-cracking behaviour of reinforced concrete elements subjected to pure tension. The prediction of the load-deflection responses of tension specimens, including the influence of both transverse cracks and splitting cracks, is presented. Equations are proposed for predicting tension stiffening, transverse crack spacings and transfer lengths. The effect of concrete strength and steel fibres on the tensile stress-strain response of concrete, particularly after cracking is illustrated. Also, means of predicting the influence of epoxy coatings on the widths of cracks in beams and slabs is investigated.

5.1 CRACK ANALYSIS IN A REINFORCED CONCRETE TENSION SPECIMEN

Fig. 5.1 shows a tension specimen, reinforced with a single bar, before cracking. The applied tensile force is transferred from reinforcing bar to the concrete by bond stress at the end zones of the specimen. This zone is referred to as a "D" region, that is, a region in which there is a disturbed flow of stresses. Beyond the "D" region the bond stress is zero and strains in the concrete and steel are equal along the specimen, before cracking occurs. This zone is called a "B" region.

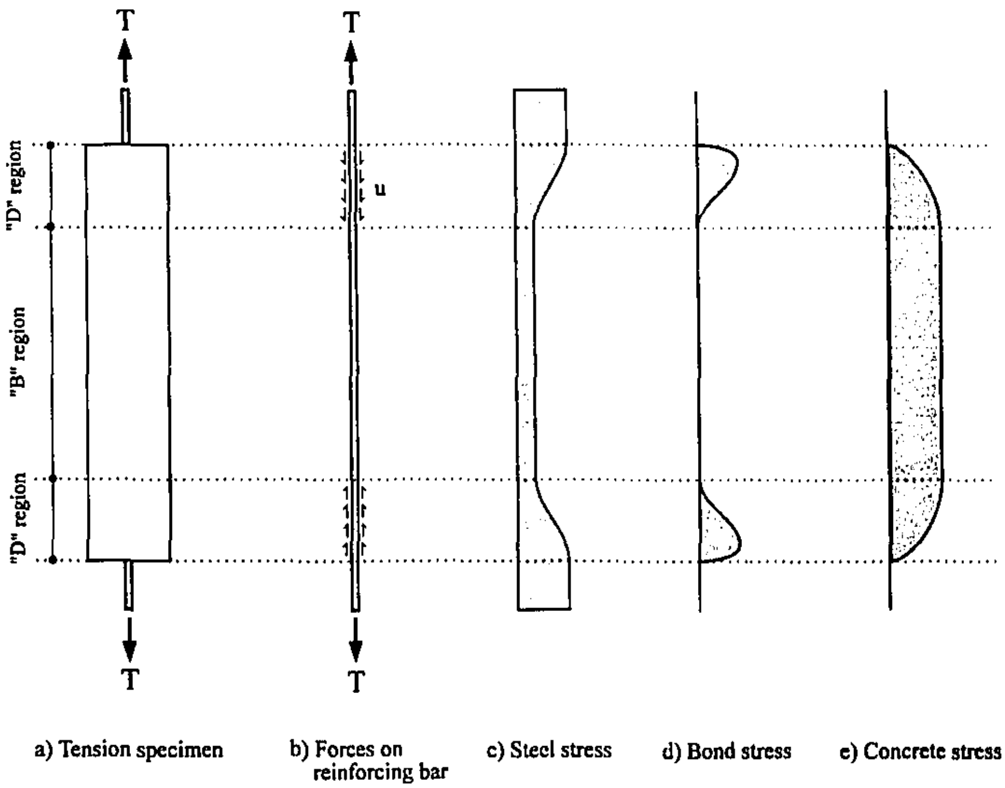

Figure 5.1: Stresses acting on concrete and steel before cracking

In general there are two types of cracking in a tension specimen, splitting cracks and transverse tensile cracks (see Fig. 5.2(a)). Splitting cracks occur in the "D" regions and transverse tensile cracks occur in the "B" region. When the splitting cracks occur, the bond stress decreases and the transfer length in the "D" region extends into the "B" region (see Fig. 5.2(b)). Along the splitting cracks the specimen acts like a bare bar and the length of the "B" region is reduced. The transverse cracks occur when the maximum longitudinal tensile stress in the concrete reaches the cracking stress, f_{cr} . After the transverse tensile cracks form, new "D" regions are formed at the crack locations (see Fig. 5.2(c)). The type of cracking depends on the bond strength between the concrete and the reinforcement and the tensile strength of the concrete.

In the "B" regions the bond stress is zero and the longitudinal tensile stress is a maximum. Therefore only transverse cracks form in the "B" regions.

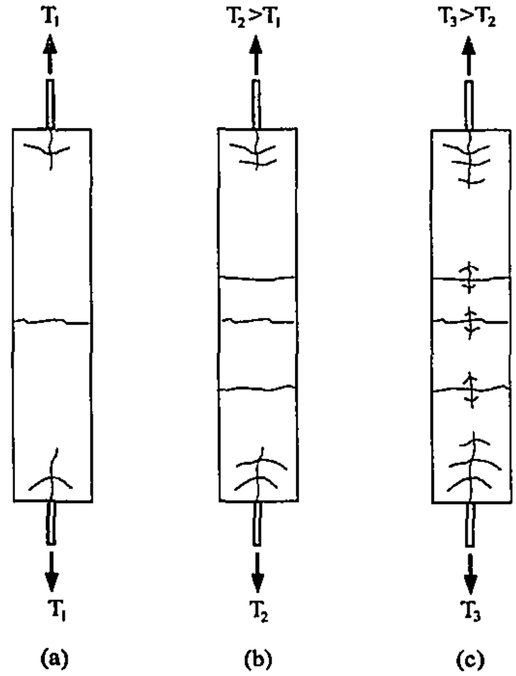

Figure 5.2: Splitting and transverse crack propagation in a tension specimen

5.1.1 Response of a Tension Specimen Reinforced with a Single Bar

Before cracking, it is typically assumed that the concrete and steel have the same strain (i.e., $\epsilon_s = \epsilon_c$). The relationship between tensile force, T , and elongation, Δ , can be written as:

$$T = K_{uc}\ \Delta \tag{5.1}$$

where K_{uc} is the stiffness of an uncracked tension specimen. The applied tensile force, T , is the summation of forces carried by the concrete and the reinforcement and can be written as:

$$T = (E_s A_s + E_c A_c)\epsilon \tag{5.2}$$

and the total elongation of the specimen having length, L , is:

$$\Delta = \epsilon L \tag{5.3}$$

where ϵ is the strain in the steel or concrete, E_s and E_c are the moduli of elasticity of the steel and concrete and A_s and A_c are the areas of the steel and the concrete, respectively. The stiffness of a bare bar having a length L is $K_s = E_s A_s / L$. Hence the pre-cracking stiffness of the specimen can be written as:

$$K_{uc} = K_s \left(1 + \frac{1}{n\rho}\right) \tag{5.4}$$

where $n = E_s / E_c$ and $\rho = A_s / A_c$. The load-deformation response up to cracking can be expressed as:

$$T = K_s \left(1 + \frac{1}{n\rho}\right) \Delta \tag{5.5}$$

In order to obtain the post-cracking response, the following expression is used:

$$T = A_c f_c + A_s f_s \quad \leq A_s f_y \tag{5.6}$$

where the average stress in the cracked concrete, f_c , is given by Collins and Mitchell (1991) as:

$$f_c = \frac{\alpha_1 \alpha_2 f_{cr}}{1 + \sqrt{500 \epsilon_{cf}}} \qquad \text{for} \quad \epsilon_{cf} > \epsilon_{cr} \tag{5.7}$$

where α_1 = factor accounting for bond characteristics of reinforcement
= 1.0 for deformed bar
= 0.7 for plain bar
= 0 for unbonded bar

and α_2 = factor accounting for sustained or repeated loading
= 1.0 for short-term monotonic loading
= 0.7 for sustained and /or repeated loads

ϵ_{cf} is the strain in the concrete caused by stress and:

$$f_s = E_s \epsilon_s \qquad < f_y \tag{5.8}$$

This approach accounts for the tension stiffening effect in the concrete. However, Eq. (5.7) assumes only the presence of transverse cracks and does not consider the important influence of splitting cracks. From the experiments reported in Section 4.1, it was found that splitting cracks reduce the bond in the vicinity of the splitting cracks and hence reduce the tension stiffening. In order to account for the detrimental effects of splitting cracks on the tension stiffening an additional factor, α_3 is introduced into Eq. (5.7) giving:

$$f_c = \frac{\alpha_1 \alpha_2 \alpha_3 f_{cr}}{1 + \sqrt{500 \epsilon_{cf}}} \qquad \text{for} \qquad \epsilon_{cf} > \epsilon_{cr} \tag{5.9}$$

It is clear from the testing that specimens with large c/d_b ratios (i.e., a small bar with significant cover) do not exhibit significant splitting cracks and hence α_3 equals 1.0. However specimens with small c/d_b ratios (i.e., larger bars with smaller cracks) can have significant reduction in the tension stiffening due to splitting. Figure 4.7 illustrates the influence of a small c/d_b ratio on the development of splitting cracks. Specimen C0-10 has a c/d_b ratio of 3.5 and does not exhibit any splitting cracks. On the other hand, specimen C0-30, with a c/d_b ratio of 1.3 exhibits splitting cracks over nearly its entire length. Figure 5.3 illustrates the response of specimen C0-30, and also shows the response predicted, using $\alpha_3 = 0$. It is interesting to note that, not only is there practically no tension stiffening after cracking, but also the stiffness of the response is reduced before transverse cracks form. This reduction in the so-called "pre-cracking" response is due to the formation of splitting cracks near the ends of the specimens.

It is clear from the test results that splitting cracks are only significant when c/d_b is less than about 2.5. It is also interesting to note that the ACI Code (ACI 1989) requires larger development length for situation with c/d_b less than 2.5 because of the influence of splitting cracks. The splitting crack factor α_3 is assumed to vary from 1.0 when c/d_b equals 2.5 to a value of 0.0 when c/d_b is about 1.3. Assuming a linear variation of this parameter gives:

$$\alpha_3 = 1.0 \qquad \text{for} \quad c/d_b \geq 2.5 \tag{5.10a}$$

$$\alpha_3 = 0.8\ c/d - 1 \qquad \text{for} \quad 1.25 \leq c/d_b \leq 2.5 \tag{5.10b}$$

$$\alpha_3 = 0 \qquad \text{for} \quad c/d_b \leq 1.25 \tag{5.10c}$$

Figure 5.4 compares the experimental load versus elongation response with the predicted response. For the predicted response, a value of α_3 of 0.27 was used, corresponding to the value calculated using Eq. (5.10) for a c/d_b ratio of 1.59. As can be seen the response is predicted well, particularly at the service load level range.

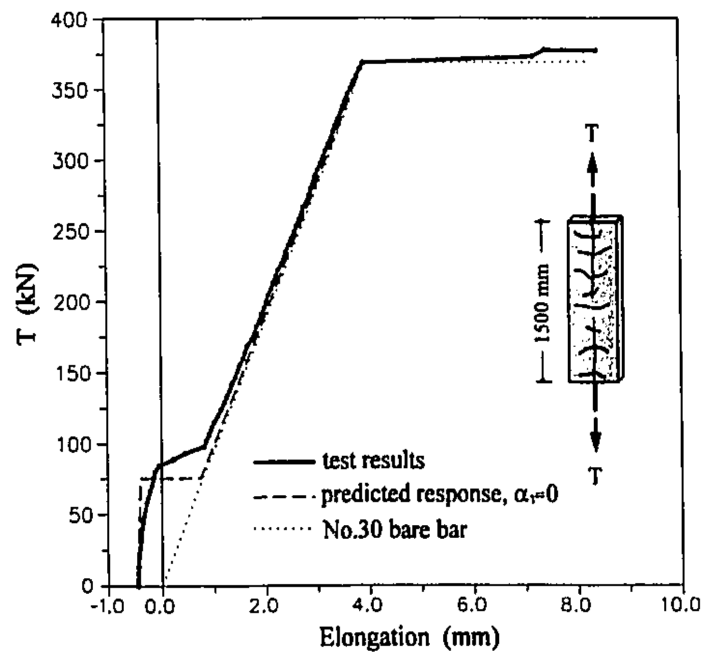

Figure 5.3: Comparison of test results and predicted response for specimen C0-30

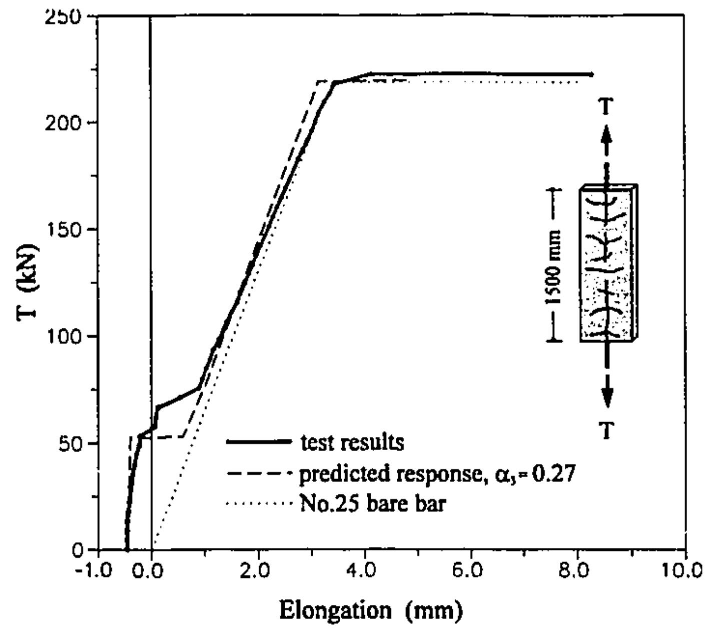

Figure 5.4: Comparison of test results and predicted response for specimen C0-25

5.1.3 Transfer Length in a Tension Specimen ("D" Region)

Fig. 5.5 shows a segment of a tension specimen in the "D" region. Using equilibrium conditions for the reinforcing bar embedded in concrete:

$$\alpha u_{max}(\pi d_b \ell_t) = T - A_s f_s \tag{5.11}$$

where αu_{max} is the average bond stress along the transfer length, ℓ_t is the transfer length and f_s is the stress in the steel at the end of the transfer length. For this elastic uncracked response the stress in the reinforcement can be expressed as:

$$f_s = \frac{T}{A_s\,(\,1 + 1/n\rho)} \tag{5.12}$$

and hence Eq. (5.11) becomes

$$\ell_t = \frac{T}{\pi \alpha u_{max}\, d_b}\left(\frac{1}{1 + n\,\rho}\right) \tag{5.13}$$

substituting the αu_{max} by the bond stress suggested by the CEB-FIP code (1991) of 1.8 f_{cr} the transfer length at the cracking load is:

$$\ell_t = \frac{T_{cr}}{1.8\, f_{cr}\ \pi d_b}\left(\frac{1}{1+n\rho}\right) \qquad \textbf{(5.13b)}$$

but the cracking load T_{cr} , can be written as:

$$T_{cr} = A_s\left(\frac{1+n\rho}{\rho}\right) f_{cr} \qquad \textbf{(5.14)}$$

Hence at the cracking load:

$$\ell_t = \frac{d_b}{7.2\ \rho} \qquad \textbf{(5.15)}$$

The minimum length of specimen required to form transverse cracks is $2\ell_t$. For specimens exhibiting splitting cracks (i.e., c/d_b less than about 2.5) a longer transfer length would be necessary.

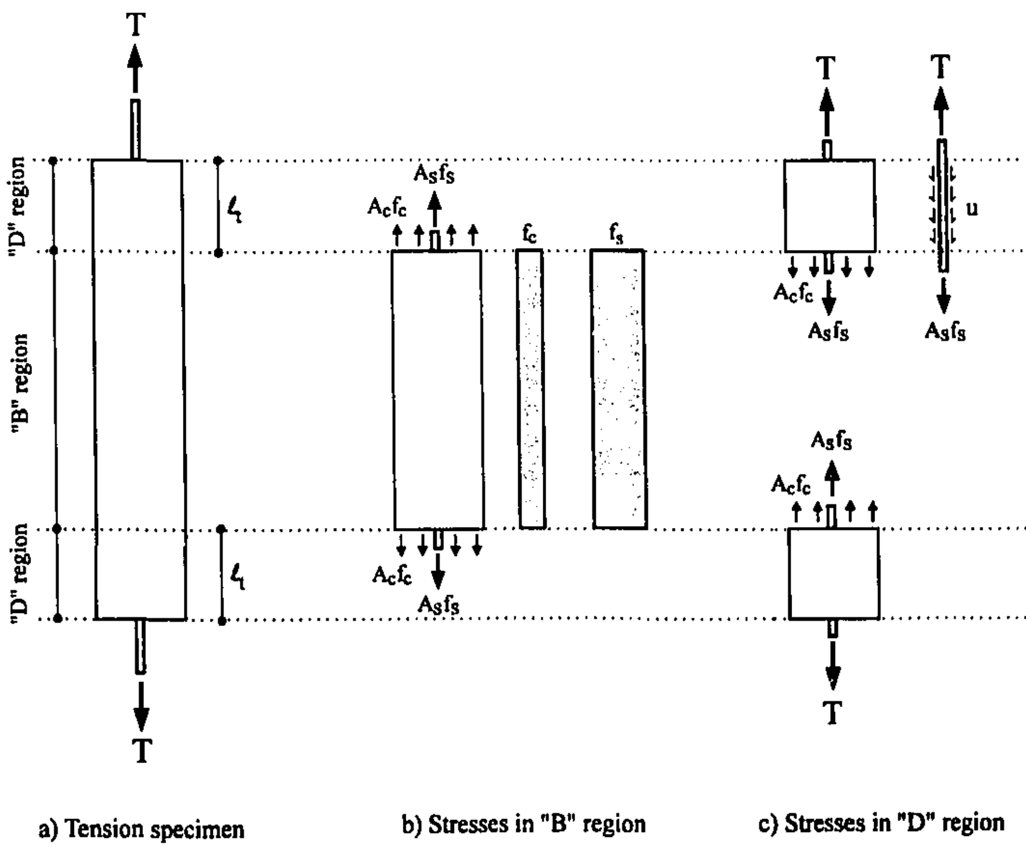

Figure 5.5: Stresses acting on concrete and reinforcing bar in "B" and "D" regions

5.1.4 Crack Spacing

Fig. 5.6 shows a segment of a tension specimen between two cracks having a length so that the concrete stress can build up to just reach f_{cr} without causing a new crack to form. That is, the length of the specimen considered is s, where s is referred to as the stabilized crack spacing. In order for the new crack to form, the stress in the concrete, f_c, must reach the cracking stress, f_{cr} (see Fig. 5.6). Considering equilibrium over length of $s/2$, gives:

$$\alpha u_{max}(\pi d_b s/2) = A_c f_{cr} \tag{5.16}$$

or:

$$s = \frac{d_b}{2\rho} \frac{f_{cr}}{\alpha u_{max}} \tag{5.17}$$

in which αu_{max} is the average bond stress between two cracks. substituting the αu_{max} by the bond stress suggested by the CEB-FIP Code (1991) of $1.8 f_{cr}$ the crack spacing can be expressed as:

$$s = \frac{d_b}{3.6\rho} \tag{5.18}$$

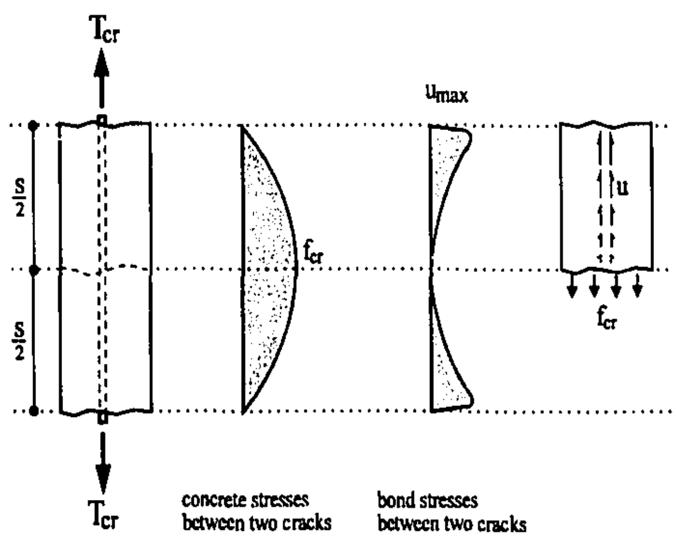

Figure 5.6: Determination of crack spacing in a tension specimen having length s

The crack spacing shown in Eq. (5.18) has the same value suggested by the CEB-FIP Code to calculate the maximum crack spacing. The CEB-FIP has estimated the maximum crack spacing as: $s_{max} = 1.5 s_{av}$ in which, s_{av} is the average crack spacing and s_{max} is the maximum crack spacing. Based on the tests on tension specimens described in Chapter 4 (see Tables 4.1 and 4.2), the average value for the ratio of s_{max}/s_{av} is 1.23 and 1.64 for the normal-strength and high-strength concrete specimens, respectively.

5.2 INFLUENCE OF CONCRETE STRENGTH AND STEEL FIBRES ON TENSION STIFFENING

Figure 5.7 illustrates the effect of steel fibres on the average tensile stress-strain response of the concrete. In the tests described in Section 4.1.3, the average strain in the specimens was determined by dividing the average of the LVDT measurements (Fig. 4.5)) by the member length of 1500 mm. At each load stage, the average strain in the reinforcing bar was assumed to be equal to the average strain measured in the specimen thus enabling the determination of the average stress in the bar. The average tensile stress in the concrete was calculated at each load stage by subtracting the average tensile force in the steel from the total load applied to the specimen and then dividing this load carried by the concrete by the concrete area. In other words:

$$f_c = \frac{T - E_s A_s \epsilon}{A_c} \tag{5.19}$$

Figure 5.7a shows the measured load-deflection responses from the modulus of rupture tests on the concrete used to construct specimens C0 and FC0 (see Table 4.5). For the specimens without fibres there is a brittle failure in the concrete at cracking. The fibres not only give a higher cracking stress, f_{cr} , but also, after cracking, result in a smaller decay of the average tensile stress in the reinforced concrete specimens (see Fig. 5.7b) determined using Eq. (5.19). The addition of fibres gives an improved post-cracking response both for the fibre-reinforced concrete material and for the fibre-reinforced concrete specimen FC0 (see Fig. 5.7a and 5.7b).

Figure 5.8 shows the average concrete tensile stress versus strain responses obtained from specimens reinforced with uncoated bars. After cracking, the specimens containing steel fibres showed higher tension stiffening than the specimens constructed without fibres in both the normal and high-strength concretes. When the first primary crack formed in the concrete, the high-strength concrete showed higher tension stiffening than normal-strength concrete but after the formation of all cracks, both the high-strength and the normal-strength concrete showed the same tension stiffening (see Fig. 4.20). In specimens C0 and HC0 (see Table 4.5), containing no fibres, the response was observed to have zero stiffness once the bar yields at the crack, that is, exhibiting no tension stiffening. This is due to the fact that all of the deformations are taking place at the cracks due to the yielding of the reinforcement.

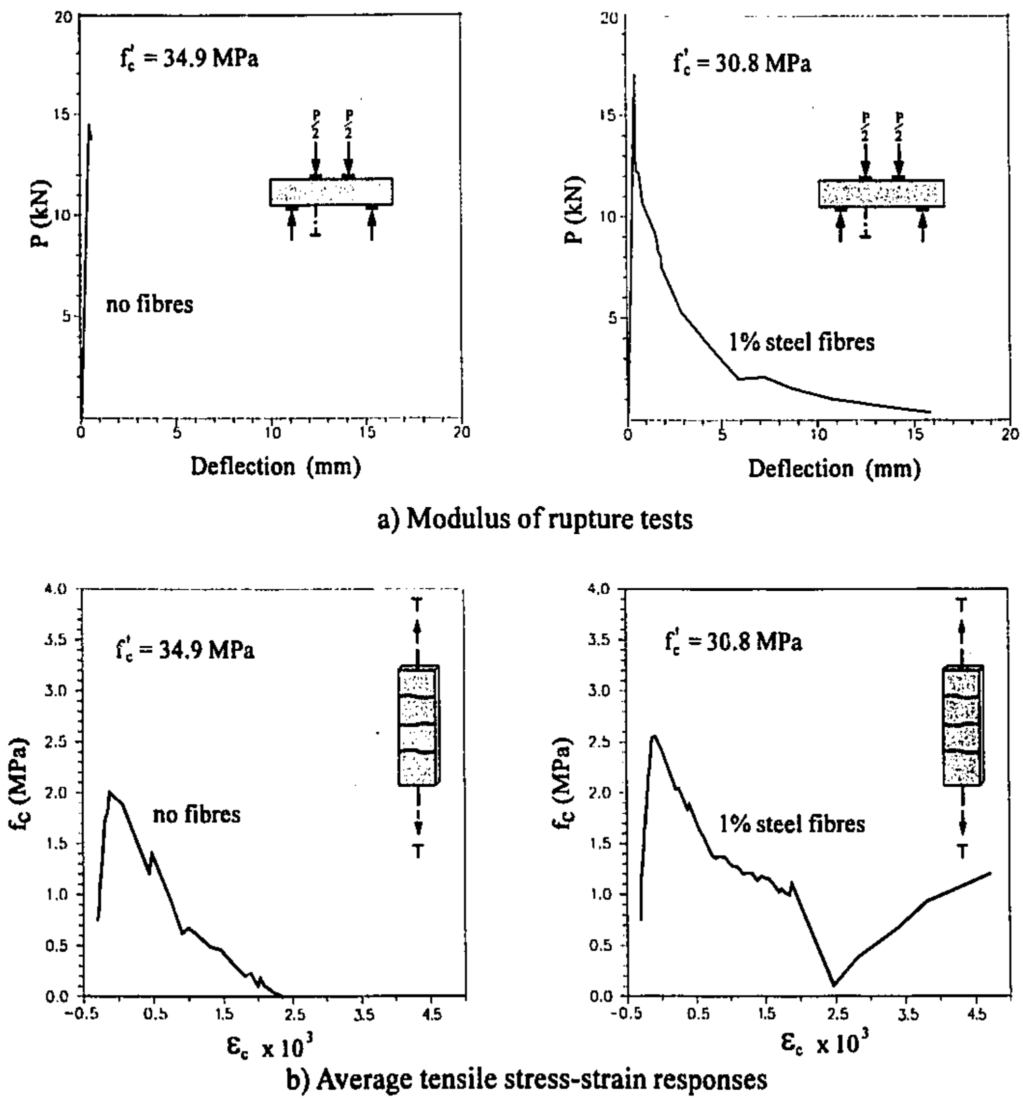

Figure 5.7: Effect of steel fibres on the tension response of concrete

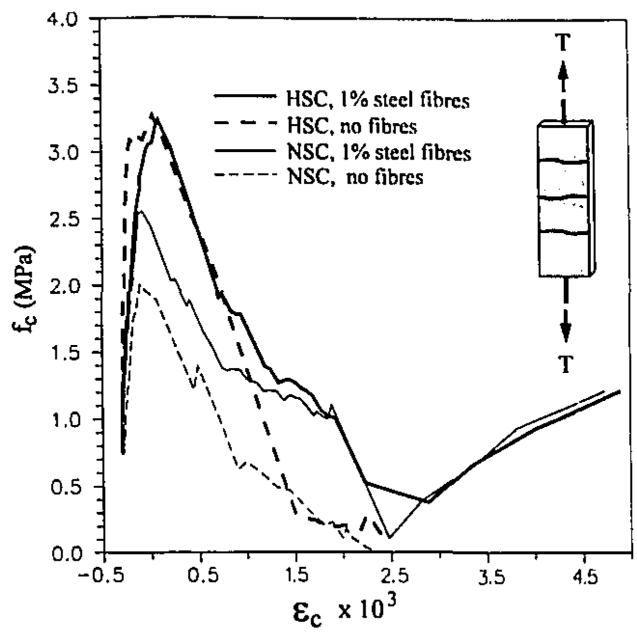

Figure 5.8: Effect of concrete strength and steel fibres on the average tensile stress-strain response for specimens with uncoated bars

5.2.1 Influence of Steel Fibres on the Response of a Tension Specimen Containing a Reinforcing Bar

Figure 5.9 shows a typical tensile response of a fibre-reinforced concrete specimen containing a reinforcing bar. Figure 5.10 shows the responses of two fibre-reinforced concrete specimens containing reinforcing bars.

The presence of fibres enables tension stiffening after yielding of the reinforcing bar (see Fig. 5.10). This is due to the ability of the fibres to help the steel reinforcing bars to resist tension across the cracks. The contribution of fibres after yielding of the reinforcing bar can be calculated as:

$$T_f = T - T_y \tag{5.20}$$

After yielding of the reinforcing bar, large straining occurs at the crack locations and the steel fibres participate in carrying the load across the cracks. At this stage, it is assumed that there is no significant tension stiffening in the concrete.

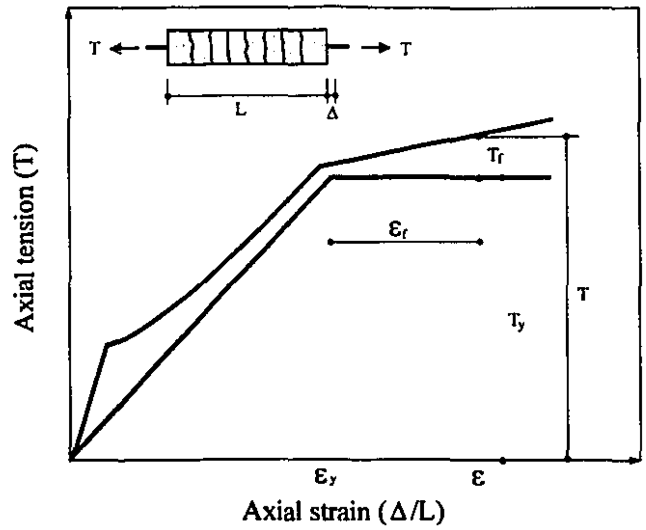

Figure 5.9: Typical response of fibre-reinforced concrete in tension

The additional tension carried by the fibres, T_f , after yielding the bar can be expressed as:

$$T_f = A_f \, E_f \, \epsilon_f \tag{5.21}$$

In which:

$$\epsilon_f = \epsilon - \epsilon_y \tag{5.22}$$

and the effective area of fibres, A_f , can be written as:

$$A_f = \frac{1}{2} \cdot \frac{1}{3} \, V_f \, A_c \tag{5.23}$$

where V_f is the percent of fibres in the specimen by volume. Equation (5.23) accounts for the fact that 1/3 of fibres will be oriented in the direction of tensile force and fifty percent of the randomly oriented fibres will pass through any given cross section. Hence:

$$T_f = \frac{V_f}{6} \, E_f \, A_c \, (\epsilon - \epsilon_y) \tag{5.24}$$

In the case of specimens FC0 and FHC0 (see Fig. 5.10), Eq. (5.24) is summarized as:

$$T_f = 53.8 \; x \; 10^6 \; (\epsilon - \epsilon_y) \tag{5.25}$$

In which, V_f = 1%, E_f = 2 x 10^5 MPa, A_c = 95 mm by 170 mm.

Figure 5.10 compares the test results with the predicted responses of the specimens FC0 and FHC0, constructed with normal-strength and high-strength concrete, respectively. The response predictions were made using tensile strengths of the fibre-reinforced concrete of 2.55 MPa and 3.25 MPa for the normal-strength and high-strength concretes, respectively. The tension stiffening effect is predicted well, particularly at the service load levels. Also the predicted responses, after yielding, are in good agreement with the test results.

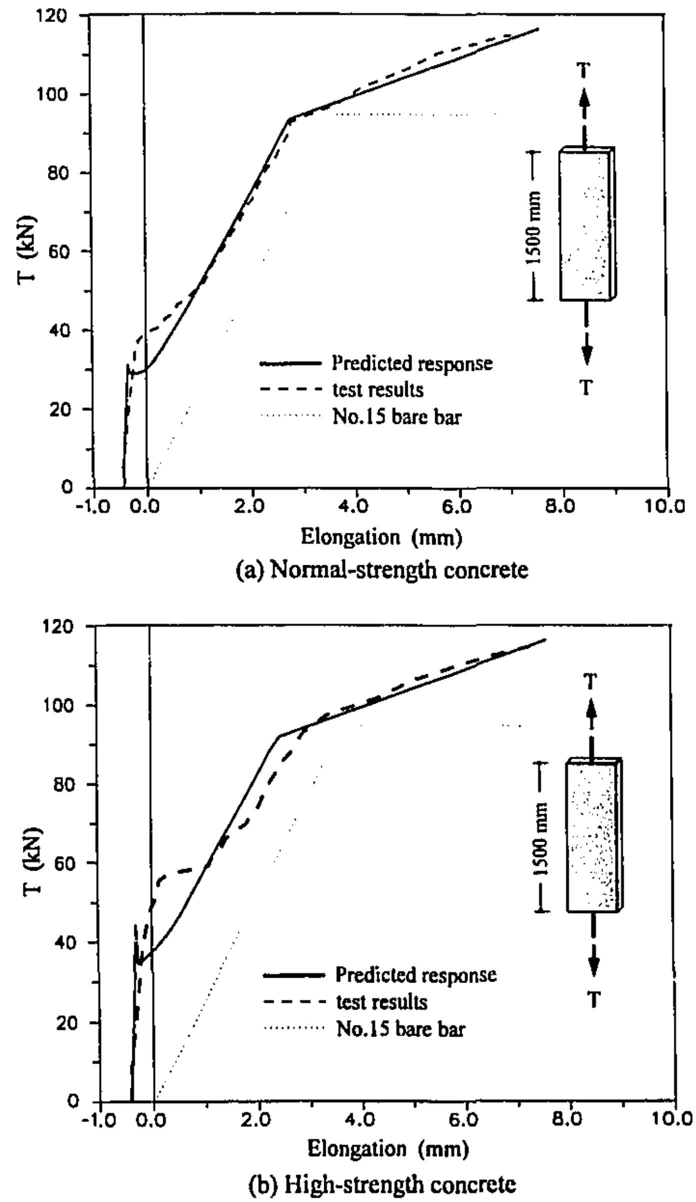

Figure 5.10: Comparison of predicted and test results for specimens containing steel fibres (FCO, FHCO)

5.3 PREDICTION OF CRACK WIDTHS IN BEAMS AND SLABS REINFORCED WITH EPOXY-COATED BARS

Many variables influence the width and spacing of flexural cracks in reinforced concrete beams and slabs. Because of the complexity of the problem, a number of empirical approaches have been developed for the determination of the width of flexural cracks. The approach suggested by Beeby (1970) for the widths in one-way slabs resulted in a better understanding of the crack mechanisms. Gergely and Lutz (1968) used experimental data from a number of researchers and studied the key parameters using a statistical approach. Much less attention has been given in past studies to the prediction of flexural crack widths in two-way slabs. Studies on crack widths in two-way slabs were conducted by Nawy *et al.* (1970) in the U.S., and by Clark (1973) in the U.K.

Because of the increased use of epoxy-coated bars in structures exposed to severely corrosive environments, more information is needed on the influence of epoxy coatings on the ability of reinforcing bars to control cracks. Experimental studies on this influence have been conducted, as part of this research for tension members (Mitchell *et al* 1994), for beams (Abrishami *et al.* 1994) and for two-way slabs (Abrishami *et al.* 1994). Details of these experiments are given in Chapter 4.

5.3.1 Prediction of Crack Widths of Concrete Beams Reinforced with Epoxy-Coated Bars

The ACI Code (1989) bases its crack control requirements on the Gergely-Lutz expression (Gergely and Lutz 1968) for maximum crack widths. The Gergely-Lutz expression is as follows:

$$w_{max} = 2.2\ \beta\ \epsilon_{scr}\ \sqrt[3]{d_c\ A} \qquad (5.26)$$

where w_{max} = maximum crack width

β = factor accounting for strain gradient

= 1.0 for uniform strain, or

= h_2/h_1 for varying strains, where h_1 is the distance from the tension steel to the neutral axis and h_2 is the distance from the extreme tension fibre to the neutral axis

ϵ_{scr} = strain in reinforcing bar at crack location

d_c = distance from extreme tension fibre to centre of closest bar

A = effective area of concrete surrounding each bar, taken as the total area of concrete in tension which has the same centroid as the tension reinforcement, divided by the number of bars.

The Gergely-Lutz expression for maximum crack width does not take into account the effect of concrete strength and presence of epoxy coating. Table 5.1 gives the maximum flexural crack widths observed on the side face of the beams tested at the level of the tension reinforcement. It is noted that the Gergely-Lutz equation gives conservative predictions for the specimens with uncoated bars. It was found that for the normal strength concrete beams, modification factors of 1.15 and 1.35 needed to be applied to Eq. 5.26 to correctly predict the maximum crack width at service load levels for the specimens with 6-8 and 10-12 mils epoxy coatings, respectively. For the high-strength concrete beams these modification factors are 0.96 and 1.04 for the specimens with 6-8 and 10-12 mils epoxy coatings, respectively. Hence for predicting the maximum crack width in the high-strength concrete beams no modification factor for epoxy coating is necessary.

Based on the results of this research the 1994 CSA Standard on the "Design of Concrete Structures" has adopted a factor of 1.2, for the influence of epoxy coating on the reinforcing bars, when calculating the crack control parameter.

Table 5.1: Observed and predicted crack widths in beams at service load level (0.6 of M_n)

	Beam	Epoxy coating (mils)	Observed maximum crack width (mm)	Predicted maximum crack width (mm)	Observed/ Predicted
Normal	UCB	0	0.22	0.26	0.85
Strength	C1B	6-8	0.30	0.26	1.15
Concrete	C2B	10-12	0.35	0.26	1.35
High	HUCB	0	0.25	0.26	0.96
Strength	HC1B	6-8	0.25	0.26	0.96
Concrete	HC2B	10-12	0.27	0.26	1.04

5.3.2 Prediction of Crack Widths in Slab-Column Connections Designed for Corrosive Environments

The ACI Code (1989) bases its crack control requirements on a modified form of the Gergely-Lutz expression (Gergely-Lutz 1968) for maximum crack widths. The Gergely-Lutz expression is valid for beams and one way slabs. As pointed out by ACI Committee 224 (1988) "Crack control equations for beams underestimate the crack widths developed in two-way slabs". The maximum crack widths in two-way slabs are influenced by the slab boundary conditions, the steel stress, the amount of reinforcement, the size and spacing of the reinforcing bars in the two directions and the concrete cover. Based on the work of Nawy and Orenstein (1970) and Nawy and Blair (1971) on cracking in two-way slabs, ACI Committee 224 recommends the following equation for predicting the maximum crack width, w_{max}:

$$w_{max} = k_1 \; \beta \; \epsilon_s \sqrt{\frac{d_{bl} \; s_2}{\rho_{tl}}} \tag{5.27}$$

where:

k_1 = coefficient, having a value of 0.81 for uniformly loaded restrained two-way square slabs and 0.90 for simply supported two-way square slabs subjected to a central concentrated load (Nawy and Orenstein 1970; Nawy and Blair 1971)

β = ratio of distance between neutral axis and tension face to distance between neutral axis and centroid of reinforcing steel (may be taken as 1.25 (Nawy and Orenstein 1970; Nawy and Blair 1971))

ϵ_s = average service load steel strain (may be taken as 0.4 ϵy (ACI Committee 224; Nawy 1992))

d_{bl} = diameter of the reinforcement in direction 1 (closest to the concrete outer fibres)

s_1 = spacing of the reinforcement in direction 1

s_2 = spacing of the reinforcement in direction 2 (perpendicular to direction 1)

ρ_{tl} = active steel ratio

= area of steel A_s per unit width $/(d_{bl} + 2c_1)$ where c_1 is the clear concrete cover measured from the tensile face of concrete to the nearest edge of the reinforcing bar in direction 1

Equation (5.27) does not take into account the effect of concrete strength and presence of epoxy coating. Table 5.2 compares the observed maximum flexural crack widths at full service load level with those predicted using Eq. (5.27) for the six test specimens. It is noted that Eq. (5.24) gives an excellent prediction for the high-performance concrete specimen with uncoated bars. It was found that for the specimens having epoxy-coated bars, an average modification factor of 1.25 needs to be applied to Eq. (5.27) to correctly predict the maximum crack width at full service load levels.

The 1994 CSA Standard on "Parking Structures" refers to this research for assessing the influence of epoxy coating on reinforcing bars on cracking.

Table 5.2: Comparison of observed and predicted maximum crack widths at full service load level for two-way slabs

	Slab	Epoxy coating (mils)	Observed maximum crack width (mm)	Predicted maximum crack width (mm)	Observed/ Predicted
Normal	C0	0	0.70	0.60	1.17
Strength	C1	6-8	0.70	0.60	1.17
Concrete	C2	10-12	0.80	0.60	1.33
High	HC0	0	0.60	0.60	1.00
Strength	HC1	6-8	0.70	0.60	1.17
Concrete	HC2	10-12	0.80	0.60	1.33

Chapter 6

CONCLUSIONS

" Perhaps the most valuable result of all education is the ability to make yourself do the things you have to do when it has to be done, whether you like it or not. "

Huxley

The purpose of this research program was to examine some of the important parameters which affect the bond of reinforcement and cracking of concrete structural elements. The experimental and analytical studies have been conducted with a view of determining the behaviour of structural concrete made with recently developed materials. The influence of high-performance concrete and fibre-reinforced concrete on the response of reinforced concrete elements was studied. The studies also examined the influence of reinforcement, including reinforcing bars, pretensioned strand and epoxy-coated reinforcing bars.

This chapter summarizes the finding of experimental and analytical studies on the bond characteristics and cracking of reinforced concrete elements.

6.1 BOND CHARACTERISTICS OF REINFORCEMENT IN CONCRETE

New testing techniques were developed to study the bond performance of reinforcing bars and pretensioned strands in concrete. These techniques were used to investigate the influence of concrete cover, bar or strand size, and the presence of epoxy coating on the bars.

6.1.1 New Testing Method to Study Bond of Reinforcing Bars

Special features of this new testing technique for studying basic bond characteristics are listed below:

1) A nearly uniformly distributed bond stress distribution is simulated which permits a more fundamental approach for studying bond characteristics.
2) Both types of failure, splitting and pullout, can be studied using this testing technique.
3) The displacement controlled testing technique demonstrated that, for uniform bond stress, the splitting type of failure is more ductile than the pullout type of failure.
4) Analytical studies showed that a combination of pullout and push-in forces can simulate uniform bond stress distribution.
5) Analytical studies showed that, in the new testing method, the maximum bond stress along the embedment length is about 10 percent greater than the average bond stress while the standard pullout test has a maximum bond stress which is about 1.4 times the average bond stress.

6.1.2 New Approach for Studying the Bond Characteristics of Pretensioned Strand

Conclusions from this new testing technique are given below:

1) This new testing technique provides a simple method for determining the bond characteristics of pretensioned strand along the transfer length and the flexural bond length. These characteristics are determined by measuring the applied forces on the strand at the top and bottom of specimen and the respective slips, rather than by the conventional method of measuring the variation of the strains in the strand or the strains on the concrete surface in a beam specimen.
2) After bond failure, a flexural bond length specimen exhibits a more ductile response, with a nearly constant bond stress, while a transfer length specimen exhibits a more brittle bond failure.
3) The bond strength, $u_{t,max}$, obtained over the simulated transfer length is greater

than the bond strength, $u_{fb,\max}$, obtained over the flexural bond length. The average ratio $u_{t,\max}/u_{fb,\max}$ is 1.5, 2.0 and 2.3 for strand sizes 9.5, 13 and 16 mm, respectively. This ratio increases with increasing strand diameter.

4) The stiffness of the bond stress versus slip response is greater in the transfer length simulation than in the flexural bond length simulation.

5) Equations have been proposed to predict the transfer length, flexural bond length and development length as functions of the concrete strength and strand size.

6.1.3 Bond Characteristics of Epoxy-Coated Bars

1) A new testing technique (pullout/ push-in) enabled the simulation of a uniform bond stress distribution along the embedment length of epoxy-coated bars.

2) The specimens containing epoxy-coated bars had a lower bond strength (up to a 17% reduction) and a lower bond stiffness than companion specimens containing uncoated bars.

6.2 CRACKING AND STRUCTURAL DEFORMATIONS

The influence of concrete strength, concrete quality, epoxy coatings on deformed bars, and the presence of steel fibres on cracking and deformation was studied. Conclusions from these studies are given below.

6.2.1 Influence of High-Strength Concrete

1) After cracking and significant deformations, reinforced concrete tension specimens made with normal and high-strength concrete showed essentially the same degree of tension stiffening.

2) Crack widths in the high-strength concrete beams tested were smaller than in normal-strength concrete beams at service load levels. Due to the increased strength and brittleness of high-strength concrete and due to its larger energy release upon cracking, the initial flexural cracks occurred at a higher load than in

the normal-strength concrete beams, but the initial cracks were longer.

3) In high-strength concrete beams without stirrups the ductility can be limited by a sudden failure, with diagonal tension cracking precipitating simultaneous bond-splitting cracks and flexure-shear crushing.

4) The high-strength concrete beams, which had the same length, cross section and reinforcement ratio as companion normal-strength concrete beams, had slightly higher stiffness and about a 5% higher ultimate strength than the normal-strength concrete beams.

6.2.2 Influence of Concrete Quality

1) Due to its lower water/cement ratio, high-performance concrete has less shrinkage, lower permeability and larger concrete strengths than normal-strength concrete.

2) The load versus average strain responses of slabs (slab-column connections) showed that the use of high-performance concrete resulted in smaller deflections than companion normal-strength concrete specimens.

3) High-performance concrete slab-column connection specimens exhibited smaller average crack widths at service load levels than companion normal-strength concrete specimens.

4) The equation proposed by Nawy and Orenstein and recommended by ACI Committee 224 gives an excellent prediction of the maximum crack width for the high-performance concrete slabs with uncoated bars.

6.2.3 Influence of Epoxy Coating on Reinforcing Bars

1) Tension specimens and beam specimens reinforced with epoxy-coated bars exhibited larger crack widths and more widely spaced cracks than specimens with uncoated bars. Larger epoxy coating thicknesses resulted in wider cracks.

2) It was found that the presence of epoxy coating did not significantly change the overall load-deflection response of either the normal or high-strength concrete beams up to yielding.

3) The beams reinforced with epoxy-coated reinforcement showed less ductility than

the beams reinforced with uncoated reinforcement.

4) It was found that for the normal-strength concrete beams, modification factors of 1.15 and 1.35 needed to be applied to the Gergely-Lutz equation to correctly predict the maximum crack width at service load levels for the beam specimens with 6-8 and 10-12 mils epoxy coatings, respectively. As a result of this research the 1994 CSA Standard A23.3 adopted an epoxy-coating factor of 1.2 when assessing flexural cracking. For the high-strength concrete beams no epoxy coating modification factor was found to be necessary to predict the flexural crack widths.

5) More splitting cracks were observed in the beams having epoxy-coated bars than the beams having uncoated bars due to the larger splitting stress arising from the smaller values of adhesion between the epoxy surface and the concrete.

6) The maximum crack width for two-way slabs reinforced with epoxy coated bars can be predicted using the Nawy-Orenstein equation multiplied by a modification factor of about 1.25. The 1994 CSA Standard S413 on "Parking Structures" cites this research for guidance on structural considerations when epoxy-coated bars are used.

7) The load versus average strain responses of two-way slabs showed that the presence of epoxy coatings could result in larger deflections.

6.2.4 Influence of Steel Fibre-Reinforced Concrete

1) Steel fibres, in the volume used, significantly increased the tensile strength and ductility of both normal-strength and high-strength concrete.

2) Steel fibres significantly increased the tension stiffening of both normal-strength and high-strength reinforced concrete in tension.

3) Steel fibres significantly reduced the crack widths in both normal and high-strength concrete specimens.

4) After yielding of the reinforcing bar, only those concrete members containing fibres showed tension stiffening.

5) Steel fibres helped to prevent bond splitting cracks from propagating in both normal and high-strength concrete tension members.

6.3 PROPOSED EQUATIONS ON BOND AND CRACKING IN STRUCTURAL CONCRETE

1) In a pullout test, at any point x , along the embedment length, the bond stress, u , and slip, δ , can be expressed as:

a) Pre-cracking response:

$$\delta(x) = c_1 e^{kx} + c_2 e^{-kx}$$

$$u(x) = E_b \left(c_1 e^{kx} + c_2 e^{-kx}\right)$$

b) Post-cracking response:

$$\delta(x) = c_3 \cos(kx) + c_4 \sin(kx) - m$$

$$u(x) = E_d (c_3 \cos(kx) + c_4 \sin(kx))$$

in which, E_b and E_d are the bond stiffnesses before and after cracking, respectively; c_1 , c_2 , c_3 and c_4 are constants depending on the boundary conditions applied to the pullout specimen; and m is $\delta_{sf}\,(E_b/E_d - 1)$.

2) The development length of a pretensioned strand is expressed as:

$$\ell_d = 0.255 \frac{f_{pi}}{\sqrt{f'_{ci}}} d_b + 0.548 \frac{(f_{ps} - f_{se})}{\sqrt{f'_c}} d_b \qquad \text{(MPa, mm)}$$

where the first term is the transfer length and second term is the flexural bond length. In this equation, d_b is the strand diameter, f_{pi} , f_{se} , f_{ps} are the initial stress, the stress after all losses and the stress at the critical section in the pretensioning strand, respectively and f'_{ci} and f'_c are the concrete strengths at the time of release of the strand and the 28-day strength, respectively.

3) A factor accounting for splitting cracks, α_3, was introduced to the tension stiffening equation to determine the concrete stress, f_c, after cracking. This resulted in the following expression:

$$f_c = \frac{\alpha_1 \alpha_2 \alpha_3 f_{cr}}{1 + \sqrt{500 \epsilon_{cf}}} \qquad \text{for} \qquad \epsilon_{cf} > \epsilon_{cr}$$

where:

$$\begin{array}{lll} \alpha_3 = 1.0 & \text{for} & c/d_b \geq 2.5 \\ \alpha_3 = 0.8\ c/d_b - 1 & \text{for} & 1.25 \leq c/d_b \leq 2.5 \\ \alpha_3 = 0 & \text{for} & c/d_b \leq 1.25 \end{array}$$

and ϵ_{cf} is the strain in the concrete caused by stress, f_{cr} is the tensile strength of the concrete, c is the concrete cover, d_b is the bar diameter and α_1 and α_2 are factors accounting for bond characteristics and loads conditions, respectively. In the case of steel fibre-reinforced concrete, f_{cr}, is taken as the tensile strength of the fibre-reinforced concrete.

4) The transfer length, ℓ_t, in a tension specimen reinforced with a single bar was determined as:

$$\ell_t = \frac{T}{\pi \alpha u_{max}\ d_b}\left(\frac{1}{1 + n\rho}\right)$$

in which, T is the applied tensile load, d_b is the bar diameter, n is the ratio of the moduli of elasticity of the reinforcement to that of the concrete, ρ is the reinforcement ratio and $\alpha\, u_{max}$ is the average bond stress along the transfer length.

5) The crack spacing, s , in a tension specimen can be expressed as:

$$s = \frac{d_b}{2\rho} \frac{f_{cr}}{\alpha u_{max}}$$

in which, d_b is the bar size, ρ is the reinforcement ratio, f_{cr} is the tensile strength of the concrete and αu_{max} is the average bond stress between two cracks.

6) Specimens containing steel fibres showed tension stiffening even after yielding the reinforcing bar. The tension carried by the steel fibres, T_f , in a tension specimen after yielding the reinforcing bar was expressed as:

$$T_f = \frac{V_f}{6} E_f A_c (\epsilon - \epsilon_y)$$

where, V_f is the volume percentage of fibres in the concrete, E_f is the modulus of elasticity of the fibres, A_c is the cross-sectional of concrete, ϵ is the average strain in the tension specimen and ϵ_y is the yielding strain of the reinforcing bars.

STATEMENT OF ORIGINALITY

Experimental and analytical studies have been conducted in order to study the bond and cracking of structural concrete elements. Ninety-seven reinforced concrete elements including forty-nine pullout specimens, thirty-six tension specimens, six beams and six two-way slabs were tested. The variables in the reinforcement included steel reinforcing bars having uncoated and two different coating thicknesses with different bar sizes, and pretensioning strands with three different strand diameters. The concrete used in the specimens included normal-strength, high-strength, high-performance and steel fibre reinforced concrete. The original contributions in this thesis are:

1) A new testing technique to simulate a more uniform bond stress distribution for reinforcing bars embedded in concrete was developed. This testing technique enables the study of splitting and pullout failures.
2) A new testing technique to study bond characteristics of pretensioned strand along both the transfer length and the flexural bond length was developed.
3) Equations for predicting the bond stress versus slip responses and bond stress distribution of different pullout specimens were formulated.
4) Equations for predicting the transfer length and development length of pretensioned strand were developed.
5) A modification to the tension stiffening expression was developed to account for the influence of splitting cracks.
6) Equations were developed for the transfer length and crack spacing of tension specimens.
7) An analytical approach was developed for predicting the complete response of reinforced concrete tension specimens containing steel fibres.

REFERENCES:

Abrams, Duff A. (1913), "Tests of Bond Between Concrete and Steel", Engineering Experiment Station, Bulletin No. 71, University of Illinois, Champaign.

Abrams, D.A. (1951), "The Readers Write; Section", Civil Engineering, Vol. 21, No. 6, pp. 51-52.

Abrishami, H.H., and Mitchell, D. (1992a), "Simulation of Uniform Bond Stress", ACI Materials Journal, Vol. 89, No. 2, pp. 161-168.

Abrishami, H.H., and Mitchell, D. (1992b), "A New Approach for Studying Bond Characteristics", International Conference on Bond in Concrete: from Research to Practice, CEB, Riga, Latvia, Vol. 1, pp. 28-37

Abrishami, H.H., and Mitchell, D. (1993), "Bond Characteristics of Pretensioned Strand", ACI Materials Journal, Vol. 90, No. 3, pp. 228-235.

Abrishami, H.H., Cook, W.D., and Mitchell, D. (1994 accepted for publication), "Influence of Epoxy-Coated Reinforcement on the Response of Normal and High-strength Concrete Beams", ACI Structural Journal.

Abrishami, H.H., Cook, W.D., and Mitchell, D. (1994 accepted for publication), "The Effect of Epoxy-coated Reinforcement and Concrete Quality on Cracking of Flat Plate Slab-Column Connections", ACI Structural Journal.

ACI Committee 208 (1945), "Proposed Test Procedure to Determine Relative Bond Value of Reinforcing Bars", ACI Journal, Vol. 16, No. 4, pp. 273-292.

ACI Committee 408 (1964), "A Guide for Determination of Bond Strength in Beam Specimens", ACI Journal, Vol. 61, No. 2, pp. 129-136.

ACI Committee 224 (1988), "Control of Cracking in Concrete Structures", Part 3, ACI Manual of Concrete Practice, American Concrete Institute, Detroit, 42 pp.

ACI Committee 318 (1963), "Building Code Requirements for Reinforced Concrete", American Concrete Institute, Detroit.

ACI Committee 318 (1971), "Building Code Requirements for Reinforced Concrete", American Concrete Institute, Detroit.

ACI Committee 318 (1983), "Building Code Requirements for Reinforced Concrete (ACI 318-83)", American Concrete Institute, Detroit, 111 pp.

ACI Committee 318 (1989), "Building Code Requirements for Reinforced Concrete (ACI 318-89) and Commentary - ACI 318R-89", American Concrete Institute, Detroit, 353 pp.

ACI Committee 318 (1992), "Building Code Requirements for Reinforced Concrete (ACI 318-89) and Commentary - ACI 318R-92", American Concrete Institute, Detroit, 347 pp.

ACI Committee 363 (1992), "Review of ACI Code for Possible Revisions for High-Strength Concrete", Committee Report 363R-92, American Concrete Institute, Detroit.

ACI Committee 408 (1966), Bond Stress - The State of the Art", Journal of the American Institute, Vol. 63, No. 11, pp. 1161-1188.

ACI Committee 408 (1991), "Bond Under Cyclic Loading - State of the Art", ACI Materials Journal, Vol. 88, No. 6, pp. 669-673.

ACI Committee 544 (1974), "Fiber Reinforced Concrete", Publication SP-81, American Concrete Institute, Detroit, 532 pp.

ACI Committee 544 (1984), "Fiber Reinforced Concrete", Publication SP-81, American Concrete Institute, Detroit, 452 pp.

ADINA (1981), Engineering, ADINA-A, "Finite Element Program for Automatic Dynamic Incremental Nonlinear Analysis", Report AE81-1, ADINA Engineering, Inc. Watertown, MA.

Ahmad, S.H., Khaloo, A.R., and Poveda, A. (1986), "Shear Capacity of Reinforced High-Strength Concrete Beams", ACI Journal, Vol. 83, No. 2, pp. 297-305.

Ahmad, S.H., and Lue, D.M. (1987), "Flexural-Shear Interaction of Reinforced High-Strength Concrete Beams", ACI Structural Journal, Vol. 84, No. 4, pp. 330-341.

Armstrong, W.E.I. (1949), "Bond in Prestressed Concrete", Journal of the Institution of Civil Engineers, Vol. 33, pp. 19-40.

ASCE (1982), "Finite Element Analysis of Reinforced Concrete", American Society of Civil Engineering, New York, 545 pp.

ASTM (1988), C 234-86 "Standard Test Method for Comparing Concretes on the Basis of the Bond Developed with Reinforcing Steel", Annual Book of ASTM Standards, Section 4, Construction.

ASTM (1990), A 775 / A 775 M-89 a, "Standard Specification for Epoxy-Coated Reinforcing Steel Bars", American Standards for Testing and Materials, Section 1, Vol. 01.04, pp. 555-559.

Azizinamini, A., Stark, A., Roller, J.J. and Ghosh, S.K. (1993), "Bond Performance of Reinforcing Bars Embedded in High-Strength Concrete", ACI Structural Journal, Vol. 90, No. 5, pp. 554-561.

Bažant, Z.P., and Sener, S. (1988), "Size Effect in Pullout Tests", ACI Materials Journal, Vol. 85, No. 5, pp. 347-351.

Bažant, Z.P. and Kazemi, M.T. (1991), "Size Effect on Diagonal Shear Failure of Beams without Stirrups", ACI Structural Journal, Vol. 88, No. 3, pp. 268-276

Bažant, Z.P., (1992) " Fracture Mechanics of Concrete Structures", Elsevier Applied Science, Proceedings of the First International Conference on Fracture Mechanics of Concrete Structures, Breckenridge, Colorado.

Beeby, A.W. (1970), "An Investigation of Cracking in Slabs Spanning One Way", Technical Report TRA 433, Cement and Concrete Association, London, 33 pp.

Berggren, L. (1965), "Utdragsprov med kor vidhaftningsland:, Division of Concrete Structures, Chalmers University of Technology, Publication No. 686.

Bertero, V.V., and Bresler, B. (1968), "Behavior of Reinforced Concrete Under Repeated Loading", Journal of The Structural Division, ASCE, Vol. 94, No. ST6.

Bertero, V.V., Popov, E.P., and Viwathanatepa, S. (1978), "Bond of Reinforcing Steel: Experiments and a Mechanical Model", IASS Symposium on Non-Linear Behavior of Reinforced Concrete Spatial Structures, Darmstadt, West Germany, Vol. 2, pp. 3-17

Broms, B.B. (1963), "Mechanism of Tension Cracking in Reinforced Concrete Members", Phase II, Report 311, Department of Structural Engineering, Cornell University.

Carrasquillo, Ramon L., Nilson, A.H., and Slate, F.O. (1981),"Properties of High-Strength Concrete Subjected to Short-Term Loading", ACI Journal, Vol. 78, No. 3, pp. 171-178.

CEB Task Group VI (1981), "Bond Action Behaviour of Reinforcement - State of the Art Report", Comité Euro-International du Béton, 153 pp.

CEB Manual (1985), "Design Manual on Cracking and Deformations", Comité Euro-International du Béton, Ecole Polytechnique Fédérale de Lusanne.

CEB-FIP (1978), "CEB-FIP Model Code for Concrete Structures, "Comité Euro-International du Béton and Fédération Internationale de la Précontrainte, Third Edition, CEB, Paris, 348 pp.

CEB-FIP (1991), "CEB-FIP Model Code 1990 for Concrete Structures", Comité Euro-International du Béton and Fédération Internationale de la Précontrainte, 437 pp.

Chinn, J., Ferguson, M.P., and Thompson, J.N. (1955), "Lapped Splices in R.C. Beams", ACI Journal, Vol. 52, No. 2, pp. 201-214.

Choi, O., Darwin, D., and MacCabe, S.L. (1990), "Bond Strength of Epoxy-Coated Reinforcement to Concrete", SM Report No. 25, University of Kansas Center for Research, Lawrence, Kansas, 217 pp.

Ciampi, V., Eligehausen, R., Bertero, V.V., and Popov, E.P. (1982), "Analytical Model for Concrete Anchorages of Reinforcing Bars Under Generalized Excitations", Report No. EERC 82-83, Earthquake Engineering Research Center, University of California, Berkeley, California.

Clark, L.A. (1973), "Flexural Cracking in Slab Bridges", Technical Report 42.479, Cement and Concrete Association, London, 12 pp.

Cleary, D.B., and Ramirez, J.A. (1991), "Bond Strength of Epoxy-Coated Reinforcement, ACI Materials Journal, Vol. 88, No. 2, pp. 146-149.

Clifton, J.R., Beeghley, H.F., and Mathey, R.G. (1974), "Non-Metallic Coatings for Concrete Reinforcing Bars", U.S. National Bureau of Standards, Report No. FHWA-RD-74-18, PB 236 424.

Collins, M.P., and Mitchell, D. (1991), "Prestressed Concrete Structures", Prentice-Hall Inc. Englewood Cliffs, N.J.

Collins, M.P., and Poraz, A. (1989), "Shear Design for High-Strength Concrete," CEB Bulletin d'Information No. 193, pp. 77-83.

Collins, M.P., Mitchell, D. and MacGregor, J.G. (1993), "Structural Design Considerations for High-Strength Concrete", ACI, Concrete International, Vol. 15, No. 5, pp. 27-34.

Considère (1899), "Influence des armatures metalliques sur le propriétes des mortiers et bétons" (Influence of Metal Reinforcement on the Properties of Mortar and Concrete), Le Génie Civil, Vol. 34, No. 15, pp. 229-233.

CPCA (1987), ADOSS, "Analysis and Design of Slab Systems", Canadian Portland Cement Association, Ottawa.

CSA (1984), CSA-A23.3-M84, "Design of Concrete Structures for Buildings", Canadian Standards Association, Rexdale, 281 pp.

CSA (1990), CSA-A23.1-M90, "Concrete Materials and Methods of Concrete Construction", Canadian Standards Association, Rexdale, 273 pp.

CSA (1994a), CSA-S413-94, "Parking Structures", Canadian Standards Association, Rexdale.

CSA (1994b), CSA-A23.3-M94, "Design of Concrete Structures", Canadian Standards Association, to be published.

Cousins, T.E., Johnston, D.W., and Zia, P. (1990), "Transfer and Development Length of Epoxy Coated and Uncoated Prestressing Strand," PCI Journal, Vol. 55, No. 4, pp. 92-103

Deatherage, J.H., and Burdette, E.G. (1990), "Development Length and Lateral Spacing Requirements of Prestressed Strand for Prestressed Concrete Bridge Products", Transportation Center, The University of Tennessee, Knoxville.

Deatherage, J.H., Burdette, E.G., and Chew, C.K. (1994), "Development Length and Lateral Spacing Requirements of Prestressing Strand for Prestressed Concrete Bridges", PCI Journal, Vol. 39, No. 1, pp. 70-83.

Edwards, A.D., and Yannopoulos, P.J. (1979), "Local Bond Stress to Slip relationships for Hot Rolled Deformed Bars and Mild Steel Plain Bars", ACI Journal, Vol. 76, No. 3, pp. 405-420.

Eligehausen, R., Popov, E.P., and Bertero, V.V., (1983), "Local Bond Stress-Slip Relationships of Deformed Bars Under Generalized Excitations", Report No. UCB/EERC 83-23, Earthquake Engineering Research Center, University of California, Berkeley, California.

El-Zanaty, A.H., Nilson A.H., and Slate, F.O. (1986a), "Shear Capacity of Reinforced Concrete Beams Using High-Strength Concrete", ACI Journal, Vol. 83, No. 2, pp. 290-296.

El-Zanaty, A.H., Nilson A.H., and Slate, F.O. (1986b), "Shear Capacity of Prestressed Concrete beams Using High-Strength Concrete", ACI Journal, Vol. 83, No. 3, pp. 359-368.

Ezeldin, A., and Balaguru, P. (1989), "Bond Behavior of Normal and High-Strength Fiber Reinforced Concrete," ACI Materials Journal, Vol. 86, pp. 515-524.

Ezeldin, A., and Balaguru, P. (1990), "Bond Performance of Reinforcing Bars Embedded in Fiber Reinforced Concrete and Subjected to Monotonic and Cyclic Loads," Proceeding of ASCE Materials Engineering Congress, Denver, Colorado, pp. 145-154.

Falkner, H., "Zur Frage der Rißbildung durch Eigen-und Zwangspannungen infolge Temperatur in Stahbetonbauteilen", Deutscher Ausschuß für Stahbetonbauteilen, (Cracking of Reinforced Concrete Members due to Residual and Restraining Stresses Caused by Temperature), Deutscher Ausschuß für Stahlbeton, 208, 1969, 99 pp.

FIP (1982), Federation Internationale de la Precontrainte, "Report on Prestressing Steel: 7. Test for the determination of tendon transmission length under static conditions", 19 pp.

Gergely, P. and Lutz, L.A. (1968), "Maximum Crack Width in Reinforced Concrete Flexural Members", Causes, Mechanism, and Control of Cracking in Concrete, SP-20, American Concrete Institute, Detroit, pp. 87-117.

Gerstle, W., Ingraffea, A.R., and Gergely P. (1982), "Tension Stiffening, A Fracture Mechanics Approach", Bond in Concrete (P. Bartos, ed.), Applied Science Publishers, London, pp. 97-106.

Ghoneim, G.A.M. (1978), "Nonlinear Analysis of Concrete Structures", Ph.D. Thesis, Department of Civil Engineering, University of Calgary, Canada, 249 pp.

Goto, Y. (1971), "Cracks formed in Concrete Around Deformed Tension Bars", ACI Journal, pp. 244-251.

Guiriani, E. (1981), "Experimental Investigation on the Bond-Slip Law of Deformed Bars in Concrete", IABSE Colloquium Delft 1981, IABSE, Zurich, pp. 121-142.

Gunther, G., and Mehlhorn, G. (1991), "Local Bond Between Reinforcing Steel and Concrete," IABSE Colloquium, Structural Concrete, Stuttgart, pp. 141-146.

Gylltoft, K., Cederwall, K., Elfgren, L., and Nilsson, G. (1982), "Bond Failure in Reinforced Concrete under Monotonic and Cyclic Loading : A Fracture Mechanics Approach", SP-75, Fatigue of Concrete Structures, ACI, Detroit, pp. 269-288.

Hajnal-Kónyi, K. (1957), "Suggestions for the Comparison of the Bond Resistance of Various Types of Reinforcing Bar", RILEM, Symposium on Bond and Cracking Formation in Reinforced Concrete, Stockholm, Vol 1, pp. 137-146.

Hamad, B.S. and Jirsa, J.O. (1979), "Effect of Casting Position on Development of Anchored Reinforcement", University of Texas at Austin.

Hamad, B.S., Jirsa, J.O., and d'Abreu d'Paolo, N.I. (1990), "Effect of Epoxy Coating on Bond and Anchorage of Reinforcement in Concrete Structures", Center for Transportation Research, The University of Texas at Austin, 242 pp.

Hanson, N., and Kaar, P. (1959), "Flexural Bond Tests of Pretensioned Prestressed Beams," ACI Journal, V. 56, No. 1, pp. 783-802.

Hoyer, E., and Friedrich, E. (1939), "Beitrag zur Frage der Haftspannung in Eisenbetonbauteilen" (Contribution towards the Question of Bond Strength in Reinforced Concrete Members), Beton und Eisen, Berlin, Vol. 38, No. 6, pp. 107-110.

Hwang, S.H., Lee, Y.Y., and Lee C.S. (1994), "Effect of Silica Fume on the Splice Strength of Deformed Bars of High-Performance Concrete", ACI Structural Journal, Vol. 91, No. 3, pp. 294-302.

Janney, J.R. (1954), "Nature of Bond in Pretensioned Prestressed Concrete", Journal of American Concrete Institute, pp. 717-736.

Johnson, M.K. and Ramirez, J.A. (1989), "Minimum Shear Reinforcement in Beams with Higher Strength Concrete", ACI Structural Journal, Vol. 86, No. 4, pp. 376-382.

Kaar, P.H., LaFraugh, R.W., and Mass, M.A. (1963)," Influence of Concrete Strength on Strand Transfer Length," PCI Journal, Vol. 8, No. 5, pp. 47-67.

Kani, M.W., Huggins, M.W. and Wittkopp, R.R. (1979), "Kani on shear in Reinforced Concrete", Department of Civil Engineering, University of Toronto, Canada, pp. 225.

Keuser, M. and Mehlhorn, G. (1987), "Finite Element Models for Bond Problems", ASCE, Journal of Structural Engineering, Vol. 113, No. 10, pp. 2160-2173.

Kim, W. and White, R.N. (1991), "Initiation of Shear Cracking in Reinforced Concrete Beams with no Web Reinforcement", ACI Structural Journal, Vol. 88, No. 3, pp. 301-308.

Lim, T.Y., Paramasivam, P., and Lee, L. (1987), "Analytical Model for Tensile Behavior of Steel-Fiber Concrete", ACI Materials Journal, Vol. 84, No. 4, pp. 286-298.

Leonhardt, F. (1977), "Crack Control in Concrete Structures", IABSE Surveys No. S-4/77, International Association for Bridge and Structural Engineering, Zurich, 26 pp.

Losberg, A. and Olsson, P.A. (1979), "Bond Failure of Deformed Reinforcing Bars Based on the Longitudinal Splitting Effect of the Bars", ACI Journal, Vol. 76, No. 1, pp. 5-17.

Lutz, A.L., Gergely, P., and Winter, G. (1966), "The Mechanics of Bond and Slip of Deformed Reinforcing Bars in Concrete", Report 324, Department of Structural Engineering, Cornell University.

Lutz, L.A. (1970), "Analysis of Stresses in Concrete Near a Reinforcing Bar Due to Bond and Transverse Cracking", ACI Journal, Vol. 67, No. 10. pp. 778-787.

Mathey, R.C., and Watstein, D. (1961), "Investigation of Bond in Beam and Pullout Specimens with High-Yield-Strength Deformed Bars", ACI Journal, Vol. 57, No. 9, pp. 1071-1090.

Mirza, M.S., and Hsu, C.T. (1969), "Investigation of Bond in Reinforced Concrete Models - Eccentric Pullout Test", Proceedings, International Conference on Shear, Torsion, and Bond in Reinforced and Prestressed Concrete, Coimbatore, India.

Mirza, S.M., and Houde, J. (1979),"Study of Bond Stress-Slip Relationships in Reinforced Concrete", ACI Journal, Vol. 76, No. 1, pp. 19-46.

Mitchell, D., Cook, W.D., Khan, A.A., and Tham, T. (1993), "Influence of High-Strength Concrete on Transfer Length and Development Length of Pretensioning Strand," PCI Journal, Vol. 38, No. 3, pp. 52-66.

Mitchell, D., Abrishami, H.H., and Mindess S. (1994 accepted for publication), "The Effect of Steel Fibers and Epoxy-Coated Reinforcement on Tension Stiffening and Cracking of Reinforced Concrete", ACI Materials Journal.

Mörsch, E. (1902); "Concrete-Steel Construction", McGraw-Hill, New York, 1909, 368 pp. (English translation by E.P. Goodrich of third edition of Der Eisenbetonbau, first edition).

Nawy, E.G. (1992), "Designing Concrete Structures for Serviceability and Safety", SP-133, American Concrete Institute, Detroit, pp. 1-32.

Nawy, Edward G., and Blair, Kenneth W. (1971)," Further Studies on Flexural Crack Control in Structural Slab Systems", Cracking Deflection, and Ultimate Load of Concrete Slab System, SP-30, American Concrete Institute, Detroit, pp. 1-41.

Nawy, E.G., and Orenstein, G.S. (1970), "Crack Width Control in Reinforced Concrete Two-Way Slabs", Journal of the Structural Division, ASCE, Vol. 96, N0. ST3, pp. 701-721.

Nilson, A.H. (1972), "Internal Measurment of Bond Slip"", ACI, Journal, Vol.69, No.7, pp. 439-441.

Ouyang, C., and Shah, S.P. (1994), "Fracture Energy Approach for Predicting Cracking of Reinforced Concrete Tensile Members", ACI Structural Journal, Vol.91, No. 1, pp. 69-78.

Pastor, J.A., Nilson, A.H. and Slate, F.O. (1984), "Behavior of High-Strength Concrete Beams", Research Report No. 84-3, Department of Structural Engineering, Cornell University, Ithaca.

PCA (1991), "Fiber Reinforced Concrete", Portland Cement Association, Skokie, Illinois, 48 pp.

Pillai, S.U., and Kirk, D.W. (1988), "Reinforced Concrete Design", Royal Military College of Canada, 1988.

Plaines, P., Tassios, T., and Vintzeleou, E. (1982), "Bond Relaxation and Bond-Slip Creep Under Monotonic and Cyclic Actions", Bond in Concrete (P. Bartos, ed.), Applied Science Publishers, London, pp. 193-204.

Popovics, S. (1973), "A numerical Approach to the complete Stress-Strain Curve of Concrete," Cement and Concrete Research, Vol. 3,No. 5, pp. 583-599.

Reineck, K.H. (1991), "Model for Structural Concrete Members without Transverse Reinforcement", Structural Concrete, IABSE Colloquium, Stuttgart, pp. 643-648.

Reinhardt, H.W. (1991), "Imposed Deformation and Cracking", IABSE Colloquium, Structural Concrete, Stuttgart, pp. 101-110.

Roller, John J., and Russell, Henry G. (1990), "Shear Strength of High-Strength Concrete Beams with Web Reinforcement", ACI Structural Journal, Vol. 87, No. 2, pp. 191-198.

Romualdi, J.P., and Batson, G.B. (1963), "Mechanics of Crack Arrest in Concete," Proceedings of the American Society of Civil Engineers, Structural Division, Vol. 89, EM3, New York, pp. 147-168.

Romualdi, J.P., and Mandel, J.A. (1964), "Tensile Strength of Concrete Affected by Uniformly Distributed Closely Spaced Short Lengths of Wire Reinforcement," Journal of the American Concrete Institute, Vol. 61, No. 6, pp. 657-671.

Russo, G., Zingone, G., and Romano, F. (1990),"Analytical Solution for Bond-Slip of Reinforced Bars in R.C. Joints", ASCE, Journal of Structural Engineering, Vol.116, No.2, pp. 336-355.

Scott, R.H., and Gill, P.A.T. (1987), "Short-Term Distribution of Strain and Bond Stress along Tension Reinforcement," Structural Engineer, Vol. 65B,, No. 2, pp. 39-48.

Shah, S.P., and Somayayi, S. (1981), "Bond Stress versus Slip Relationships and Cracking Response of Tension Members", ACI Journal, Vol. 78, No. 3, pp. 217-225.

Spencer, R. A., Panda, A. K., and Mindess, S. (1982), "Bond of Deformed Bars in Plain and Fiber Reinforced Concrete under Reversed Cyclic Loading," International Journal of Cement and Composites, Vol. 4, No. 1, pp. 3-18.

Stevens, N.G., Uzumeri, S.M., Collins, M.P., and Will, G.T. (1991), "Constitutive Model for Reinforcement Concrete Finite Element Analysis", ACI Materials Journal, Vol. 88, No.1, pp. 49-59.

Swamy, R.N., and Al-Noori, K. (1974), "Bond Strength Of Steel Fibres Reinforced Concrete", Concrete (Great Britain), Vol. 8, pp. 36-37.

Tabatabai, H., and Dickson, T.J. (1993), "The History of the Pertstressing Strand Development Length Equation," PCI Journal, Vol. 38, No. 6, pp. 64-75.

Tassios, T.P., and Koroneos, E.G. (1984), "Local Bond-Slip Relatioships by Means of the Moire Method", ACI Journal, Vol. 81, No. 1, pp. 27-34.

Tepfers, Ralejs (1973), "A Theory of Bond Applied to Overlapped Tensile Reinforcement Splices for Deformed Bars", Division of Concrete Structures, Chalmers University of Technology, Goteborg, Sweden, Publication 73:2, 328 pp.

Thorenfeldt, E., Tomaszewicz, A., and Jensen, J.J. (1987), "Mechanical Properties of High-Strength Concrete and Application in Design," Proceedings of the Symposium "Utilization of High Strength Concrete", Tapir, Trondheim, pp. 149-159.

Treece, R. A., and Jirsa, J. O. (1987), "Bond Strength of Epoxy-Coated Reinforcing Bars," PMFSEL Report 87-1, Ferguson Structural Engineering Laboratory, Department of Civil Engineering, The University of Texas at Austin, 85 pp.

Treece, R. A., and Jirsa, J. O. (1989), "Bond Strength of Epoxy-Coated Reinforcing Bars," ACI Materials Journal, Vol. 86, No. 2, pp. 167-174.

Vecchio, F.J., and Collins, M.P. (1986), "The Modified Compression Field Theory for Reinforced Concrete Elements Subjected to Shear", ACI Journal, Vol. 83, No. 2, pp. 219-231.

Viwathanatepa, S., Popov, E.P., and Bertero, V.V. (1979), "Effect of Generalized Loading on Bond of Reinforcing Bars Embedded in Confined Concrete Blocks", Report No. VCB/EERC-79/22, Earthquake Engineering Research Center, University of California, Berkely, 304 pp.

Weerasekera, I.R.A. (1991), "Transfer and Flexural Bond in Pretensioned Prestressed Concrete", Ph.D. Thesis, University of Calgary.

Wicke, M. (1991), "Cracking and Deformation in Structural Concrete", IABSE Colloquium, Structural Concrete, Stuttgart, pp. 49-57.

Wilhelm, W.J., Kemp, E.L., and Lee, Y.T. (1971), "Influence of Deformation Height and Spacing on the Bond Characteristics of Steel Reinforcing Bars", Civil Engineering Studies Report No. 2013, Department of Civil Engineering, West Virginia University.

Williams, A. (1986), "Tests on Large Reinforcement Concrete Elements Subjected to Direct Tension", Technical Report No. 562, Cement and Concrete Association, Wexham Spring, UK, 56 pp.

Yan, C. (1992), "Bond Between Reinforcing Bars and Concrete Under Impact Loading", Ph.D. Thesis, Department of Civil Engineering, The University of British Columbia.

Yankelevsky, D.Z. (1985), "Bond Action Between Concrete and a Deformed Bar -- A New Model", ACI Journal, Vol.82, No. 2, pp. 154-161.

Yannopoulos, P.J., and Tassios, T.P. (1991), "Reinforced Concrete Axial Elements Analyzed under Monotonic and Cyclic Actions," ACI Materials Journal, Vol. 88, No. 1, pp. 3-11.

Yerex II, L., Wenzel, T.H. and Davies, R. (1985), "Bond Strength of Mild Steel in Polypropoiene Fiber Reinforced Concrete", ACI Journal, Vol. 82, No. 1, pp. 40-45.

Zia, P., and Mostafa, P. (1977), "Development Length of Prestressing Strand," PCI Journal, V. 22, No. 5, pp. 54-66.

"The best part of our knowledge is that which teaches us where knowledge leaves off and ignorance begins."

Oliver Wendell Holmes

....So there is still much to learn and I am still learning